INFORMATION TO USERS

This manuscript has been reproduced from the microfilm master. UMI films the text directly from the original or copy submitted. Thus, some thesis and dissertation copies are in typewriter face, while others may be from any type of computer printer.

The quality of this reproduction is dependent upon the quality of the copy submitted. Broken or indistinct print, colored or poor quality illustrations and photographs, print bleedthrough, substandard margins, and improper alignment can adversely affect reproduction.

In the unlikely event that the author did not send UMI a complete manuscript and there are missing pages, these will be noted. Also, if unauthorized copyright material had to be removed, a note will indicate the deletion.

Oversize materials (e.g., maps, drawings, charts) are reproduced by sectioning the original, beginning at the upper left-hand corner and continuing from left to right in equal sections with small overlaps. Each original is also photographed in one exposure and is included in reduced form at the back of the book.

Photographs included in the original manuscript have been reproduced xerographically in this copy. Higher quality 6" x 9" black and white photographic prints are available for any photographs or illustrations appearing in this copy for an additional charge. Contact UMI directly to order.

UMI

A Bell & Howell Information Company
300 North Zeeb Road, Ann Arbor MI 48106-1346 USA
313/761-4700 800/521-0600

"The important thing is not to stop questioning. Curiosity has its own reason for existing. One cannot help but be in awe when he contemplates the mysteries of eternity, of life, of the marvelous structure of reality. It is enough if one tries merely to comprehend a little of this mystery every day. Never lose a holy curiosity."

-Albert Einstein

University of Alberta

Chemistry and Preliminary Biological Evaluation of Novel Radioiodinated Iodoazomycin Arabinoside (IAZA) Metabolites as Potential SPECT Brain and Tumor Imaging Agents

by

Herbert Chi-Ho Lee ©

A thesis submitted to the Faculty of Graduate Studies and Research in partial fulfillment of the requirements for the degree of Doctor of Philosophy

in

Pharmaceutical Sciences

Faculty of Pharmacy and Pharmaceutical Sciences

Edmonton, Alberta

Spring 1998

National Library of Canada
Bibliothèque nationale du Canada

Acquisitions and Bibliographic Services
Acquisitions et services bibliographiques

395 Wellington Street
Ottawa ON K1A 0N4
Canada

395, rue Wellington
Ottawa ON K1A 0N4
Canada

Your file Votre référence

Our file Notre référence

The author has granted a non-exclusive licence allowing the National Library of Canada to reproduce, loan, distribute or sell copies of this thesis in microform, paper or electronic formats.

L'auteur a accordé une licence non exclusive permettant à la Bibliothèque nationale du Canada de reproduire, prêter, distribuer ou vendre des copies de cette thèse sous la forme de microfiche/film, de reproduction sur papier ou sur format électronique.

The author retains ownership of the copyright in this thesis. Neither the thesis nor substantial extracts from it may be printed or otherwise reproduced without the author's permission.

L'auteur conserve la propriété du droit d'auteur qui protège cette thèse. Ni la thèse ni des extraits substantiels de celle-ci ne doivent être imprimés ou autrement reproduits sans son autorisation.

0-612-29061-1

Canada

University of Alberta

Faculty of Graduate Studies and Research

The undersigned certify that they have read, and recommend to the Faculty of Graduate Studies and Research for acceptance, a thesis entitled **Chemistry and Preliminary Biological Evaluation of Novel Radioiodinated Iodoazomycin Arabinoside (IAZA) Metabolites as Potential SPECT Brain and Tumor Imaging Agents** submitted by Herbert Chi-Ho Lee in partial fulfillment of the requirements for the degree of Doctor of Philosophy in Pharmaceutical Sciences.

Dr. John R. Mercer (Supervisor)

Dr. Leonard I. Wiebe (Co-supervisor)

Dr. Edward E. Knaus

Dr. Stephen A. McQuarrie

Dr. Matthew B. Parliament

Dr. Hsing-Jang Liu

Dr. Michael J. Adam (External Examiner)

Date: April 6, 1998

DEDICATION

Upon completion of this milestone in my life,
I would like to dedicate this thesis to:

My father, George Lee, and my mother, Mary Tsui,
for their unparalleled and continual support, love, care,
understanding, patience, encouragement
and advice throughout my life,
and particularly during the course of my studies.

My younger brothers, Thomas and Peter,
for their caring support and enormous help in the family
so that I could concentrate on my research and studies.

My uncle, Stephen Chin,
for his altruistic help, support and care
during my early days in Canada.

My friends (in alphabetical order)
for their warm friendships, goodwill and good memories:
Akino, Christine, Edgar, Ernie, ESS members, Fay, Frank, Hattie, Heng,
Henry C., Henry L., Herman, Hideaki, Jason, Karima, Ken-Ichi, Kenneth,
Kenway, Kevin, Luc, Maggie, Pauline, Regina, Tatsuya and Yukari.

ABSTRACT

Two arabinofuranosyl sugars, methyl 5-deoxy-5-iodo-D-arabinofuranoside (3) and methyl 2,3-di-*O*-acetyl-5-deoxy-5-iodo-α-D-arabinofuranoside (4), and one arabinofuranosyl nucleoside, 1-(5-deoxy-5-iodo-α-D-arabinofuranosyl)-2-amino-imidazole (iodoaminoimidazole arabinoside: IAIA (5)), were chemically synthesized, radioiodinated and biologically evaluated in mice as potential SPECT brain and tumor imaging agents. In particular, compound 5 is a possible [^{123}I]IAZA metabolite that could be responsible for the highly unusual brain uptake of radioactivity observed in advanced cancer patients receiving diagnostic doses of [^{123}I]IAZA.

Direct synthesis from D-(-)-arabinose was the preferred synthetic method for the sugar analogs. The stereospecific synthesis of IAIA was extensively studied. It involved the glycosylation of 2-trifluoroacetamidoimidazole with 1-bromo-2,3,5-tri-*O*-benzoyl-α-D-arabinofuranose. The protected α nucleoside was obtained in 44% yield.

Radioiodination of the sugar analogs was achieved by exchange labeling by the pivalic acid "melt" method. Radiochemical yields greater than 90% were obtained for both sugars by this method. The solvent exchange method in 2-propanol was preferred for the radioiodination of IAIA because of its shorter reaction time. This method gave radiochemical yields of 40-45% for IAIA.

In vivo biodistribution studies of the radioiodinated sugar analogs (in normal mice) and IAIA (in normal and EMT-6 tumor-bearing mice) showed no active accumulation of brain radioactivity. The abnormal brain uptake of radioactivity observed in the [^{123}I]IAZA patients thus could not be explained by this study. However, the maximum tumor-to-blood ratio for IAIA was 4.3 at 4 h with 0.83% of

the injected dose per gram of tumor. Liver radioactivity was found to be unusually high at 24 h with a liver-to-blood ratio of about 30, accounting for 0.32% of the injected dose. All three compounds showed rapid whole-body elimination (>95% at 4 h for the sugar analogs and >97% at 24 h for IAIA). Although a promising tumor-to-blood ratio was obtained, high background radioactivity is likely to hinder tumor imaging with this agent. On the other hand, its high liver-to-blood ratio may be exploited in potential liver imaging.

The present glycosylation studies provided an impetus for the reinvestigation of the anomeric configuration in the chemical structure of IAZA. Based on several types of evidence, it was concluded that IAZA is actually the α anomer.

ACKNOWLEDGEMENTS

I would like to express my deepest gratitude and my indebtedness to my supervisor Dr. John R. Mercer, Assistant Professor of the Faculty of Pharmacy and Pharmaceutical Sciences, for his excellent supervision, thoughtful guidance and warm mentorship. His patience, advice, encouragement and valuable criticism made the successful completion of this thesis possible. I particularly appreciate his patience in the painstaking task of reading the thesis manuscript and his encouragement for me to participate in the Japan research exchange program. His enormous contribution to my professional career will always be remembered.

My deepest thanks and appreciation are also extended to Dr. Leonard I. Wiebe, Professor and Associate Dean of the Faculty of Pharmacy and Pharmaceutical Sciences, for his excellent mentorship, guidance and co-supervision. His advice, encouragement and valuable comments also contributed much in the successful completion of this thesis. I am particularly thankful to him for providing me with a reference for the Japan research exchange program. His enormous contribution to my professional career will equally be remembered.

I am very grateful for the valuable suggestions and criticisms on different aspects of this thesis given by all the committee members: Dr. Matthew B. Parliament, Assistant Professor of the Department of Radiology and Diagnostic Imaging, Faculty of Medicine; Dr. Edward E. Knaus, Professor, Faculty of Pharmacy and Pharmaceutical Sciences; Dr. Stephen A. McQuarrie, Associate Professor, Faculty of Pharmacy and Pharmaceutical Sciences; Dr. Hsing-Jang Liu, Professor, Department of Chemistry; and Dr. Michael Adam (external reader) of TRIUMP in Vancouver. I

am especially thankful to Dr. Matthew B. Parliament for useful discussions on [^{123}I]IAZA patients and their SPECT images.

My sincere thanks are also extended to Dr. Piyush Kumar, Faculty of Pharmacy and Pharmaceutical Sciences, for his valuable help in the laboratory and in the chemical syntheses of some of the sugar analogs and derivatives. I particularly thank him for his continual support, goodwill, friendship and advice throughout my studies, as well as providing me with references on a few occasions.

I would like to thank Ms. Carrie Morin, Department of Nuclear Medicine, Cross Cancer Institute, for letting me examine the SPECT images of some [^{123}I]IAZA patients, and to Mr. Ken Golberg for providing me with a color copy of a SPECT image of an [^{123}I]IAZA patient. I am very grateful to Ms. Haiyan Xia, AltaRex Corp., for providing EMT-6 cells as a generous gift and for her valuable help in biodistribution studies. I am also thankful to Dr. Angelina Morales-Izquierdo in the Mass Spectrometry Laboratory of the Department of Chemistry for her kind help in obtaining mass spectra despite her extremely busy schedule. The great help of Dr. Vishwa Somayaji, Faculty of Pharmacy and Pharmaceutical Sciences, in obtaining numerous NMR spectra, especially NOE studies on IAIA, is deeply appreciated.

I would also like to thank the Faculty of Pharmacy and Pharmaceutical Sciences, Dr. R.E. Moskalyk, Dean of the Faculty, and Taiho Endowed Research Fund for making my research exchange in Japan possible. My sincere thanks are also extended to Ms. Evelyn Mattern, Ms. Theresa Atcheson, and Ms. Joyce Johnson for their constant help and goodwill, to Mr. Gordon McRae for his assistance in computer matters, to Mr. Jeff Turchinsky for his kind help in obtaining laboratory

supplies, and to all the professors and staff in the Faculty of Pharmacy and Pharmaceutical Sciences for their goodwill.

The financial support by the Faculty of Pharmacy and Pharmaceutical Sciences in the form of part-time teaching assistantship is deeply appreciated. This work was funded by a grant from the Alberta Cancer Board Research Initiatives Fund, Grant #RI-14, and by Central Research Fund.

At the Health Sciences University of Hokkaido (HSUH), Hokkaido, Japan:

I would like to express my deep gratitude to Dr. Koh-Ichi Seki, Professor, Faculty of Pharmaceutical Sciences, for his enormous help, patience, advice and hospitality when I was in Japan. His valuable advice, suggestions and keen interest in my project helped make the completion of this thesis possible. I particularly thank him for his wonderful company during a symposium in Kumamoto, Japan and his interesting explanations of Japanese culture and history. I am very much indebted to him for the improvement of my Japanese language ability, especially in the preparation of my Japanese speech for the Faculty of Nursing and Social Welfare at HSUH.

I am equally thankful to Dr. Kazue Ohkura, Assistant Professor, Faculty of Pharmaceutical Sciences, for her generous help, company, advice and hospitality. Her kind assistance in the laboratory and useful discussions in chemistry are gratefully acknowledged. I particularly thank her for taking a keen interest in my project, for helping me improve my Japanese through many interesting conversations, and for her sincere care in my adjustment of Japanese life.

I would also like to express my gratitude to Ms. Yukari Noguchi, Lecturer, Faculty of Pharmaceutical Sciences, for her warm friendship, company, help and

hospitality. My thanks are also extended to Mr. Ken-Ichi Nishijima and Mr. Hideaki Nakamura for their help and great company in the laboratory, and for introducing me to their wonderful friends. I would also like to thank Dr. Masanao Terashima, Emeritus Professor, Faculty of Pharmaceutical Sciences, for his warm welcome and interesting discussions on my project and on Japanese history and language.

I am very grateful to Ms. Masako Ueda and all the staff in the Office of Public Affairs for coordinating the research exchange between Hokkaido and Alberta. The kind and warm assistance of Ms. Ueda in translation and non-academic matters during my stay in Japan is deeply appreciated. Special thanks are also extended to Dr. Howard Tarnoff and Dr. Chie Terayama for their goodwill and for introducing me to the English Speaking Society (ESS) on HSUH campus. Furthermore, the wonderful hospitality and company of all ESS members, as well as Dr. Sansei Nishibe, Dr. Kiyoshi Horita and their pharmacognosy group, are gratefully acknowledged. I would also like to acknowledge the generous financial supports from the Association of International Education, Japan (AIEJ) and the Health Sciences University of Hokkaido.

TABLE OF CONTENTS

1. Introduction..... 1

2. Survey of Related Literature.....11

2.1. Radiolabeled hexopyranosyl sugar analogs for metabolic brain and tumor imaging.....11

2.1.1. 2-Deoxy-2-[^{18}F]fluoro-D-glucose (2-[^{18}F]FDG).....11
2.1.2. Other PET sugar analogs.....16
2.1.3. SPECT hexopyranosyl sugar analogs.....26
2.1.3.1. Rationale for investigating potential SPECT sugar analogs.....26
2.1.3.2. ^{123,131}I-labeled glucose and other sugar analogs.....28
2.1.3.3. Technetium-99m-labelled sugar analogs.....34

2.2. Radiolabeled sugar-coupled derivatives (nucleosides) for hypoxic tumor imaging: metabolic trapping in hypoxic cells.....37

2.2.1. Tumor oxygenation and changes in oxygen supply-demand relationships: causes and detection of tissue hypoxia.....37
2.2.2. Mechanisms of hypoxic tissue radiosensitization by nitroimidazoles.....40
2.2.3. Nature of the reductive adducts.....43
2.2.4. Radioiodinated sugar-coupled 2-nitroimidazoles as hypoxic cell markers.....48

2.3. Chemistry and radioiodination of arabinofuranosyl sugars and nucleosides.....54

2.3.1. Chemistry of glycosylation reactions with arabinofuranosyl sugars..... 54
2.3.2. Methods to differentiate between α and β anomers of arabinofuranosyl nucleosides.....56
2.3.2.1. NMR spectroscopy.....57
2.3.2.2. Chiroptical methods.....61
2.3.2.3. X-ray crystallography.....63
2.3.2.4. Chemical reactions.....64
2.3.3. Chemistry of radioiodination of arabinofuranosyl nucleosides....65
2.3.3.1. Exchange labeling methods.....65
2.3.3.2. Direct synthesis with radioiodide.....66

2.4. New and current developments in medical diagnostic imaging.....67

2.4.1. Role of ^{123}I and some potential newcomers in SPECT.....67
2.4.2. Instrumentation for PET and SPECT and PET-SPECT dual cameras.....69
2.4.3. Present and future trends.....72

3. Experimental.....73

3.1. Materials.....73
3.1.1. Chemicals, Solvents, Gases, and Equipment.....73
3.1.2. Instruments.....74
3.1.3. Radioisotopes.....76
3.1.4. Animals.....76
3.1.5. Tumor cell line.....76

3.2. Methods.....77
3.2.1. Synthesis of methyl 5-deoxy-5-iodo-D-arabinofurnoside (3).....77
3.2.1.1. Chemical cleavage from IAZA (1A).....77
3.2.1.2. Chemical synthesis from D-(-)-arabinose (61).....79
3.2.2. Methyl 2,3-di-*O*-acetyl-5-deoxy-5-iodo-α-D-arabinofuranoside (6).....80
3.2.3. General procedure for the cleavage reactions 3-6 (section 4.1.1.) the preparation of 59.....81
3.2.4. General procedure for the deacetylation reactions 1 & 2 (section 4.1.1.) of 59.....82
3.2.5. Chemical synthesis of 1-(5-deoxy-5-iodo-α-D-arabinofuranosyl)-2-aminoimidazole (Iodoaminoimidazole arabinoside: IAIA (5))...82
3.2.5.1. Chemical reduction from AZA (7) and subsequent iodination.....82
3.2.5.2. Chemical synthesis from D-(-)-arabinose (61).....83
3.2.5.2.1. Starting materials.....83
3.2.5.2.2. Glycosylation reactions.....86
3.2.5.2.3. Deprotection reactions.....88
3.2.6. General procedure for glycosylation reactions with silylation of 2-aminoimidazole derivatives (Reactions 1 & 9, section 4.4.1.).....91
3.2.7. General procedure for glycosylation reactions in dichloromethane (Reactions 7 & 8, section 4.4.1.).....92
3.2.8. General procedure for the radioiodination of methyl 5-deoxy-5-[^{125}I]iodo-D-arabinofuranoside ([^{125}I]-3) and methyl 2,3-di-*O*-acetyl-5-deoxy-5-iodo-α-D-arabinofuranoside ([^{125}I]-6) in pivalic acid.....92

3.2.9. General procedure for the radioiodination of 1-(5-deoxy-5-[^{125}I]iodo-α-D-arabinofuranosyl)-2-aminoimidazole (Iodoamino-imidazole arabinoside: IAIA (5))....94
3.2.9.1. Pivalic acid "melt" method....94
3.2.9.2. Solvent exchange method....94
3.2.10. Purification of methyl 5-deoxy-5-[^{125}I]iodo-D-arabinofurnoside (3) and methyl 2,3-di-*O*-acetyl-5-deoxy-5-iodo-α-D-arabinofurano-side ([^{125}I]-6)....95
3.2.11. Purification of 1-(5-deoxy-5-[^{125}I]iodo-α-D-arabinofuranosyl)-2-aminoimidazole (Iodoaminoimidazole arabinoside: IAIA (5))....95
3.2.12. Animal studies....96
3.2.12.1. Preparation of the animal model....96
3.2.12.2. Administration of radiopharmaceuticals....96
3.2.12.3. Collection of tissue samples....97
3.2.12.4. Biodistribution studies....98

4. Results and Discussions

4.1. Methyl 5-deoxy-5-iodo-D-arabinofuranoside (3)....99
4.1.1. Chemistry....99
4.1.2. Radioiodination....106
4.1.3. Biodistribution and elimination....109
4.1.4. Stability....116

4.2. Methyl 2,3-di-*O*-acetyl-5-deoxy-5-iodo-α-D-arabinofuranoside (4)....117
4.2.1. Chemistry....117
4.2.2. Radioiodination....118
4.2.3. Biodistribution and elimination....123
4.2.4. Stability....127

4.3. 1-(5-Deoxy-5-iodo-α-D-arabinofuranosyl)-2-aminoimidazole (Iodoamino-imidazole arabinoside: IAIA (5))....130
4.3.1. Chemistry....130
4.3.2. Radioiodination....133
4.3.3. Biodistribution and elimination....141
4.3.4. Stability....154

4.4. Chemistry of glycosylation reactions between arabinofuranosyl sugars and N^2-protected 2-aminoimidazoles....156
4.4.1. Studies on the glycosylation reaction....156
4.4.2. Studies on the deprotection reaction....163

4.5. Investigations that led to the conclusion of the chemical structure of α-IAZA (1A)....169
4.5.1. Initial observations: Studies with AIA (6)....169
4.5.2. Literature evidence....176
4.5.3. Previous ^{1}H and ^{13}C NMR data of AZA and IAZA....181
4.5.4. X-ray crystallography structure analyses....184

5. Conclusions....187

References....191

Appendices....208
Appendix 1. Brief assessment on the SPECT images obtained from 10 selected [^{123}I]IAZA advanced cancer patients[2,4] during 1991-1994....208
Appendix 2. Sample calculations of the two-sample *t*-test....210

LIST OF TABLES

Table 1. Some examples of PET and SPECT radiopharmaceuticals currently used as brain imaging agents.....5

Table 2. Some examples of radiopharmaceuticals used for PET and SPECT studies of cancer.....7-8

Table 3. Comparisons of relative kinetic constants of glucose analogs with structural modifications at carbons 2,3 and 4 and hexokinase.....13

Table 4. Cleavage reactions under various reaction conditions.....100

Table 5. Deacetylation reactions of **59**.....103

Table 6. Summary of radioiodination results for **3** (1 mg) in DMF (100 μL) or pivalic acid (3 mg).....106

Table 7. Radiochemical purity determination for [^{125}I]-**3**.....109

Table 8. Biodistribution of [^{125}I]-**3** following i.v. administration in normal mice at various time intervals.....110

Table 9. Thyroid radioactivity as percent injected dose of [^{125}I]-**3** per organ in normal mice (n=4 & 3).....111

Table 10. Radiochemical stability assessment for [^{125}I]-**3**.....116

Table 11. Iodination and acetylation reaction for α-**62**.....118

Table 12. Summary of radioiodination results for **4** (0.5 mg) in pivalic acid (1.5 mg).119

Table 13. Radiochemical purity determination for [^{125}I]-**4**.....123

Table 14. Biodistribution of [^{125}I]-**4** following i.v. administration in Balb/c mice at various time intervals.....124

Table 15. Thyroid radioactivity as percent injected dose of [^{125}I]-**4** per organ in normal mice (n=4).....126

Table 16. Whole-body elimination and blood clearance data for [^{125}I]-**4**.....127

Table 17. Radiochemical stability of [^{125}I]-**4** in saline, 10% DMSO in saline and 20% EtOH in saline.....128

Table 18. Summary of radioiodination results for IAIA (**5**) in pivalic acid or 2-propanol 134-136

Table 19. Purification results for [^{125}I]IAIA (**5**) 138-139

Table 20. Biodistribution of [^{125}I]IAIA following i.v. administration in Balb/c mice at various time intervals 142

Table 21. Biodistribution of [^{125}I]IAIA following i.v. administration in Balb/c mice bearing EMT-6 tumors at various time intervals 143

Table 22. Thyroid radioactivity as percent injected dose of [^{125}I]IAIA (**5**) per organ in normal and EMT-6 tumor-bearing Balb/c mice (n=3) 145

Table 23. Chemical and radiochemical stability assessment for **5** 149

Table 24. Glycosylation trials between N^2-protected 2-aminoimidazoles (**66** or **69**) with 2,3,5-tri-*O*-benzoyl-α-D-arabinofuranosyl bromide (**64**) 157

Table 25. Deprotection reactions of selected glycosylation products 164

Table 26. Comparison of ^{1}H NMR and mass data of the unknown side product and AIA (**6**) 166-167

Table 27. ^{1}H NMR data comparison between the two AIA (**6**) nucleosides synthesized by two different methods 169-170

Table 28. ^{1}H NMR and melting point data reported in literature 177

Table 29. Glycosylation methods reported in literature 180

Table 30. Previous ^{1}H and ^{13}C NMR data of AZA and IAZA 181

LIST OF FIGURES

Figure 1. Unusual brain uptake of radioactivity in the SPECT brain images of an [^{123}I]IAZA advanced cancer patient 2

Figure 2. Determination of the anomeric configuration of sugar derivatives.....57

Figure 3. Differentiation of anomeric arabinofuranosyladenine by NOE.....60

Figure 4. Radioiodination yields of 3.....107

Figure 5. Determination of labeling efficiency of [^{125}I]-3 by TLC.....108

Figure 6. Purification and collection profile for [^{125}I]-3.....108

Figure 7. Tissue-to-blood ratios of radioactivity at various time intervals following i.v. administration of [^{125}I]-3 in normal mice.....113

Figure 8. Tissue-to-blood ratios of radioactivity at various time intervals following i.v. administration of [^{125}I]-3 in normal mice.....114

Figure 9. Whole-body elimination and blood clearance of radioactivity following i.v. administration of [^{125}I]-3 in normal mice.....115

Figure 10. Radioiodination results for 4.....120

Figure 11. Determination of labeling efficiency of [^{125}I]-4 by TLC.....121

Figure 12. Collection profile for [^{125}I]-4 (Run 1).....122

Figure 13. Collection profile for [^{125}I]-4 (Run 2).....122

Figure 14. Labeling efficiency for IAIA (5).....137

Figure 15. Determination of labeling efficiency of [^{125}I]IAIA (5) by TLC.....137

Figure 16. Collection profile for [^{125}I]IAIA (5).....140

Figure 17. Radiochemical purity of [^{125}I]IAIA (5).....141

Figure 18. Tissue-to-blood ratios of radioactivity at various time intervals following i.v. administration of [^{125}I]IAIA (5) in normal Balb/c mice.....146

Figure 19. Tissue-to-blood ratios of radioactivity at various time intervals following i.v. administration of [^{125}I]IAIA (5) in normal Balb/c mice.....147

Figure 20. Tissue-to-blood ratios of radioactivity at various time intervals following i.v. administration of [^{125}I]IAIA (**5**) in Balb/c mice.....150

Figure 21. Tissue-to-blood ratios of radioactivity at various time intervals following i.v. administration of [^{125}I]IAIA (**5**) in Balb/c mice.....151

Figure 22. Whole-body clearance of radioactivity following i.v. administration of [^{125}I]IAIA (**5**) in normal and tumor-bearing Balb/c mice.....152

Figure 23. Blood clearance of radioactivity following i.v. administration of [^{125}I]IAIA (**5**) in normal and tumor-bearing Balb/c mice.....153

Figure 24. ^{1}H-^{1}H COSY spectrum of AIA (**6**).....171

Figure 25. ^{1}H-^{1}H NOESY spectrum of AIA (**6**).....172

Figure 26. MO calculations on AIA (**6**) of intramolecular distances relevant in NOE correlation studies.....174

Figure 27. MO calculations on β-AIA (**76**) of intramolecular distances relevant in NOE correlation studies.....175

Figure 28. MO calculations on AIA (**6**): dihedral angles and other selected intra-molecular distances.....175

Figure 29. ^{1}H-^{1}H COSY spectrum of IAZA (**1A**).....182

Figure 30. ^{1}H-^{1}H ROESY spectrum of IAZA (**1A**).....183

Figure 31. X-ray crystallography structure analysis of IAZA (**1A**).....185

Figure 32. X-ray crystallography structure analysis of AZA (**7**).....186

LIST OF SCHEMES

Scheme 1. A proposed metabolic pathway for [^{123}I]IAZA (**1A**).....4

Scheme 2. Metabolic trapping of 2-[^{18}F]FDG in tissues.....14

Scheme 3. Metabolic trapping of 2-[^{18}F]FDGal in liver tissues.....22

Scheme 4. Mechanism of action of nitroimidazoles.....41

Scheme 5. Possible biologically important reactions of 2-hydroxylaminoimidzoles.....44

Scheme 6. Postulated pathway for the formation and subsequent reduction of the bimolecular, azoxy, azo and hydrazo derivatives.....44

Scheme 7. Reactions of 2-hydroxylaminoimidazoles in aqueous solutions under hypoxic conditions.....45

Scheme 8. Reactions of 2-hydroxylaminoimidazoles with glutathione.....46

Scheme 9. Chemical synthesis of a C_1'-C_2' *cis* arabinofuranosyl nucleoside.....56

Scheme 10. Differentiation of anomeric nucleosides by evidence of cyclonucleoside formation.....64

Scheme 11. Chemical synthesis of **3** from IAZA (**1A**) by base cleavage.....102

Scheme 12. Expected deacetylation reaction of **59**.....103

Scheme 13. Chemical synthesis of **3** from D-(-)-arabinose (**61**).....104

Scheme 14. Radioiodination of **3**.....105

Scheme 15. Chemical synthesis of **4** from D-(-)-arabinose (**61**).....117

Scheme 16. Radioiodination of **4**.....119

Scheme 17. Chemical synthesis of IAIA (**5**) from AZA (**7**).....130

Scheme 18. Chemical synthesis of IAIA (**5**) from D-(-)-arabinose (**61**).....131

Scheme 19. Radioiodination of IAIA (**5**).....133

LIST OF ABBREVIATIONS

2-BDG	2-deoxy-2-bromo-D-glucose
2-DG	2-deoxy-D-glucose
2-FDA	2-deoxy-2-fluoro-D-altrose
2-FDG	2-deoxy-2-fluoro-D-glucose
2-FDG-6-P	2-deoxy-2-fluoro-D-glucose-6-phosphate
2-FDGal	2-deoxy-2-fluoro-D-galactose
2-FDM	2-deoxy-2-fluoro-D-mannose
2-FDT	2-deoxy-2-fluoro-D-talose
2-FIG	2-deoxy-2-fluoro-2-iodo-D-glucose
2-FIM	2-deoxy-2-fluoro-2-iodo-D-mannose
2-IDG	2-deoxy-2-iodo-D-glucose
3-BDG	3-deoxy-3-bromo-D-glucose
3-FDG	3-deoxy-3-fluoro-D-glucose
3-IDG	3-deoxy-3-iodo-D-glucose
4-FDG	4-deoxy-4-fluoro-D-glucose
4-FIG	4-deoxy-4-iodo-D-glucose
Å	angstrom (10^{-10} m)
ABGA	1,3,4,6-tetra-*O*-acetyl-*N*-(*m*-iodobenzoyl)glucosamine
Ac_2O	acetic anhydride
AcOH	acetic acid
AIA	aminoimidazole arabinoside
Anal.	analysis (elemental)
ara-A	arabinofuranosyladenine
AZA	azomycin arabinoside
AZR	azomycin riboside
β-CIT	methyl 3β-(4-iodophenyl)tropane-2β-carboxylate
BBB	blood-brain barrier
BGA	2-deoxy-2-*N*-iodobenzoyl-D-glucosamine
BGO	bismuth germanate

br s	broad singlet (NMR)
Calcd.	calculated
CD	circular dichroism
cm	centimeter
CMG	3-[^{11}C]-methyl-D-glucose
^{1}H-^{1}H COSY	proton-proton shift correlations spectroscopy
CT	computed tomography
d	doublet (NMR)
dd	doublet of doublets (NMR)
df	degrees of freedom (statistical analysis)
DMF	*N,N*-dimethylformamide
DMSO	dimethyl sulfoxide
DNA	deoxyribonucleic acid
dpm	disintergrations per min
dt	doublet of triplets (NMR)
DTPA	diethylenetriaminepentaacetic acid
E^{1}_{7}	one electron reduction potential
EDTA	ethylenediaminetetracetic acid
EI MS	electron impact mass spectrometry
ESI MS	(positive mode) electrospray ionization mass spectrometry
Et_3N	triethylamine
EtOAc	ethyl acetate
EtOH	ethanol
FAG	*N*-fluoroacetyl-D-glucosamine
FDOPA	6-fluoro-L-dihydroxyphenylalanine
FIAZP	1-(2-fluoro-4-iodo-2,4-dideoxy-β-L-xylopyranosyl)-2-nitro-imidazole
fMRI	functional magnetic resonance imaging
g	gram
GBq	gigabecquerel

GH	glucoheptonate
GIT	gastrointestinal tract
GSH	glutathione
h	hour
HEADTOME	hybrid emission advanced dynamic tomograph
HIDA	heptabilliary iminodiacetic acid
HMPAO	hexamethylpropylene amine oxime
HPLC	high pressure liquid chromatography
HR MS	high resolution mass spectrometry
Hz	hertz
i.v.	intravenous
IAIA	iodoaminoimidazole arabinoside
IAZA	iodoazomycin arabinoside
IAZG	iodoazomycin galactoside
IAZP	iodoazomycin pyranoside
IAZR	iodoazomycin riboside
IAZXP	β-D-iodoazomycin xylopyranoside
IBG	2-deoxy-2-*O*-(iodobenzoyl)-D-glucose
IBZM	3-iodo-6-methoxybenzamide
IMP	isopropyl-*p*-iodoamphetamine
IMT	3-iodo-α-methyl-L-tyrosine
IUdR	5-iodo-2'-deoxyuridine
J	spin-spin vicinal coupling constant (NMR)
kBq	kilobecquerel
keV	kiloelectron volts
K_M	Michaelis constant, the substrate concentration at which the enzyme reaction rate is half of its maximal value, V_{max}
L-2-FDG	2-deoxy-2-fluoro-L-glucose
LCMRGlc	local cerebral metabolic rate of glucose
LR MS	low resolution mass spectrometry

m	multiplet (NMR)
m/z	mass-to-charge ratio (MS)
MBDG	methyl 2-deoxy-2-bromo-β-D-glucopyranoside
MBq	megabecquerel
MEK	methyl ethyl ketone
MeOH	methanol
MIBG	metaiodobenzylguanidine
MIDG	methyl 2-deoxy-2-iodo-β-D-glucopyranoside
MISO	misonidazole
MO	molecular orbitals
MeV	million electron volts
mg	milligram
min	minute
mL	milliliter
mm	millimeter
mmol	millimole
mol	mole
mp	melting point
mV	millivolt
μCi	microcurie
μg	microgram
μL	microliter
μm	micron or micrometer
MTBG	methyl 3,4,6-tri-*O*-acetyl-2-deoxy-2-bromo-β-D-glucopyranoside
MTIG	methyl 3,4,6-tri-*O*-acetyl-2-deoxy-2-iodo-β-D-glucopyranoside
N	normal
NIS	*N*-iodosuccinimide
nm	nanometer
NMR	nuclear magnetic resonance
NOE	nuclear Overhauser effect

NOESY	two-dimensional nuclear Overhauser spectroscopy
ORD	optical rotatory dispersion
P	octanol:water partition coefficient
p	probability value
PBGA	1,3,4,6-tetra-*O*-pivaloyl-*N*-(*m*-iodobenzoyl)glucosamine
PDT	photodynamic therapy
PET	positron emission tomography
ϕ	dihedral angle between the C-H bonds **H-C-C-H**
POSFAB MS	positive ion fast atom bombardment mass spectrometry
ppm	parts per million
R_f	ratio to front (TLC)
RNA	ribonucleic acid
ROESY	rotating frame two-dimensional nuclear Overhauser spectroscopy
s	singlet (NMR)
SPECT	single photon emission computed tomography
t	two-sample t-test
t	triplet (NMR)
$t_{1/2}$	half-life
TLC	thin layer chromatography
TMS	tetramethylsilane (NMR internal standard)
UV	ultraviolet
v/v	volume percent
V_{max}	maximal rate at which the enzyme active sites are saturated with substrate

1. Introduction

[^{123}I]Iodoazomycin arabinoside ([^{123}I]IAZA, **1A**), an arabinofuranosyl 2-nitro-imidazole nucleoside used in hypoxic cells imaging, has been shown to have selective uptake into hypoxic tissues in both animal studies[1] and preliminary human studies with cancer patients[2]. Hypoxia, a state of oxygenation between the absolute absence of oxygen (anoxia) and the normal state of oxygenation of healthy tissues, is caused by the reduction of oxygen supply to tissue below physiological levels[3]. In tumors, low oxygenation is most often due to inadequate blood supplies to meet their metabolic demands. Recently [^{123}I]IAZA has been under investigation in advanced cancer patients, where it is used to assess tumor hypoxia[4], and in patients with diabetes mellitus[5]. A very *unexpected* observation in the imaging of about one-third of patients (3 out of 10 patients) from those preliminary studies[2,4] (Appendix 1) was the brain uptake of radioactivity in the later images (18-24 h) which was sufficiently intense to provide excellent images of the brain (Figure 1). The time course of this highly unusual uptake was not consistent with perfusion images and has been postulated to represent metabolic trapping of radioactivity in the brains of [^{123}I]IAZA patients (McEwan, unpublished results).

If a single-photon-emitting, radioiodinated sugar analog that was produced through metabolism of [^{123}I]IAZA were actively accumulated in the brain tissues as observed in the [^{123}I]IAZA patients, then this might be a valuable SPECT agent for brain imaging. It would also be a very attractive SPECT metabolic alternative to 2-[^{18}F]FDG and would extend its medical application to nuclear medicine facilities.

Figure 1. Unusual brain uptake of radioactivity in the SPECT brain images of an [^{123}I]IAZA advanced cancer patient (McEwan, unpublished results).

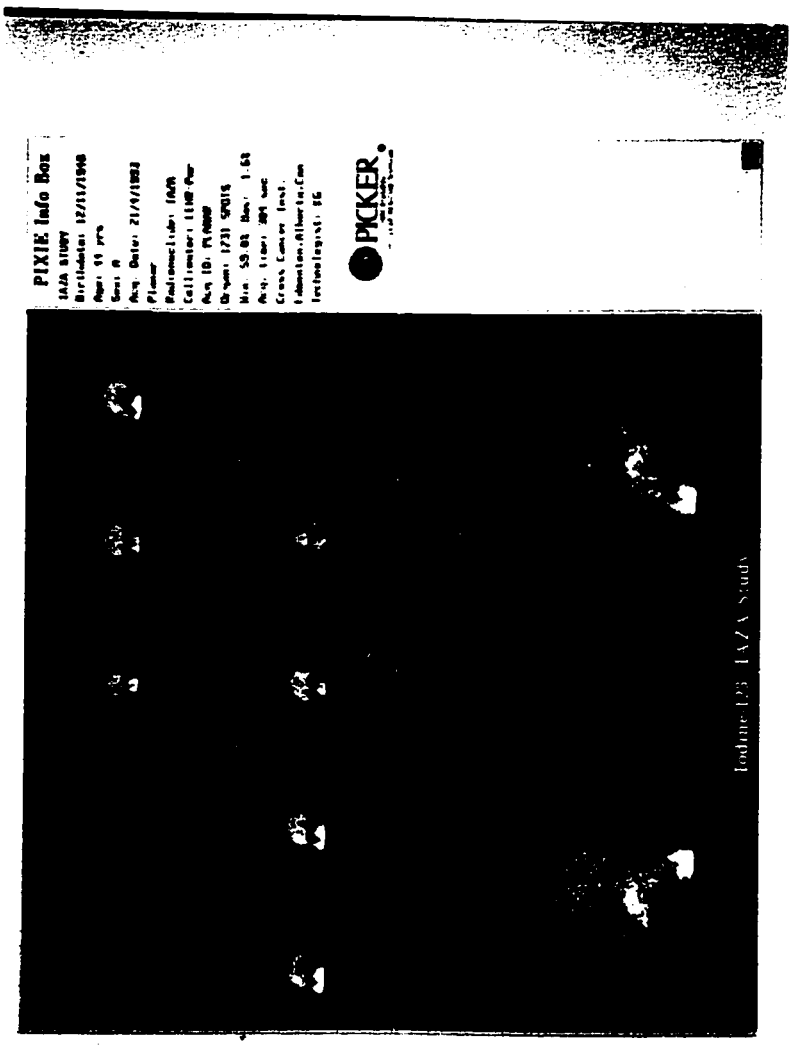

The actual species or metabolites causing this abnormal uptake of radioactivity have not been identified. Two possible metabolic pathways are proposed. Metabolites from each of these pathways were evaluated in this preliminary study for their roles in the observed accumulation of brain radioactivity in the [^{123}I]IAZA patients.

Proposed Metabolic Pathway I

The first hypothesized metabolic route involves the enzymatic cleavage of the N^1-glycosidic bond between the 2-nitroimidazole nucleobase and the radioiodinated arabinofuranosyl sugar moiety. [^{123}I]IAZA has been observed to undergo metabolism *in vivo* and the decoupled radioiodinated arabinofuranosyl sugar **2** is a probable initial product of this process (Scheme 1) (McEwan, unpublished results). The metabolized [^{123}I]IAZA yields a radioiodinated sugar analog **2** which then undergoes passive or active uptake into brain tissues and hence becomes metabolically trapped. This radioiodinated sugar derivative **2** is postulated to be a likely candidate responsible for this anomalous brain uptake of radioactivity in the brains of the [^{123}I]IAZA patients. It is known that many enzymes exist for the metabolic cleavage of the N^1-glycosidic bond in nucleosides. One such enzyme is thymidine phosphorylase[6,7] which is used to assess the relative resistance to enzymatic cleavage by the ribofuranosyl and arabinofuranosyl structure[1,8]. Although a number of arabinofuranosyl nucleosides have been shown to be more stable than their ribofuranosyl counterparts *in vivo* and *in vitro*[9], it is conceivable that *in vivo* enzymatic cleavage of the arabinofuranosyl nucleoside could still occur to an appreciable degree to allow sufficient quantities of the metabolite to accumulate in the brain.

Scheme 1. A proposed metabolic pathway for [^{123}I]IAZA (1A).

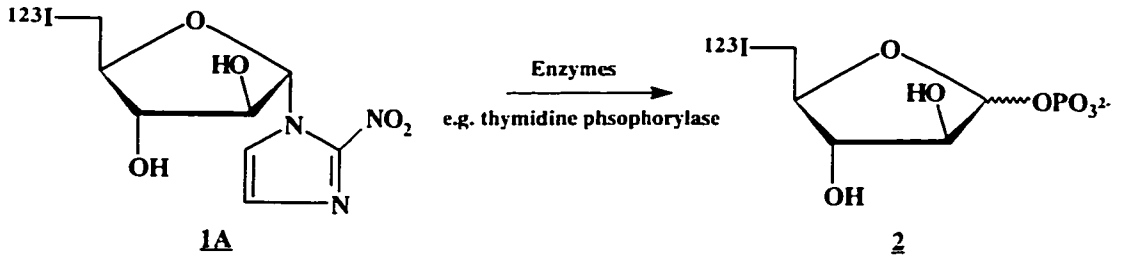

This type of metabolic trapping behavior has been recognized and exploited with the radiofluorinated sugar 2-deoxy-2-[^{18}F]fluoro-D-glucose (2-[^{18}F]FDG) to achieve metabolic and functional brain imaging using positron emission tomography (PET) techniques. 2-[^{18}F]FDG has been widely used to detect many metabolic abnormalities in the brain[10] and can indicate disease states even when conventional imaging indicates no structural change in the brain. It is also highly successful in the detection of tumors and the evaluation of tumor metabolism[11,12].

Despite the tremendous potential of 2-[^{18}F]FDG, studies are generally limited to PET centers that have medical cyclotron facilities available for the production of the short-lived (110 min) fluorine-18. This is a severe limitation on the widespread clinical application of this agent. The current lack of a SPECT metabolic brain imaging agent also provides an impetus for the studies on radioiodinated sugar analogs metabolized from [^{123}I]IAZA as potential SPECT brain imaging agents. At present radiopharmaceuticals for brain imaging can be classified into the following categories[10] (Table 1).

Table 1. Some examples of PET and SPECT radiopharmaceuticals currently used as brain imaging agents[10].

Types of imaging agents	*PET*	*SPECT*
Blood-brain barrier (BBB) agents	[^{68}Ga]EDTA [^{13}N]Glutamate	[^{99m}Tc]Pertechnetate (TcO_4^-) [^{201}Tl]Thallous chloride (TlCl)
Cerebral perfusion agents	[^{15}O]H_2O [^{15}O]O_2	[^{99m}Tc]Hexamethylpropylene amine oxime ([^{99m}Tc]HMP-AO) Isopropyl-*p*-[^{123}I]iodoamphetamine ([^{123}I]IMP)
Cerebral receptor-binding agents	[^{18}F]Methylspiperone analogs 3-*N*-[^{11}C]Methylspiperone	3-[^{123}I]Iodo-6-methoxybenzamide ([^{123}I]IBZM)
Cerebral neurotransmitter agents	[^{18}F]FDOPA	None reported to date
Cerebral dopamine-transporter agents	[^{11}C]β-CIT (cocaine analog)	[^{123}I]β-CIT
Cerebral metabolic agents	2-[^{18}F]FDG 1-[^{11}C]-2-Deoxy-D-glucose	None reported to date
Monoclonal antibodies	[^{124}I]3F8	[^{131}I]3F8

Many compounds cannot cross the blood-brain barrier (BBB) in the normal brain but do so in some brain pathologies because of the breakdown of the BBB. These are called BBB agents. In contrast, cerebral perfusion agents cross the BBB and localize in the normal brain tissue but have altered uptake in abnormal tissues.

Cerebral receptor-binding agents bind specifically to brain receptors (e.g. dopamine and opiate receptors) while cerebral neurotransmitter agents give a cerebral distribution of neurotransmitter activities which are often different for normal and abnormal tissues. Table 1 shows that the lack of a direct SPECT measure of bio-energetics is now the only significant difference between PET and SPECT tracers.

Proposed Metabolic Pathway 2

[^{123}I]IAZA, like its 2-nitroimidazole predecessors, has been demonstrated to be a radiosensitizer for hypoxic tissues. Radiosensitizers are agents that sensitize hypoxic cells to the lethal effects of ionizing radiation. 2-Nitroimidazoles typically undergo a preliminary reversible intracellular reduction step in all cells. In hypoxic cells where the O_2 concentration is low, they can undergo further bioreduction to reactive intermediates (nitroso and hydroxylamine) that bind to cellular components (See Scheme 4), contributing to tissue sensitization of ionizing radiation.

The amino derivative, which cannot be further reduced, is the final product of this bioreduction process. This radioiodinated 2-aminoimidazole nucleoside is thus a potential metabolite of [^{123}I]IAZA and is speculated to be another possible candidate responsible for the observed brain radioactivity. It is conceivable that after bio-reduction, this 2-aminoimidazole metabolite leaves the cell and then undergoes passive or active uptake into the brain and is once again metabolically trapped. This brain uptake could be facilitated by specific nucleoside and/or amine transporters[13], while its subsequent brain accumulation could be effected by a pH-dependent trapping mechanism in which the amino group is protonated by the slightly lower cerebral pH[14].

This 2-aminoimidazole nucleoside is also a potential SPECT tumor imaging agent. At present, tumor imaging agents comprise a number of different classes as shown in Table 2[15]. This table illustrates that a considerable number of biochemical (e.g. hypoxic cell agents) or physiological processes (e.g. perfusion) are involved in tumor uptake mechanisms. The agents listed in Table 2 are either clinically useful or those which have clinical potential. If this 2-aminoimidazole nucleoside were found to be selectively localized in tumor cells, it would have the potential to be added to this list of useful tumor imaging agents.

Table 2. Some examples of radiopharmaceuticals used for PET and SPECT studies of cancer[15].

Type of processes	*PET radiopharmaceutical*	*SPECT radiopharmaceutical*
General biochemical and physiological processes: Glucose metabolism	2-[^{18}F]FDG	None reported to date
Perfusion	[^{13}N]NH_3, [^{15}O]H_2O	[^{99m}Tc]HMPAO *N*-Isopropyl-*p*-[^{123}I]-iodoamphetamine
Oxygen metabolism	[^{15}O]O_2	None
Amino acid uptake and protein synthesis	[^{11}C]Methionine [^{13}N]Glutamate	3-[^{123}I]Iodo-α-methyl-L-tyrosine ([^{123}I]IMT)
Nucleic acid metabolism (DNA replication)	[^{11}C]Thymidine	5-[^{123}I]Iodo-2'-deoxy-uridine ([^{123}I]IUdR)
Glucosamine uptake	[^{18}F]Fluoroacetyl-D-glucosamine (2-[^{18}F]FAG)	*m,o*-2-Deoxy-2-*N*-([^{123}I]-iodobenzoyl)-D-glucosamine (*m, o*-[^{123}I]BGA).

Table 2 (Cont'd). Some examples of radiopharmaceuticals used for PET and SPECT studies of cancer[15].

Types of Processes	*PET radiopharmaceuticals*	*SPECT radiopharmaceuticals*
Organ-specific or other specialized biochemical and physiological processes:		
BBB permeability	[^{82}Rb]RbCl [^{68}Ga]EDTA	[^{99m}Tc]Glucoheptonate ([^{99m}Tc]GH) [^{99m}Tc]Diethylenetriamine-pentaacetic acid ([^{99m}Tc]DTPA)
Receptor-specific ligands	[^{18}F]Fluoroestradiol	[^{111}In-DTPA-D-Phe]-Octreotide (OctreoScan®) [^{123}I-Tyr-3]-Octreotide
Monoclonal antibodies	[^{124}I]HMFG1 [^{124}I]3F8	[^{111}In]OncoScint® [^{99m}Tc]Anti-CEA (a Fab fragment)
Hypoxic cell agents	[^{18}F]Fluoromisonidazole	[^{123}I]IAZA
Nucleoside analogs	[^{18}F]Fluorodeoxyuridine	[^{123}I]IUdR
Hepatobilliary agent	None	[^{99m}Tc]Hepatobilliary iminodiacetic acid ([^{99m}Tc]HIDA)
Adrenal medulla accumulating agent	[^{124}I]Metaiodobenzyl-guanidine ([^{124}I]MIBG) [^{18}F]Metafluorobenzyl-guanidine ([^{18}F]MFBG)	[^{131}I]Metaiodobenzyl-guanidine ([^{131}I]MIBG)
Other processes (e.g. protein-binding agents, Na^+-K^+ pump uptake agents)	[^{68}Ga]Gallium citrate	[^{67}Ga]Gallium citrate [^{201}Tl]TlCl

These two metabolic pathways provided a rationale for the chemical syntheses and radioiodination of the two deoxyiodo sugars, anomeric methyl 5-deoxy-5-iodo-D-arabinofuranoside (3) and methyl 2,3-di-*O*-acetyl-5-deoxy-5-iodo-α-D-arabinofuranoside (4), and the 2-aminoimidazole nucleoside, 1-(5-deoxy-5-iodo-α-D-arabinofuranosyl)-2-aminoimidazole (iodoaminoimidazole arabinoside: IAIA, 5). These proposed metabolites were then biologically evaluated in mice to determine if they could have had roles in the observed SPECT brain images of [^{123}I]IAZA patients. The chemistry of the glycosylation reaction with N^2-protected 2-aminoimidazoles was also extensively investigated.

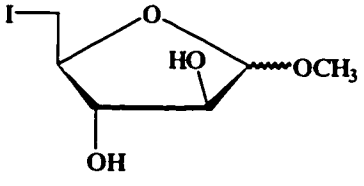

3

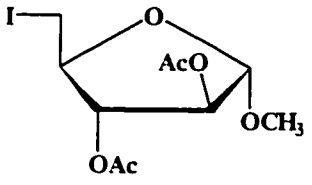

4

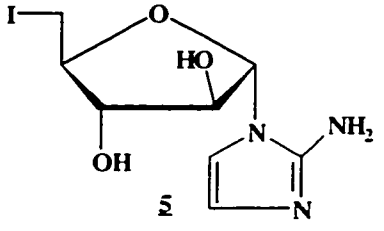

5

During the course of this investigation, the ^{1}H NMR spectrum of aminoimidazole arabinoside (AIA, 6), which is believed to be the α nucleoside, was found to be identical to the sample chemically reduced from azomycin arabinoside (AZA, 7). This observation appears to contradict the β anomeric configuration of IAZA (1A) in literature[1] and provided an impetus for further investigations.

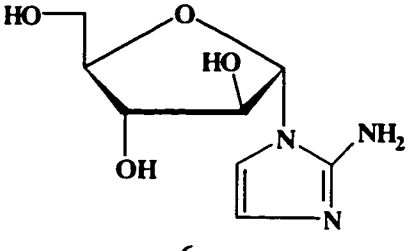

6

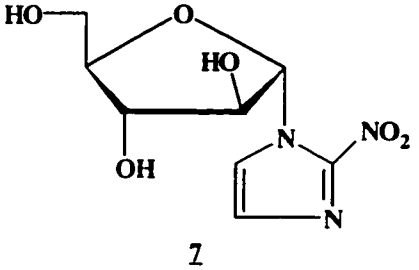

7

Section 2.1 provides a survey of radiolabeled sugar analogs that have been studied or are in current clinical use. Hexopyranosyl sugars as PET and SPECT agents are reviewed because no corresponding studies with radiolabeled pento-furanosyl sugars have been reported to date. Since the proposed metabolites are sugar analogs and derivatives, and this study is motivated by the possible development of a SPECT radioiodinated sugar analog, a review of the most common hexopyranosyl sugars used in PET and SPECT imaging is important. However, this review does not suggest that the mechanisms of uptake and accumulation in cells are the same for both hexopyranosyl and pentofuranosyl sugars, nor are the roles of hexopyranosyl sugars in bioenergetics the same as their pentofuranosyl counterparts.

The chemical syntheses, radioiodination reactions, biological evaluations of the proposed metabolites, as well as investigations that led to the conclusion of the α anomeric configuration in the chemical structure of IAZA (**1A**), are the subject of this thesis and are included in Section 4.

2. Survey of Related Literature

2.1. Radiolabeled hexopyranosyl sugar analogs for metabolic brain and tumor imaging

2.1.1. 2-Deoxy-2-[^{18}F]fluoro-D-glucose (2-[^{18}F]FDG)

Of the positron emission tomography (PET) metabolic agents, 2-[^{18}F]FDG (8) is the most widely used in the metabolic studies of the brain and in the detection of tumors[11,12,16,17]. Unlike the heart, which uses several other metabolic substrates such as non-esterified (free) fatty acids (e.g. palmitate) and ketone bodies (e.g. aceto-acetate), the brain uses glucose (9) almost exclusively (99%) as its energy source. 2-[^{18}F]FDG as a glucose analog becomes a primary metabolic marker of cerebral glucose utilization. This cerebral glucose metabolism indicates average cerebral metabolic rate for the entire brain and hence provides only a measure of global cerebral function. In order to detect and identify any particular task or malfunction of the brain, small and subtle changes in the local cerebral metabolic rate of glucose (LCMRGlc)[18] have to be detected and measured by PET. This LCMRGlc has been successfully measured in humans[18]. For example, up to a twofold increase in LCMRGlc has been observed in the visual cortex from the nonstimulated state (eyes-closed control group) to complex visual stimulation by a visual scene in a park[18]. Indeed, mapping of functional activity caused by sensory stimuli (visual, auditory, tactile) in the brain with 2-[^{18}F]FDG has been demonstrated[19].

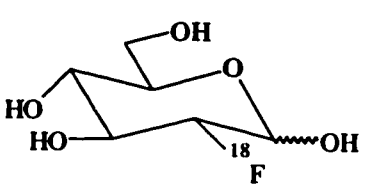

8

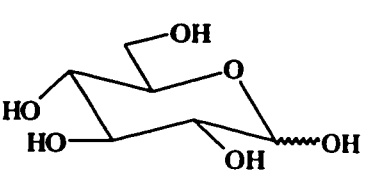

9

Numerous cerebral disorders have been detected by 2-[^{18}F]FDG. Regional cerebral glucose hypometabolism (decreased 2-[^{18}F]FDG uptake) was reported to occur in the majority of partial epilepsy patients[20] and in patients with Alzheimer's disease[21,22]. 2-[^{18}F]FDG has further been used to probe other clinical disorders such as trauma[23,24], stroke[25,26], Parkinson's disease[27], dementia[28,29], and sleep deprivation[30,31]. Its high accumulation in sites of cerebral inflammation has recently been demonstrated[32,33].

2-[^{18}F]FDG also plays a very important role in the detection of brain tumors. It is used for brain tumor grading[34,35], detection of recurrent or residual tumors[36,37], and prediction of clinical outcome[38,39]. Additionally, 2-[^{18}F]FDG has been used to evaluate cerebral lesions in AIDS patients[40] and to differentiate recurrent tumors from radiation necrosis in patients receiving radiotherapy[41].

Since 2-[^{18}F]FDG has an immense value as a probe for detecting abnormalities in tissues that have a high glycolytic demand (such as heart, brain, and tumors), it is not surprising that it is one of the most widely used PET radio-pharmaceuticals today. Indeed, the usefulness of 2-[^{18}F]FDG is based completely on the principle of metabolic trapping first exploited by Sols and Crane[42] in 1954. The use of 2-deoxy-D-glucose (2-DG, **10**) as a substrate for the enzyme hexokinase "isolates the hexokinase reaction" in that the hexose phosphate formed is metabolically trapped and does not enter into the subsequent metabolic steps of glycolysis. This important property led to the work of Sokoloff, Reivich *et al.*[43] in which they measured the rates of glucose consumption in the different structural and functional components of brain *in vivo* using [^{14}C]-**10** and quantitative autoradiography. This in turn stimulated the development of labeled

analogs of **10** which might allow measurement of regional brain glucose metabolism in humans using emission tomography. A gamma or positron-emitting radionuclide that would not significantly change the biochemical properties of **10** is desired. The use of fluorine-18 as a radiolabel at C_2 was chosen on the following basis:

1. The hexokinase reaction has been demonstrated to be relatively insensitive to structural modifications at C_2 of glucose[44,45] (Table 3). 2-FDG is a good substrate for yeast hexokinase (K_m = 0.19 mM) when compared with glucose (K_m = 0.17mM). K_m, the Michaelis constant, is the substrate concentration at which the reaction rate is half of its maximal value, V_{max}. In this case, K_m is the concentration of substrate at which half the active sites of hexokinase are filled. 3-Deoxy-3-fluoro-D-glucose (3-FDG, **11**) and 4-deoxy-4-fluoro-D-glucose (4-FDG, **12**), on the other hand, are poor substrates with K_m values (~ 80 mM) much larger than that of glucose.

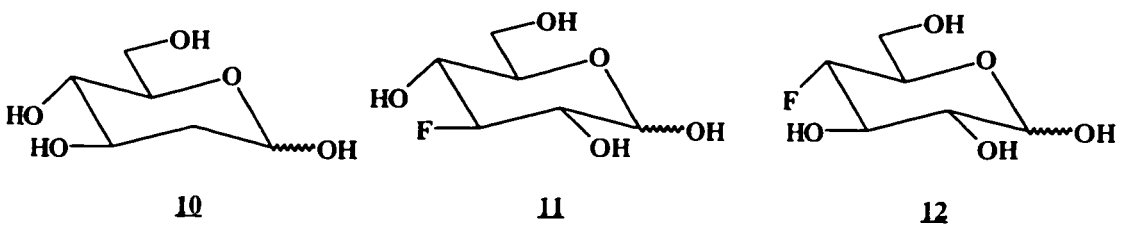

10 **11** **12**

Table 3. Comparisons of relative kinetic constants of glucose analogs with structural modifications at carbons 2, 3 and 4[45] and hexokinase.

Substrate	*K_m(mM)*	*Relative V_{max}*
D-Glucose (**9**)	0.17	1.00
2-DG (**10**)	0.59±0.11	0.85
2-FDG (**8**)	0.19±0.03	0.83
3-FDG (**11**)	70±30	0.10
4-FDG (**12**)	84±30	0.10

2. 2-FDG is known to be a suitable substrate for hexokinase[44,45] (Scheme 2) but 2-deoxy-2-fluoro-D-glucose-6-phosphate (2-FDG-6-P), the only observed product of this hexokinase reaction[46], is a relatively poor substrate for subsequent metabolic steps[47]. Consequently, this species is trapped in tissues with high hexokinase activity and released at a very slow rate, permitting determination of regional glucose metabolism which would be difficult if metabolism were to proceed.

Scheme 2. Metabolic trapping of 2-[^{18}F]FDG in tissues.

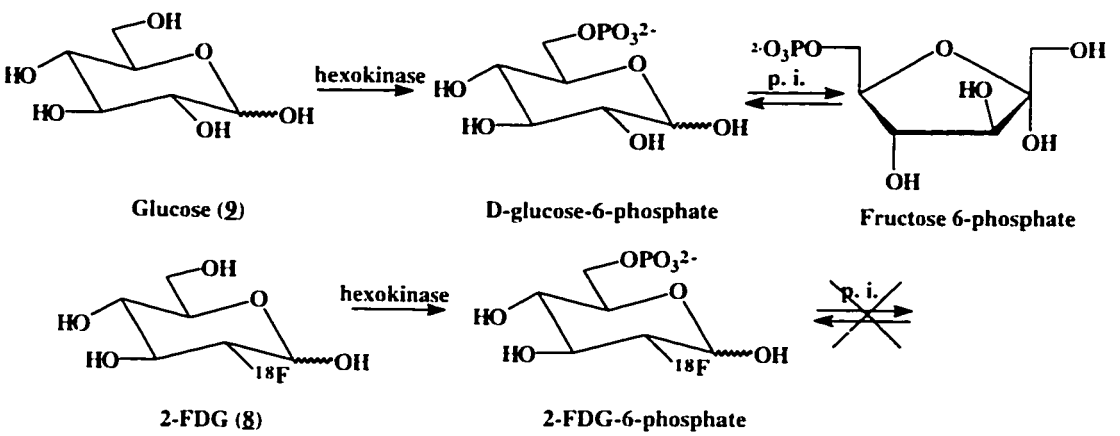

p. i. = phosphoglucose isomerase

3. The fluorine atom is similar in size as measured by its van der Waal radius (1.35 Å) compared to the hydrogen atom (1.20 Å). The bond length of a carbon-fluorine bond (1.39 Å) is comparable to that of a carbon-hydrogen bond (1.09 Å). The fluorine atom thus mimics a hydrogen atom in 2-DG (**10**) with respect to steric requirements at the enzyme-receptor site[48].

4. Since the strong carbon-fluorine bond (485 kJ/mol) exceeds that of a carbon-hydrogen bond (410 kJ/mol), substitution with fluorine increases the oxidative and

thermal stability of the molecule. This usually results in both chemical and biological stability of the fluorine-18 label.

5. The replacement of hydrogen with fluorine usually increases the lipophilicity of the molecule. The presence of the highly electronegative fluorine atom is believed to decrease the hydrogen bonding abilities of other hydroxyl groups on glucose, resulting in faster rates of passive transport and subsequent absorption.

6. The characteristics of fluorine-18 for PET, radiopharmaceutical synthesis and for patient dosimetry are nearly ideal. Fluorine-18, like carbon-11, decays by positron (β^+) emission (97%) and emits two 511-keV photons 180^0 from each other as a consequence of annihilation of the positron with an electron. These decay characteristics are well suited for the modern PET camera. Its production can be achieved by either the $^{20}Ne(d, \alpha)^{18}F$ or $^{18}O(p, n)^{18}F$ nuclear reaction with simple and low-energy cyclotrons.

2-[^{18}F]FDG is therefore an extremely useful probe for measuring regional glucose utilization which in turn reflects energy metabolism and functional activities. Obviously, 2-[^{18}F]FDG would not be too useful as a quantitative marker if all tissues, including normal and abnormal, were to have same glycolytic activities. Indeed, the value of metabolic markers in general, and 2-[^{18}F]FDG in particular, lies in their abilities to differentiate tissues with *different* rates of glycolysis. For example, regional glucose hypometabolism is reported to occur in the temporal lobe of the brain in most partial epilepsy patients[20], and in the temporo-parietal areas in patients with Alzheimer's disease[21,22].

In the case of tumors, the important distinction lies in the *increased* level of glycolytic activities in tumor tissues compared to normal tissues. This glucose hyper-metabolism was first demonstrated more than fifty years ago[50]. Studies using Morris hepatoma cell lines, which are slow-growing and considered to be well-differentiated, revealed that the degree of increased glycolysis and the activity of key enzymes in glycolysis, such as hexokinase, correlated with the rate of tumor growth[51]. However, it has yet to be determined whether a high glycolytic rate is essential for cancer cells or is a consequence of other metabolic processes[52]. Nevertheless, 2-[^{18}F]FDG has been successful in diagnosing various tumors based on this tumor metabolic imaging principle.

2.1.2. Other PET sugar analogs

Carbon-11-Labeled sugar analogs

A number of ^{11}C-labeled glucose analogs have been synthesized for studying cerebral and myocardial energy metabolism. [^{11}C]D-Glucose[53] was initially un-successful in measuring the *in vivo* cerebral and myocardial energy metabolism because of its low extraction from the coronary circulation and its widespread distribution to other organs[54-56]. Since glucose transport is a passive and carrier-facilitated process, selective accumulation within a tissue against a concentration gradient does not occur; there is only an equilibrium between intracellular and extracellular glucose concentrations[57]. Furthermore, glucose rapidly enters numerous metabolic pathways and the tendency toward equilibrium would continuously affect net glucose influx, resulting in redistribution of its ^{11}C-labeled metabolites and, ultimately, the loss of radioactivity from the organ. For this reason, a glucose analog

suitable for imaging has to be constructed in such a way that it would be transported and phosphorylated as a normal glucose molecule but would then not undergo a metabolic transformation unique to the analog. In other words, it is necessary to design a glucose analog that is intracellularly trapped *longer* than a glucose molecule in order to effect imaging.

However, Hara *et al.*[58] have reported preliminary studies of using the mixture of 1-[^{11}C]D-glucose and 1-[^{11}C]D-mannose as specific tumor markers to visualize tumors *in vivo*. Furthermore, recent studies have indicated that 1-[^{11}C]D-glucose can be used in conjunction with mathematical modeling to determine accurate measurements of blood-to-brain glucose transport and cerebral glucose metabolism *in vivo* even under conditions of severe hypoglycemia[59]. This mathematical model includes another rate constant which accounts for regional egress of all ^{11}C-labeled metabolites. Feasibility of imaging pentose cycle glucose metabolism in human gliomas with PET in rat brain tumor models have also been explored using this radiolabeled glucose and the results have been promising[60].

2-Deoxy-D-glucose (2-DG, **10**) was the forerunner of 2-FDG and has been used in the study of various aspects of carbohydrate metabolism for over two decades. Its ^{11}C-labeled analog 1-[^{11}C]-**10** has been synthesized and used to measure regional glucose metabolic rate[61-64]. Even though this tracer is a natural analog of glucose, it is not as widely used as 2-[^{18}F]FDG in metabolic studies of the brain. This is possibly due to the very short half life of carbon-11 (20 min), making routine clinical studies impractical.

Another ^{11}C-labeled glucose analog, 3-[^{11}C]-methyl-D-glucose[65,66] (CMG, **13**) has been used to assess regional glucose transport across the blood-brain barrier (BBB)[67,68]. CMG has a high affinity for the glucose transporter and it showed rapid brain and heart uptake[65] in mice. It is therefore a valuable agent for the study of ischemic brain disease[69], although it is not a substrate for hexokinase and is not metabolically tapped inside the cell.

1-[^{11}C]-D-Glucosamine (**14**), a structural unit of many biologically interesting macromolecules (see page 18), has also been biologically evaluated. Its biodistribution studies in rats showed that the intact BBB substantially lowered its availability to the brain[70]. No further evaluations of this ^{11}C-labeled amino sugar have been reported.

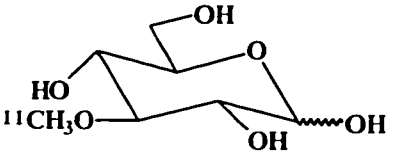

13

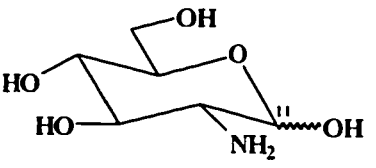

14

These four glucose analogs are all radiolabeled with the physiological radionuclide carbon-11. Therefore, their biological behavior is expected to be virtually identical to their unlabeled counterparts. Despite this advantage, they showed different mechanisms of uptakes and only 1-[^{11}C]-2-DG (1-[^{11}C]-**10**) was shown to be metabolically trapped analogous to 2-[^{18}F]FDG. The short half-life of carbon-11 makes shipment from a remote site of preparation to a hospital or nuclear medicine clinic impractical. These complicating factors with ^{11}C-labeled analogs have contributed to the widespread popularity of the more versatile and longer-lived 2-[^{18}F]FDG.

Fluorine-18-labeled glucose analogs

3-Deoxy-3-fluoro-D-glucose (3-FDG, **11**) is a substrate for hexokinase[45] despite its considerably larger K_m when compared to 2-FDG and glucose itself (Table 3). Animal biodistribution studies of 3-[^{18}F]-**11** in mice and dogs revealed that significant amounts of radioactivity were localized in brain and heart and were retained there longer than in other organs[71,72]. Tumor uptakes of 3-[^{18}F]-**11** in rats was also found to parallel those observed in 2-[^{18}F]FDG[73]. Comparative studies with 3-[^{18}F]-FDG and CMG (**13**) revealed that 3-[^{18}F]-**11** could be considered as a CMG analog for *in vivo* determination of local glucose perfusion and transport rates. *In vivo* kinetic studies using ^{19}F NMR have also been performed with this glucose analog in diabetic rat brains[74]. However, no studies with 3-[^{18}F]-**11** in humans have been reported.

4-Deoxy-4-fluoro-D-glucose (4-FDG, **12**) was observed to behave similarly to **11** as a hexokinase substrate (Table 3) and thus it is expected to be carried into cells by glucose transporters. The presence of hydrogen bonding between the fluorine atom at C_4 in the D-*gluco* configuration and the glucose transporter provides a structural requirement for transport[75]. 4-[^{18}F]FDG has been successfully synthesized[76] but no biological data have been reported to date.

D-Glucosamine and its derivatives are structural components of many biologically important molecules such as membrane glycoproteins and mucopolysaccharide[77]. It was reported that the invasive VX-2 carcinoma (previously called V2 carcinoma) grown in rabbits contained larger amounts of hyaluronic acid than when grown in nude mice[78], where it is less aggressive. Hyaluronic acid is the most abundant mucopolysaccharide present in cell membrane and in the extracellular

ground substance of the connective tissues of vertebrates[79]. Since repeating units of hyaluronic acid is a disaccharide composed of D-glucuronic acid and *N*-acetyl-D-glucosamine linkages, the tumor uptake of *N*-[^{18}F]fluoroacetyl-D-glucosamine ([^{18}F]FAG, **15**), a structural analog of *N*-acetyl-D-glucosamine, was studied.

[^{18}F]FAG was first synthesized by the Japanese group at Tohoku University[80] and its incorporation into hyaluronic acid was shown by Winterbourne *et al* [81]. Fujiwara *et al.*[77] showed that there were high uptakes of **15** in tumor, liver and kidney but relatively low uptakes were observed in the brains of mice and rabbits. It could thus have a potential for detecting tumors in humans.

None of the three ^{18}F-labeled glucose analogs have been studied in humans. 3-[^{18}F]FDG has the most clinical potential among the three because of its promising animal biodistribution data. Although no biological data have yet been reported for 4-[^{18}F]FDG, its biological properties might be quite similar to those for 3-[^{18}F]FDG because of their comparable K_m values (Table 3). [^{18}F]FAG, on the other hand, has a very different mechanism of uptake (incorporation into hyaluronic acid). These literature findings show that 2-[^{18}F]FDG continues to be the preferred PET imaging agent.

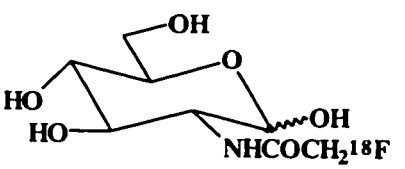

15

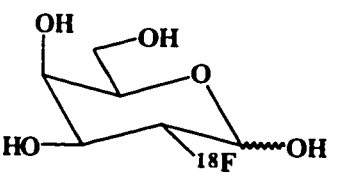

16

Other Fluorine-18 sugar analogs

2-Deoxy-2-[^{18}F]fluoro-D-galactose[82,83] (2-[^{18}F]FDGal, **16**), although not used in brain imaging, has proven to be of value in evaluating liver metabolism[84-86] and hepatomas[87]. D-galactose is actively transported into the cell and is phosphorylated to galactose-1-phosphate by galactokinase, and is finally used for glycoprotein synthesis or changed to glucose to be used as an energy source[87]. 2-[^{18}F]FDGal is localized competitively with D-galactose in the liver, and is phosphorylated by galactokinase. It is subsequently trapped after a second (uridylation) step of the galactose pathway (Scheme 3)[86].

Uptake of **16** directly reflects galactose metabolic activity in the tissue. Although this marker has high uptakes in well-differentiated, spontaneous hepatoma of C3H mice and well-differentiated Morris hepatoma, it has very low uptakes in poorly-differentiated hepatomas and metastatic liver tumors of other origins. 2-[^{18}F]-FDG is thus more useful than **16** in detecting hepatomas; in the latter sugar, uptakes in normal livers are even higher than those in well-differentiated hepatomas. However, 2-[^{18}F]-**16** could still be used to assess galactose metabolism in tumors.

Scheme 3. Metabolic trapping of 2-[^{18}F]FDGal in liver tissues[86].

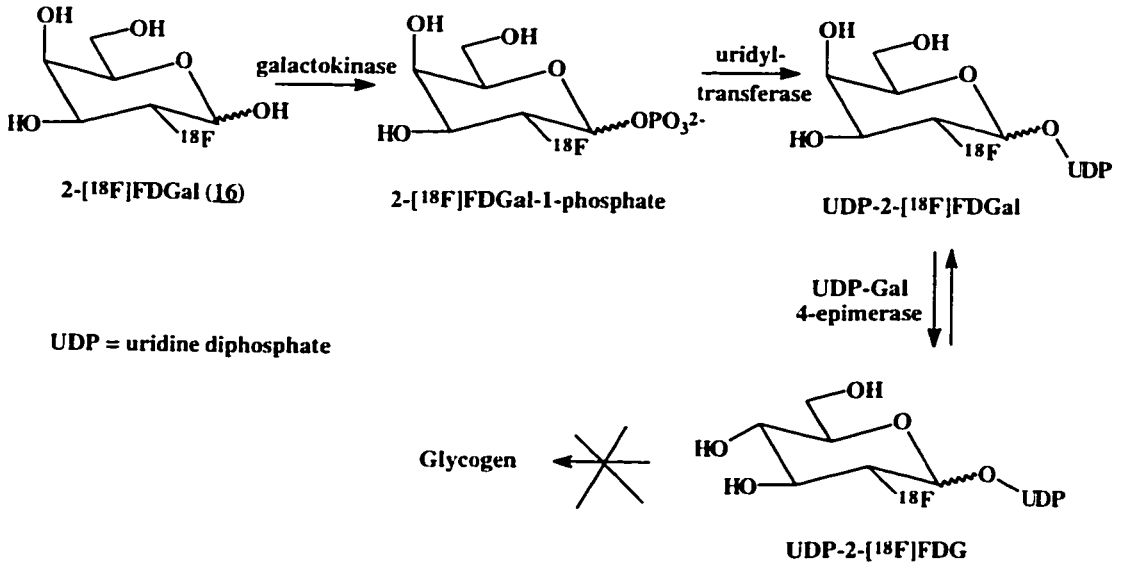

2-Deoxy-2-fluoro-D-mannose (2-FDM), a C_2 epimer of 2-FDG, has been extensively used for studies of glycoprotein biosynthesis and function[88] and its ^{18}F-labeled counterpart[89] (**17**) has been reported to be a useful radiopharmaceutical for cancer diagnosis in humans by PET[90]. Furthermore, 2-deoxy-2-[^{18}F]fluoro-β-mannosyl [^{18}F]fluoride (**18**), a glycosidase inhibitor, has been synthesized and observed to form a covalent glycosyl-enzyme intermediate *in vitro* which may allow glycosidase activity in the brain to be imaged by PET[91,92].

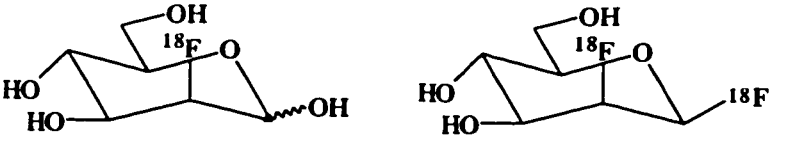

17 **18**

In a comparative study with 2-[^{18}F]FDGal (**16**), 2-deoxy-2-[^{18}F]fluoro-D-altrose (2-[^{18}F]FDA, **19**) and 2-deoxy-2-[^{18}F]fluoro-L-glucose (L-2-[^{18}F]FDG, **20**), biodistribution studies were performed[93]. 2-[^{18}F]FDA was found to be rapidly cleared from all organs, and 2-L-[^{18}F]FDG was also rapidly excreted via the kidney and

cleared moderately rapidly from other tissues. No accumulation in the liver, as was the case for 2-[^{18}F]FDGal, was reported for these two glucose analogs.

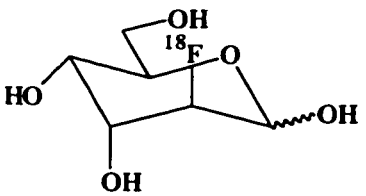

19

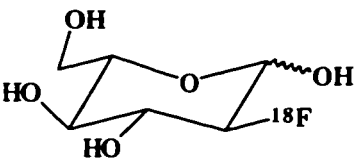

20

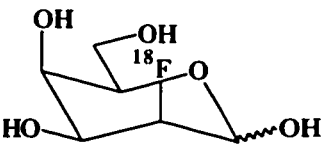

21

2-Deoxy-2-[^{18}F]fluoro-D-talose[94,95] (2-[^{18}F]FDT, **21**), another C_2 epimer of 2-[^{18}F]FDGal, has been shown to behave similarly as 2-[^{18}F]FDGal. 2-[^{18}F]FDT enters the D-galactose metabolic pathway and undergoes a metabolic trapping via 2-[^{18}F]FDT-1-phosphate which is phosphorylated by galactokinase in the liver and tumor. Therefore, 2-[^{18}F]FDT is likely to be a promising radiopharmaceutical for the measurement of galactokinase activity by PET in the future.

D-Fructose, a physiological ketohexose, behaves analogously to D-glucose for energy production in humans[96]. Although D-fructose is known to be phosphorylated to fructose-6-phosphate by hexokinase, its affinity for this enzyme is significantly lower than that for D-glucose[97]. It is primarily converted to D-fructose-1-phosphate by fructokinase in human tissues such as the liver, gut and kidneys. Therefore, the metabolism of D-fructose by fructokinase could be blocked by introducing a fluorine atom at C_1 of D-fructose and might be subjected to metabolic trapping analogously to 2-[^{18}F]FDG. 1-Deoxy-1-[^{18}F]fluoro-D-fructose (**22**) has been synthesized and its biodistribution studies in rats indicated that there was initial high uptake and subsequent rapid washout of radioactivity in kidney, liver, and small intestine,

suggesting no metabolic trapping in these organs[98]. The uptake in brain was also low, probably due to the low BBB permeability of this tracer.

Among these six ^{18}F-labeled sugar analogs, 2-[^{18}F]FDGal appears to be the most promising in its role in assessing liver metabolism. 2-[^{18}F]FDT is also found to be another interesting alternative to 2-[^{18}F]FDGal. The remaining ^{18}F-labeled sugar analogs have little or no metabolic trapping in the brain, liver or tumor.

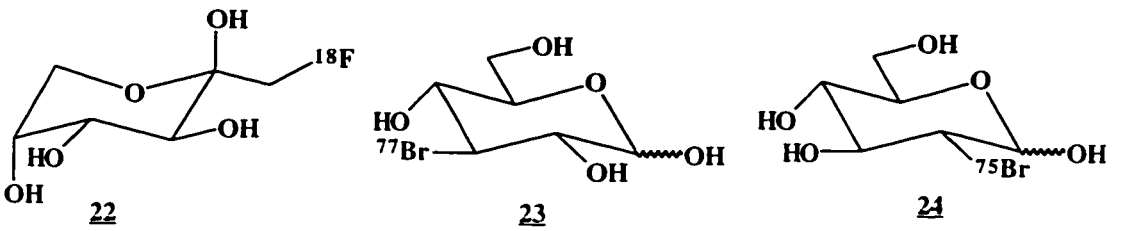

Bromine-labeled glucose analogs

A number of glucose analogs labeled with bromine-75 ($t_{1/2}$ = 1.6 h) have been evaluated as potential PET tracers for glucose utilization in heart and brain by Kloster *et al* [99-101]. 3-Deoxy-3-[^{77}Br]bromo-D-glucose (3-[^{77}Br]BDG, **23**) was investigated based on the results of 3-FDG described earlier[71,72]. Although **23** is a substrate for hexokinase and is metabolically stable, it is not suitable for *in vivo* studies because the brain uptake was far too low and the heart-to-blood and lung-to-blood ratios were considerably less than unity. These factors make myocardial studies impossible[101].

The Stöcklin group was not able to synthesize 2-deoxy-2-[^{75}Br]bromo-D-glucose (2-[^{75}Br]BDG, **24**)[100]. However, Zhou *et al.*[102,103] succeeded in preparing **24** and showed its biological data was significantly inferior to that of 2-FDG. Consequently, studies with **24** were not further pursued.

The Stöcklin group turned their attention to the intermediates in the synthesis of 2-BDG from 3,4,6-tri-*O*-acetyl-D-glucal (**25**)[101]. Two bromo intermediates, methyl 2-deoxy-2-[^{75}Br]bromo-β-D-glucopyranoside ([^{75}Br]MBDG, **26**) and methyl 3,4,6-tri-*O*-acetyl-2-deoxy-2-[^{75}Br]bromo-β-D-glucopyranoside ([^{75}Br]MTBG, **27**) were prepared and evaluated as potential tracers for glucose transport rate. Biodistribution studies in mice showed that **26** behaved as a glucose transport tracer: after rapidly entering most tissues, it was washed out parallel to its elimination from blood. Brain radioactivity was, however, low.

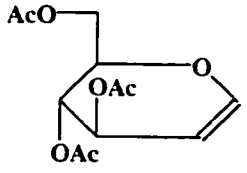

25

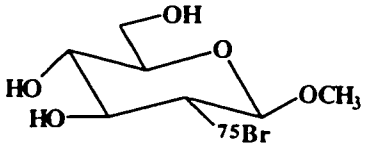

26

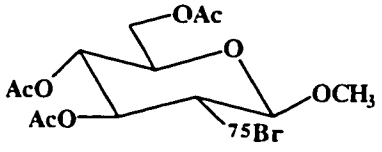

27

The tri-*O*-acetyl derivative **27**, on the other hand, reached high brain radioactivity concentrations and the brain uptake was larger than that of any other compound studied by the Stöcklin group. The mechanism by which **27** entered the brain is still unknown. If **27** is a substrate for the glucose transporter at the BBB, it may be a useful longer-lived alternative to 3-[^{11}C]methyl-D-glucose (**13**) as a PET tracer for regional glucose transport rate.

Although bromine-75 is more easily handled than fluorine-18, the introduction of a bromine atom inevitably changes the electronic and steric properties of the molecule. This change would likely have a pronounced effect in its interactions with enzymes such as hexokinase. Not surprisingly, with the exception of [^{75}Br]MTBG (**27**) which had unusually high brain uptakes of radioactivity in mice, the remaining

three deoxybromo sugars had little or no biological significance. Furthermore, the weaker carbon-bromine bond (276 kJ/mol) relative to the carbon-fluorine bond makes radiobrominated compounds more susceptible to *in vivo* debromination. The resulting radiobromide ion has a long plasma clearance half-life and causes high background radioactivity. These disadvantages make radiobrominated sugar analogs less attractive than 2-[^{18}F]FDG.

2.1.3. SPECT hexopyranosyl sugar analogs

2.1.3.1. Rationale for investigating potential SPECT sugar analogs

Although PET sugar analogs such as 2-[^{18}F]FDG have been extremely useful in studying regional glucose metabolism in humans, the positron-emitting radionuclides ^{11}C and ^{18}F pose some serious practical problems. In general, radionuclides used in nuclear medicine are artificial, which means that they are produced in a cyclotron or a reactor. The types of radionuclides that can be produced in a cyclotron or a reactor depends on 1) the irradiating particle (protons, neutrons, deuterons, α particles or ^{3}He particles), its 2) energy of the irradiating particle (from a few kiloelectron volts (keV) to several billion electron volts (BeV)) and 3) the target nuclei (e.g. ^{20}Ne for the production of ^{18}F). Since cyclotrons and reactors are usually expensive, they are available only in a limited number of institutions. A number of medically important short-lived PET radionuclides (^{11}C, ^{13}N, ^{15}O, ^{18}F) can be generated only in the institutions that are close to cyclotron facilities and they cannot be supplied to remote (< 4-5 h shipping time for ^{18}F) hospitals or nuclear medicine facilities because their activities decay too rapidly. For this reason, hospitals and

nuclear medicine facilities must be geographically located in proximity to a cyclotron in order to effect practical imaging studies.

Single photon emission computed tomography (SPECT) agents have the advantage of longer half-lives (e.g. ^{123}I) or generator production (e.g. ^{99m}Tc from ^{99}Mo generator). Unlike PET agents, SPECT agents are single-photon emitters where the nature of the emitted radiation is very different. These photons are individually emitted and thus spatially and temporally uncorrelated. Such γ-rays that are associated with isomeric transitions and electron capture form the basis of SPECT[95]. Among the single-photon emitting radionuclides, iodine-123 has gained considerable importance in nuclear medicine because of its useful decay characteristics. It decays by electron capture with a half-life of 13.2 hours and γ-ray emission of 159 keV (86%). The two most common nuclear reactions for the production of iodine-123 are $^{124}Te(p, 2n)^{123}I$ and $^{127}I(p, 5n)^{123}Xe \rightarrow {}^{123}I$. Although a cyclotron is still necessary for the production of iodine-123, its relatively long half-life of 13.2 hours makes it a very attractive alternative to fluorine-18 (110 min). Iodine-123 can thus be reasonably transported from one place to another with sufficient activity remaining for radiochemical synthesis, purification, formulation and subsequent imaging studies.

Faced with the higher costs of PET instrumentation and facilities, researchers have turned to investigate glucose analogs which can be labeled with iodine-123 or iodine-131, two radionuclides readily useable by all nuclear medicine facilities.

2.1.3.2. [^{123,131}I]-labeled glucose and other sugar analogs

3-Deoxy-3-[^{123}I]iodo-D-glucose (3-[^{123}I]IDG, **28**) has been prepared by Kloster *et al.*[99-101] using the same method used for 3-[^{77}Br]BDG (**23**). In a patent application[104] it is stated that **28** was identical to glucose in absorption, distribution and metabolism in the body of mice with the exception of the brain. In their own study, however, the Stöcklin group found that **28** had much lower and rapidly falling concentrations of radioactivity in brain while the decrease in radioactivity was slower for the heart when compared with **23**. The metabolic stability of the ^{123}I-label in **28** was good and less than 0.7% of the administered dose was found in the thyroid at all time intervals after i.v. administration. However, it could not be used for *in vivo* studies because of its low brain-to-blood and heart-to-blood ratios.

Recently, Abbadi *et al.* have successfully synthesized 4-deoxy-4-iodo-D-glucose (4-IDG) and its ^{125}I-labeled counterpart[105]. No biological data have been reported to date.

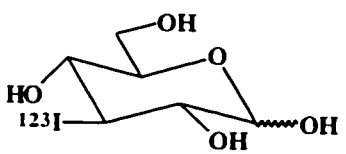

28

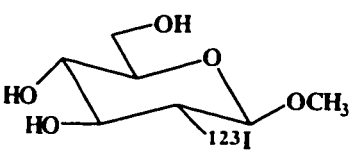

29

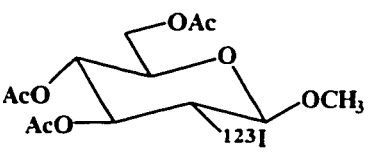

30

The Stöcklin group also prepared the β-methyl glucoside ([^{123}I]MIDG, **29**) and the triacetyl β-methyl glucoside ([^{123}I]MTIG **30**) bearing an ^{123}I-label at C_2, analogous to the bromo counterparts. Biodistribution data for **29** in mice paralleled those for [^{75}Br]MBDG (**26**) in which brain radioactivity was low. However, metabolic stability

of **29** was good: less than 0.5% of the administered dose was observed in the thyroid at any time.

The tri-*O*-acetyl derivative **30** showed high brain uptake in mice but this uptake was lower than that of its bromo counterpart [^{75}Br]MTBG (**27**). The uptake was fairly constant for the first 3-5 min after i.v. injection. This behavior is not expected for a glucose transporter tracer but it resembles that of a blood flow tracer[101]. Heart-to-blood and lung-to-blood ratios were less than unity and thus **27** is not likely to be used in myocardial studies.

Although the Stöcklin group was not able to synthesize 2-deoxy-2-iodo-D-glucose (2-[^{131}I]IDG, **31**) in agreement with the Wolf group[61], Honda and Takiura[106] reported the synthesis of unlabeled **31**. It was stable for at least 2 days in triethylamine solution but it rapidly deiodinated on neutralization and dilution of the solution. The stability of **31** could have a strong dependence on the pH and the ionic strength of the solution. Decomposition was thought to occur through an α-iodo aldehyde in the open chain form of the sugar. Due to its *in vivo* instability, further biological studies have not been pursued.

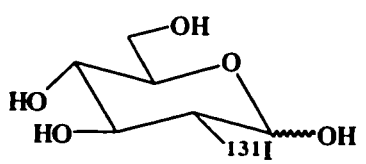

31

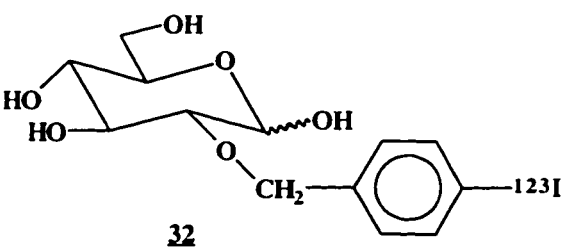

32

In an attempt to improve the stability of radioiodinated glucose analogs and derivatives, 2-deoxy-2-*O*-(*p*-[^{123}I]iodobenzyl)-D-glucose (4-[^{123}I]IBG, **32**) and its *ortho*- and *meta*- isomers were synthesized and evaluated *in vivo* by Magata *et al.*[107]

and Lutz *et al* [108]. With an iodinated benzene ring, [^{123}I]IBG analogs have the required structural configuration to remain stable *in vitro* and *in vivo*. However, these compounds were found to be poor substrates for hexokinase, and their overall tissue uptakes were too low to be used as heart or brain imaging agents. Although tissue uptake differences among the isomers were observed (possibly due to iodine position and hence lipophilicity), they are still far inferior to 2-[^{18}F]FDG.

Radioiodinated glucosamine analogs

According to Maley and Hardy[109], various glucosamine derivatives have been reported as competitive inhibitors of hexokinase. Of these, the *N*-benzoyl glucosamine analog was considered the most promising candidate to be evaluated as a clinical agent. Magata *et al.*[110] reported the syntheses of *ortho*-, *meta*-, and *para*-2-deoxy-2-*N*-([^{125}I]-iodobenzoyl)-D-glucosamine ([^{125}I]BGA) derivatives and studied their interaction with hexokinase. Their studies concentrated mainly on the *m*- and *p*-[^{125}I]BGA (**33**, **34**) due to labeling difficulties with ^{125}I in the *o*-[^{125}I]BGA isomer (**35**). *m*-BGA (**33**) had little or no brain uptake but showed a more rapid clearance from the blood with higher systemic stability than its *para* isomer **34**. These observations suggested that it is highly possible to develop a clinically feasible ^{123}I-labeled radioligand on glucose that could monitor the quantitative changes and biodistribution of hexokinase.

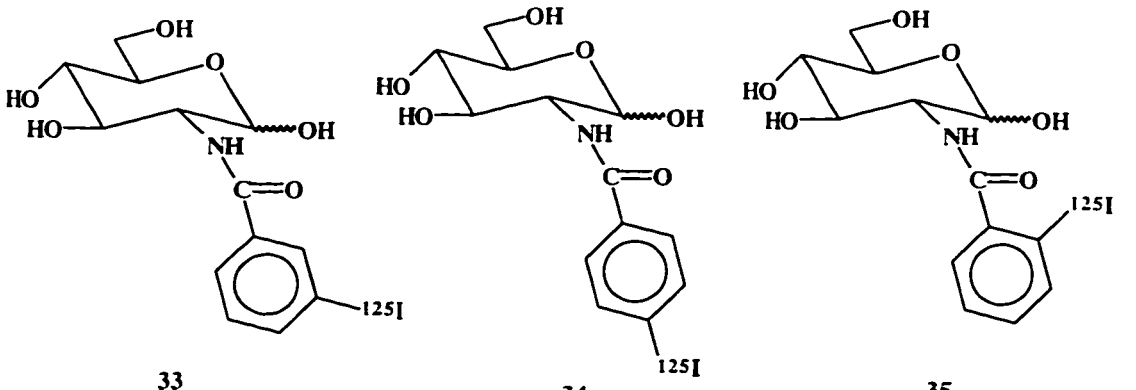

33 34 35

Encouraged by the results of **33**, Lutz *et al.*[111] further studied these [^{125}I]BGA analogs to determine the effect of iodine position and lipophilicity on tissue distribution. They were able to radiolabel all three [^{125}I]BGA isomers with good radiochemical yields for biodistribution studies in mice. Although **33** exhibited good blood clearance as reported by Magata *et al.*[110], **35** displayed the highest uptake in heart with the best blood clearance. A rabbit image recorded at 14 h post injection showed significant heart uptake of **35**. However, the mode of accumulation of **35** remains unclear.

Two esterified glucosamine analogs, 1,3,4,6-tetra-*O*-acetyl-*N*-(*m*-[^{125}I]-iodobenzoyl)glucosamine ([^{125}I]ABGA, **36A**) and 1,3,4,6-tetra-*O*-pivaloyl-*N*-(*m*-[^{125}I]-iodobenzoyl)glucosamine ([^{125}I]PBGA, **36B**), were also studied[112]. The permeability of **33** into the brain was enhanced by esterification. However, *in vitro* and *in vivo* studies showed that only **36A** released free **33** by brain esterases, while no changes were detected with **36B**. The tetra-*O*-acetyl derivative **36A** could thus have the potential to function as a prodrug of **33** and deliver it into the brain.

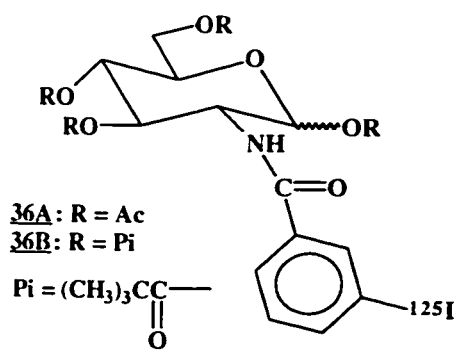

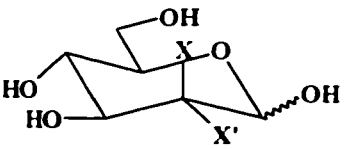

37A: X = I ; X' = F
37B: X = F; X' = I

Other radioiodinated sugar analogs

A pair of 2-deoxy-2-fluoro-2-iodo-D-hexoses have recently been prepared and evaluated as substrates for hexokinase from either yeast or bovine heart *in vitro*[113,114]. 2-Deoxy-2-fluoro-2-iodo-D-mannose (2-FIM, **37A**) and 2-deoxy-2-fluoro-2-iodo-D-glucose (2-FIG, **37B**) were shown to be stable in physiological saline for several days at room temperature. The ^{123}I analog of **37A** was also successfully prepared with a radiochemical yield of 63%. However, neither analog was found to be a substrate for hexokinase *in vitro*. The sugar analogs are hence not likely to be useful as ^{123}I-labeled analogs of 2-FDG for imaging of glucose metabolism but may be useful in studying glucose transport.

Adding to the list of radioiodinated sugar analogs, a D-allose derivative, (*E*)-3-*C*-[^{125}I]iodovinyl-D-allose (**38**) has been studied[115]. Although biodistribution studies of this ^{125}I-labeled analog in rats did not show any significant brain and heart uptake, the study demonstrated that an iodovinyl moiety could stabilize radioiodide on a sugar, minimizing *in vivo* deiodination. Flanagan *et al.*[116] have also reported the radiochemical synthesis and biodistribution studies with 6-[^{125}I]iodo-6-deoxy-D-galactose (**39**) in rats. Although designed as a glucose transporter marker, hepatic

accumulation was not observed and scintigrams of rats injected with [^{131}I]-39 offered little potential as a tissue imaging agent in rats.

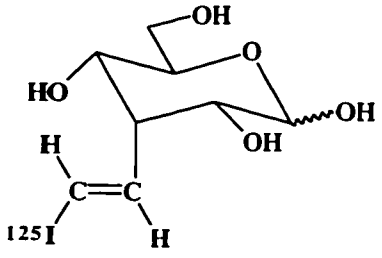

38

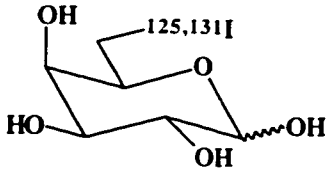

39

A series of ester derivatives of ^{123}I-labeled *n*-propyl-β-D-glucosides (40) were biologically evaluated in mice as metabolic tracers in SPECT medical imaging[117], but the levels of radioactivity observed in the organs of interest (heart or brain) remained low. Recently an ^{123}I-labeled D-maltose, 6'-deoxy-6'-[^{123}I]iodo-D-maltose (41) was studied *in vitro* and the preliminary results suggested that it interacts with the glucose transporter and thus has the potential as a useful SPECT radiotracer for glucose transporters[118]. No biological studies with radioiodinated pentofuranosyl sugar derivatives are reported to date.

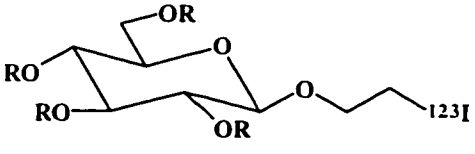

40

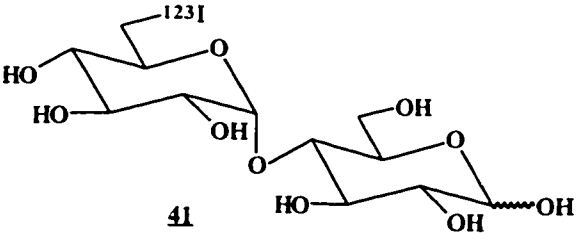

41

The direct introduction of the even larger iodine atom (than a bromine atom) on glucose causes severe steric effects because an iodine atom is much larger than a fluorine atom. The electronic properties of the molecule are also affected by this substitution because iodine is much less electronegative than fluorine. The relatively

weak carbon-iodine bond further increases the possibility of deiodination. Therefore, these studies with ^{123}I-labeled sugar analogs showed that the direct introduction of an iodine atom on glucose severely changes the chemical and biological properties of the sugar molecule. These iodinated glucose analogs did not show any significant brain or heart uptakes in mice. The relatively weak carbon-iodine bond makes the radio-iodine label chemically and biologically unstable. To counter this *in vivo* deiodination, the iodine atom was introduced in sites further from the glucose molecule as in the case of the [^{125}I]BGA derivatives. Improved biological data have indeed been obtained, but they were still far inferior to 2-[^{18}F]FDG.

2.1.3.3. Technetium-99m-labeled sugar analogs

To date no ^{99m}Tc-labeled sugar analogs for metabolic imaging have been reported. This is not surprising since the biggest problem with ^{99m}Tc is its chemistry. Technetium, which has atomic number 43 and belongs to Group VIIB in the periodic table, is a transition metal and has electronic configuration [Kr]$4d^5 5s^2$. The loss of a fixed number of electrons from the *s* suborbit or the *d* suborbit or hybridized orbitals results in any of the seven oxidation states (+7 to -1) for technetium. Unlike labeling with fluorine-18, labeling with metallic technetium requires chelation of this metal with carrier molecules (ligands). The resulting coordination complex profoundly changes the chemical and biological properties of the isolated ligand molecules and this complex becomes a compound that no longer behaves biologically like the original ligand molecule.

An excellent example to illustrate this point is the SPECT BBB agent ^{99m}Tc-glucoheptonate (^{99m}Tc-GH, 42). Glucoheptonate (gluceptate, 43)[119] is a salt of the

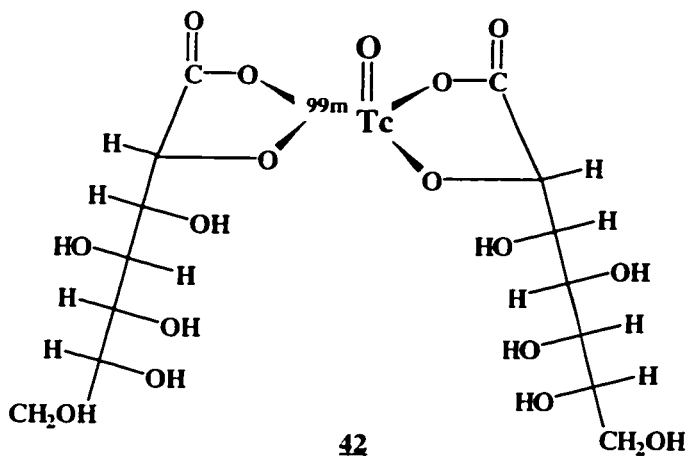

42

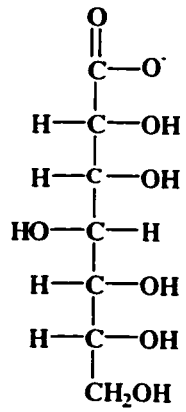

43

parent seven-carbon aldoheptonic acid which is derived from the seven-carbon heptose sugar. The proposed structure of this technetium-sugar coordination com-pound is a dimeric complex consisting of two glucoheptonate ligands. It can easily be prepared from a commercial kit containing sodium glucoheptonate, stannous chloride ($SnCl_2$) and pertechnetate (TcO_4^-). The reduction of TcO_4^- (+7 oxidation state) with the Sn(II)-glucoheptonate (from $SnCl_2$ and sodium glucoheptonate) complex followed by chelation with the excess glucoheptonate ligand results in the dimeric complex in which the oxidation state of technetium is +5. In contrast with sugars (e.g. 2-[^{18}F]FDG), ^{99m}Tc-GH is not a metabolic agent. It is a BBB agent which normally does not localize in the normal brain. It does so only in abnormal tissues because of the breakdown of the BBB caused by primary and metastatic tumors or injury. Therefore, any uptake of this BBB agent will result in a positive scan indicating brain abnormalities. ^{99m}Tc-GH is also widely used in renal imaging and its processing in the kidneys includes glomerular filtration, tubular secretion and cellular uptake which are

all very different from metabolic trapping. Therefore, ^{99m}Tc-GH provides an excellent example of how coordination with technetium fundamentally alters the chemical and biological properties of the sugar molecule, and the resulting new complex behaves in a totally different manner from the original sugar molecule.

2.2. Radiolabeled sugar-coupled derivatives (nucleosides) for hypoxic tumor imaging: metabolic trapping in hypoxic cells

2.2.1. Tumor oxygenation and changes in oxygen supply-demand relationships: causes and detection of tissue hypoxia

All mammalian tissues need a continuous supply of oxygen to meet their metabolic requirements. When oxygen supplies are diminished, systems are down-regulated (which result in negative feedback) to maintain viability. For very short periods (seconds), cellular demand for oxygen could exceed the oxygen supply, but an oxygen "debt" occurs which must be repaid[120]. If this oxygen debt becomes un-manageable, cellular integrity would be threatened. For this reason, normal tissues have many mechanisms to ensure adequate supplies of oxygen. For example, in the metabolic mechanism of blood flow regulation, a decrease in the oxygen supply-demand ratio of a tissue releases one or more vasodilator metabolites (such as CO_2 and/or nitric oxide) that dilate arterioles (the smallest branches of arteries with the highest blood flow resistance) and thereby enhances the oxygen supply[121].

Many diseases arise due to an impairment in this oxygen supply-demand relationship. Although hypoxia can be secondary to low amounts of inspired oxygen or other lung disorders, the most common cause (especially in tumors) is ischemia which is due to the lack of blood. In tumors, for instance, the increased cell mass produced during rapid cell proliferation requires additional oxygen supplies to keep the cells alive. To meet this demand tumors often release several growth factors (and/or cause surrounding normal tissue to release growth factors) that stimulate proliferation of vascular endothelium and penetration of new blood vessels into the tumor (tumor angiogenesis)[122]. These growth factors include angiogenin, TGF-α, and vascular

endothelial growth factor (VEGF). If this new vascular growth cannot keep pace with tumor cell proliferation, which is usually the case, tumor growth can produce zones of poorly perfused tissue with oxygen concentrations below physiological levels. Therefore, the increased supply of oxygen from this new vascular growth may still not be able to accommodate the increased demand for oxygen, inevitably causing a portion of the tumor mass to become hypoxic. Measurement of perfusion would no longer accurately characterize the entire tumor mass.

These hypoxic cells, although chronically lacking oxygen, are viable and are about three times more resistant to the damaging effects of ionizing radiation than are normally oxygenated cells[123]. The susceptibility of well-oxygenated cells to ionizing radiation is due to the ability of oxygen to "fix" radiation damage, a process known as the oxygen effect[124]. Molecular oxygen can act as a radical scavenger, reacting with both aqueous electrons and hydrogen radicals formed from water radiolysis, converting them to superoxide anions ($O_2^{-\bullet}$). Oxygen may also enhance radical damage in DNA by "fixing" target radicals in DNA. These target radicals in DNA, which can be directly formed by ionization due to ionizing radiation or indirectly produced by reactive and diffusible free radicals generated from radiolysis of water[125], are prime targets for oxygen. Reactions of oxygen with these target radicals in DNA could make the radicals longer-lived, or make the repair of DNA more difficult. A given dose of therapeutic radiation is thus more effective if delivered in the presence of oxygen.

Hypoxic cells are therefore resistant to therapeutic radiation and could lead to local recurrence of some human cancers following a course of radiotherapy[126]. Tumor

oxygenation status becomes an important predictor of tumor response to radiation and a non-invasive method, which could quantify tumor hypoxia and predict for radioresistance using modern available equipment, would greatly assist in the development and assessment of treatment strategies and in the evaluation of the progress of reoxygenation of hypoxic tissues.

A variety of tools and methods such as oxygen electrodes and flow cytometry techniques (which have been reviewed elsewhere[123,127]) have been explored to assess tissue hypoxia. Unfortunately, these methods are either invasive or impractical in the clinical setting. The concept of a suitable SPECT radiotracer would be a very attractive alternative to assess tumor oxygenation status indirectly and non-invasively. The next question to explore is what classes of compounds could reflect tumor oxygenation levels *in vivo*. Although oxygen-15, a PET radionuclide ($t_{1/2}$ = 123 s), can be detected non-invasively in living tissues[123], its broad application is severely restricted by its limited resolution of tumor volume and its extremely short half-life which requires on-site cyclotron facilities for its production. Compounds which behave differently in well-oxygenated (oxic) cells and in hypoxic cells could be potential chemical markers for cell oxygenation status and thus for hypoxic cells detection. Nitroimidazoles, especially N^1-substituted derivatives of 2-nitroimidazole (azomycin), are found to be such compounds.

The selective activity of 2-nitroimidazoles against hypoxic cells make them an extremely interesting group of agents. 2-Nitroimidazoles have been investigated as radiosensitizers of hypoxic cells[128], as cytotoxins of hypoxic cells[129,130], as chemo-sensitizers of hypoxic cells to a variety of anti-cancer agents[130], and as markers of

tumor and tissue oxygenation status[131]. The common underlying mechanism is the ability of 2-nitroimidazoles to preferentially undergo nitro-reduction to reactive intermediates (hydroxylamine and nitroso) in an hypoxic environment. These reductive intermediates are highly reactive and form covalent linkages with cellular macromolecules within hypoxic cells. This important property of 2-nitroimidazoles has been capitalized by Chapman *et al.* who showed that [^{14}C]misonidazole ([^{14}C]-MISO) is bound selectively to metabolizing hypoxic cells in both single and multicellular systems and might be marking for the first time at a histological level those cells which are hypoxic and resistant to radiation[132]. These promising experimental data could be extended into clinical applications by labeling an appropriate hypoxic cell radiosensitizer with a suitable γ-emitting radionuclide (e.g. ^{123}I). The resulting hypoxic cell chemical marker could be used in nuclear medicine for a SPECT assessment of the extent and location of hypoxia within tumors in cancer patients. Such a non-invasive procedure would provide valuable information on the role of tumor oxygenation at initial diagnosis, tumor oxygenation after therapy, and tumor reoxygenation during treatment on tumor response and cure[123].

2.2.2 Mechanisms of hypoxic tissue radiosensitization by nitroimidazoles

Nitroimidazoles undergo a preliminary, reversible intracellular reduction step in all cells while in the absence of oxygen, they can be further reduced to more reactive intermediates that bind to cellular components as shown in Scheme 4[133].

Scheme 4. Mechanism of action of nitroimidazoles[133].

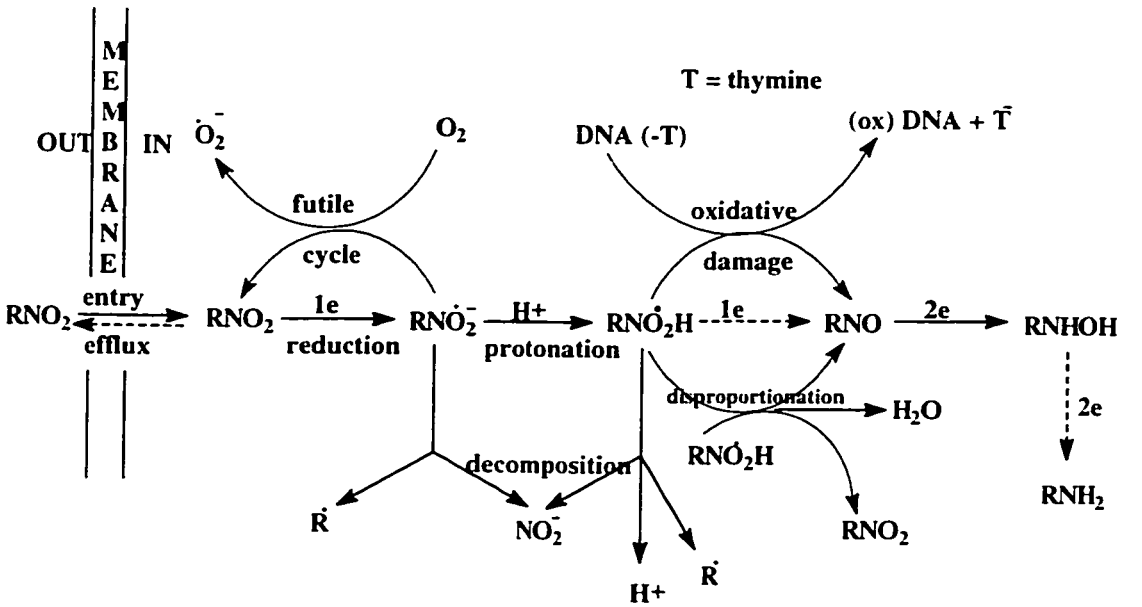

Nitroimidazole compounds typically enter cells by passive diffusion with the ability to cross cell membranes primarily determined by lipophilicity of the compounds. Obviously, to exert their radiosensitizing effect, nitroimidazoles must be transported to the site of hypoxic cells and preferentially accumulated there. For nitroimidazoles it is found that lipophilicity (as measured by the partition coefficient *P*) plays a significant role in determining the relative nitroimidazole concentration in tumors[134]. However, the balance between lipophilicity and hydrophilicity is essential. As clinical radiosensitizers, nitroimidazoles should possess high water solubility because high doses are usually required to rapidly achieve peak drug concentrations in hypoxic cells. Neurotoxicity to the brain can also be minimized by the BBB. As hypoxic cell markers, their partition coefficients should be high enough to allow passive diffusion to both well-perfused and poorly-perfused tissues. However, they should also be relatively hydrophilic to facilitate renal and urinary excretion of the

radiolabeled marker. This delicate balance of lipophilicity and hydrophilicity is best achieved if the octanol-water partition coefficient is in the range of 0.1-10[134], a range that seems to apply to both radiosensitizers and diagnostic radiolabeled hypoxic cell markers.

Once nitroimidazoles enter the cell, they undergo a one-electron reduction step to the nitro radical anion, a reaction that is reversible in the presence of oxygen. Molecular oxygen, with its one-electron reduction potential (E^1_7, measured at pH 7) of -155 mV, remains the best known biological electron acceptor. It will readily reverse the initial reduction and reform the original nitroimidazoles with the concomitant production of the superoxide anion ($^{\bullet}O_2^-$). This process is known as "futile cycling"[135] and is dependent on both the intracellular oxygen levels and the one-electron reduction potential (electron affinity) of the nitroimidazoles[136]. At lower oxygen levels nitroimidazoles with higher (more positive) reduction potentials are more resistant to futile cycling than those with lower (more negative) reduction potentials[136]. For example, metronidazole, a 5-nitroimidazole derivative (E^1_7 = -486 mV), undergoes futile cycling at a lower oxygen concentration than that required for misonidazole, a 2-nitroimidazole derivative (E^1_7 = -389 mV)[136]. In general, the higher the reduction potential of a compound, the better its ability to accept electrons from the cytochrome system. This explains why 2-nitroimidzoles are much better than 5-nitroimidazoles in their radiosensitizing effectiveness in low oxygen environments.

In summary, the rate of oxidation (futile cycling) of nitroimidazole anion radicals is dependent on the intracellular oxygen levels and thus the initial one-electron reduction step is susceptible to oxygen. Further reductions occur in those tissues with

low oxygen tension because reoxidation of the original nitroimidazoles is slowed, permitting additional reductive reactions to take place. The formation of these reductive products, which are highly reactive, bind with cellular macromolecules and undergo selective metabolic trapping in hypoxic cells.

2.2.3. Nature of the reductive adducts

The exact nature and reactivity of these reductive adducts produced following the intracellular uptake of nitroimidazoles remain elusive. Reduction of nitroheterocyclic compounds in general, and nitroimidazoles in particular, proceeds stepwise and involves the formation of three reduction species, the nitroso, hydroxylamine and amine derivatives corresponding to two, four and six electron reductions, respectively[137]. One or more of these intermediates have been shown to bind with various cellular constituents predominately in hypoxic cells, including DNA, RNA, protein and non-protein sulfhydryl compounds[138,139]. Among these three reduction species, the hydroxylamine appears to be the most likely candidate because it is chemically more reactive than the amine. The nitroso derivative is very electron-affinic and in most reducing situations it will be rapidly reduced to the hydroxylamine[140]. The hydroxylamine derivative, as shown in Scheme 5, is capable of undergoing the following chemical reactions.

Oxidation. Aqueous solutions of 2-hydroxylaminoimidazoles are oxidized in air under neutral conditions to form the azoxy derivative as shown in Scheme 6. The azoxy derivative is believed to be formed from the oxidation of the hydroxylamine to the nitroso derivative followed by a condensation of nitroso with hydroxylamine. The

concomitant formation of H_2O_2 in the presence of oxygen may play a role in biological damages since H_2O_2 is an excellent source of hydroxyl radicals.

Scheme 5. Possible biologically important reactions of 2-hydroxylaminoimidazoles[140].

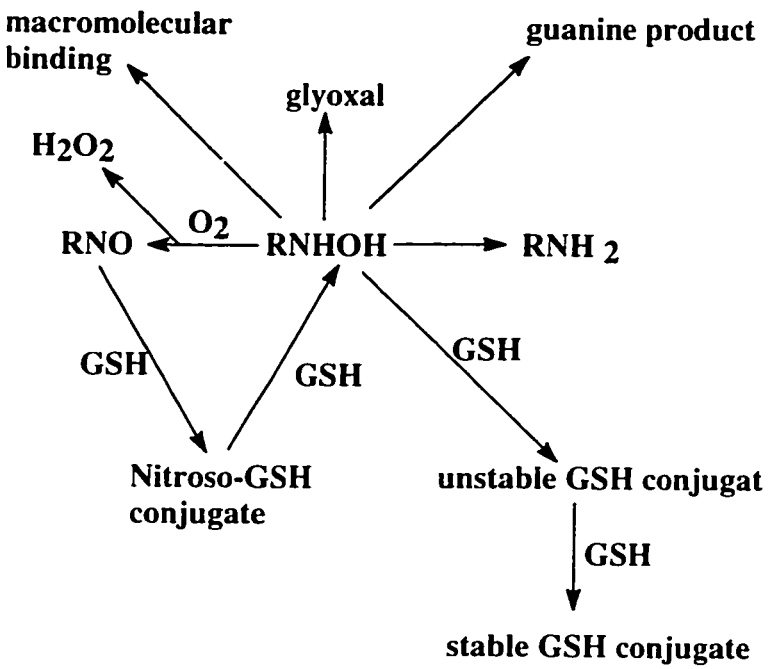

Scheme 6. Postulated pathway for the formation and subsequent reduction of the bimolecular, azoxy, azo and hydrazo derivatives[137].

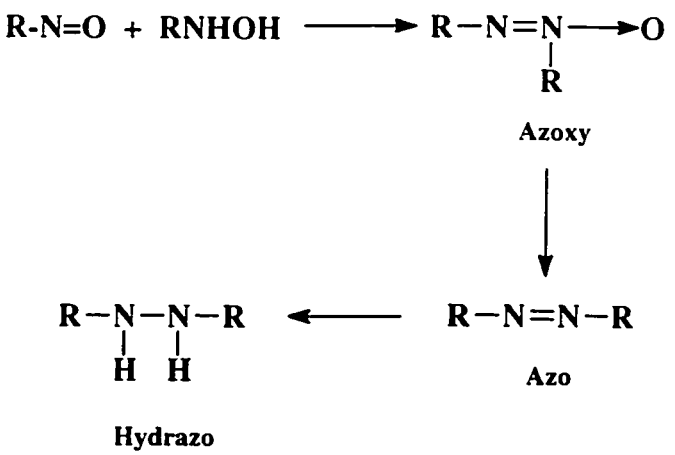

Scheme 7. Reactions of 2-hydroxylaminoimidazoles in aqueous solutions under hypoxic conditions[137,140,141].

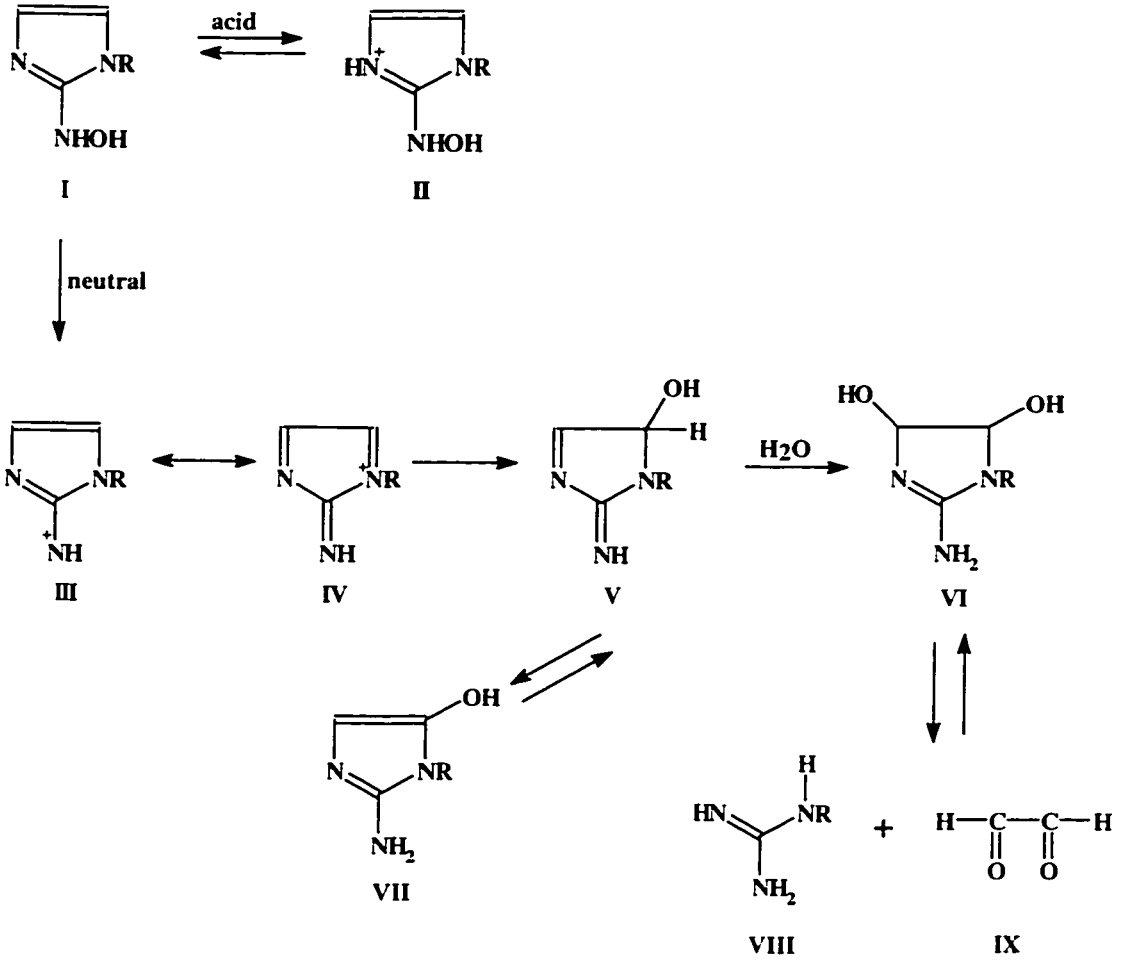

Reactions in aqueous solutions. Scheme 7 shows the postulated reactions for 2-hydroxylaminoimidazoles in aqueous solutions under hypoxic conditions. At low pH the imidazole nitrogen is protonated (II) which prevents molecular rearrangement. However, at neutral pH, the formation of a stabilized nitrenium ion (III, IV) allows nucleophilic attack on the imidazole ring, resulting in the formation of a Bamberger type rearrangement (V, VII) which on adding water yields the dihydroxy derivative (VI)[140]. This dihydroxy derivative may in turn be fragmented into glyoxal (IX) and a guanidine derivative (VIII). These reactions are highly pH dependent and at neutral

pH the lifetime of the 2-hydroxylaminoimidazole may be minutes or less and may also vary somewhat with the nature of N_1 substitution[140,141].

Scheme 8. Reactions of 2-hydroxylaminoimidazoles with glutathione[137,142,143].

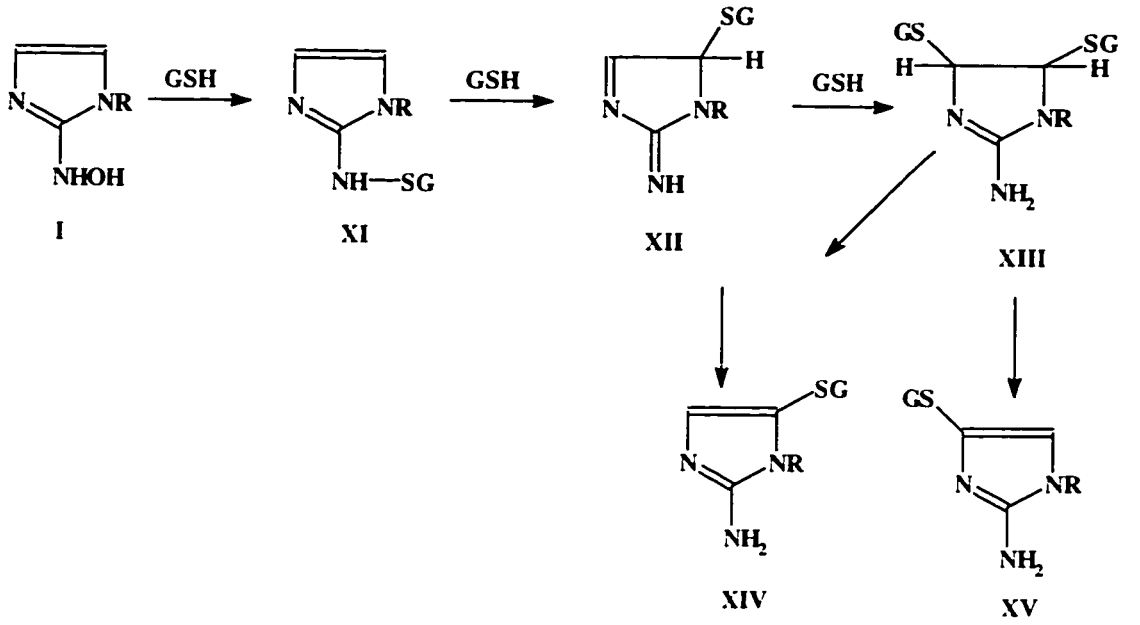

Reactions with GSH. Prolonged exposure of mammalian cells to 2-nitroimidazoles under hypoxic conditions has been shown to reduce the intracellular level of glutathione[142,143]. The reactions of glutathione with 2-nitroimidazoles are summarized in Scheme 8. Remarkable similarities to those reactions illustrated in Scheme 7 are observed. Initially the GSH reacts with the hydroxylamine to produce an unstable GS conjugate which in excess GSH undergoes further reactions to yield two stable GS adducts (XIV, XV) and a saturated product (XIII). This saturated product can undergo loss of GSH to produce one of the two stable amino products containing a GS adduct on either the C_4 or C_5 position of the imidazole ring. The initial hydroxylamine-GS adduct (XI) is a reactive species which on exposure to air

under neutral conditions forms the azoxy derivative, and, on reacting with guanine, forms the guanine-glyoxal adduct as depicted in Scheme 7.

Another important question is whether these reactions occur in biological systems. The earliest indication that reduction of 2-nitroimidazoles occurred in biological systems was the presence of the amine in homogenates of cells exposed to MISO under hypoxic conditions[144]. Further experiments demonstrated the existence of the amino derivative in the urine of animals[144] and in patients[145,146] following exposure to 2-nitroimidazoles. Because the amine is the final step of reduction, its formation is often indicative of the formation of its precursor, the hydroxylamine. Further evidence also showed that the hydroxylamine is likely to bind to nucleic acids, proteins and DNA via the guanine-glyoxal adducts depicted in Scheme 7. These observations suggested that 2-nitroimidazoles undergo bioreductive activation and the major reactive product is likely to be the hydroxylamine. The hydroxylamine itself or its reactive derivatives could explain many of the biological phenomena reported for the 2-nitroimidzoles. However, the exact mechanisms by which some of these occur has yet to be determined.

Recent studies have indicated that another reactive intermediate, the nitroso derivative, is a potent chemosensitizer, enhancing melphalan (L-PAM) cytotoxicity at micromolar concentrations under either aerobic or hypoxic conditions. In contrast, the hydroxylamine and amine derivatives failed to modify cell kill by L-PAM even at millimolar concentrations[147]. Glutathione and protein thiol depletion, followed by an increase in intracellular calcium levels, were also observed[148].

These studies indicated that the nitroso compound seems to be responsible for chemosensitization while the hydroxylamine derivative is for radiosensitization of hypoxic cells. Obviously, nitro-reduction is not the only way that nitroimidazoles can be metabolized in biological systems. Other metabolic pathways include ring fragmentation, conjugation, nitro displacement, and dealkylation and hydroxylation which are also known to contribute to hypoxic binding. These and other metabolic pathways have been reviewed elsewhere[149].

2.2.4. Radioiodinated sugar-coupled 2-nitroimidazoles as hypoxic cell markers

Over the last decade a large number of 2-nitroimidazole derivatives have been synthesized, radiolabeled and evaluated *in vitro* and *in vivo* as potential chemical markers in hypoxic cells. These derivatives have been extensively reviewed elsewhere[149,150]. The following brief discussion will entirely focus on radioiodinated sugar-coupled 2-nitroimidazoles.

Radioiodinated sugar-coupled 2-nitroimidazoles were developed collaboratively by the groups of Wiebe at the University of Alberta and Chapman at Fox Chase Cancer Center, Philadelphia (formerly at the Cross Cancer Institute in Edmonton, Alberta). These sugar derivatives or nucleosides are designed to provide a balance between the lipophilicity of the iodine atom on the sugar and the hydrophilicity of the sugar hydroxyl groups. As described in Section 2.2.2., a proper balance between lipophilicity and hydrophilicity is crucial in the radiosensitizing effectiveness of a compound. Furthermore, the introduction of an iodine atom conveniently provides a site for radioiodination and subsequent SPECT imaging.

The first iodinated sugar-coupled azomycin, iodoazomycin riboside (IAZR, **44**) was synthesized from azomycin riboside (AZR, AR, **45**), a known radiosensitizer and sugar-containing homolog of MISO, by Jette *et al.*[151,152] in 1986. Although [^{125}I]IAZR (P = 2.1)[151] showed promising radiosensitization of hypoxic cells *in vitro*, it was radiochemically unstable *in vivo*[152]. Its rapid renal clearance and appreciable deiodination severely limit the use of [^{123,131}I]IAZR as an *in vivo* marker of hypoxic tissues in the animal models studied.

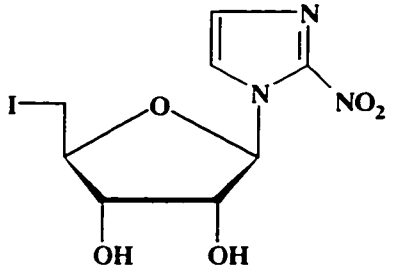

44

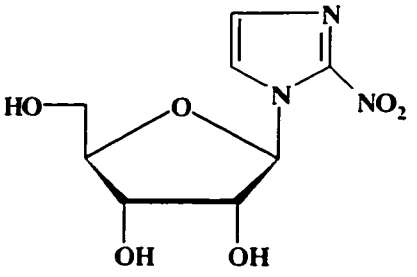

45

In an attempt to minimize *in vivo* deiodination which is believed to occur following enzymatic cleavage of the N^1-glycosidic bond rather than by directly from the intact [^{125}I]IAZR[152], Mannan *et al.*[1] synthesized iodoazomycin arabinoside* (IAZA, **1A**) by altering the stereochemistry of the hydroxyl group at C_2' of the sugar moiety. Studies have shown that the arabinofuranosyl nucleosides are more stable than their ribofuranosyl counterparts both *in vitro* and *in vivo*[9] and thus improved *in vivo* stability of IAZA might be anticipated. Indeed, [^{123}I]IAZA is the first SPECT hypoxic cell marker to proceed to clinical studies. Some of the clinical studies with [^{123}I]IAZA have already been mentioned in the Introduction section[1,2,4,5].

---

*Although IAZA (**1A**) has previously been reported as the β anomer, subsequent investigations revealed that it is actually the α anomer.

[^{123}I]IAZA has further been used to study the oxygenation status of both non-treated and photodynamic therapy (PDT)-treated Dunning prostate tumors in rats[153]. Recently, its pharmacokinetics have been extensively studied[3,154] and its potential in detecting brain hypoxia has also been evaluated in the Gerbil Stroke model[155]. Its relatively high lipophilicity (P = 4.98)[1] results in slower blood clearance and the choice of 24 h post infusion as an optimal imaging time in the [^{123}I]IAZA patients. At this imaging time, the hypoxic tissue-to-blood ratio would be at a maximum[3] of 5.6. The high radioactivity in the thyroid and liver at short time periods after injection are evidence that the tracer kinetic data consisted of the pharmacokinetics of [^{123}I]IAZA, its radiolabeled metabolites and [^{123}I]iodide. Some of the probable metabolites were studied and evaluated in this thesis. These observations implied that the stereo-chemical change at C_2' of IAZA seemed to marginally reduce *in vivo* deiodination. In addition, the pharmacokinetics of [^{123}I]IAZA was found to be very complicated.

A third member of this class is iodoazomycin galactoside (IAZG, **46**) in which the pentose sugar was replaced by the hexose D-galactose. Mannan *et al.*[149,156] reported a low tumor-to-blood ratio of 1.6 at 4 h for [^{125}I]IAZG (P = 0.57) with similar *in vivo* deiodination as [^{125}I]IAZA. However, the Chapman group have recently studied [^{125}I]IAZG and reported a tumor-to-blood ratio of 11.1 at 8-24 h[157]. These results confirmed the earlier reinvestigations in which the tumor-to-blood ratios for [^{125}I]IAZG were actually much higher than previously reported (Mannan, unpublished results). In this study, the Chapman group concluded that **46** has the lowest partition coefficient (P = 0.63), the fastest plasma clearance rate, and the maximal tumor-to-blood ratio. It thus showed superior hypoxia marking properties relative to IAZA.

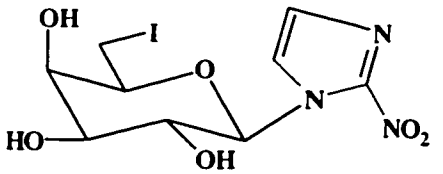

46

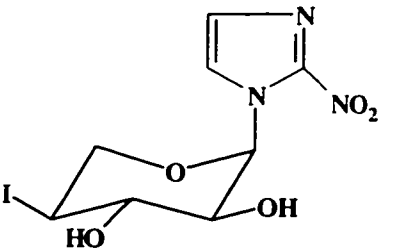

47

The next member of this iodoazomycin nucleoside series, iodoazomycin pyranoside (IAZP, 47), is also very interesting. IAZP, which had been reported to be the β anomer, was shown to have a very high tumor-to-blood ratio (13.9) in mice at 24 h post injection[155]. The hexose sugar in IAZP was changed from D-galactopyranose to a 6-deoxy pentopyranose sugar, L-xylopyranose. The iodine atom was also moved from a primary carbon at C_6' to a secondary carbon closer to the sugar ring at C_4' in order to reduce *in vivo* deiodination. Indeed, the high tumor-to-blood ratios and extent of deiodination showed that [^{125}I]IAZP is superior to [^{125}I]IAZA in murine studies.

However, the Chapman group synthesized the α anomer of IAZP (IAZXP) (P = 1.29)[157] and compared it with the reported IAZP (P = 0.89)[158]. The ^{1}H NMR chemical shifts (CD_3OD) and C_1'-C_2' coupling constants were nearly identical for IAZP and IAZXP: δ6.15 and 9 Hz for IAZP, and δ6.126 and 8.91 Hz for IAZXP. Their melting points were also identical (175-176°C). Furthermore, biological data of these two compounds were very similar. IAZP had a tumor-to-blood ratio of 13.9 (24 h post injection) while the value for IAZXP was 11.7 (8-24 h post injection). Based on these observations, the Chapman group claimed that IAZP is identical in all respects to IAZXP and concluded that IAZP is in fact the α anomer and not the reported β

anomer. Further investigations on the original samples of IAZP are currently underway (Kumar, personal communications).

The fifth member in this class is 1-(2-fluoro-4-iodo-2,4-dideoxy-β-L-xylo-pyranosyl)-2-nitroimidazole (FIAZP, **48**)[159] in which the hydroxyl group at C_2' was replaced with a fluorine atom. This isosteric approach changes the lipophilicity (P = 6.26) and the hydrogen bonding patterns of the sugar molecule. The tumor-to-blood ratio for [^{125}I]FIAZP was found to be 6 at 24 h post injection. Compared to the previous iodoazomycin nucleosides in this series, *in vivo* deiodination in [^{125}I]-**48** was found to be comparable to [^{125}I]IAZP. At 24 h, less than 6% of the whole-body activity was found in the thyroid. This is not surprising because FIAZP, like IAZP, consists of a stronger carbon-iodine bond on a secondary carbon as reflected in the necessity for direct radioiodination of these two compounds.

These biological data suggested that [^{125}I]FIAZP appears to undergo hypoxia-dependent binding in tumor tissues at level comparable to other iodinated sugar-coupled 2-nitroimidazoles in this series. The high liver radioactivity up to 24 h could limit its potential in imaging tumors near the liver, but it may still be a useful probe for non-invasive assessment of hypoxia in other sites of the body. Another interesting feature of FIAZP is that the magnitude of its C_1'-C_2' coupling constant (8.6 Hz) in ^{1}H NMR was also quite similar to that of IAZP (9 Hz). Obviously, the substitution of a fluorine atom at C_2' might have an effect on the C_1'-C_2' coupling constant. Indeed, an original sample of FIAZP was reinvestigated and its anomeric configuration at C_1' was determined to be α by X-ray crystallography (Kumar, unpublished results).

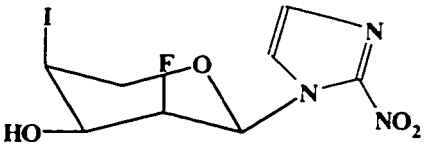

48

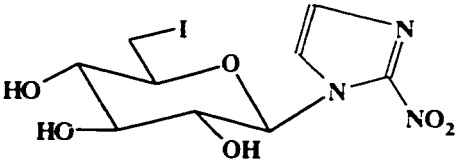

49

Four additional iodoazomycin nitroimidazoles were evaluated by the Chapman group[157]. These are 1-(6-deoxy-6-iodo-β-D-glucopyranosyl)-2-nitroimidazole (a glucose-coupled 2-nitroimidazole, **49**), 1-(6-deoxy-6-iodo-β-D-glucopyranosyl)-4-nitroimidazole (a glucose-coupled 4-nitroimidazole, **50**), 1-(4-deoxy-4-iodo-β-D-xylopyranosyl)-2-nitroimidazole (a D-enantiomer of IAZXP, **51**) and 1-(4-deoxy-4-iodo-β-L-lyxopyranosyl)-2-nitroimidazole (**52**). These compounds all had low partition coefficients ($P < 1.30$) but had tumor-to-blood ratios of > 7. They were inferior in respect to their lower water solubility, slow plasma clearance rates and lower tumor-to-blood ratios when compared with the results of [^{125}I]IAZG and [^{125}I]IAZXP.

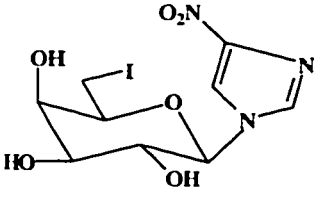

50

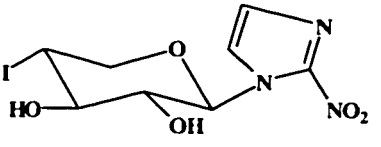

51

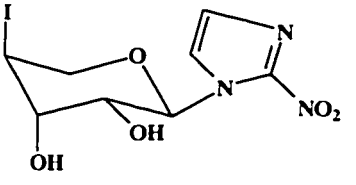

52

It should be noted that the chemical synthesis, radiolabeling and biodistribution studies of α-IAZA (**1A**) were reported by the Chapman group. In particular, its ^{1}H NMR data were included in the investigations described in section 4.5.

2.3. Chemistry and radioiodination of arabinofuranosyl sugars and nucleosides

2.3.1. Chemistry of glycosylation reactions with arabinofuranosyl sugars

The preparation of β-arabinofuranosyl nucleosides (C_1'-C_2' *cis* nucleosides) has traditionally been difficult. The benzoyl group (C_6H_5CO) is commonly used to protect the three hydroxyl groups on the sugar moiety during glycosylation reactions. However, the presence of this participating benzoyl group (or any other acyl groups) at C_2 directs the reaction pathway to a C_1'-C_2' *trans* nucleoside as defined by the *trans* rule of nucleoside synthesis[160]. With the benzoyl group at C_2 *cis* to a halogen (e.g. bromine) at C_1, simple inversion would predominate; with a C_1-C_2 *trans* halide, participation of the benzoyl group at C_2 in the displacement of the halogen results in either no net inversion or formation of an ortho ester derivative (**53**). Therefore, whether the starting acylated arabinofuranosyl halide is α or β, the product will almost always be exclusively α (C_1'-C_2' *trans*) nucleoside.

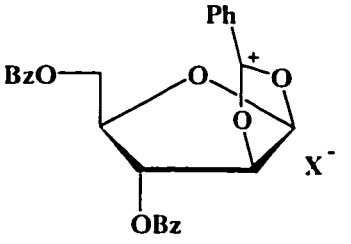

53

A wide variety of special methods have been devised for the synthesis of C_1'-C_2' *cis* arabinofuranosyl nucleosides. In general they fall into the following two methods: inverting the configuration of C_2' in a C_1'-C_2' *trans* nucleoside[161-170] or using an arabinofuranosyl halide in which the hydroxyl group at C_2 is masked with a group which does not participate in the displacement of the halogen at C_1[171-176]. In the first

method, the configuration of C_1'-C_2' *trans* nucleosides could be inverted via the 2',3'-anhydro epoxide[161] (54), the 8,2'-*O*-anhydronucleoside (for arabinofuranosyladenine)[162,163] (55), or through DMSO oxidation[165,166] (56). This method provides a convenient way to overcome the difficulties with the direct synthesis of a C_1'-C_2' *cis* nucleoside.

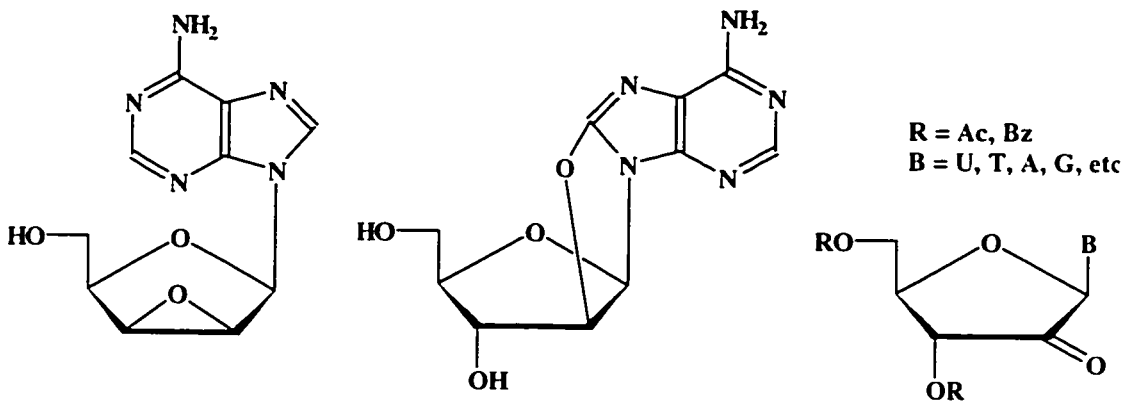

54 55 56

Undoubtedly, these difficulties are mainly due to the presence of a participating protecting group at C_2 of the sugar molecule. A direct synthesis could be accomplished if the identity of the protecting group at C_2 was changed. Indeed, the second method uses almost exclusively 2,3,5-tri-*O*-benzyl-D-arabinofuranosyl chloride (57) as the protected glycosyl halide. The absence of a reactive carbonyl on the benzyl substituent makes this blocking group incapable of neighboring group participation. The hydroxyl groups can be readily masked as benzyl ethers which can easily be cleaved by catalytic hydrogenation. The chloride was also found to be markedly more stable than the corresponding bromide[177]. These features of the chloride make it a convenient tool for the synthesis of C_1'-C_2' *cis* arabinofuranosyl

nucleosides. For example, 9-β-D-arabinofuranosylguanine (araG) has been synthesized and isolated as the sole product in 33% yield using this method (Scheme 9)[174].

Scheme 9. Chemical synthesis of a C_1'-C_2' *cis* arabinofuranosyl nucleoside[174].

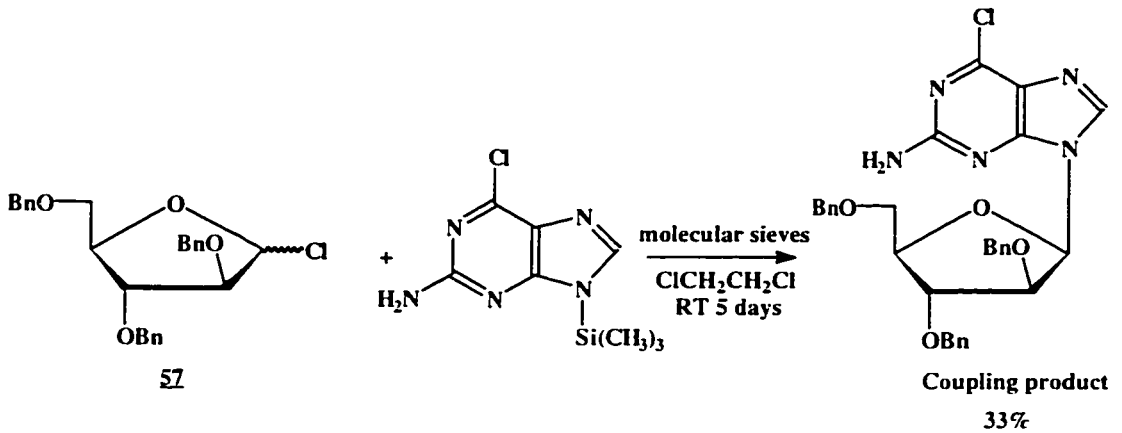

2.3.2. Methods to differentiate between α and β anomers of arabinofuranosyl nucleosides

For carbohydrate derivatives (and nucleosides) the new center of chirality generated by hemiacetal ring formation is called the anomeric center. The two stereoisomers are referred to as anomers, designated α or β according to the configurational relationship between the anomeric center and a specified anomeric reference atom[178]. In the case of nucleosides, this anomeric reference atom is the same as the configurational atom, the highest numbered chiral carbon atom that dictates whether a given sugar belongs to the D or L series. In the α anomer, the exocyclic oxygen atom at the anomeric center is formally *cis*, in the Fischer projection, to the oxygen attached to the anomeric reference atom; in the β anomer these oxygen atoms are formally *trans*[178] (Figure 2).

Figure 2. Determination of the anomeric configuration of sugar derivatives.

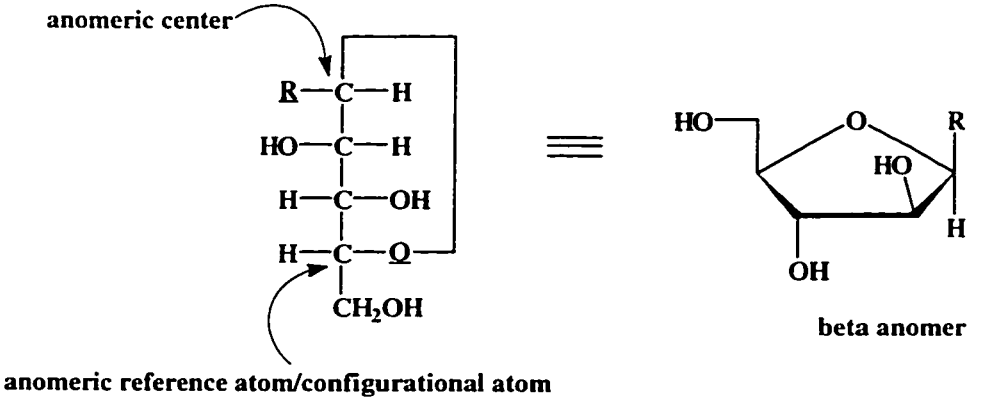

This rule shows that for β-D-arabinofuranosyl nucleosides (C_1'-C_2' *cis* nucleosides) the nucleobase will always be in an "up" configuration and vice versa for the α anomer. Since anomers are stereoisomers and thus have different physical, chemical and even biological properties, it is important to distinguish them unambiguously. The following selected methods of determining anomeric configurations are briefly discussed.

2.3.2.1. NMR Spectroscopy

^{1}H NMR Spectroscopy

In general, ^{1}H NMR spectroscopy can usually be used, but not always, for the assignment of anomeric nucleosides. The chemical shifts and H_1'-H_2' coupling constants are the most important indicators. It has been reported that the anomeric proton of the β anomer of arabinofuranosyl nucleosides always appeared downfield from the anomeric proton of the corresponding α anomer[179]. This observation is consistent with the reported trend in ribofuranosides[180] that the chemical shift of the anomeric proton of a C_1'-C_2' *cis* nucleoside appears at lower field (usually around 0.5 ppm) than the peak observed for the anomeric proton of the corresponding C_1'-C_2'

trans nucleoside. This downfield shift probably results from the deshielding of the anomeric proton by the vicinal *cis* hydrogen atom in a C_1'-C_2' *cis* nucleoside[181].

The spin-spin vicinal coupling constant between neighboring (vicinal) protons over three bonds ($^3J_{H\text{-}C\text{-}C\text{-}H}$) varies with the dihedral angle ϕ as depicted in the Karplus curve[182]. It is known that in a five-membered ring the dihedral angle between vicinal *cis* hydrogens and vicinal *trans* hydrogens can vary from 0-45^0 and 75-165^0 which can produce coupling constants, using the Karplus equation in a range of about 3.5-8.0 Hz and 0-8.0 Hz, respectively[183]. Therefore, an assignment of anomeric configuration can be made only if the coupling constant is less than about 3.5 Hz, but preferably a smaller ^3J value (less than about 1.0 Hz) is desirable. If a given arabinofuranosyl nucleoside has a ^3J value of 5 Hz, for example, unambiguous assignment cannot be obtained based on the above observations.

^{13}C NMR Spectroscopy

^{13}C NMR spectroscopy can be used to complement ^1H NMR because the chemical shift difference between the anomers is usually larger (around 5 ppm) than that in ^1H NMR. For example, the C_1 atom of the α anomer of methyl D-arabinofuranoside (*trans*) resonates at a lower field (109.3 ppm) than the corresponding C_1-C_2 *cis* β anomer (103.2 ppm)[184]. The anomers are thus more clearly identified in a ^{13}C NMR spectrum.

1-D NOE difference spectroscopy

Questions of stereoisomerism are often investigated by NOE (nuclear Overhauser effect). In general, irradiation of a proton results in enhancement of the signal of the nucleus to which the proton is directly bonded. For example, it is

standard practice in ^{13}C NMR spectroscopy to use NOE to improve the sensitivity of NMR measurements with the less sensitive ^{13}C nucleus which has a low magnetogyric ratio γ and a natural abundance of only 1.108%. This NOE can also operate between non-bonded protons through space but only over a short distance and with a smaller effect, which decreases as the inverse of the sixth power of the distance through space between the nuclei[185]. This spatial interaction has observable enhancement usually less than 20%.

An NOE difference spectrum is obtained by subtracting an ^{1}H spectrum from a specific-proton-irradiated spectrum. The data are stored in two different blocks of the computer memory and the Overhauser enhancement remains as the NOE difference spectrum. This form of NOE spectroscopy is very sensitive and allows the detection of very small intensity differences (as low as 3%), because the signals from experiments with and without irradiation are recorded practically under identical conditions[186]. A measurable effect can be expected between protons over a spatial distance of up to about 4 Å (0.4 nm).

To apply this NMR technique to arabinofuranosyl nucleosides, Seela *et al.*[187,188] have studied a series of anomeric nucleosides and unambiguously assigned the configuration in each pair of nucleosides. Figure 3 illustrates how NOE can be used to differentiate the anomeric arabinofuranosyladenine (ara-A)[188].

Figure 3. Differentiation of anomeric arabinofuranosyladenine by NOE[188].

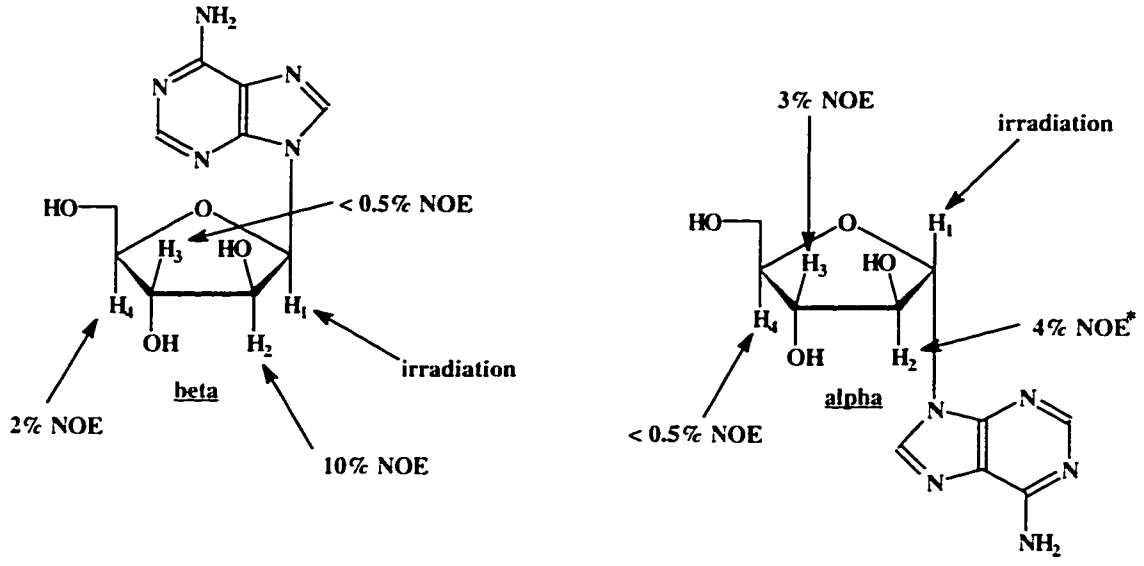

*additional partial saturation of 2'-OH

The anomeric configuration of arabinofuranosyl nucleosides can be unambiguously assigned by irradiating H_1' and measuring the NOE enhancement factors at H_3' and H_4'. An NOE of the H_4' signal indicates β configuration while an NOE at H_3' confirms α configuration.

2-D NOE Spectroscopy (NOESY)

It is possible to assemble all of the ^1H-^1H NOE enhancement effects in a molecule into a single spectrum called NOESY. The 1-D ^1H spectrum appears on the diagonal and the nonbonding ^1H-^1H interactions with protons that are nearby in space are found in the non-diagonal cross peaks. Essentially NOESY gives the same information as 1-D NOE difference spectroscopy. The enhancement effects appear as cross peaks in NOESY and their presence or absence can indicate protons of different spatial proximities. For example, in the ara-A example[188], one would expect to find cross peaks at H_1'-H_2' and H_1'-H_4', but not H_1'-H_3', for the β anomer.

2.3.2.2. Chiroptical methods

Chiroptical properties are properties of chiral substances arising from their nondestructive interaction with anisotropic radiation (polarized light), properties that can differentiate between the two enantiomers of a chiral compound[189]. These chiroptical methods include polarimetry (optical activity), optical rotatory dispersion (ORD), and circular dichroism (CD). Optical activity results from the refraction of right and left circularly polarized light to different extents by chiral molecules. The source of this rotation is unequal slowing of right and left circularly polarized light as the light passes through a sample[189]. This method can also be applied to the detection of anomeric sugars and nucleosides. For example, the specific rotation value, $[\alpha]_D^{25}$, which denotes the specific rotation for light of the wavelength of the sodium D-line (589 nm) at 25°C, was found to be +128.8° (*c* 0.3, H_2O) for the α-anomer and -24.0° (*c* 0.3, H_2O) for the β anomer of an arabinofuranosyl nucleoside[179]. Although polarimetry provides results rather fast, the information is often not very precise nor is it necessarily very accurate. The optical rotation is affected by numerous variables: wavelength of light used, presence or absence of solvent, the nature of the solvent used, concentration of the solution, temperature, and the presence of impurities. Precise reproduction of published rotation values, from laboratory to laboratory, or even from day to day in the same laboratory, is difficult to achieve[189]. Therefore, polarimetry should only be used as a rough guide in the assignment of anomeric nucleosides.

The other two chiroptical methods, ORD and CD, are thus increasing replacing polarimetry in studying chiral compounds. ORD is the measurement of specific

rotation as a function of wavelength. The absolute value of the rotation increases as wavelength decreases (towards the ultraviolet region). ORD curves can be simple or they can be complicated by the Cotton effect (showing both a maximum and a minimum, and a point of inflection)[189]. The sign of the ORD curve reflects the configuration of the chromophore, or of the stereogenic centers (such as the anomeric center in sugars and nucleosides) that perturb the chromophore, even in the presence of other stereocenters. A positive Cotton effect occurs when the rotation first increases as the wavelength decreases; conversely, a negative Cotton effect arises when the rotation first decreases when going towards shorter wavelengths. ORD has been used to study anomeric nucleosides and nucleotides[190]. The study found that configuration at the anomeric carbon determines the sign of the Cotton effect and that at C_2' profoundly affects the amplitude of the ORD curve. α-D-Arabinofuranosyl nucleosides were found to exhibit negative Cotton effects while β-D-arabinofuranosyl nucleosides gave positive Cotton effects.

Circular dichroism (CD) spectra arise from the differential absorption of left and right circularly polarized radiation by chiral molecules . CD is the measurement of the ellipticity [θ] (analogous to the measurement of [α] in ORD) as a function of wavelength. The ellipticity measures the extent of elliptical polarization caused by the absorption of the incident linearly polarized light by the sample. The signs of the CD curve and that of the corresponding ORD curve in the region of an anomaly (Cotton effect) are the same[189]. Both ORD and CD spectra gave similar information, although CD spectra are less cluttered, bands are better separated, and easier to interpret. Therefore, where a choice is possible, CD spectra are preferred over ORD.

2.3.2.3. X-ray crystallography

X-ray diffraction is by far the most powerful technique for the structural determination of crystalline compounds[189]. In this method, X-rays of appropriate wave-lengths are allowed to impinge on a single crystal, 0.1-1 mm in length, of the material to be investigated. The X-rays are scattered by the atoms (by their electrons rather than by the nuclei) and the interference of the scattered radiation is displayed as a diffraction pattern. The diffraction pattern is then mathematically analyzed to provide the necessary structural data for the molecules. Although X-ray crystallography requires single-crystal samples, it is a very attractive method for the determination of the absolute configuration of a chiral compound. All the other methods mentioned in this section measure only the *relative* configuration of chiral compounds. In other words, they determine the configuration of one chiral center relative to another, either in the same molecule or another[189]. For example, NMR spectroscopy can differentiate between a C_1'-C_2' *cis* or C_1'-C_2' *trans* nucleoside but it cannot provide information on whether it is an α-D-*ribo* or β-D-*arabino* for C_1'-C_2' *cis*, or β-D-*ribo* or α-D-*arabino* for C_1'-C_2' *trans*. Obviously, if the absolute configuration of one chiral center in the molecule is known (e.g. *arabino* configuration at C_2'), that of C_1' and the other chiral carbons follow. But without this prior knowledge, only the relative configuration can be obtained. Therefore, the attractiveness of X-ray crystallography lies in its ability to determine absolute configuration of a molecule provided that its chemical structure is known.

2.3.2.4. Chemical reactions

The use of chemical reactions in structural elucidation has a long history, although its importance has been replaced by recent advances in spectroscopy, especially NMR spectroscopy. Nevertheless, chemical reactions can sometimes be used to complement spectroscopic data. For example, Prisbe *et al.*[191] showed that a cyclonucleoside of the β anomer of the ribofuranosyl 2-aminoimidazole nucleoside was formed upon heating (100°C) in an inert solvent (e.g. DMF) while there was no similar reaction for the α anomer (Scheme 10).

Scheme 10. Differentiation of anomeric nucleosides by evidence of cyclo-nucleoside formation[191].

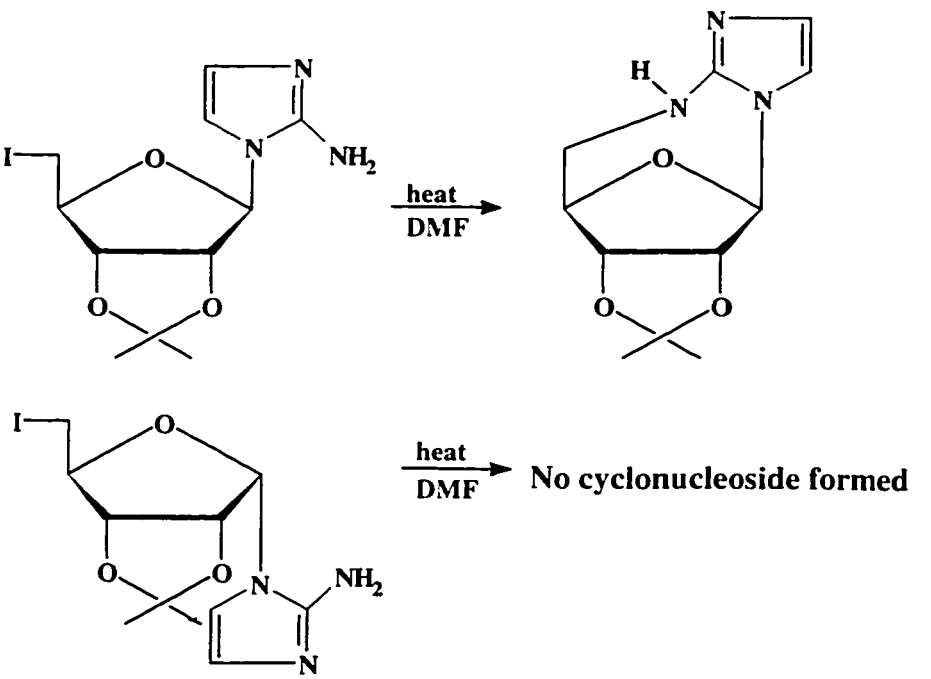

2.3.3. Chemistry of radioiodination of arabinofuranosyl nucleosides

2.3.3.1. Exchange labeling methods

Radioiodine can be introduced into organic compounds by numerous methods depending on the structure of the compound to be radioiodinated. If high specific activity is not essential, exchange labeling reactions by nucleophilic radioiodination represent a viable method. Advantages of the method include ease of radioiodination, characterization, and handling of the cold, stable iodinated compound. No complicated separation techniques are usually necessary because the cold iodinated compound and the radioiodinated product are chemically identical.

Isotope exchange of aliphatic iodides can be conducted in a refluxing solvent such as acetone, methyl ethyl ketone (MEK), water or dimethylformamide (DMF)[192]. Alternatively, radioiodination can be carried out at elevated temperatures in a "melt" fashion. The molten reaction medium must possess a sufficiently high dielectric constant to solubilize both the substrate and radioiodide[193]. Examples of such media include benzoic acid[194], acetamide[195] and ammonium sulfate[196]. Ammonium sulfate seems to be particularly useful in solid-phase exchange radioiodination between no-carrier-added radioiodide and unactivated aryl iodides[196]. However, these methods generally afforded low yields of radioiodinated products.

Isotope exchange reactions essentially occur via S_N2 nucleophilic substitution and are affected by the acidity of the reaction medium. To improve the labeling efficiency, a homolog of acetic acid, trimethylacetic acid (pivalic acid)[193], has been chosen because it possesses sufficient acidity, appropriate melting (33°C) and boiling (164°C) points, and relative chemical inertness due to steric hindrance by the methyl

groups. Indeed, pivalic acid has been successfully employed in the radioiodination of a wide variety of organic compounds with good to excellent radiochemical yields (55-99%). This method is also suitable for radioiodination with ^{123}I because of short labeling times. In fact [^{123}I]IAZA has been radioiodinated using the pivalic acid "melt" method with a radiochemical yield of 92.6%[2]. An efficient, high specific activity radioiodination of a 2'-deoxyuridine nucleoside in pivalic acid "melt" has also been reported[197].

2.3.3.2. Direct synthesis with radioiodide

Radioiodine can also be directly incorporated into non-iodinated organic molecules by electrophilic radioiodination, especially in aromatic compounds. The most common mechanism is iododestannylation which gives aromatic radioiodinated tracers rapidly in high yields and specific activities from trialkylarylstannanes. A typical radioiodination reaction normally requires the presence of a suitable oxidizing agent, such as Iodogen, chloramine-T, or peracetic acid. The pH of the reaction medium is extremely important in the radiochemical yields of the radioiodination. Respectable radiochemical yields are generally obtained at pH up to 5.8; at pH 7.0 no desired radioiodinated product is obtained[198]. Glacial acetic acid or phosphoric acid is used to provide this acidic reaction medium. For example, a radiochemical yield of about 60% has been obtained with the radiosynthesis of β-CIT (at pH 2.9 in peracetic acid), a dopamine transporter imaging agent[198].

Direct radioiodination is sometimes necessary to incorporate radioiodine into aliphatic non-primary carbon atoms. Exchange labeling works best with primary carbon atoms because the carbon-iodine bond in a primary carbon is relatively weak.

In a secondary carbon, however, the increased steric hindrance and the stronger carbon-iodine bond make exchange labeling, which is essential an S_N2 reaction, more difficult. An excellent example to illustrate this point is the direct radioiodination of FIAZP (48)[159]. [^{125}I]FIAZP was prepared by direct radioiodination with Na^{125}I in pyridine and triphenylphosphine after previous treatment with Iodogen. The difficulties with direct radioiodination are reflected by longer reaction times (16 h) compared to exchange labeling (1-3 h) and lower radiochemical yields (15%). Similar radioiodination results have been obtained with [^{125}I]IAZP (47), although exchange labeling with ^{123}I was successful in preparing [^{123}I]IAZP in high specific activity (50 GBq/mmol)[158]. The radiochemical yield of this exchange labeling on a secondary carbon atom was not reported.

Armed with these versatile radioiodination methods, radiopharmaceutical chemists can now radiolabel desired compounds with ^{123}I or ^{131}I for SPECT imaging studies. As previously described, ^{123}I is an important player in SPECT imaging today. Whether or not ^{123}I will continue to play this important role in nuclear medicine remains an open question. Undoubtedly, it has more clinical applications than PET radionuclides such as ^{18}F, yet it is not as popular as the rather inexpensive ^{99m}Tc. These and other related issues are briefly discussed in the next section.

2.4. New and current developments in medical diagnostic imaging

2.4.1. Role of ^{123}I and some potential newcomers in SPECT

In the United States more than 80% of all diagnostic procedures are carried out using techetium-99m. In the last three decades, the number of diagnostic procedures has increased almost fourfold from 7.9 to 28.3 per 1,000 population[199]. This

unprecedented popularity with technetium-99m is due largely to its ideal decay properties, ease of production by a generator, and relatively low cost factors which have been described in Section 2.1.3. Iodine-123, on the other hand, is especially important in Canada and Europe because of available domestic sources (e.g. Nordion International in Canada). The lack of a domestic supplier of iodine-123 and its high cost in the United States limits its share in the diagnostic nuclear medicine market, and only 9% of all diagnostic procedures are performed using iodine-123[199]. Iodine-123 has a longer half-life than the physiological PET radionuclides and hence can be conveniently transported. Unfortunately, due to required cyclotron production, the high cost of iodine-123 remains a considerable barrier to widespread commercial use.

Besides iodine-123, some potential SPECT newcomers have been identified that could occupy an important position in the future practice of nuclear medicine. These include ruthenium-97, indium-111, thallium-201, and lead-203[199]. Two of these radio-nuclides, indium-111 and thallium-201, are already commercially available. Furthermore, they all have half-lives between 2-3 days and gamma ray energies suitable for imaging studies with conventional gamma camera systems, although lead-203 has a higher gamma ray energy (279 keV). Despite these potential newcomers, technetium-99m will continue to enjoy its popularity in diagnostic imaging. Whether any of them would become another technetium-99m success story does not seem too likely in the foreseeable future, although it is not impossible[199].

2.4.2. Instrumentation for PET and SPECT and dual PET-SPECT cameras

PET instrumentation

Traditionally PET provides the best resolution for functional and metabolic imaging. The two 511-keV annihilation photons simultaneously emitted 180° apart following positron-electron annihilation form the basis of PET. It has been found that these two annihilation photons offer substantial advantages over single gamma ray photons for *in vivo* nuclear medicine imaging. These advantages include very accurate compensation for the attenuation of the radiation in tissues, resulting in the production of quantitative images measuring the local concentration of a radiotracer. Attenuation refers to the process of absorption or scattering of gamma rays during which the observed count rates are reduced and images distorted[200].

A typical modern PET camera operates as follows. The two 511-keV photons, which are emitted in opposite directions after annihilation of a positron and an electron, are detected by two detectors in coincidence; data collected over many angles around the patient's body are used to reconstruct the image of activity distribution in the area of interest. With PET scanners continually increasing in complexity, a modern PET camera typically consists of several rings with as many as 512 detectors per ring around the patient. Each detector is connected to the opposite detector by a coincidence circuit. Hence all coincidence counts from different slices over 360^0 angles around the patient are acquired simultaneously. The most common detector material used in PET scanners is bismuth germanate (BGO) because of its high density (7.13 g/cm^3) and an effective atomic number of 75, leading to very high detection

efficiencies for 511-keV photons and short radiation lengths in the detector[201]. Current technological features of PET include the use of radio-pharmaceuticals which closely mimic endogenous compounds, its ability to accurately measure the actual three-dimensional radiotracer distribution, its ability to rapidly acquire a dynamic set of tomographic images through a volume of tissue, and the capability to acquire tomographic whole body images[202]. It is the combination of these four features that enables PET to model and quantitate *in vivo* biochemical or physiological processes.

SPECT instrumentation

The most common SPECT systems are comprised of a typical gamma camera with one to three NaI (Tl) detector heads mounted on a gantry, an on-line computer for acquisition and processing of data and a display system. Computerized reconstruction of data follows the accumulation of a series of images taken as the gamma camera moves around the patient at small angle increments for 180^0 or 360^0 angular sampling. Three-head SPECT systems are presently the most sophisticated instruments for SPECT, having high resolution (6-9 mm), reliable performance and low costs[203]. Recent computer advances have provided SPECT images with comparable resolution to PET, making any differences relatively inconsequential in clinical applications. Dual-isotope imaging (e.g. with ^{99m}Tc and ^{123}I) has been demonstrated with SPECT and this imaging opportunity is not possible with PET. Therefore, SPECT imaging can no longer be viewed as "a poor man's PET" but as a mature technology of independent merit[203].

Dual-camera technology

One solution to the high costs of PET is the development of the so-called Hybrid Emission Advanced Dynamic Tomograph (HEADTOME) in the early 1980s which includes PET and SPECT in one system[204]. The HEADTOME was redesigned as the multi-ring version HEADTOME II[205], HEADTOME III[206], and HEADTOME IV[207], although the latter two have been redesigned as high-performance PET systems. In HEADTOME the detector array consists of 64 NaI crystals in a 42 cm diameter circle. Two collimator sets can slide axially on the inner face of the crystal ring to change from SPECT to PET imaging[204]. The SPECT collimator consists of 64 units each containing a main tungsten fin and five sub-fins which are synchronously driven by a large wheel gear to swing back and forth up to 30^0 in each direction. Therefore, all collimated rays can simultaneously sweep across the field of view. In the PET collimator, photons that contribute to image noise are eliminated. It contains a slice mask which rejects photons originating outside the slice plane and is made up of two doughnut shaped lead plates of 1 cm thickness. The space between the two plates can be selected at 12, 20, and 28 mm. A scatter mask is also included which is made of a 0.5 mm thick lead belt covering the NaI crystal face to reduce low energy scattered photons and improve spatial resolution[204]. This hybrid camera has been successfully used to study the BBB using $^{99m}TcO_4^-$ or ^{68}Ga-EDTA.

Recently the technology for FDG-SPECT has been developed using a relatively inexpensive gamma camera[208]. This technology is based on previous documentation that multi-headed camera systems with a conventional high-energy collimator or a 511-keV collimator can be used to image FDG myocardial uptake[209]. Preliminary

studies showed that relative to the sensitivity for technetium, a 9% sensitivity has been reported for 511-keV photon capture with FDG SPECT. Despite this shortcoming, FDG SPECT images are interpretable and adequate for cardiac or oncological diagnosis. Although it is far inferior to PET, FDG SPECT equipped with the 511-keV collimator gives adequate images from which equivalent information about myocardial viability can be obtained.

2.4.3. Present and Future Trends

Obviously, medical diagnostic imaging is not limited to PET and SPECT. Computed tomography (CT), functional magnetic resonance imaging (fMRI), and ultrasound are routinely used for imaging. With costs likely to remain the determining factor in today's health care industry, alternative imaging technologies are continuing to be developed to replace the expensive costs of PET. Although in its infancy, optical imaging using light has been studied[210-213]. The idea of using a light bulb is indeed exceedingly attractive: light bulbs are small, they don't emit X-rays and they are low power[211]. The major obstacle, of course, is that very little light will go through the body because more than 99.9999% of the light will be absorbed by molecules or scatter off cells and cell organelles. To truly cut imaging costs, one vision has been described:

> "If someone comes into an office and says 'I have this lesion,' you stick a light probe onto it and image the lesion. And the computer, using the absorption and scattering characteristics, can tell you whether this is normal or a cancer. That's more than just a pipe dream."[211]

But until such visions could be achieved, SPECT imaging remains a feasible alternative for medical diagnostic imaging.

3. Experimental

3.1. Materials

3.1.1. Chemicals, Solvents, Gases, and Equipment

Melting points were determined on a Hoover capillary apparatus and are uncorrected. All chemicals were reagent grade unless otherwise specified. Where dry solvents were required these were dried by standard methods. Gases were purchased from LINDE Union Carbide, Canada and were of research grade purity. Thin layer chromatography (TLC) was carried out on silica gel MK6F 60 F_{254} (2.5 x 7.6 cm) microplates (Whatman) and plastic-backed Silica Gel 60 F_{254} (20 x 20 cm) pre-coated plates (Merck) for radiochemical yield and purity determinations. Preparative TLC was carried out on silica gel PK5F 150 F_{254} (1000 μm layer thickness, 20 x 20 cm) plates. Silica gel MN-Kieselgel 60 (70-230 mesh) was purchased from Rose Scientific, Edmonton, Alberta, Canada. Fractions from column chromatography were collected a Gilson® FC205 Fraction Collector (Mandel Scientific). Reverse-phase chromatography was carried out on C_{18} reverse phase Sep-Pak® cartridges (Waters). A Bηchi rotavapor (model R-114) and a B-169 vacuum system were employed for vacuum drying. Radiochemical syntheses were generally carried out in Pierce Reacti-Vials™ sealed with teflon-rubber septa or capped with Mininert® valves, with heating by a Baxter Multi-blok Module heater. Eppendorf micropipettes and Hamilton MICRO-LITER syringes were used for measuring micro quantities of solvents. Beckman Poly-Q™-Vials (6 & 18 mL) were used for counting radioactivity on TLC plates and in biological samples.

In the work performed in the Faculty of Pharmaceutical Sciences at the Health Sciences University of Hokkaido (HSUH) in Ishikari-Tobetsu, Hokkaido, Japan, gases were purchased from Daido-Hokusan, Japan. Thin layer (silica gel and aluminum oxide) chromatography was conducted on silica gel 60 F_{254} pre-coated (Merck) and on aluminum oxide 60 F_{254} neutral (Type E, Merck) plates (20 x 20 cm), respectively. Preparative TLC was conducted on silica gel 60 F_{254} pre-coated plates (20 x 20 cm) for preparative layer chromatography (Merck).

3.1.2. Instruments

Animal tissue samples and TLC plates for radiochemical yield and purity determinations were counted in a Beckman Gamma 8000 gamma scintillation counter or Minaxi γ Auto-Gamma® 5000 Series Gamma counter. ^{1}H and ^{13}C NMR spectra were measured with a Bruker AM 300 MHz spectrometer, and chemical shifts are given on the δ (ppm) scale with tetramethylsilane (TMS) as an internal standard. ^{1}H NMR spectra of IAZA (**1A**, Batch #4) were measured with a Varian Unity 500 (500 MHz) spectrometer, and its ^{1}H-^{1}H COSY and ROESY spectra with a Varian Infinity 600 (600 MHz) spectrometer in the Department of Chemistry, University of Alberta, Edmonton, Alberta, Canada (Kumar, unpublished results). Elemental analyses (for compounds **3** and **4**) were performed on an EA1108-Elemental Analyzer (Carlo Erba Instruments) at the MicroAnalytical Service Laboratory in the Department of Chemistry. Low resolution positive ion fast atom bombardment (POSFAB) mass spectra (for compounds **3** and **4**) were recorded on an AEI-Kratos MS-9 spectrometer (matrix: Cleland (dithiothreitol/dithioerythritol = 6:1)) while low and high resolution positive mode electrospray ionization (ESI) mass

spectra (for compound 5) were recorded on a Micromass ZabSpec Hybrid Sector-TOF at the Mass Spectrometry Laboratory in the Department of Chemistry. X-ray crystallography data on IAZA (1A) were obtained on a Siemens P4/RA diffractometer with graphite-monochromated Mo K_α radiation (λ= 0.71073 Å) at the Structure Determination Laboratory in the Department of Chemistry.

At HSUH, Japan, NOE correlation studies, ^{1}H and ^{13}C NMR, ^{1}H-^{1}H COSY, ^{1}H-^{13}C COSY and ^{1}H-^{1}H NOESY spectra were measured with JEOL JNM-EX400 (400 MHz) and JEOL JNM-LA300 (300 MHz) spectrometers. Low and high resolution mass spectra were recorded on JEOL JMS-HX110 spectrometer for POSFAB MS (matrix: glycerol or 3-nitrobenzyl alcohol), and on a JEOL JMS-DX303 spectrometer for electron impact (EI) MS at Hokkaido University, Sapporo, Hokkaido, Japan. X-ray crystallography data on AZA (7) were determined on an MXC18K diffractometer with graphite-monochromated Cu K_α radiation (λ=1.5418 Å) by MAC Science in Nagoya, Japan. High pressure liquid chromatography (HPLC) was used to purify selected glycosylation products. Silica gel HPLC was conducted on a Shim-pac PRC-Sil (H) column (25 cm x 20 mm i.d. for preparative scale) (Shimadzu) and on a Shim-pac HRC-SIL column (25 cm x 4 mm i.d. for analytical scale), using a Shimadzu LC-6A apparatus with monitoring at 254 nm. Reverse-phase HPLC was performed at the Isotope Research Center at HSUH on a Shim-pac STR-ODS II (25 cm x 4 mm i.d. for analytical scale) column and a Shim-pac PREP-ODS (25 cm x 20 mm i.d. for preparative scale) eluting with aqueous methanol, using the same Shimadzu apparatus. Molecular orbital (MO) calculations were performed by the PM3 method with CAChe MOPAC version 94 (Release 3.7,

CAChe Scientific) running on a personal computer, Power Macintosh 8100/100AV (Apple Computer).

3.1.3. Radioisotopes

Radioiodine was the radionuclide used in animal studies. Iodine-125 was purchased from Amersham as no-carrier-added solutions of NaI in 0.1 *N* NaOH.

3.1.4. Animals

Black female B6D2F1/J mice ([^{125}I]-**3**) weighing 20-25 grams were purchased from Jackson Laboratories in Bar Harbor, Maine, USA. White female Balb/c mice ([^{125}I] **4** and [^{125}I]-**5**) weighing 20-25 grams were purchased from Health Sciences Laboratory Animal Services (HSLAS), University of Alberta. All animals were maintained *ad lib* with rodent food pellets and tap water in standard plastic cages (5 mice per cage).

3.1.5. Tumor cell line

EMT-6 tumor cells were used for *in vivo* biodistribution studies on [^{125}I]-**5**. Tumor cells were generous gifts from Ms. Haiyan Xia in Dr. Leonard I. Wiebe's research group in the Faculty of Pharmacy and Pharmaceutical Sciences, University of Alberta. EMT-6 cell suspensions contained approximately 10^7 viable cells per mL of normal saline.

3.2. Methods

3.2.1. Chemical synthesis of methyl 5-deoxy-5-iodo-D-arabinofuranoside (3)

3.2.1.1. Chemical cleavage from IAZA (1A)

(1-(2,3-Di-O-acetyl-5-deoxy-5-iodo-α-D-arabinofuranosyl)-2-nitroimidazole (1B)

IAZA (1A) (208 mg, 0.59 mmol) was dissolved in dry pyridine (3 mL) and acetic anhydride (4 mL) and the resulting mixture was stirred at 25^{0}C for 15 h. Ice (1 mL) was added to destroy any excess acetic anhydride and the solution was concentrated to dryness. The residue was chromatographed on a column containing silica gel using an elution gradient of toluene-ethyl acetate (19:1, 9:1, 85:15 and 4:1 (v/v) successively) to give 236 mg (91%) of 1B as a crystalline solid with a mp of 126-128^{0}C. ^{1}H NMR ($CDCl_3$): δ 7.39 (1 H, d, J = 0.9 Hz, C_5-H), 7.21 (1 H, d, J = 0.9 Hz, C_4-H), 6.68 (1 H, d, $J_{1'-2'}$ = 1.1 Hz, C_1'-H), 5.46 (1 H, br s, C_2'-H), 5.20 (1 H, dd, $J_{3'-2'}$ = 1.8 Hz, $J_{3'-4'}$ = 2.0 Hz, C_3'-H), 4.67 (1 H, dt, $J_{4'-3'}$ = 2.0 Hz, $J_{4'-5'}$ = 6.8 Hz, C_4'-H), 3.48 & 3.43 (2 H, dd, $J_{5'-5'}$ = 10.7 Hz, $J_{5'-4'}$ = 6.8 Hz, 2 x C_5'-H), 2.21 (3H, s, C_2'-$OCOCH_3$), 2.02 (3 H, s, C_3'-$OCOCH_3$). ^{13}C NMR ($CDCl_3$): δ 173.2 (C_2'-$OCOCH_3$ & C_3'-$OCOCH_3$), 148.6 (C_2), 142.2 (C_4), 139.2 (C_5), 85.2 (C_1'), 83.0 (C_2'), 73.8 (C_3'), 68.3 (C_4'), 18.2 (C_5').

Methyl 5-deoxy-5-iodo-D-arabinofuranoside (3)

A solution of (1B) (100 mg, 0.23 mmol) was dissolved in dry dichloromethane (5 mL) and cooled to 0°C. Stannic chloride ($SnCl_4$) in dichloromethane solution (1 mL, 1 mmol) was added to the cooled solution and the resulting mixture was stirred for 5 minutes before methanol (2 mL) was added. The reaction was complete in 30

minutes as indicated by TLC. After evaporation, the residue was deacetylated by the addition of methanolic ammonia (5 mL) and kept at 0°C for 15 h. The solution was subsequently concentrated to dryness and the residue was applied to a silica gel column using toluene-ethyl acetate (9:1 (v/v)) to give **3** as a syrup (57 mg, 82% yield from **1A**). The α-β ratio in **3** was approximately 1:1. ^{1}H NMR ($CDCl_3$): δ 4.96 (1H, d, $J_{1\alpha,2}$ = 1.7 Hz, $C_{1\alpha}$-H), 4.86 (1H, d, $J_{1\beta,2}$ = 5.0 Hz, $C_{1\beta}$-H), 4.17 (1H, br s, $C_{2\alpha}$-H), 4.11 (2H, m, $C_{3\alpha,\beta}$-H), 4.04 (1H, m, $C_{2\beta}$-H), 3.92-4.00 (2H, m, $C_{4\alpha,\beta}$-H), 3.48 (3H, s, OCH_3-β), 3.42 (3H, s, OCH_3-α), 3.30-3.40 (4H, m, $C_{5\alpha,\beta}$-H, $C_{5'\alpha,\beta}$-H). ^{13}C NMR ($CDCl_3$): δ109.0 ($C_{1\alpha}$), 102.0 ($C_{1\beta}$), 85.1 ($C_{4\alpha}$ and $C_{2\alpha}$), 81.6 ($C_{4\beta}$ and $C_{2\beta}$), 80.9 ($C_{3\alpha}$), 78.6 ($C_{3\beta}$), 55.6 (OCH_3-β), 55.1 (OCH_3-α), 7.9 ($C_{5\beta}$), 6.5 ($C_{5\alpha}$). POSFAB MS *m/z* (%): 275($[M+H]^+$, 3), 243(79), 225(44). *Anal.* Calcd. for $C_6H_{11}IO_4$: C, 26.28; H, 4.01; I, 46.35. Found: C, 26.43; H, 4.13; I, 46.06.

For comparison, **3α** was obtained. ^{1}H NMR ($CDCl_3$)(**3α**): δ 4.97 (1H, s, C_1-H), 4.17 (1H, br s, C_2-H), 4.11 (1H, m, C_3-H), 3.92 (1H, br s, C_4-H), 3.42 (3H, s, OCH_3), 3.39 (2H, m, C_5-H and $C_{5'}$-H). ^{13}C NMR ($CDCl_3$): δ109.0 (C_1), 85.2 (C_4 and C_2), 80.9 (C_3), 55.1 (OCH_3-α), 6.5 (C_5).

^{1}H NMR (CD_3OD) (**3α**): δ 4.76 (1H, d, $J_{1,2}$ = 1.7 Hz, C_1-H), 3.98 (1H, dd, $J_{2,1}$ = 1.7 Hz, $J_{2,3}$ = 3.8 Hz, C_2-H), 3.79 (1H, dd, $J_{3,4}$ = 6.2 Hz, C_3-H), 3.74 (1 H, m, $J_{4,5}$ = 2.6 Hz, C_4-H), 3.45 (1H, dd, $J_{5,5'}$ = 10.6 Hz, C_5-H), 3.36 (3H, s, OCH_3-α), 3.29 (1H, m, $C_{5'}$-H). ^{13}C NMR (CD_3OD): δ110.6 (C_1), 83.9 (C_4), 83.7 (C_2), 82.2 (C_3), 55.4 (OCH_3), 6.5 (C_5).

3.2.1.2. Chemical synthesis from D-(-)-arabinose (61)

Methyl D-arabinofuranoside (62)

The synthesis of **62** was performed according to published procedures[157, 214,215] starting from D-(-)-arabinose **61** (7.0 g, 0.047 mol) in saturated methanolic hydrogen chloride (44 mL) and methanol (140 mL). The reaction was stirred at 25^{0}C for 12 h after which the solution no longer reduced Fehling's solution (absence of reducing sugars). Successive neutralizations with pyridine and subsequent evaporation gave **62** as a light yellow syrup in essentially quantitative yields and was used without further characterizations.

Methyl 5-deoxy-5-iodo-D-arabinofuranoside (3)

To a solution of the anomeric **62** (0.9 g, 5.49 mmol) in dry pyridine (25 mL) was added triphenylphosphine (2.88 g, 10.98 mmol) and iodine (1.40 g, 5.49 mmol) and the resulting solution was heated at 50^{0}C for 1 h. The reaction was quenched with methanol (2 mL) after which the mixture was taken to dryness under vacuum. The residue was chromatographed on a silica gel column. Triphenylphosphine oxide was washed from the column with chloroform, and **3** was subsequently eluted with chloroform-methanol (9:1 (v/v)) to give 1.0 g (67%) of syrup after evaporation of the solvent. It was found to be identical to that prepared in section 3.2.1.1. by TLC and NMR.

3.2.2. Methyl 2,3-di-*O*-acetyl-5-deoxy-5-iodo-α-D-arabinofuranoside (6)

Methyl α-D-arabinofuranoside (62α)

The anomeric **62** (5.0 g, 0.030 mol) was chromatographed on a column containing silica gel (35 mm x 440 mm) using dichloromethane-methanol (19:1 (v/v)). A UV active component was washed from the column and **62α** was subsequently eluted using the same solvent system to give 1.1 g (22% from **62**, 15% from **61**) as a syrup. No crystallization of **62α** was attempted. Literature mp 65-67^{0}C[216]. ^{1}H NMR (CD_3OD): δ 4.74 (1H, d, $J_{1,2}$ = 1.4 Hz, C_1-H), 3.98 (1H, dd, $J_{2,1}$ = 1.4 Hz, $J_{2,3}$ = 3.5 Hz, C_2-H), 3.89 (1H, dd, $J_{4,3}$ = 5.9 Hz, $J_{4,5}$ = 3.3 Hz, C_4-H), 3.82 (1 H, dd, $J_{3,4}$ = 5.9 Hz, $J_{3,2}$ = 3.5 Hz, C_3-H), 3.73 (1H, dd, $J_{5,5'}$ = 11.9 Hz, $J_{5,4}$ = 3.3 Hz, C_5-H), 3.62 (1H, dd, $J_{5',5}$ = 11.9 Hz, $J_{5',4}$ = 5.4 Hz), 3.36 (3H, s, OCH_3). ^{13}C NMR (CD_3OD): δ110.6 (C_1), 85.6 (C_4), 83.4 (C_2), 78.8 (C_3), 63.1 (C_5), 55.2 (OCH_3). These NMR data were found to be in agreement with those reported in literature[217,218].

Methyl 2,3-di-O-acetyl-5-deoxy-5-iodo-α-D-arabinofuranoside (6)

To a solution of **62α** (0.9 g, 5.49 mmol) in dry pyridine (25 mL) was added triphenylphosphine (2.88 g, 10.98 mmol) and iodine (1.40 g, 5.49 mmol) and the resulting solution was stirred at 50^{0}C for 1 h after which the solution was concentrated to dryness. The residue **3α** was purified by column chromatography as described for **3** in section 3.2.1. The anomerically pure **3α** was used for NMR studies (section 3.2.1.1.).

To a solution of **3α** (0.8 g, 2.92 mmol) in dry pyridine (20 mL) was added acetic anhydride (10 mL) and the resulting solution was kept at 25^{0}C for 15 h. Ice (2

mL) was subsequently added to destroy any excess reagent. The solution was concentrated to dryness and the residue was chomatographed on a column containing silica gel using hexane-ethyl acetate (4:1 (v/v)) to give **6** as a syrup (0.72 g, 69%). An anomeric mixture of **6** has been prepared but no NMR data were reported[219]. ^{1}H NMR ($CDCl_3$): δ5.09 (1H, d, $J_{1,2}$ = 1.5 Hz, C_1-H), 4.95 (1H, br s, C_2-H), 4.89 (1H, d, $J_{3,2}$ = 1.4 Hz, $J_{3,4}$ = 5.4 Hz, C_3-H), 4.06 (1H, dd, $J_{4,3}$ = 4.0 Hz, $J_{4,5}$ = 6 Hz, C_4-H), 3.52 (1H, dd, $J_{5,5'}$ = 10.8 Hz, $J_{5,4}$ = 4.8 Hz, C_5-H), 3.43 (1H, dd, $J_{5',5}$ = 10.8 Hz, $J_{5',4}$ = 6 Hz, C_5'-H), 3.41 (3H, s, OCH_3), 2.11 (6H, s, $COOCH_3$). ^{13}C NMR ($CDCl_3$): δ170.2 & 169.7 (2 x C=O), 106.6 (C_1), 81.9 (C_4), 81.3 (C_2), 80.3 (C_3), 54.9 (OCH_3), 20.7 (2 x OAc), 5.0 (C_5). POSFAB MS *m/z* (%): 359($[M+H]^+$, 16), 327(100), 267(46). *Anal.* Calcd. for $C_{10}H_{15}IO_6$: C, 33.52; H, 4.19; I, 35.47. Found: C, 33.72; H, 4.01; I, 35.74.

3.2.3. General procedure for the cleavage reactions 3-6 (section 4.1.1.) and the preparation of 59

To a solution of **1B** (46.4 - 236.4 mg, 0.107 mmol - 0.545 mmol) in glacial acetic acid (0.16 mL - 1 mL) was added acetic anhydride (0.04 mL - 0.25 mL) and the resulting solution was allowed to stir for 9 h - 3 days at 100^{0}C. Ice (1 - 2 mL) was subsequently added to the solution to destroy any excess acetic anhydride. The solution was concentrated to dryness and the residue was chromatographed on a column containing silica gel using hexane-ethyl acetate (4:1 (v/v)) to give **59** as an oily residue (12 - 152 mg, 30-70%). The α anomer predominated its β counterpart by about 8:1. ^{1}H NMR (CD_3OD): δ 6.37 (1H, d, $J_{1\beta\text{-}2}$ = 5.0 Hz, $C_{1\beta}$-H), 6.15 (1H, s, $C_{1\alpha}$-H), 5.25-5.35 (2H, m, $C_{2\beta}$-H & $C_{3\beta}$-H), 5.16 (1H, d, $J_{2,3}$ = 1.4 Hz, $C_{2\alpha}$-H), 4.98 (1H, dd, $J_{3,4}$ = 5.0 Hz, $J_{3,2}$ = 1.4 Hz, $C_{3\alpha}$-H), 4.18 (1H, dd, $J_{4,3}$ = 5.0 Hz, $J_{4,5}$ = 5.1 Hz, $C_{4\alpha}$-H), 4.10-4.15 (1H,

m, $C_{4\beta}$-H), 3.52 (1H, dd, $J_{5,5'}$ = 10.9 Hz, $J_{5,4}$ = 5.1 Hz, $C_{5\alpha}$-H), 3.42 (1H, dd, $J_{5',5}$ = 10.9 Hz, $J_{5',4}$ = 4.7 Hz, $C_{5'\alpha}$-H), 3.30-3.50 (2H, m, $C_{5'\beta}$-H), 2.09-2.11 (18H, 9 x $OCOCH_3$). ^{13}C NMR (CD_3OD): δ169.9, 169.4, 168.8 (3 x C=O, β), 169.7, 169.2, 168.9 (3 x C=O, α), 99.2 ($C_{1\alpha}$), 93.7 ($C_{1\beta}$), 83.4 ($C_{4\alpha}$), 81.5 ($C_{4\beta}$), 80.9 ($C_{2\alpha}$), 79.8 ($C_{3\alpha}$), 77.5 ($C_{2\beta}$), 75.9 ($C_{3\beta}$), 21.0, 20.8, 20.6 (3 x $OCO\underline{C}H_3$, β), 20.9, 20.7, 20.4 (3 x $OCO\underline{C}H_3$, α), 5.5 ($C_{5\beta}$), 4.0 ($C_{5\alpha}$). No further studies were performed with **59**.

3.2.4. General procedure for the deacetylation reactions 1 & 2 (section 4.1.1.) of 59

To a residue of **59** (120 mg, 0.31 mmol) was added methanolic ammonia (20 mL, previously saturated at 0^0C) and the resulting solution was kept at 0^0C for 16 h (Reaction 1) or -20^0C for 8 h (Reaction 2). The solution was concentrated to dryness and the residue was chromatographed on a column containing silica gel using dichloromethane-methanol (19:1, 9:1, 85:15 and 1:1 in reaction 1 (v/v)) or purified by preparative TLC using chloroform-methanol (85:15 (v/v)) to give three major products (11.8 mg, 14.5 mg, 49.6 mg, respectively) which were shown not to be the expected deacetylated product **60** by ^1H and ^{13}C NMR. The formation of **60**, if any, was not observed in these two reactions.

3.2.5. Chemical synthesis of 1-(5-deoxy-5-iodo-α-D-arabinofuranosyl)-2-aminoimidazole (Iodoaminoimidazole arabinoside: IAIA (5))

3.2.5.1. Chemical reduction from AZA (7) and subsequent iodination

1-(α-D-Arabinofuranosyl)-2-aminoimidazole (AIA, 6)

A solution of **7** (100 mg, 0.41 mmol) in 95% ethanol (5 mL) was reduced under 1 atmosphere of hydrogen at 25^0C for 2 h in the presence of palladium on activated carbon (12.2 mg). The mixture was filtered and the filtrate was evaporated to give **6**

(90 mg, 88%) as a residue which was used directly. ^{1}H NMR (D_2O): δ 6.77 (1H, d, J = 2 Hz, C_5-H), 6.48 (1H, d, J = 2 Hz, C_4-H), 5.40 (1H, d, $J_{1',2'}$ = 6 Hz, C_1'-H), 4.33 (1H, t, $J_{2',3'}$ = 6.2 Hz, C_2'-H), 4.06 (1H, m, C_3'-H), 3.99 (1H, m, C_4'-H), 3.66 & 3.56 (2H, m, 2 x C_5'-H). Full characterizations of **6** are provided in section 3.2.5.2.3.

1-(5-Deoxy-5-iodo-α-D-arabinofuranosyl)-2-aminoimidazole (IAIA, 5)

To a solution of **6** (78 mg, 0.36 mmol) in dry pyridine (2 mL) was added triphenylphosphine (221.5 mg, 0.73 mmol) and iodine (185 mg, 0.73 mmol) and the resulting solution was stirred at 25^{0}C for 2 h. The solution was concentrated to dryness and the residue was chromatographed on a column containing silica gel using chloroform-methanol (19:1 (v/v)) to give 47 mg (40%) as an oily residue. ^{1}H NMR (D_2O): δ 6.93 (1H, d, J = 2.6 Hz, C_5-H), 6.74 (1H, d, J = 2.6 Hz, C_4-H), 5.64 (1H, d, $J_{1',2'}$ = 5.2 Hz, C_1'-H), 4.45 (1H, t, $J_{2',3'}$ = 5.5 Hz, C_2'-H), 4.10 (2H, m, $J_{4',5'a}$ = 4.3 Hz, C_3'-H & C_4'-H), 3.43 (1H, dd, $J_{5'a,5'b}$ = 10.0 Hz, $J_{5'a,4}$ = 4.3 Hz, C_5'-H_a), 3.33 (1H, m, $J_{5'b,5'a}$ = 10.0 Hz, $J_{5'b,4}$ = 5.3 Hz, C_5'-H_b). ^{13}C NMR (D_2O): δ 147.2 (C_2), 114.8 (C_4), 113.8 (C_5), 88.8 (C_1'), 83.8 (C_4'), 79.9 (C_2'), 78.7 (C_3'), 6.6 (C_5'). LR (ESI) MS *m/z* (%): 326([M+H]$^+$, 100). HR (ESI) MS ($C_8H_{13}N_3IO_3$): Calcd. mass 326.000168. Exact mass 326.000624.

3.2.5.2. Chemical synthesis from D-(-)-arabinose (61)

3.2.5.2.1. Starting materials

Methyl 2,3,5-tri-O-benzoyl-α-D-arabinofuranoside (63)

The title compound **63** was prepared from D-(-)-arabinose **61** (10.0 g, 0.067 mol) according to published procedures[157,214,215]. Crystalline **63** was obtained from absolute ethanol and was used directly (17.4 g, 54%). Melting point 99-101^{0}C

(Literature mp[214] 100-101.5^{0}C). TLC R_f = 0.39 (hexane-ethyl acetate 4:1 (v/v)). ^{1}H NMR ($CDCl_3$): δ 7.28-8.13 (15H, m, 3 x C_6H_5), 5.58 (1H, d, $J_{3,4}$ = 4.9 Hz, C_3-H), 5.51 (1H, d, $J_{2,3}$ = 1.2 Hz, C_2-H), 5.18 (1H, s, C_1-H), 4.84 (1H, dd, $J_{5,5'}$ = 12.0 Hz, $J_{5,4}$ = 3.4 Hz, C_5-H), 4.69 (1H, dd, $J_{5',5}$ = 12.0 Hz, $J_{5',4}$ = 4.9 Hz, $C_{5'}$-H), 4.57 (1H, dd, $H_{4,5'}$ = 4.9 Hz, $H_{4,5}$ = 3.4 Hz, C_4-H). ^{13}C NMR ($CDCl_3$): δ 165.8-167.0 (3 x C=O), 128.3-133.5 (3 x C_6H_5), 106.9 (C_1), 82.2 (C_4), 80.9 (C_2), 78.0 (C_3), 63.7 (C_5), 55.0 (OCH_3). ^{1}H-^{1}H NOESY ($CDCl_3$): H_4 had cross peaks with methyl protons in OCH_3, confirming its α configuration.

*1-Bromo-2,3,5-tri-O-benzoyl-α-D-arabinofuranose (**64**)*

The sugar bromide **64** was prepared from **63** (1.0 g, 2.10 mmol) in hydrogen bromide-acetic acid (25%) according to published procedures[157,214,215]. Crystalline **64** (475 mg, 43%) was obtained from absolute ether (5 mL) after keeping the ethereal solution in the dark for 15 h at 0^{0}C. TLC indicated a single spot (R_f = 0.38 in ethyl acetate-hexane 3:7(v/v)) with no UV active spots at R_f = 0. (Literature TLC[157] R_f = 0.38 in ethyl acetate-hexane 3:7(v/v)). Melting point 100-102^{0}C (Literature mp[214] 103-104^{0}C). ^{1}H NMR ($CDCl_3$): δ 7.28-8.16 (15H, m, 3 x C_6H_5), 6.63 (1H, s, C_1-H), 5.96 (1H, s, C_2-H), 5.63 (1H, d, $J_{3,4}$ = 4.4 Hz, C_3-H), 4.92 (1H, dd, $J_{5,4}$ = 3.2 Hz, $J_{5,5'}$ = 11.0 Hz, C_5-H), 4.87 (1H, dt, $J_{4,5}$ = 3.2 Hz, $J_{4,5'}$ = 4.4 Hz, C_4-H), 4.78 (1H, dd, $J_{5',5}$ = 11.0 Hz, $J_{5',4}$ = 4.4 Hz, $C_{5'}$-H). ^{13}C NMR ($CDCl_3$): δ 166.0, 165.7, 165.1 (3 x C=O), 128.4-133.8 (3 x C_6H_5), 88.5 (C_1), 85.7 (C_4), 84.6 (C_2), 77.2 (C_3), 62.6 (C_5).

*2-Acetamidoimidazole (**69**)*

To a stirred suspension of finely powdered 2-aminoimidazole sulfate **65** (2.01 g, 15 mmol) in acetic anhyride (20 mL) was added triethylamine (2.5 mL, 18 mmol) and the resulting suspension was stirred at 25^{0}C for 42 h. Absolute ethanol (50 mL) was subsequently added to the resulting clear solution and the ethanolic solution was further stirred at 25^{0}C for 15 min and then under reflux (at 80^{0}C) for 20 h. After evaporation of the solvent, the residue was treated with chloroform (30 mL) to afford crude solids (1.44 g). The mother liquor was concentrated and the resulting syrupy material gave a further 231 mg of crystalline product on standing (total crude yield: 1.67 g, 88%). Recrystallization from 2-propanol (100 mL) gave **69** as light brown needles (1.28 g, 67%). Melting point 238-240^{0}C (Literature mp 287^{0}C[220] and 284-285^{0}C[221]). ^{1}H NMR (CD_3OD): δ 6.77 (2H, s, C_4-H & C_5-H), 2.15 (3H, s, $NHCOCH_3$). TLC R_f = 0.25 in chloroform-methanol 9:1 (v/v). LR (EI) MS *m/z* (%): 125(M^+, 32), 83(100). *Anal.* Calcd. For $C_5H_7N_3O$: C, 47.98; H, 5.65; N, 33.58. Found: C, 48.06; H, 5.64; N, 33.53 (Literature values[221]: C, 48.22; H, 5.50; N, 33.43).

*2-Trifluoroacetamidoimidazole (**66**)*

To a cooled, stirred suspension of finely powdered 2-aminoimidazole sulfate **65** in trifluoroacetic anhydride (10 mL) was added dropwise triethylamine (3.2 mL, 23 mmol). The resulting clear solution was stirred at 25^{0}C for 15 h after which the solution was concentrated to a thick syrup. 2-Propanol (30 mL) was added and the resulting suspension was filtered to give 0.80 g (60%) of milky white solids which were used directly. An analytical sample was prepared by recrystallization in 2-propanol. Melting point 233-235^{0}C. TLC R_f = 0.33 in ethyl acetate-hexane 3:2 (v/v).

^{1}H NMR (CD_3OD): δ6.94 (2H, s, C_4-H and C_5-H). LR (EI) MS *m/z* (%): 179(M^+, 100). HR (EI) MS ($C_5H_4N_3F_3O$): Calcd. mass 179.0306. Exact mass 179.0296.

3.2.5.2.2. Glycosylation reactions

1-(2,3,5 Tri-O-benzoyl-α-D-arabinofuranosyl)-2-acetamidoimidazole (71)

To a stirred suspension of 2-acetamidoimidazole **69** (11 mg, 0.088 mmol) and potassium carbonate (24 mg, 0.17 mmol) in dry acetonitrile (10 mL) under argon was added the sugar bromide **64** (30.5 mg, 0.058 mmol) and the resulting suspension was stirred at 25^{0}C in a sealed reaction flask for 13 h after which a clear solution resulted. TLC indicated the formation of two major products. The solution was allowed to stir at 25^{0}C for an additional 47 h and then under reflux for 3 h. After evaporation of the solvent, the residue was treated with chloroform (20 mL) and the filtered chloroform solution was washed successively with saturated sodium bicarbonate (20 mL) and water (20 mL). The dried solution (Na_2SO_4) was concentrated to give a residue (24 mg) which was purified by preparative TLC using ethyl acetate-methanol (19:1 (v/v)) to give **67** (9 mg, 28%) as a syrup. ^{1}H NMR ($CDCl_3$): δ 7.35-8.11 (15H, m, 3 x C_6H_5), 7.05 (1H, br s, C_5-H), 6.90 (1H, br s, C_4-H), 6.38 (1H, br s, C_1'-H), 6.10 (1H, br s, C_2'-H), 5.72 (1H, br s, C_3'-H), 4.92 (1H, m, C_4'-H), 4.75 (2H, m, 2 x C_5'-H), 2.11 (3H, s, $NHCOCH_3$). ^{13}C NMR ($CDCl_3$): δ 165.0-166.1 (4 x C=O), 128.4-133.8 (3 x C_6H_5, C_2, C_4 & C_5), 90.0 (C_1'), 83.9 (C_4'), 80.4 (C_2'), 77.9 (C_3'), 63.9 (C_5'), 21.0 ($NHCO\underline{C}H_3$). LR (EI) MS *m/z* (%): 569(M^+, 0.43), 105(100). HR (FAB) MS ($C_{31}H_{28}O_8N_3$): Calcd. mass 570.1876. Exact mass 570.1854.

Another product with a higher R_f value was isolated (11 mg, 19%) and confirmed to be *1,3-bis (2,3,5-tri-O-benzoyl-α-D-arabinofuranosyl)-2-acetamido-*

imidazole (72). ^{1}H NMR ($CDCl_3$): δ 7.28-8.04 (30H, m, 6 x C_6H_5), 6.94 (2H, s, C_4-H & C_5-H), 6.60 (2H, s, 2 x C_1'-H), 6.00 (2H, s, 2 x C_2'-H), 5.52 (2H, s, 2 x C_3'-H), 4.78 (2H, m, 2 x C_4'-H), 4.72 & 4.63 (4H, m, 2 x C_5'-H), 1.83 (3H, s, $NHCOCH_3$). LR (FAB) MS *m/z* (%): 1014($[M+H]^+$, 15), 105(100).

1-(2,3,5 Tri-O-benzoyl-α-D-arabinofuranosyl)-2-trifluoroacetamidoimidazole (67)

To a suspension of 2-trifluoroacetamidoimidazole **66** (100 mg, 0.56 mmol) and potassium carbonate (92 mg, 0.67 mmol) in dry acetonitrile (100 mL) was added dropwise a solution of the sugar bromide **64** (295 mg, 0.56 mmol) in dry benzene (30 mL) under argon over a period of 1-1.5 h. The resulting suspension was stirred in the dark at 25^{0}C for 15 h in a sealed reaction flask. After filtration of the gray suspension the solvent was evaporated and the residue was treated with chloroform (30 mL). The filtered solution of chloroform was concentrated to a light yellow foam (371 mg) which was submitted to silica gel HPLC (preparative scale) using dichloromethane followed by dichloromethane-ethyl acetate (97:3 (v/v), flow rate = 6.0 mL/min) to give 152.3 mg (44%) of **67** as a syrup. TLC R_f = 0.56 in ethyl acetate-hexane (1:1 (v/v)). ^{1}H NMR ($CDCl_3$): δ 11.84 (1H, br s, NH), 7.34-8.11 (15H, m, 3 x C_6H_5), 6.96 (1H, d, J = 2.44 Hz, C_5-H), 6.88 (1H, d, J = 2.44 Hz, C_4-H), 6.43 (1H, d, $J_{1',2'}$ = 3.9 Hz, C_1'-H), 6.20 (1H, t, $J_{2',1'}$ = 3.9 Hz, $J_{2',3'}$ = 4.1 Hz, C_2'-H), 5.86 (1H, t, $J_{3',4'}$ = 4.4 Hz, C_3'-H), 5.08 (1H, dt, $J_{4',5'a}$ = 4.9 Hz, $J_{4',5'b}$ = 3.9 Hz, C_4'-H), 4.80 (1H, dd, $J_{5'a,5'b}$ = 12.2 Hz, $J_{5'a,4'}$ = 4.9 Hz, C_5'-H_a), 4.70 (1H, dd, $J_{5'b,5'a}$ = 12.2 Hz, $J_{5'b,4'}$ = 3.9 Hz, C_5'-H_b). ^{13}C NMR ($CDCl_3$): δ 164.3-166.1 (4 x C=O), 149.4 (C_2), 128.3-133.8 (3 x C_6H_5), 112.8 (C_4 & C_5), 89.2 (C_1'), 82.7 (C_4'), 80.8 (C_2'), 77.5 (C_3'), 64.2 (C_5'). LR (FAB) MS *m/z* (%): 624

([M+H]$^+$, 68), 105(100). HR (FAB) MS ($C_{31}H_{25}O_8N_3F_3$): Calcd. mass 624.1594. Exact mass 624.1581.

Another product with a slightly higher R_f value (0.60 in ethyl acetate-hexane 1:1 (v/v)) was isolated (39.5 mg, 7%) and confirmed to be *1,3-bis (2,3,5-tri-O-benzoyl-α-D-arabinofuranosyl)-2-trifluoroacetamidoimidazole (73)*. ^{1}H NMR ($CDCl_3$): δ 7.35-8.10 (30H, m, 6 x C_6H_5), 7.15 (2H, s, C_4-H & C_5-H), 6.71 (2H, $J_{1',2'}$ = 2.45 Hz, 2 x C_1'-H), 5.93 (2H, t, $J_{2',3'}$ = 2.2 Hz, 2 x C_2'-H), 5.64 (2H, t, $J_{3',4'}$ = 2.4 Hz, 2 x C_3'-H), 4.93 (2H, dt, $J_{4',5'a}$ = 5.9 Hz, $J_{4',5'b}$ = 4.9 Hz, 2 x C_4'-H), 4.81 (2H, dd, $J_{5'a,5'b}$ = 11.9 Hz, $J_{5'a,4}$ = 5.9 Hz, 2 x C_5'-H_a), 4.69 (2H, dd, $J_{5'b,5'a}$ = 11.9 Hz, $J_{5'b,4}$ = 4.9 Hz, 2 x C_5'-H_b). LR (FAB) MS *m/z* (%): 1068([M+H]$^+$, 18), 445(100).

3.2.5.2.3. Deprotection reactions

1-(α-D-Arabinofuranosyl)-2-acetamidoimidazole (74)

To a solution of **71** (30.5 mg, 0.054 mmol) in absolute methanol (10 mL) was saturated with NH_3 at 0^0C for 15 min. The resulting solution was kept at 4^0C for 22 h after which the solvent was evaporated. The residue (23 mg) was purified by preparative TLC using chloroform-methanol (7:3 (v/v)) to give **74** (10.1 mg, 73%) as a syrup. TLC R_f = 0.46 in chloroform-methanol (7:3 (v/v)). ^{1}H NMR (CD_3OD): δ 7.33 (1H, s, C_5-H), 6.90 (1H, s, C_4-H), 5.60 (1H, d, $J_{1',2'}$ = 3.9 Hz, C_1'-H), 4.28 (1H, t, $J_{2',3'}$ = 4.4 Hz, C_2'-H), 4.15 (1H, m, $J_{4',5'a}$ = 3.4 Hz, C_4'-H), 4.09 (1H, m, $J_{3',4'}$ = 4.9 Hz, C_3'-H), 3.75 (1H, dd, $J_{5'a,5'b}$ = 12.1 Hz, $J_{5'a,4'}$ = 3.4 Hz, C_5'-H_a), 3.66 (1H, dd, $J_{5'b,5'a}$ = 12.1 Hz, $J_{5'b,4'}$ = 4.9 Hz, C_5'-H_b), 2.13 (3H, s, $NHCOCH_3$). LR (EI) MS *m/z* (%): 257(M^+, 5.5), 43(100).

1-(α-D-Arabinofuranosyl)-2-aminoimidazole (6) (Trial 2, Section 4.4.2.)

To a solution of **74** (1 mg, 0.004 mmol) in absolute ethanol (0.75 mL) was added 1 *N* KOH in D_2O (0.25 mL) and the resulting solution was refluxed for 3 h. The solution was then concentrated to dryness to give **6** (0.5 mg, 50%) as an oily residue. ^{1}H NMR spectrum showed that the acetamide was cleaved. ^{1}H NMR (D_2O): δ 6.81 (1H, s, C_5-H), 6.49 (1H, s, C_4-H), 5.30 (1H, m, C_1'-H), 4.30 (1H, m, C_2'-H), 4.00 (2H, m, C_3'-H & C_4'-H), 3.60 (2H, m, C_5'-H_a & C_5'-H_b). Full characterizations of **6** are given below.

1-(α-D-Arabinofuranosyl)-2-trifluoroacetamidoimidazole (68)

To a solution of **67** (17.3 mg, 0.028 mmol) in absolute methanol (5 mL) was saturated with NH_3 at 0^0C for 10 min. The resulting solution was kept at 25^0C for 15 h after which it was concentrated to dryness. The residue (6 mg) was chromatographed on a column containing silica gel (3 g) using chloroform-methanol (7:3 (v/v)) to give 3.5 mg (42%) of **68** as an oily residue. TLC R_f = 0.59 in chloroform-methanol (7:3 (v/v)). ^{1}H NMR (CD_3OD): δ 7.30 (1H, d, J = 2.44 Hz, C_5-H), 6.97 (1H, d, J = 2.44 Hz, C_4-H), 6.04 (1H, d, $J_{1',2'}$ = 3.9 Hz, C_1'-H), 4.36 (1H, t, $J_{2',3'}$ = 4.4 Hz, C_2'-H), 4.23 (1H, m, $J_{4',5'a}$ = 3.9 Hz, $J_{4',5'b}$ = 4.9 Hz, C_4'-H), 4.14 (1H, t, $J_{3',4'}$ = 4.9 Hz, C_3'-H), 3.76 (1H, dd, $J_{5'a,5'b}$ = 12.0 Hz, $J_{5'a,4'}$ = 3.9 Hz, C_5'-H_a), 3.68 (1H, dd, $J_{5'b,5'a}$ = 12.0 Hz, $J_{5'b,4'}$ = 4.9 Hz, C_5'-H_b). LR (EI) MS *m/z* (%): 311(M^+, 1), 110(100).

1-(α-D-Arabinofuranosyl)-2-aminoimidazole (6) (Trial 5, Section 4.4.2.)

To a solution of **67** (33.3 mg, 0.054 mmol) in absolute methanol (10 mL) was saturated with NH_3 at 0^0C for 10 min. The resulting solution was stored at 25^0C for 18 h after which it was concentrated to dryness. Ammonia water (29%, 10 mL) was

subsequently added to the residue and the aqueous ammonia solution was refluxed for 30 min. The solution was then concentrated to a syrup (19.5 mg) which was chromatographed by reverse-phase HPLC (analytical scale) twice, eluted with water-methanol (1:0, 1:1, 0:1 (v/v), flow rate = 0.6 mL/min, retention time = 11.02-12.09 min) to give **6** (5 mg, 44%) as an oily residue. ^{1}H NMR (D_2O): δ 6.81 (1H, d, J = 1.95 Hz, C_5-H), 6.53 (1H, d, J = 1.95 Hz, C_4-H), 5.43 (1H, d, $J_{1',2'}$ = 6.35 Hz, C_1'-H), 4.36 (1H, t, $J_{2',1'}$ = 6.35 Hz, $J_{2',3'}$ = 6.3 Hz, C_2'-H), 4.08 (1H, t, $J_{3',2'}$ = 6.35 Hz, C_3'-H), 4.01 (1H, m, C_4'-H), 3.68 (1H, dd, $J_{5'a,5'b}$ = 12.7 Hz, $J_{5'a,4'}$ = 2.9 Hz, C_5'-H_a), 3.59 (1H, dd, $J_{5'b,5'a}$ = 12.7 Hz, $J_{5'b,4'}$ = 4.9 Hz C_5'-H_b). ^{13}C NMR (D_2O): δ 150.4 (C_2), 125.0 (C_4), 113.9 (C_5), 87.8 (C_1'), 83.7 (C_4'), 80.1 (C_2'), 75.1 (C_3'), 61.7 (C_5'). LR (FAB) MS *m/z* (%): 216([M+H]$^+$, 69), 185(80), 93(100). HR (FAB) MS ($C_8H_{14}O_4N_3$): Calcd. mass 216.0984. Exact mass 216.0991. ^{1}H-^{1}H COSY, ^{1}H-^{1}H NOESY, NOE correlation studies are reported in section 4.4.2.

^{1}H NMR (CD_3CN): δ 13.68 (2H, br s, NH protons), 6.76 (1H, d, J = 1.47 Hz, C_5-H), 6.48 (1H, d, J=1.47 Hz, C_4-H), 5.40 (1H, d, $J_{1',2'}$ = 5.4 Hz, C_1'-H), 4.27 (1H, t, $J_{2',3'}$ = 4.75 Hz, C_2'-H), 4.07 (1H, t, $J_{3',2'}$ = 5.4 Hz, C_3'-H), 4.02 (1H, m, C_4'-H), 3.69 (1H, dd, $J_{5'a,5'b}$ = 12.2 Hz, $J_{5'a,4'}$ = 2.9 Hz, C_5'-H_a), 3.59 (1H, dd, $J_{5'b,5'a}$ = 12.2 Hz, $J_{5'b,4'}$ = 4.4 Hz C_5'-H_b).

Another product was isolated from reverse-phase HPLC (retention time = 8.48-9.56 min) and its structure was proposed to be the pyranosyl isomer of **6**, *1-(α-D-arabinopyranosyl)-2-aminoimidazole* (**75**). ^{1}H NMR (D_2O): δ 6.90 (1H, br s, C_5-H), 6.69 (1H, br s, C_4-H), 5.52 (1H, d, $J_{1',2'}$ = 5.5 Hz, C_1'-H), 4.39 (1H, m, C_2'-H), 4.10 (2H, m, C_3'-H & C_4'-H), 3.70 & 3.62 (2H, m, 2 x C_5'-H). LR (FAB) MS *m/z* (%): 216

([M+H]$^+$, 100), 185(48), 93(68). HR (FAB) MS ($C_8H_{14}O_4N_3$): Calcd. mass 216.0984. Exact mass 216.0995. ^{1}H-^{1}H COSY, ^{1}H-^{1}H NOESY, NOE correlation studies are reported in section 4.4.2.

^{1}H NMR (CD_3CN): δ 6.89 (1H, d, J = 2.44 Hz, C_5-H), 6.74 (1H, d, J = 2.44 Hz, C_4-H), 5.61 (1H, d, $J_{1',2'}$ = 3.4 Hz, C_1'-H), 4.29 (1H, t, $J_{2',3'}$ = 3.9 Hz, C_2'-H), 4.20 (1H, dd, $J_{4',3'}$ = 4.4 Hz, $J_{4',5'a}$ = 3.4 Hz, $J_{4',5'b}$ = 4.2 Hz, C_4'-H), 4.16 (1H, t, $J_{3',2'}$ = 3.9 Hz, $J_{3',4'}$ = 4.4 Hz, C_3'-H), 3.71 (1H, dd, $J_{5'a,5'b}$ = 12.1 Hz, $J_{5'a,4'}$ = 3.4 Hz, C_5'-H_a), 3.64 (1H, dd, $J_{5'b,5'a}$ = 12.1 Hz, $J_{5'b,4'}$ = 4.2 Hz C_5'-H_b).

1-(5-Deoxy-5-iodo-α-D-arabinofuranosyl)-2-aminoimidazole (IAIA, 5)

The iodination procedures of **6** are identical to those described in section 3.2.5.1.

3.2.6. General procedure for glycosylation reactions with silylation of 2-aminoimidazole derivatives (Reactions 1 & 9, section 4.4.1.)

These glycosylation reactions were modified from published procedures[191]. A suspension of **66** (15 mg, 0.080 mmol) or finely powdered **65** (16.4 mg, 0.116 mmol) in hexamethyldisilazane (1-5 mL) was refluxed for 2.5-3 h after which the excess reagent was evaporated to give an oily residue. A solution of the sugar bromide **64** (30 mg, 0.058 mmol) in dry acetonitrile (10 mL) or dry benzene (20 mL) and mercuric cyanide (28.3-49.6 mg, 0.11-0.196 mmol) were added to the silylated residue and the reaction mixture was refluxed for 12 h. After evaporation of the solvent, the filtered chloroform solution (20-30 mL) was successively washed with 30% potassium iodide solution (20-30 mL), saturated sodium bicarbonate (30 mL) and water (20-30 mL). The dried solution (Na_2SO_4) was concentrated to give a residue (15-27.2 mg) which

was purified by preparative TLC using ethyl acetate-hexane (4:1 or 3:7 (v/v)) to give 6 major products (0.6-4.4 mg, total 15.8 mg) in Reaction 1 and 9 major products (0.8-4.3 mg, total 19 mg) in Reaction 9. These products showed very complex ^{1}H NMR data and were not further studied.

3.2.7. General procedure for glycosylation reactions in dichloromethane (Reactions 7 & 8, section 4.4.1.)

A solution of the sugar bromide **64** (30 mg, 0.058 mmol) in dry dichloromethane (10 mL) was added to a suspension of **69** (21 mg, 0.116 mmol) in dry dichloromethane (50-120 mL) and the resulting suspension was stirred at 25-28^{0}C for 10.5 days (Reaction 7) and 3.5 days (Reaction 8). The solvent was evaporated and the filtered solution of chloroform (10-20 mL) was washed successively with saturated sodium bicarbonate (10-20 mL) and water (10-20 mL). The dried solution (Na_2SO_4) was concentrated to give a syrup (30-50 mg) which was purified by preparative TLC to give 4 major products (1-11.3 mg, total 18.5 mg) in Reaction 7 and 5 major products (0.5-13.2 mg, total 27.8 mg) in Reaction 8. The glycosylation product **67** was isolated in both reactions (4.2 mg, 12% and 8.3 mg, 23%, respectively) and was found to be identical to that obtained in Reaction 6 by ^{1}H NMR.

3.2.8. General procedures for the radioiodination of methyl 5-deoxy-5-[^{125}I]-iodo-D-arabinofuranoside ([^{125}I]-3) and methyl 2,3-di-*O*-acetyl-5-deoxy-5-[^{125}I]iodo-α-D-arabinofuranoside ([^{125}I]-6) in pivalic acid

In a typical radioiodination reaction, no-carrier-added Na[^{125}I]I supplied as a solution in 10 μL of 0.1 *N* NaOH, was diluted to the desired specific concentrations (0.2 MBq for radioiodination trials and 9.2 MBq for biodistribution studies, in 5 μL of aqueous NaOH for both **3** and **6**). The solution was concentrated to dryness in a

1.0 mL Reacti-vial® under a stream of argon gas. A solution of **3** (1.0 mg, 3.6 μmol) or **6** (0.5 mg, 1.4 μmol) in 100 μL of methanol (**3**) or dichloromethane (**6**) was added to the Reacti-vial® and the solvent was subsequently evaporated. A solution of pivalic acid (3 mg, 0.029 mmol for **3** or 1.5 mg, 0.014 mmol for **6**) in methanol (100 μL, **3**) or dichloromethane (100 μL, **6**) was added to the Reacti-vial® and the solvent was again evaporated. The vial was then sealed with a teflon-rubber septum or capped with a Mininert® valve and heated (71-130^{0}C) for 1-3 h at which radioiodine exchange occurred in a pivalic acid "melt"[193].

The contents of the vial were then dissolved in 100 μL of methanol ([^{125}I]-**3**) or dichloromethane ([^{125}I]-**6**). A 1.0 μL sample was analyzed by TLC using chloroform-methanol (85:15 (v/v)) for [^{125}I]-**3** or hexane-ethyl acetate (4:1 (v/v)) for [^{125}I]-**6**. Unlabeled standards of these sugar analogs were used as reference compounds. The plastic-backed TLC plate was covered with transparent Scotch™ tapes and cut into six ([^{125}I]-**3**) or ten ([^{125}I]-**6**) fractions and each part was separately counted for radioactivity in a gamma counter. The radiochemical yield (labeling efficiency) was calculated by dividing the radioactivity on the portion of the plate co-eluting with the "cold" standards (as observed under UV) by the total radioactivity on the TLC plate. The best radiochemical yield obtained for **3** was 92% and that of **6** was 91%.

3.2.9. General procedures for the radioiodination of 1-(5-deoxy-5-[^{125}I]iodo-α-D-arabinofuranosyl)-2-aminoimidazole (Iodo-aminoimidazole arabinoside: IAIA (5))

3.2.9.1. Pivalic acid "melt" method

In a typical radioiodination reaction, no-carrier-added Na[^{125}I]I supplied as a solution in 10 μL of 0.1 *N* NaOH, was diluted to the desired specific concentrations (0.4-0.8 MBq for radioiodination trials in 5-10 μL of aqueous NaOH. The radio-iodination trials were performed in pivalic acid (0.3-5 mg, 0.003-0.048 mmol) and the radiochemical yields were determined as described in section 3.2.8. The best radio-iodination result for 5 was about 46% but it required a reaction time of more than 5 h.

3.2.9.2. Solvent exchange method

In a typical radioiodination reaction for biodistribution studies, no-carrier-added Na[^{125}I]I supplied as a solution in 10 μL of 0.1 *N* NaOH, was diluted to the desired specific concentrations (5.6-9.2 MBq in 10-20 μL of aqueous NaOH). The solution was concentrated to dryness in a 1.0 mL Reacti-vial® under a stream of argon gas. A solution of 5 (0.5-1.0 mg, 1.5-3.1 μmol) in 100 μL of methanol was added to the Reacti-vial® and the solvent was subsequently evaporated. 2-Propanol (100 μL) was added and the vial was capped with a Mininert® valve and heated at 88^{0}C for 2-3.5 h.

The vial was cooled after which the solvent was evaporated. Subsequent determinations of radiochemical yields are described in section 3.2.8. (TLC solvent chloroform-methanol-ammonia (85:15:1 (v/v)). The radiochemical yields averaged about 42% and this method was preferred over the pivalic acid "melt" method.

3.2.10. Purification of methyl 5-deoxy-5-[^{125}I]iodo-D-arabinofuranoside ([^{125}I]-3) and methyl 2,3-di-*O*-acetyl-5-deoxy-5-[^{125}I]iodo-α-D-arabinofuranoside ([^{125}I]-6)

The crude products ([^{125}I]-3 and [^{125}I]-6) were chromatographed on a short column (Pasteur pipette) containing silica gel using dichloromethane-methanol (19:1 (v/v)) for [^{125}I]-3 or hexane-ethyl acetate (4:1 (v/v)) for [^{125}I]-6. Twenty fractions each containing approximately 0.5 mL were collected. Each collected fraction (1 μL) was spotted on a small TLC plate which was then counted for radioactivity by a gamma counter. The fractions containing the most amounts of radioactivity were combined and evaporated to give the purified [^{125}I]-3 or [^{125}I]-6. Radiochemical purity of these compounds was determined by the same TLC method and it was found to be over 99% and 97%, respectively.

3.2.11. Purification of 1-(5-deoxy-5-[^{125}I]iodo-α-D-arabinofuranosyl)-2-aminoimidazole (Iodoaminoimidazole arabinoside: IAIA (5))

The crude product [^{125}I]-5 was purified by reverse-phase Sep-Pak® cartridges (Waters). The cartridge was fitted with a 10-mL syringe in which the added solvent exerted solvent pressure to increase the gravity flow rate. The cartridge was first pre-conditioned with methanol (5 mL) followed by normal saline (5 mL). A solution of [^{125}I]-5 in saline (50 μL) was added to the top of the cartridge through the syringe. The vial was washed further with saline (50 μL) which was combined with the previous saline solution. Saline (9-10 mL) was then added to the syringe as an eluant and to maintain the solvent pressure on the cartridge (flow rate was about 1 mL/min). Twenty fractions each containing approximately 2 mL were collected. Each collected fraction (0.5 μL) was spotted on a small TLC plate which was then counted for

radioactivity by a gamma counter. The fractions containing the most amounts of radioactivity were combined and evaporated to give the purified [^{125}I]-**5**. Its radiochemical purity was determined by the same TLC method (TLC solvent chloroform-methanol-ammonia (85:15:1 (v/v/v)) and it was found to be over 95%.

3.2.12. Animal studies

3.2.12.1. Preparation of the animal model

Murine EMT-6 cells were obtained as a suspension in normal saline from Ms. Haiyan Xia in the Wiebe research group in this faculty, at a concentration of about 1×10^7 cells/mL. The cell suspension (0.1 mL, 1×10^6 cells) was subcutaneously injected into the left flank of each Balb/c mouse briefly anesthetized by inhalation with halothane. The mice were caged in standard plastic cages (5 mice per cage) and maintained with water and rodent food pellets *ad lib*. After 14-16 days, when the tumors reached the desired size of about 300 mg (8 mm diameter), the animals were used for biodistribution studies. The average size of tumors used in this study was about 238 mg.

3.2.12.2. Administration of radiopharmaceuticals

Radiolabeled compounds were stored dry and frozen, and were reconstituted with physiological saline ([^{125}I]-**3**) or 20% ethanol in saline ([^{125}I]-**6**) just prior to injection. In the reconstitution of [^{125}I]-**5**, an appropriate amount of ultra-pure and sterile water was added to the residue to maintain isotonicity of the injected saline solution just prior to injection. For biodistribution studies, each mouse received 0.10-0.15 mL of solution and the radioactivity present was 10-15 kBq (0.3-0.4 μCi)

in [^{125}I]-3 and [^{125}I]-4, and 10-60 kBq (0.3-1.6 μCi) in [^{125}I]-5. Reconstituted radiopharmaceuticals were injected via the dorsal vein in a single bolus injection.

3.2.12.3. Collection of tissue samples

Tissue samples of the mice that received single bolus injections of radiopharmaceuticals were collected by the following general procedure.

The mice were sacrificed by asphyxiation with carbon dioxide (dry ice), followed by cardiac puncture and exsanguination. In addition to the blood, other recovered samples were the brain, heart, lungs, liver, kidneys, spleen, gastrointestinal tract (GIT), stomach, muscle, bone, tumor (when tumor-bearing mice were used), thyroid, skin, and tail. Entire organs of the above samples were dissected and collected into small plastic vials (Beckman Poly-Q™-Vials, 6 mL) and weighed wet using an electronic balance. Stomach and small intestine samples were emptied of their food contents. Other organs were blotted to remove surface blood contamination. The muscle sample was taken from the upper hind leg, and the femur of this leg was removed as a representative bone sample. A skin sample containing fur was taken from the upper back. The thyroid was collected with the trachea attached with surrounding tissues. The remaining carcass was divided into two portions and placed into large counting vials (Beckman Poly-Q™-Vials, 18 mL) and weighed by an electronic balance.

3.2.12.4. Biodistribution studies

B6D2F1/J mice (in [^{125}I]-**3** studies) and Balb/c mice (normal and EMT-6 tumor-bearing) were given i.v. doses of the radioiodinated compounds and were then sacrificed at various time intervals after injection. Biological samples were collected by the procedure described in section 3.2.12.3.

The tissue samples containing iodine-125 were counted in a Beckman Gamma 8000 gamma scintillation counter. The disintegrations per min value (dpm) of each tissue sample was determined in the preset ^{125}I window with correction for background. Dpm values were used for all calculations. Percent injected dose per gram values were calculated by this formula:

$$\% \text{ ID/g} = \frac{\text{Tissue activity (dpm) / Total injected dose (dpm)}}{\text{weight of wet tissue (g)}}$$

The data from three to five animals at each time period were analyzed with the help of an animal distribution computer program. Statistical analyses on these biodistribution data were performed by the Analysis ToolPak in Microsoft® Excel version 5.0.

4. Results and Discussion

4.1. Methyl 5-deoxy-5-iodo-D-arabinofuranoside (3)

4.1.1. Chemistry

The title sugar 3 was synthesized by the procedures described in section 3.2.1. An initial synthetic route to 3 involved chemical cleavage of the N^1-glycosidic bond of two nucleosides: 1-(5-deoxy-5-iodo-β-D-arabinofuranosyl)uracil (58A) and 1-(5-deoxy-5-iodo-α-D-arabinofuranosyl)-2-nitroimidazole (iodoazomycin arabinoside: IAZA, 1A). The hydroxyl groups in these two nucleosides were first protected by acetylation to give the respective diacetylated derivatives (58B and 1B) which were then used for various cleavage reactions (Table 4).

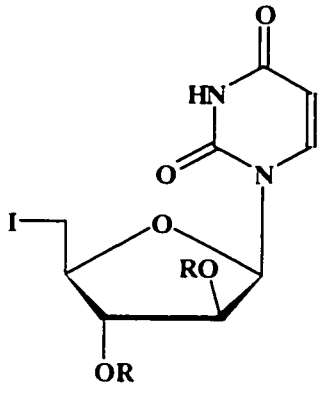

58A R=H
58B R=Ac

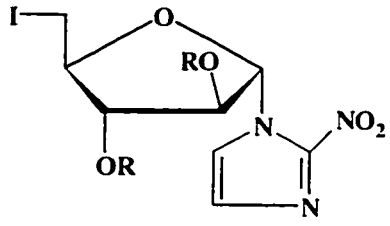

1A R=H
1B R=Ac

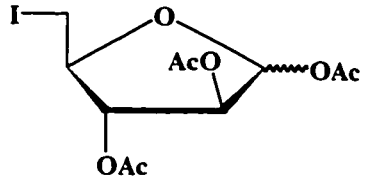

59

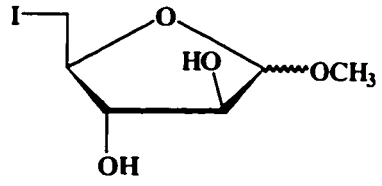

3

Table 4. Cleavage reactions under various reaction conditions.

Cleavage Reaction	*Nucleoside*	*Reaction Conditions*	*Desired Product*	*Cleaved Product Obtained*	*% yield*
1	**58B**	glac. AcOH, 50-80^{0}C, 8 days	**59**	No	N/A
2	**58B**	glac. AcOH, 100^{0}C, 4 days	**59**	No	N/A
3	**1B**	glac. AcOH/ Ac_2O, 100^{0}C, 3 days	**59**	Yes	30%
4	**1B**	glac. AcOH/ Ac_2O, 100^{0}C, 3 days	**59**	Yes	72%
5	**1B**	glac. AcOH/ Ac_2O, 100^{0}C, 12 h	**59**	Yes	71%
6	**1B**	glac. AcOH/ Ac_2O, 100^{0}C, 9 h	**59**	Yes	70%
7	**1B**	$SnCl_4/CH_2Cl_2$ MeOH, 0^{0}C, 30 min	**3**	Yes	90%

Reactions 1 and 2 were attempted with the di-*O*-acetylated uridine derivative **58B**. The desired sugar product of these reactions (**59**) was not obtained in these two reaction trials. The reaction mixtures were found to contain two compounds (as shown by TLC and by ^{1}H NMR) which remained acetylated at the 2' and 3' positions, respectively. There was no evidence (TLC) to suggest the cleavage of the N^1-glycosidic bond and hence the formation of any "free" sugars. When TLC plates were sprayed with a visualization agent such as H_2SO_4/methanol, "free" sugars were

expected to give a positive reaction by appearing as brown color on TLC plates. At the same time these sugars would give little or no UV response on TLC plates. A strong UV signal is expected from any uracil-containing sugar fragments due to the presence of the uracil base. Therefore, a spot on the TLC plate that gives no UV response but turns brown with the visualization agent suggests a cleaved sugar. No such spots were found in these two reactions and, together with confirmation by ^{1}H NMR, it appeared that the N^1-glycosidic bond was not cleaved under these conditions.

The difficulties with the first two cleavage reactions may lie in the relative stability of the N^1-glycosidic bond in **58B**. The presence of a strong electron withdrawing group on the nucleobase could weaken the N^1-glycosidic bond and facilitate chemical cleavage by conventional agents shown in Table 4. The next five reactions were devoted to this investigation. IAZA (**1A**) was chosen as the starting nucleoside for three reasons: (1) it can be obtained relatively easily; (2) it possesses a strong electron withdrawing group (NO_2) on the nucleobase; (3) IAZA is the basis for the hypotheses involving sugar analogs and these cleavage reactions would be analogous to the proposed metabolic pathway *in vivo*.

The target sugar in Reactions 3-6 (**59**) was prepared from **1B** using acetic acid/acetic anhydride at 100^{0}C. The success of these four reactions implied that the introduction of a strong electron withdrawing group could facilitate the cleavage of the N^1-glycosidic bond. Although not studied in detail, the mechanism of cleavage could be protonation on the 2-nitroimidazole base followed by an S_N1 or S_N2 attack on the anomeric carbon by the acetate ion. Since an anomeric mixture was observed, the reaction might have predominately proceeded in S_N1.

In the last reaction the target sugar was the methyl arabinofuranoside 3. To obtain 3 stannic chloride ($SnCl_4$) and methanol were utilized, and very good yields were obtained in a short reaction time (30 min). The first protection step was necessary to protect the reactive hydroxyl groups during base cleavage. This step was quite straightforward and diacetyated IAZA (1B) was isolated in 91% yield. It was then subjected to base cleavage using stannic chloride in dichloromethane. The relative ease of cleavage was probably due to the Lewis acid catalyst, stannic chloride, which helped direct electron density on the 2-nitroimidazole ring to itself and thus weakened the N^1-glycosidic bond. Stannic chloride is known to cleave the N^1-glycosidic bond in nucleosides[222] and it has also been used in glycosylation reactions with different bases[223]. Methanol could then attack the anomeric carbon and form 3 in an anomeric mixture, suggesting an S_N1 mechanism. After deacetylation by methanolic ammonia at 0^0C, 3 was obtained in 90% overall yield (from IAZA, 1A). The synthesis is outlined in Scheme 11.

Scheme 11. Chemical synthesis of 3 from IAZA (1A) by base cleavage.

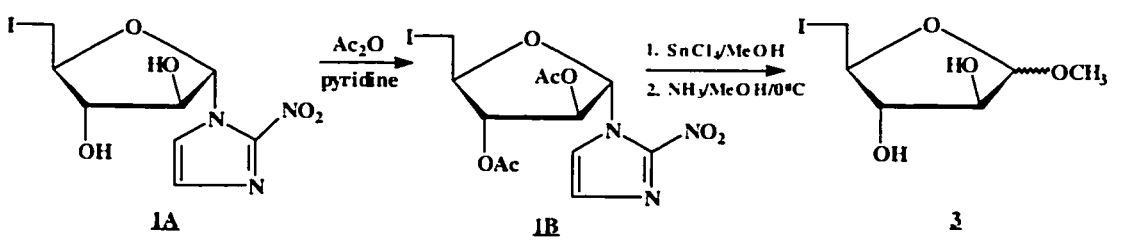

Deacetylation

The results of deacetylation reactions of **59** under standard conditions are listed in Table 5.

Table 5. Deacetylation reactions of 59.

Deacetylation reaction	*Protected sugar*	*Reaction conditions*	*Desired product*	*Fully deacetylated product obtained*
1	**59**	NH_3/MeOH 0^0C, 16 h	**60**	No
2	**59**	NH_3/MeOH -20^0C, 8 h	**60**	No

Scheme 12. Expected deacetylation reaction of 59.

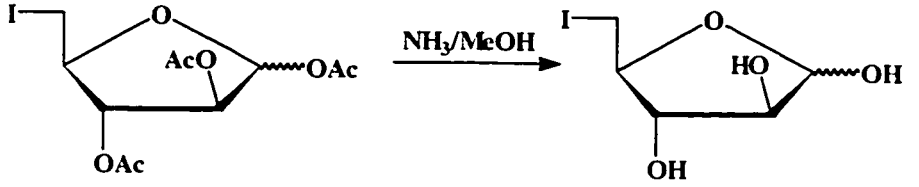

59 **60**

Scheme 12 illustrates the expected deacetylation reaction of **59**. The "free" sugar **60** was not observed (^{1}H NMR) in these two reactions. Presumably **60**, once formed, was chemically unstable and underwent rapid decomposition.

The "free" sugar **60** thus may not be a suitable sugar candidate for biological investigation because of its observed chemical instability in this study. It is also likely to be biologically unstable if it is chemically unstable; enzymatic hydrolysis at the anomeric center and deiodination at the primary carbon atom (C_5) might jointly operate to open the sugar ring, generating an open-chain sugar. The sugar **59** may

however be a suitable precursor or prodrug to deliver **60** in the acetylated form. Although **59** is chemically stable, high levels of esterase (acetylase) activity in blood[152] could rapidly deacetylate **59** and regenerate **60**. By replacing the anomeric acetyl group with a methoxy group to produce **3**, the stability of the "free" sugar (**60**) could be enhanced. Methyl furanosides are known to be chemically stable[224] and their methyl pyranoside counterparts have been used for biological investigations[100,101].

Although this synthetic method from nucleosides provided **3** in high yields, it is not the best method from a chemical viewpoint. This synthetic method involves the degradation of a costly synthetic end product (IAZA, **1A**). Alternatively, **3** can be synthesized from D-(-)-arabinose (**61**). Treatment of **61** with saturated methanolic hydrogen chloride gave the anomeric methyl D-arabinofuranosides (**62**). Iodination with I_2/PPh_3/pyridine afforded **3** in 65% yield from **62** (Scheme 13).

Scheme 13. Chemical synthesis of 3 from D-(-)-arabinose (61).

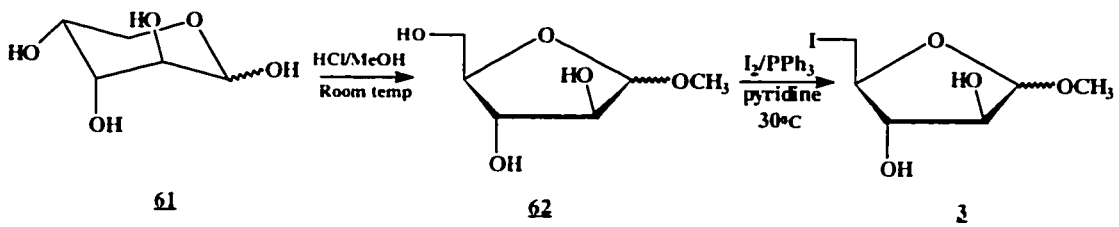

The first step of the synthesis was based on standard procedures[157,214,215]. Since the desired anomeric methyl furanosides **62** were the kinetic products, it was essential to stop the reaction when the reaction solution no longer reduced Fehling's solution (absence of reducing sugars). Otherwise, the reaction would proceed to the thermodynamic products, the anomeric methyl pyranosides. After successive

evaporation with pyridine, the anomeric furanosides were recovered as a syrup in essentially quantitative yields.

The resulting syrup was directly iodinated with iodine-triphenylphosphine-pyridine which is a well-known reagent system for iodination at primary carbons on sugars and nucleosides[1]. The role of pyridine may be similar to the role of imidazole in the triphenylphosphine-iodine-imidazole reagent system[225]. The overall yield of 3 was 67% from 61.

4.1.2. Radioiodination

Scheme 14 shows the two methods of exchange radioiodination of 3 used in this study. Method A employed dimethylformamide (DMF) as the exchange medium while Method B was a "melt" method using pivalic acid[190]. Sixteen radioiodination trials were performed in various reaction conditions (Table 6). Method B was extensively studied and it was found that the best radioiodination condition consisted of 1 mg of 3 and 3 mg of pivalic acid in a "melt" at a temperature of 100^{0}C for 2 h. The labeling efficiency obtained for the crude reaction mixture was close to 92% (Table 6) as detected by TLC.

Scheme 14. Radioiodination of 3.

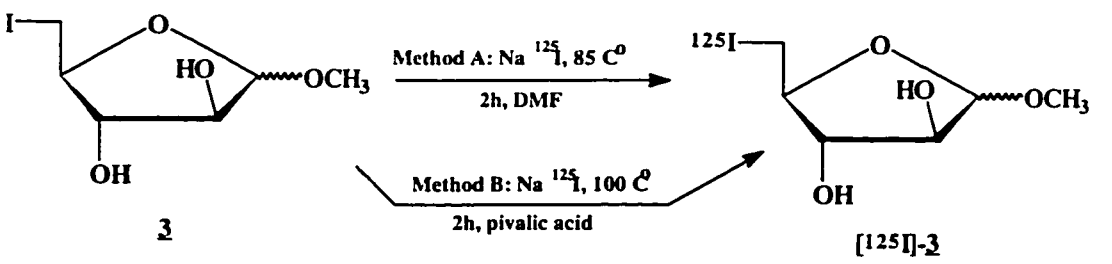

Table 6. Summary of radioiodination results for 3 (1 mg) in DMF (100 μL) or pivalic acid (3 mg).

Radio-iodination Trial	*Reaction Medium*	*Reaction Temp. (^0C)*	*Reaction Time (h)*	*Na[^{125}I]I (MBq)*	*Estimated Specific Activity (MBq/ mmol)*	*Labeling Efficiency (%)*
1	DMF	85	1.0	0.2	27.1	53.1
2	DMF	85	1.5	0.2	36.5	71.5
3	pivalic acid	71	2.0	0.2	28.4	55.5
4	pivalic acid	85	1.25	0.2	41.9	82.0
5	pivalic acid	85	1.5	0.2	40.0	78.3
6	pivalic acid	85	2.0	0.2	44.3	86.6
7	pivalic acid*	85	1.5	0.2	39.0	76.3
8	pivalic acid	100	1.25	0.2	42.6	83.3
9	pivalic acid	100	1.5	0.2	43.3	84.8
10	**pivalic acid**	**100**	**2.0**	**0.2**	**46.8**	**91.6**
11	pivalic acid	115	1.0	0.2	45.1	88.3
12	pivalic acid	115	1.25	0.2	43.6	85.3
13	pivalic acid	115	1.5	0.2	46.0	90.0
14	pivalic acid	115	2.0	0.2	46.6	91.2
15	pivalic acid	130	0.75	0.2	34.0	66.5
16	pivalic acid	130	1.0	0.2	16.0	31.4
17**	pivalic acid	100	2.0	9.3	2340.6**	91.6

*5 mg of pivalic acid was used. **Used in *in vivo* studies.

Early indications (Trials 3-4) suggested that Method B would give higher radioiodination yields of 3 and thus this method was chosen for further investigations. Although solvent exchange in DMF at 85^{0}C for 1.5 h (Method A) gave a lower labeling efficiency (71.5%) than Method B, other reaction conditions might have improved the radioiodination yields. In Method B, a higher reaction temperature correlated positively with radioiodination yields in this study. In general, a longer reaction time was also found to increase the radioiodination yields at 85^{0}C, 100^{0}C, and 115^{0}C.

However, there seemed to be an upper limit to the reaction temperature. At 130^{0}C, the labeling efficiency fell sharply to 31% after 1 h. Based on these observations, the preferred radioiodination condition was chosen at a lower temperature (100^{0}C) which essentially produced the same radioiodination yields as when the temperature was at 115^{0}C.

Figure 4. Radioiodination yields of 3.

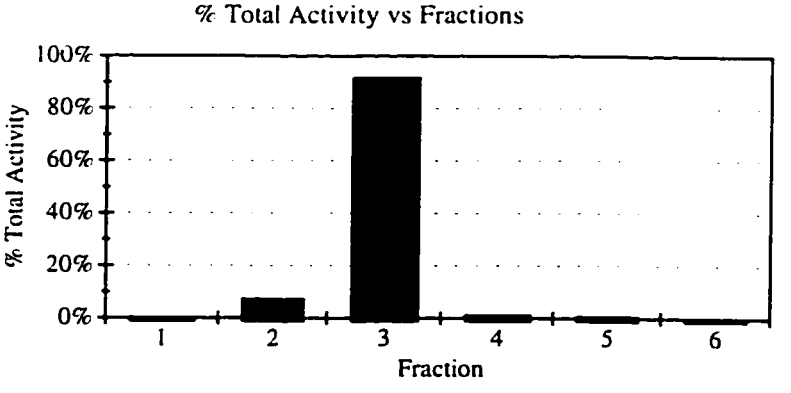

Figure 4 shows that in Trial 10, for example, 92% of the total activity was found on Fraction 3 ([^{125}I]-3). Visualization on TLC plates was enhanced by co-

spotting with the "cold" sugar analog. Figure 5 illustrates the position of various components on the original TLC plate.

Figure 5. Determination of labeling efficiency of [^{125}I]-3 by TLC.

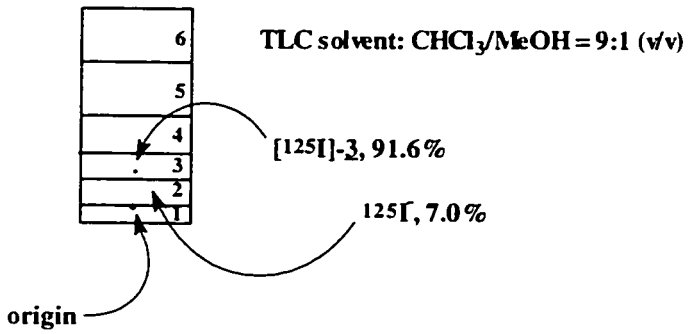

The crude reaction mixture containing the desired [^{125}I]-3 and "free" radio-iodide was separated by column chromatography. Twenty fractions each containing about 0.5 mL were collected and the collection profile was shown in Figure 6.

Figure 6. Column chromatographic purification and collection profile for [^{125}I]-3.

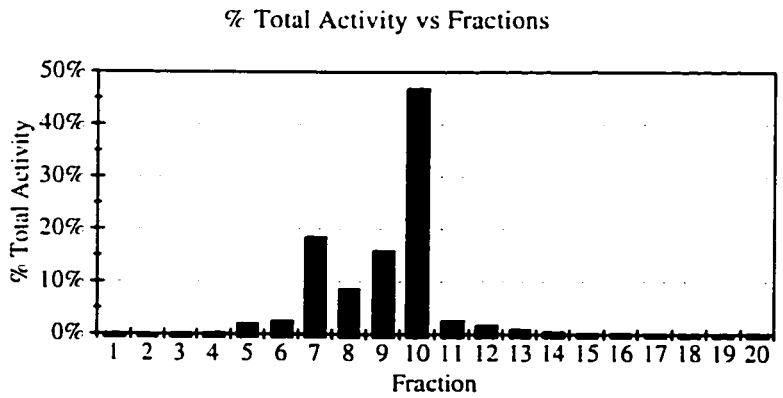

Table 7. Radiochemical purity determination for [^{125}I]-3.

Fraction	*Counts (dpm)*	*Counts-Background (dpm)*	*% Total*
S	966727	966427	99.6%
S'	4305	4005	0.4%
Total		970432	100.0%
Background	300		

Note: Fraction S : Fraction containing [^{125}I]-3
Fraction S': The rest of TLC fractions

The apparent two maxima observed in the collection profile (Figure 6) were probably due to variability in fraction volumes. Fractions 7-13 were subsequently combined and evaporated and the resulting TLC determination indicated that the radiochemical purity of [^{125}I]-3 was > 99%, suggesting that these fractions essentially contained [^{125}I]-3 . The actual amount of radioactivity of radiochemically pure [^{125}I]-3 was determined by successive (three) dilutions of the original reaction vial. After adjustments for counting efficiencies, the amount of radioactivity contained in [^{125}I]-3 was calculated to be 239.4 µCi with an estimated specific activity of 2.3 GBq/mmol.

4.1.3. Biodistribution and elimination

Table 8 shows the *in vivo* biodistribution of [^{125}I]-3 at five time intervals in B6D2F1/J mice. The specific activity of the injected compound was 2-3 GBq/mmol. Each animal received an intravenous bolus injection of 11-15 kBq containing 1-2 μg of [^{125}I]-3. The data are presented as percent injected dose per gram of tissue and as tissue-to-blood ratios of ^{125}I activity.

Table 8. Biodistribution of [^{125}I]-3 following i.v. administration in normal mice at various time intervals.

	Time (Hours)				
Tissue	0.25	0.50	1	2	4
Blood	3.29±0.22	1.35±0.09	1.26±0.13	0.45±0.12	0.23±0.07
Heart	1.67±0.17	0.83±0.18	0.75±0.06	0.23±0.04	0.13±0.02
	0.51±0.02	***0.63±0.17***	***0.60±0.04***	***0.52±0.07***	***0.58±0.06***
Lungs	2.37±0.11	1.40±0.17	1.08±0.10	0.43±0.10	0.20±0.05
	0.72±0.02	***1.05±0.19***	***0.86±0.06***	***0.95±0.04***	***0.91±0.10***
Liver	2.43±0.37	1.40±0.24	1.01±0.12	0.35±0.08	0.18±0.07
	0.74±0.08	***1.05±0.22***	***0.80±0.04***	***0.77±0.07***	***0.77±0.04***
Spleen	1.40±0.11	0.90±0.16	0.72±0.05	0.29±0.06	0.19±0.02
	0.43±0.02	***0.68±0.15***	***0.57±0.04***	***0.66±0.05***	***0.94±0.27***
Kidney	5.72±0.18	2.02±0.39	1.63±0.22	0.44±0.14	0.21±0.06
	1.74±0.12	***1.51±0.36***	***1.29±0.11***	***0.96±0.08***	***0.91±0.08***
Stomach	2.61±0.23	2.70±0.31	2.88±0.76	2.41±0.25	1.28±0.75
	0.79±0.07	***2.03±0.35***	***2.32±0.69***	***5.70±1.72***	***5.30±1.47***
Small Intestine	1.99±0.24	1.26±0.27	1.36±0.36	0.95±0.20	0.58±0.49
	0.61±0.11	***0.95±0.25***	***1.06±0.21***	***2.18±0.52***	***2.21±1.09***
Muscle	1.37±0.05	0.77±0.21	0.47±0.07	0.16±0.03	0.07±0.01
	0.42±0.04	***0.57±0.15***	***0.37±0.02***	***0.36±0.05***	***0.31±0.06***
Skin	1.59±0.08	0.94±0.19	0.80±0.11	0.32±0.10	0.16±0.04
	0.48±0.04	***0.71±0.18***	***0.63±0.08***	***0.71±0.09***	***0.74±0.12***
Bone	1.04±0.23	0.63±0.03	0.54±0.03	0.24±0.06	0.15±0.08
	0.32±0.08	***0.47±0.03***	***0.44±0.05***	***0.54±0.10***	***0.65±0.18***
Brain	0.98±0.05	0.49±0.12	0.40±0.06	0.08±0.02	0.02±0.00
	0.30±0.01	***0.37±0.11***	***0.32±0.03***	***0.17±0.01***	***0.11±0.03***
Carcass	2.88±0.22	1.86±0.28	1.56±0.22	0.88±0.20	0.45±0.12
	0.88±0.02	***1.39±0.25***	***1.24±0.14***	***1.99±0.24***	***2.13±0.81***

The numbers represent the mean ± standard deviation for percent of injected dose per gram of wet tissue for 4 animals, 3 animals for 15 and 30 min.
The numbers in bold italics represent tissue-to-blood ratios.

Table 8 indicates a rapid early distribution of [^{125}I]-3 throughout the body with the brain containing the lowest radioactivity when compared to the rest of the organs. At longer time periods, between 2 and 4 h, brain radioactivity, in terms of percent injected dose per gram, continued to be the lowest in any other organs. These low brain radioactivity data did not appear to suggest any metabolic trapping of [^{125}I]-3 in the normal mouse brain. At 2 h when the brain-to-blood ratio was the highest (0.37), the ratios of other tissues were all higher than that of brain. This precludes practical brain imaging.

Table 9. Thyroid radioactivity as percent injected dose of [^{125}I]-3 per organ in normal mice (n=4 & 3).

Time (Hours)	*Percent injected dose per organ*	*Thyroid radioactivity as percentage of whole-body radioactivity*
0.25	0.28±0.07	0.73±0.15
0.50	0.03±0.02	0.14±0.13
1	0.82±0.17	5.41±1.40
2	0.80±0.90	8.55±9.02
4	1.57±0.74	30.08±10.89

On the other hand, thyroid radioactivity increased steadily as illustrated in Table 9. *In vivo* deiodination appeared to be important in these studies and as much as 30% of radioactivity of the whole body was located in the thyroid at 4 h post injection. This is not surprising because the relatively weak carbon-iodine bond has been known to undergo *in vivo* deiodinations exemplified in the cases of

[^{125}I]IAZR[151,152] and [^{125}I]-IAZA[1]. The thyroid is known to extract and accumulate circulating iodide[226].

The tissue-to-blood ratios (calculated as percent dose per gram of tissue/percent dose per gram of blood) of radioactivity for some selected organs are illustrated in Figures 7 and 8. Early hepatic radioactivity was probably due to the initial metabolism of [^{125}I]-**3** or unmetabolized [^{125}I]-**3** in liver. The exact nature of the metabolite(s), if any, is not known. The sugar **3** is a methyl glycoside with a five-membered sugar ring and an iodine atom on the terminal carbon. It thus no longer resembles a physiological sugar and could probably be metabolized as a xenobiotic by the liver, since the liver is known to play a major role in the metabolism of xenobiotics[227]. Phase 2 conjugation reactions by the liver would render the sugar even more water soluble. This was reflected in the initial high kidney radioactivity, suggesting that the renal route of elimination appeared to be predominant.

The tissue-to-blood ratio was highest (5.3-5.7) for stomach at time periods between 2 and 4 h. Corresponding values for the small intestine were also high (around 2.2) during this two-hour interval. These elevated levels of ^{125}I activity in the stomach and intestine at later time periods are indicative of "free" radioiodide being taken up in organs known to accumulate iodide[226].

The whole-body elimination and blood clearance curves of normal mice are shown in Figure 9. The whole-body elimination curve was constructed by summing radioactivity in all organs dissected for biodistribution studies plus the radioactivity in the remaining carcass. Whole blood radioactivity was calculated from an aliquot taken at the time of sacrifice, assuming blood to be 6.5% of the total body weight.

Figure 7. Tissue-to-blood ratios of radioactivity at various time intervals following i.v. administration of [^{125}I]-3 in normal mice.

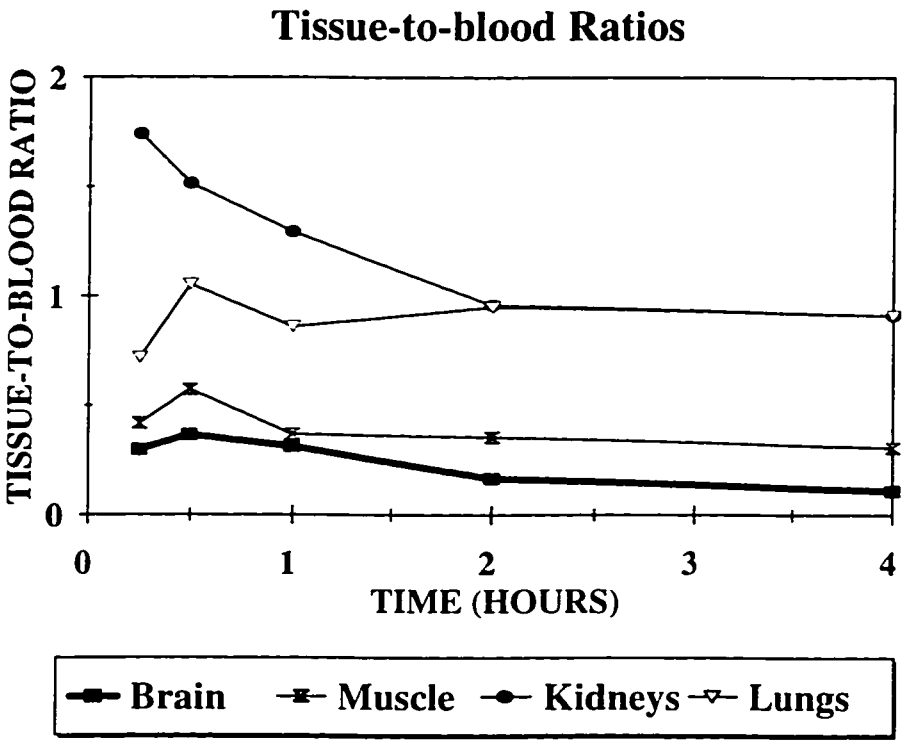

Figure 8. Tissue-to-blood ratios of radioactivity at various time intervals following i.v. administration of [^{125}I]-3 in normal mice.

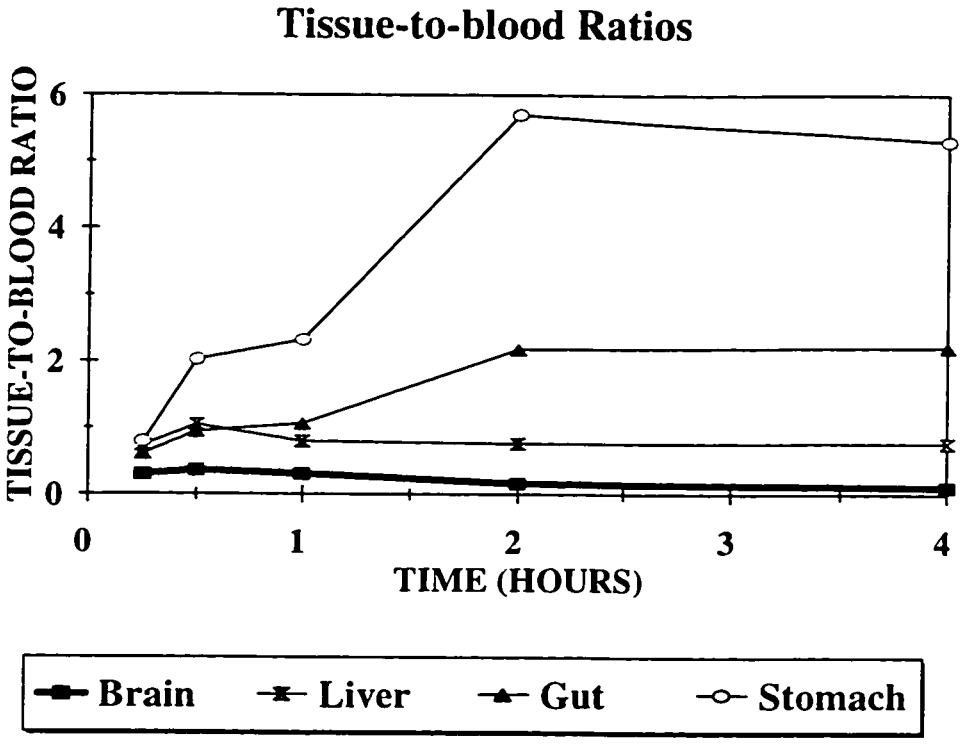

Figure 9. Whole-body elimination and blood clearance of radioactivity following i.v. administration of [^{125}I]-3 in normal mice.

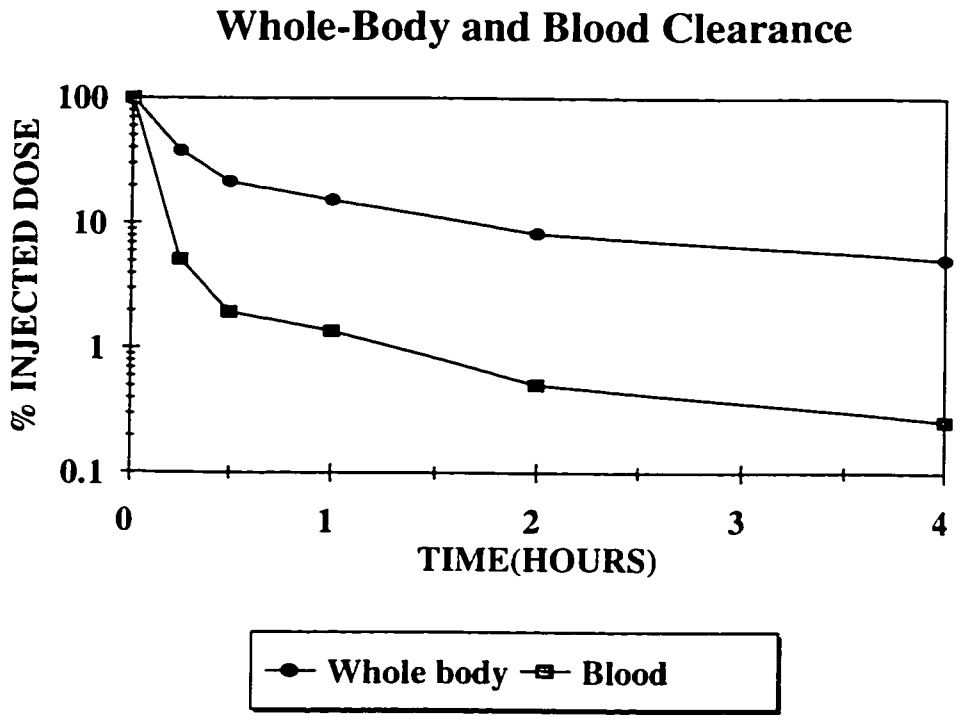

Whole-body and blood radioactivity clearance data show similar initial rapid decline in radioactivity and the elimination was likely to be biphasic. More than 60% of whole-body and 95% of blood radioactivity were eliminated by 15 min post injection. This was followed by slower clearance up to 2 h in the whole body. Between 2 and 4 h the whole-body clearance pattern was similar to that in blood clearance.

The amount of radioactivity remaining in blood and the whole body at 4 h were 0.26% and 5.13% of the injected dose, respectively. Compared with the corresponding values of about 1.0% and 20% of the injected dose at 4 h for [^{125}I]IAZA[1], the values for [^{125}I]-3 were much smaller. The sugar analog 3 was cleared four to five times faster from whole body and blood than the corresponding 2-nitroimidazole nucleoside.

Because of the observed low brain-to-blood ratios for [^{125}I]-3 (< 0.5), brain tissue imaging would not be possible. These biodistribution data with [^{125}I]-3 thus could not explain the abnormal radioactivity in the brains of [^{123}I]IAZA patients.

4.1.4. Stability

The radiochemical stability of [^{125}I]-3 at 4^{0}C in saline was monitored over a ten-month period. The radiochemical purity of [^{125}I]-3 generally decreased with time in this stability study. By the end of the second 5-month period, its radiochemical purity had dropped below 90% (Table 10). "Free" radioiodide was generally detected as a radioactive impurity in addition to other minor active components.

Table 10. Radiochemical stability assessment for [^{125}I]-3.

Date of determination	*Number of months*	*Radiochemical purity (%)*	*% "free" radioiodide*	*% other impurities*
Aug 22, 1994	0	99.6	0.4	0.0
Sep 21, 1994	1	99.0	0.6	0.4
Oct 31, 1994	2	95.5	2.9	1.6
Jan 23, 1995	5	97.7	0.0	2.3
Jun 09, 1995	10	89.1	3.6	7.3

4.2. Methyl 2,3-di-*O*-acetyl-5-deoxy-5-iodo-α-D-arabinofuranoside (4)

4.2.1. Chemistry

The title sugar 4 was synthesized from the anomerically pure furanoside (62α) followed by iodination and acetylation (Scheme 15). The preparation of 62 was identical to that previously described for the synthesis of 3 in section 4.1.1. The anomeric furanoside 62 was chromatographed on a column containing silica gel and eluted with dichloromethane. The α anomer was first eluted from the column and recovered as a syrup (47% from 61).

Scheme 15. Chemical synthesis of 4 from D-(-)-arabinose (61).

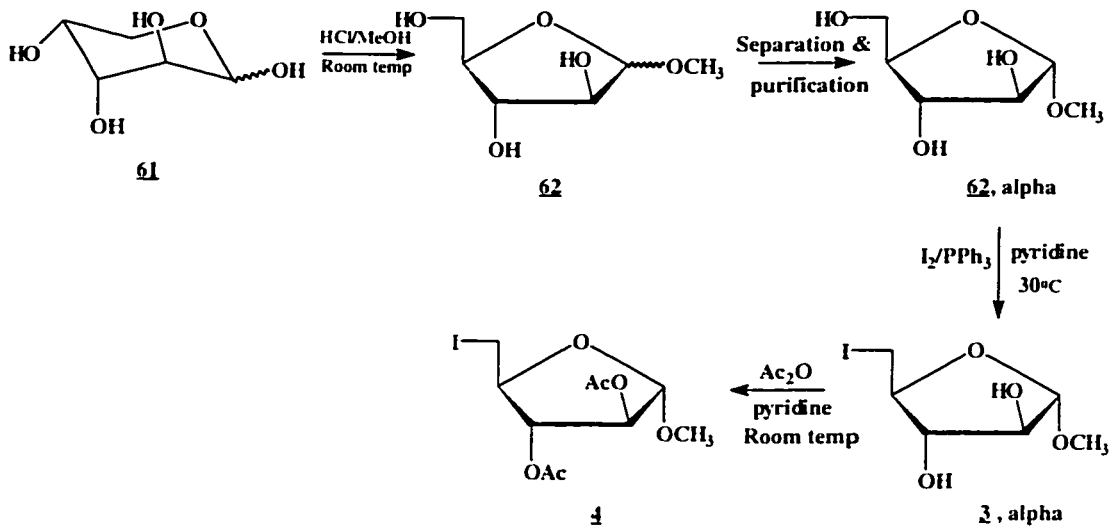

Iodination was readily achieved by the I_2/PPh_3/pyridine reagent system. Another iodination method, which consists of the *N*-iodosuccinimide (NIS)/PPh_3/DMF reagent system, was explored as an alternative to the former iodination reagent system. The NIS/PPh_3/DMF reagent system is known for the direct replacement of primary hydroxyl groups in the presence of secondary hydroxyl groups[228]. Subsequent acetylation with acetic anhydride in pyridine gave 4 (Table 11).

Table 11. Iodination and acetylation reactions for α-62.

Starting compound	*Iodination reagent/ Reaction conditions*	*Percent yield (%)*	*Acetylation reagent/ Reaction conditions*	*Percent yield (%)*
α-62	I_2/PPh_3/pyridine 50°C, 1 h	67%	Ac_2O/pyridine 25°C, 15 h	61%
α-62	NIS/PPh_3/DMF 50°C, 6 h	not isolated	Ac_2O/pyridine 25°C, 15 h	17%

The I_2/PPh_3/pyridine reagent system appeared to be superior in the preparation of 4. The reason for the poor yields obtained with the NIS/PPh_3/DMF reagent system was not investigated in details, although a shorter reaction time might minimize product decomposition. The rationale for prolonged reaction times came from the observation from TLC plates indicating little or no disappearance of the starting sugar α-62. At the end of the reaction time, TLC indicated a complex mixture of compounds. Furthermore, difficulties with evaporating the non-volatile DMF also complicated subsequent work-up procedures. Iodination with I_2/PPh_3/pyridine was thus selected to be the preferred iodination reagent system.

The overall yield of the anomerically pure (α) iodinated, di-*O*-acetylated sugar analog 4 was about 20% from 61.

4.2.2. Radioiodination

Scheme 16 shows the desired method of exchange radioiodination of 4 using the pivalic acid "melt" method as described in section 4.1.2. Nine radioiodination trials were performed to determine the optimum radioiodination condition (Table 12). The best radioiodination condition employed 0.5 mg of 4 and 1.5 mg of pivalic acid in

a "melt" with a temperature of 78^{0}C for 3 h. The labeling efficiency obtained for the crude reaction mixture was close to 91% as detected by TLC.

Scheme 16. Radioiodination of 4.

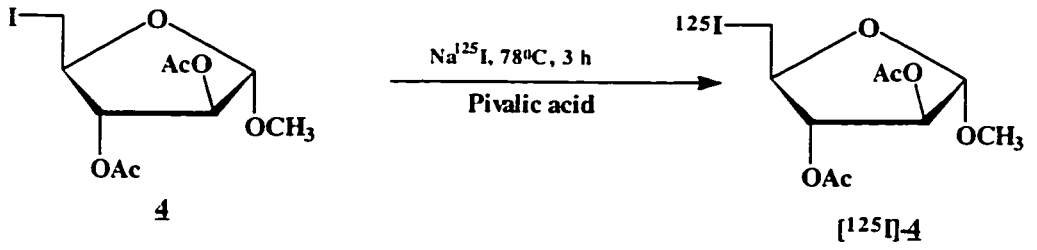

Table 12. Summary of radioiodination results for 4 (0.5 mg) in pivalic acid (1.5 mg).

Radio-iodination Trials	*Reaction Medium*	*Reaction Temp. (^{0}C)*	*Reaction Time (h)*	*Na[^{125}I]I (MBq)*	*Estimated Specific Activity (MBq/ mmol)*	*Labeling Efficiency (%)*
1	pivalic acid	80	1	0.2	105.7	80.0
2	pivalic acid	80	2	0.1	167.6	85.2
3	**pivalic acid**	**78**	**3**	**0.2**	**120.2**	**91.0**
4	pivalic acid	93	1	0.2	105.5	79.8
5	pivalic acid	90	2	0.2	107.6	81.4
6	pivalic acid	100	0.5	0.2	82.2	62.2
7	pivalic acid	100	2	0.2	92.5	70.0
8	pivalic acid	100	3	0.2	31.8	24.1
9	pivalic acid	122	2	0.2	20.5	15.5
10*	pivalic acid*	78	3	13.4	2180.4**	91.0

*2 mg of 4; 3 mg of pivalic acid. **Used in *in vivo* studies.

The labeling efficiency of 4 seemed to increase with longer reaction times. At 80^0C, labeling efficiency was highly correlated with a longer reaction time in this study. Increasing the temperature further, however, appeared to disrupt this correlation. At 100^0C, the labeling efficiency generally decreased with reaction times. At 122^0C, the labeling efficiency fell sharply to 15.5%.

In contrast to the radioiodination results of 3, reaction temperature was negatively correlated with radioiodination yields in this study. This different effect of reaction temperature on 3 and 4 was not investigated in details, although the presence of the two acetyl groups on the latter compound could make it chemically more unstable in acidic conditions at higher temperatures.

The labeling efficiencies were determined by TLC as previously described. Figure 10 shows that 91% of the total radioactivity was found on Fraction 4 ([^{125}I]-4). Figure 11 illustrates the position of various components on the original TLC plate.

Figure 10. Radioiodination results for 4.

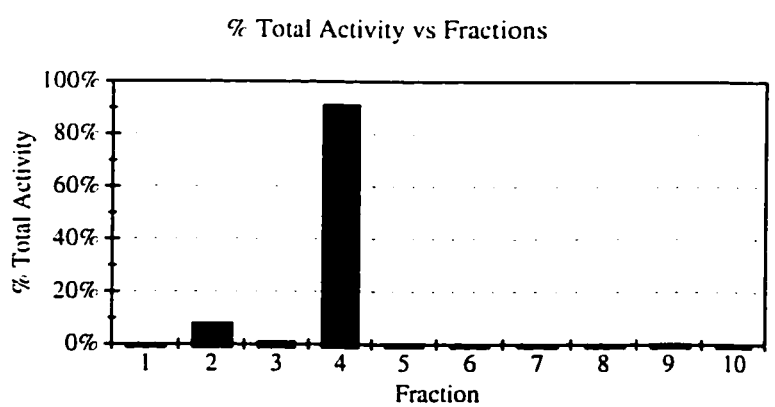

Figure 11. Determination of labeling efficiency of [^{125}I]-4 by TLC.

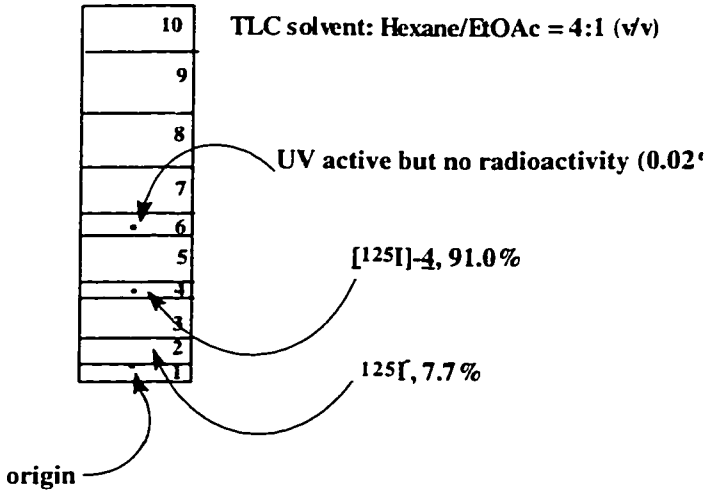

As Figure 11 illustrates, there was a UV visible spot on Fraction 6 containing no radioactivity. The identity of this compound formed during radioiodination was not determined, nor was the mechanism of its formation investigated. Presumably this compound was produced during the decomposition of 4 because the two acetyl groups could become unstable when heated for prolonged time periods (e.g. 3 h in Trial 3). Since the decomposed product contained no radioactivity, it did not affect subsequent purification steps and was not further investigated.

The crude reaction mixture containing the desired [^{125}I]-4 was separated by column chromatography. The purification was performed in two runs to ensure maximal chromatographic yields, since earlier purification attempts with [^{125}I]-4 had been more difficult than its non-acetylated counterpart 3. In each run, twenty fractions each containing approximately 0.5 mL were collected (Figures 12 and 13).

Figure 12. Collection profile for [^{125}I]-4 (Run 1).

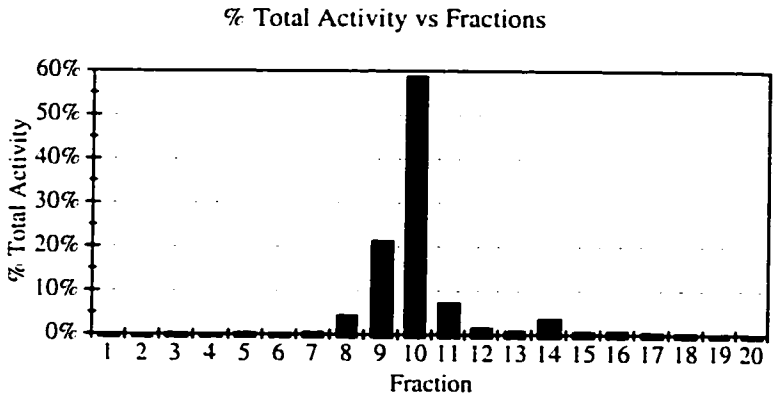

Figure 13. Collection profile for [^{125}I]-4 (Run 2).

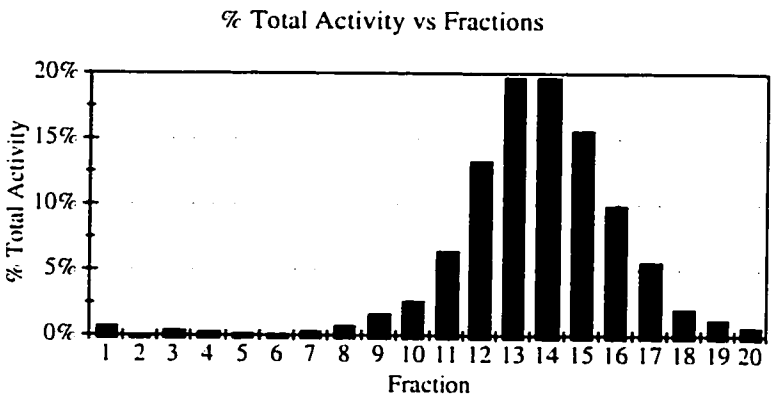

In Run 1, Fractions 9-11 were combined and evaporated and the resulting TLC determination indicated that the radiochemical purity of [^{125}I]-4 was >98%. After adjustments for counting efficiency, the amount of radioactivity contained in [^{125}I]-4 in Run 1 was estimated to be 129 μCi.

In Run 2, Fractions 12-17 were combined and evaporated and the resulting TLC determination showed that the radiochemical purity of [^{125}I]-4 was >97%. The amount of radioactivity contained in [^{125}I]-4 in Run 2 was found to be 117 μCi. The total estimated radioactivity was about 246 μCi.

The two purified products were combined and the radiochemical purity of the resultant mixture was assessed by TLC. The final radiochemical purity of [^{125}I]-4 was determined to be about 97% (Table 13) and the total amount of radioactivity was 229 μCi. Its specific activity was estimated to be 2.2 GBq/mmol.

Table 13. Radiochemical purity determination for [^{125}I]-4.

Fraction	*Counts (dpm)*	*Counts-Background (dpm)*	*% Total*
S	214411	214354	96.75%
S'	7249	7192	3.25%
Total		221546	100.00%
Background	57		

Note: Fraction S : Fraction containing [^{125}I]-4
Fraction S': The rest of TLC fractions

4.2.3. Biodistribution and elimination.

Table 14 shows the *in vivo* biodistribution of [^{125}I]-4 at two time intervals in normal Balb/c mice. The specific activity of the injected compound was 2.1-2.2 GBq/mmol. Each animal received an intravenous bolus injection of 10-13 kBq containing 2-3 μg of [^{125}I]-4. The data are presented as percent injected dose per gram of tissue and as tissue-to-blood ratios of ^{125}I activity.

Table 14. Biodistribution of [^{125}I]-4 following i.v. administration in Balb/c mice at two time intervals.

	Time (Hours)	
Tissue	0.25	4
Blood	4.50±1.99	0.32±0.13
Heart	3.14±1.02	0.15±0.05
	0.74±0.09	***0.48±0.08***
Lungs	3.85±1.34	0.24±0.11
	0.89±0.09	***0.76±0.06***
Liver	3.99±1.09	0.23±0.11
	0.96±0.18	***0.67±0.14***
Spleen	2.75±0.89	0.19±0.09
	0.64±0.08	***0.60±0.13***
Kidney	7.40±2.25	0.26±0.11
	1.75±0.33	***0.80±0.07***
Stomach	3.07±0.65	1.59±0.60
	0.79±0.30	***5.09±0.65***
Small Intestine	3.84±1.04	0.40±0.19
	0.96±0.32	***1.24±0.18***
Muscle	2.50±0.64	0.17±0.09
	0.61±0.12	***0.50±0.11***
Skin	2.64±0.86	0.28±0.12
	0.61±0.10	***0.87±0.08***
Bone	1.73±0.76	0.18±0.11
	0.42±0.15	***0.56±0.22***
Brain	2.77±0.86	0.05±0.02
	0.66±0.10	***0.16±0.03***
Carcass	2.50±0.76	0.31±0.13
	0.59±0.08	***0.97±0.15***

The numbers represent the mean±standard deviation for percent of injected dose per gram of wet tissue for 5 animals (4 h) and 4 animals (15 min).
The numbers in bold italics represent tissue-to-blood ratios.

Table 14 reveals a rapid early distribution of [^{125}I]-4 throughout the body with brain radioactivity comparable to the rest of the organs, especially muscle, stomach and spleen. At 0.25 h post injection, brain radioactivity, in terms of percent injected dose per gram, was about 2.77 which was almost three times higher than that obtained in [^{125}I]-3 (t = 3.59, p = 0.0370). The two-sample t-test was used to analyze the biodistribution data, and a sample calculation of a t-test is given in Appendix 2. The brain-to-blood ratio at this early time interval was 0.66 and its difference from [^{125}I]-3 was statistically significant (t = 6.05, p = 0.0090). At 4 h post injection, brain radioactivity data for [^{125}I]-4 was 0.05% injected dose per gram with a brain-to-blood ratio of 0.16. Furthermore, at 4 h no real differences could be inferred on brain radioactivity between [^{125}I]-3 and [^{125}I]-4 in both dose per gram values (t = 2.49, p = 0.067) and brain-to-blood ratios (t = 2.21, p = 0.0695). These observations suggested that the brain-to-blood ratios in [^{125}I]-4 were also insufficient to effect brain tissue imaging.

There was little evidence to support that differences in thyroid radioactivity in [^{125}I]-3 and [^{125}I]-4 were significant. Table 15 shows that at 0.25 h, thyroid radioactivity (dose per organ) for both compounds were similar in magnitude (t = -1.16, p = 0.298); in terms of percent whole-body radioactivity, a similar inference could be made (t = 0.44, p = 0.678). Thyroid radioactivity reached a maximum of only 11.7% of the total body radioactivity at 4 h, compared to 30% in [^{125}I]-3 (t = 3.19, p = 0.033). In [^{125}I]-4, strong evidence for *in vivo* deiodination was also observed in percent whole-body radioactivity of thyroid at 0.25 and 4 h (Table 15).

Table 15. Thyroid radioactivity as percent injected dose of [^{125}I]-4 per organ in normal mice (n=4).

Time (Hours)	*Percent injected dose per organ*	*Thyroid radioactivity as percentage of whole-body radioactivity*
0.25	0.35±0.08	0.66±0.24
4	0.67±0.02	11.69±4.20

At 0.25 h post injection, radioactivity in all organs (dose per gram values), were generally higher in the studies with [^{125}I]-4 than in [^{125}I]-3. This reflected the higher lipophilicity of [^{125}I]-4 where the two acetyl groups would likely to enable the sugar analog to more efficiently diffuse across cell membranes. At 4 h, the dose per gram values of these organs were, however, very similar in magnitude to those in [^{125}I]-3. For both sugars, less than 0.4% of the injected dose remained in the blood after 4 h. In both cases, the stomach-to-blood ratios were between 5.1-5.3 (t = -0.23, p = 0.827), providing the physiological evidence for "free" radioiodide and hence *in vivo* deiodination. Early hepatic and renal tissue-to-blood ratios were also similar in magnitude for both sugars and may suggest the role of hepatobiliary and renal clearance respectively (liver: t = 1.96, p = 0.122; kidney: t = 0.045, p = 0.966). Despite making the sugar more lipophilic through the acetylation of the arabinofuranosyl hydroxyl groups on [^{125}I]-3, renal excretion did not appear to be significantly delayed, nor was the brain radioactivity sufficiently increased or trapped. Similar experiments using a more lipophilic derivative have been reported with IAZR (44). In their study, Jette *et al.*[152] suggested that the ineffective attempts to delay renal clearance of [^{131}I]IAZR (44) by acetylation was probably due to the high levels of

esterase (acetylase) activity in blood. This high level of esterase activity in blood could possibly account for similar results obtained with [^{125}I]-4 in this mouse model.

Table 16. Whole-body elimination and blood clearance data for [^{125}I]-4.

Time post injection (hours)	*Percent body dose*	*Percent blood dose*
0.25	59.09±19.80% ***37.97± 1.37%****	5.96 ± 2.65% ***5.14 ± 0.24%***
4	6.33 ± 2.24% ***5.13 ± 1.04%***	0.42 ± 0.17% ***0.26 ± 0.06%***

****The numbers in bold italics represent the corresponding values for [^{125}I]-3.***

Based on the percent body dose and percent blood dose data at 0.25 h, there was no strong statistical evidence to suggest that [^{125}I]-4 was cleared more slowly than [^{125}I]-3 (body dose: t = -1.84, p = 0.163; blood dose: t = -0.533, p = 0.63). At 4 h, these values for the sugars were also comparable (body dose: t = -0.94, p = 0.38; blood dose: t = -1.76, p = 0.139). Presumably the high esterase activity in blood efficiently deacetylated [^{125}I]-4 and regenerated the more polar [^{125}I]-3 in an anomerically pure form.

These biodistribution data provided no evidence to suggest any brain uptake of radioactivity for [^{125}I]-4; its low brain-to-blood ratios and generally high background in various organs would render practical brain tissue imaging very difficult.

4.2.4. Stability

The radiochemical stability of [^{125}I]-4 in saline was very poor. A summary of tests performed on samples of [^{125}I]-4 in saline, 10% DMSO in saline, and 20% EtOH in saline is shown in Table 17. In saline, the radiochemical purity of [^{125}I]-4 ranged from 62 to 86% which was not acceptable for biodistribution studies. Since [^{125}I]-4

contains two acetyl groups which make it more lipophilic, solubility and radiochemical stability in saline were expected to be lower. A saline solution containing small amounts of an organic solvent could be an alternative to overcome this solubility problem. Indeed, by adding 10% (v/v) dimethyl sulfoxide (DMSO) in saline, the radiochemical stability increased to about 80% (Table 17).

Table 17. Radiochemical stability of [^{125}I]-4 in saline, 10% DMSO in saline and 20% EtOH in saline.

Trial	*Storage conditions*	*Radiochemical purity (%) of[^{125}I]-4*	*% radioiodide*	*% major decomposition product*
1	4^{0}C, 18-24 h, 10 min sonication, saline	85.8	7.1	7.1
2	10 min sonication, saline	79.2	5.4	5.9
3	4^{0}C, 2 days, saline	62.1	13.4	12.4
4	10% DMSO in saline, 10 min sonication	81.4	4.6	6.2
5	20% EtOH in saline, 10 min sonication,	95.2	4.1	0.1
6	sample from 5, stored at 4^{0}C for 1 week	88.2	8.8	2.0
7	sample from 5, stored at 4^{0}C for 5 months	87.5	7.9	3.0

To further increase the radiochemical stability of [^{125}I]-4, 20% ethanol (v/v) was added to saline. Twenty percent is the maximum limit of ethanol that can be added in saline with no major physiological effect to the animal following injection. Greater than 95% radiochemical purity was obtained if the resulting saline/ethanol solution was immediately used for animal injection (Table 17). When the solution was stored at 4 ^{0}C for 1 week or up to 5 months, the radiochemical purity determined thereafter was around 88%, which was still higher than that in 10% DMSO in saline, or in plain saline. These observations confirmed that 20% EtOH in saline was a suitable solution medium for animal injection.

4.3. 1-(5-Deoxy-5-iodo-α-D-arabinofuranosyl)-2-aminoimidazole (Iodoamino-imidazole arabinoside: IAIA (5))

4.3.1. Chemistry

The title 2-aminoimidazole nucleoside 5 was synthesized by two methods. The first method involved the chemical reduction of AZA (7) with hydrogen in the presence of palladium-carbon to give AIA (6) in 88% yield. Subsequent iodination with iodine-triphenylphosphine-pyridine afforded 5 in 40% yield (Scheme 17).

Scheme 17. Chemical synthesis of IAIA (5) from AZA (7).

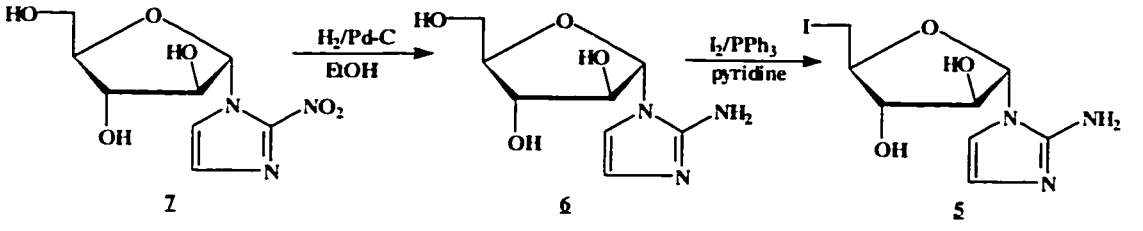

The second synthetic method started from commercially available D-(-)-arabinose (61) and proceeded in numerous steps to the final desired nucleoside IAIA (5) . The glycosylation reaction and the problems associated with it were studied in detail (see section 4.4). Scheme 18 shows the preferred route for the synthesis of 5.

The preparation of methyl 2,3,5-tri-*O*-benzoyl-α-D-arabinofuranoside (63) was performed according to standard procedures[157,214,215]. The crystalline 63 was isolated in 54% yield from 61. The sugar bromide 64 was prepared by the HBr/HOAc method according to the same published procedures[157,214,215]. ^{1}H NMR showed that crystalline 64 was pure and stable for months at -20^{0}C. After a series of trial reactions, the best protecting group on 2-aminoimidazole sulfate (65) for glycosylation was found to be the trifluoroacetyl group.

Scheme 18. Chemical synthesis of IAIA (5) from D-(-)-arabinose (61).

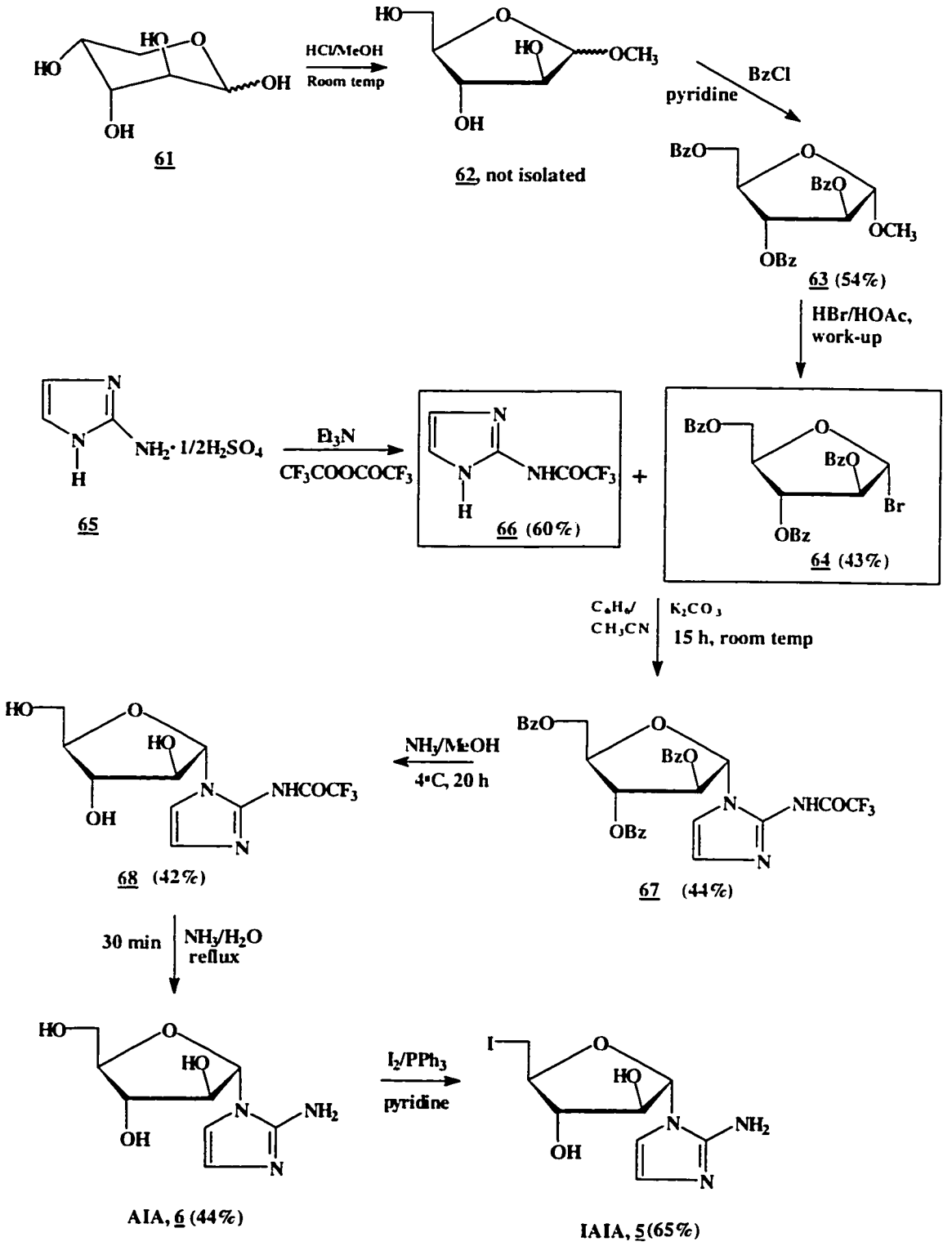

Because of the electron-withdrawing fluorine atoms, the trifluoroacetamide is expected to be more easily cleaved than its acetamide counterpart.

The glycosylation between **64** and **66** was conducted in a mixed solvent system ($CH_3CN:C_6H_6$ = 10:3 (v/v)) in the presence of potassium carbonate for 15 h at room temperature. Potassium carbonate probably functioned as a solid acid acceptor similar to the role of molecular sieves[171]. This base-catalyzed approach eliminated the need for the highly toxic Lewis acid catalyst, mercuric cyanide. Silylation, the traditional procedure for base activation, was also found to be unnecessary in this case, although it is not known whether silylation of **66** would considerably increase the yield of **67**. This approach afforded **67** in 44% yield from **64**.

The deprotection reactions involved two separate steps as shown in Scheme 15. Some difficulties were encountered in the second deprotection reaction and these are discussed in section 4.4. The first deprotection step with NH_3/MeOH was a straightforward reaction, giving the debenzoylated but still *N*-protected nucleoside **68** in about 42% yield from **67**. This 42% chemical yield was lower than the reported values for the debenzoylation of "free" 2-aminoimidazole ribofuranoside where the yields were in the range of 60-83%[191]. The reason for this lower debenzoylation yield in **67** is not clear, although the presence of a trifluoroacetyl group on the 2-aminoimidazole base could influence the course of the debenzoylation reaction.

The second deprotection reaction was more difficult because it involved the formation of a major side product. This side product had virtually identical ^{1}H NMR properties (including NOE and NOESY) to **6**. Despite the presence of the fluorine

atoms on the amide, it still required a relatively vigorous reaction condition to cleave the trifluoroacetamide (Scheme 18). Compound 6 was isolated in 44% yield from 68.

Iodination of 6 afforded 5 in about 40% yield as previously described. The overall yield of 5 from D-(-)-arabinose (61) was approximately 2%, although the most important step, the glycosylation reaction, was achieved in 44% yield.

4.3.2. Radioiodination

Twenty-four radioiodination trials were performed to determine the optimum radioiodination condition (Table 18). The best radioiodination condition used 0.5-1.0 mg of 5 in 2-propanol (100 μL) at 88^{0}C for 2 h (Scheme 19). The labeling efficiency obtained for the crude reaction mixture was about 43% as detected by TLC.

Scheme 19. Radioiodination of IAIA (5).

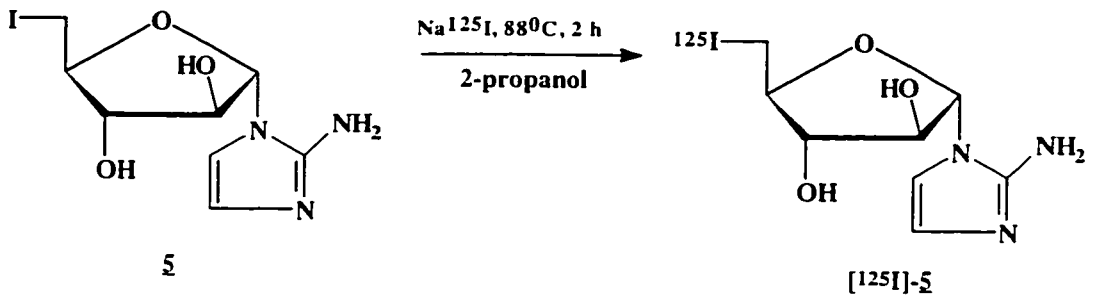

In the pivalic acid "melt" method, labeling efficiencies were negatively correlated with reaction temperature in this study. At 85^{0}C, there was a good positive correlation between reaction time and labeling efficiencies. A further increase on temperature (110^{0}C) reversed the correlation trend from positive to negative. These results suggested that the optimum reaction temperature was 85^{0}C, but in this method a reaction time of 5.5-7.5 h was necessary to achieve labeling efficiencies of over 45%.

Table 18. Summary of radioiodination results for IAIA (5) in pivalic acid or 2-propanol.

Radio-Iodination Trials	*Reaction Medium*	*Reaction Temp.(^{0}C)/ Reaction Time (h)*	*Na[^{125}I]I (MBq)*	*Amount of 5 used (mg)*	*Estimated Specific Activity (MBq/ mmol)*	*Labeling Efficiency (%)*
1	pivalic acid (0.3 mg)	85/1.5	0.37	0.1	334	27.8
2	pivalic acid (3.3 mg)	85/1.5	0.37	0.1	461	38.4
3	pivalic acid (3.0 mg)	85/1.5	0.74	0.1	851	35.4
4	pivalic acid (3.0 mg)	85/3.5	0.74	0.1	976	40.6
5	pivalic acid (3.0 mg)	85/5.5	0.74	0.1	1103	45.9
6	pivalic acid (3.0 mg)	85/7.5	0.74	0.1	1117	46.5
7	pivalic acid (5.0 mg)	85/3.5	0.74	0.1	817	34.0
8	pivalic acid (3.3 mg)	95/0.25	0.74	0.1	581	24.2
9	pivalic acid (3.3 mg)	95/0.50	0.74	0.1	803	33.4

Table 18 (Cont'd). Summary of radioiodination results for IAIA (5) in pivalic acid or 2-propanol.

Radio-Iodination Trials	*Reaction Medium*	*Reaction Temp.(^{0}C)/ Reaction Time (h)*	*Na[^{125}I]I (MBq)*	*Amount of 5 used (mg)*	*Estimated Specific Activity (MBq/ mmol)*	*Labeling Efficiency (%)*
10	pivalic acid (3.3 mg)	95/0.75	0.74	0.1	781	32.5
11	pivalic acid (3.3 mg)	95/1.0	0.74	0.1	742	30.9
12	pivalic acid (5.0 mg)	95/2.0	0.74	0.1	324	13.5
13	pivalic acid (3.3 mg)	110/0.50	0.56	0.1	629	34.9
14	pivalic acid (3.3 mg)	110/0.75	0.56	0.1	258	14.3
15	pivalic acid (3.3 mg)	110/1.0	0.74	0.1	300	12.5
16	pivalic acid (3.3 mg) + DMF (100 µL)	85/3.5	0.56	0.1	451	25.0
17	pivalic acid (3.3 mg) + 2-propanol (100 µL)	85/3.5	0.56	0.1	575	31.9

Table 18 (Cont'd). Summary of radioiodination results for IAIA (5) in pivalic acid or 2-propanol.

Radio-iodination Trials	*Reaction Medium*	*Reaction Temp.(^{0}C)/ Reaction Time (h)*	*Na[^{125}I]I (MBq)*	*Amount of 5 used (mg)*	*Estimated Specific Activity (MBq/ mmol)*	*Labeling Efficiency (%)*
18	pivalic acid (0.1 mg) + 2-propanol (100 µL)	85/3.5	7.40	0.1	9851	41.0
19	2-propanol (100 µL)	85/3.5	0.74	0.1	1016	42.3
20	2-propanol (100 µL)	88/2.0	0.56	0.1	7046	39.1
21	2-propanol (100 µL)	88/2.0	0.56	0.5	142	39.4
22	2-propanol (100 µL)	88/2.0	5.55	0.5	1500*	41.6
23	2-propanol (100 µL)	88/2.0	6.66	1.0	941*	43.5
24	2-propanol (100 µL)	88/2.0	9.25	1.0	1288*	42.9

*Used in *in vivo* studies.

The effect of adding a solvent on the pivalic acid "melt" was thus examined. This solvent exchange method in DMF did not produce a satisfactory labeling efficiency. Another solvent, 2-propanol, was thus selected and was found to give acceptable labeling efficiencies. When the amount of pivalic acid was reduced, slight increases on the radioiodination yields were observed. A shorter reaction time (e.g. 2

h) did not significantly alter this yield (>40%). Therefore, solvent exchange in 2-propanol was selected to be the preferred radioiodination method because it required a shorter reaction time to achieve comparable 40% radioiodination yields observed in the pivalic acid "melt" method. The labeling efficiency of Trial 23, for example, was obtained as shown in Figures 14 and 15.

Figure 14. Labeling efficiency for IAIA (5).

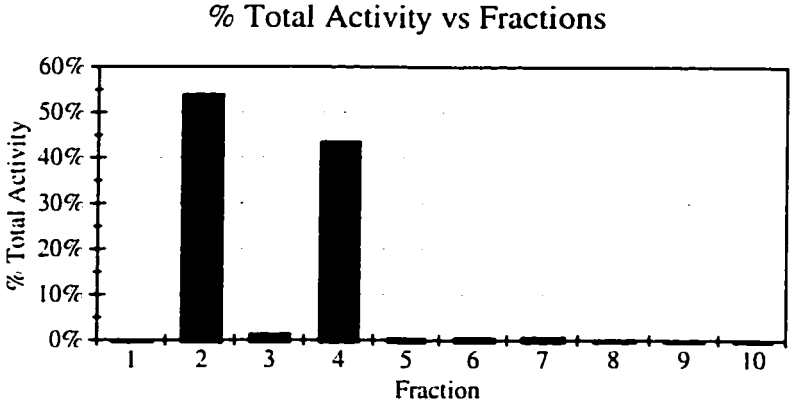

Figure 15. Determination of labeling efficiency of [^{125}I]IAIA (5) by TLC.

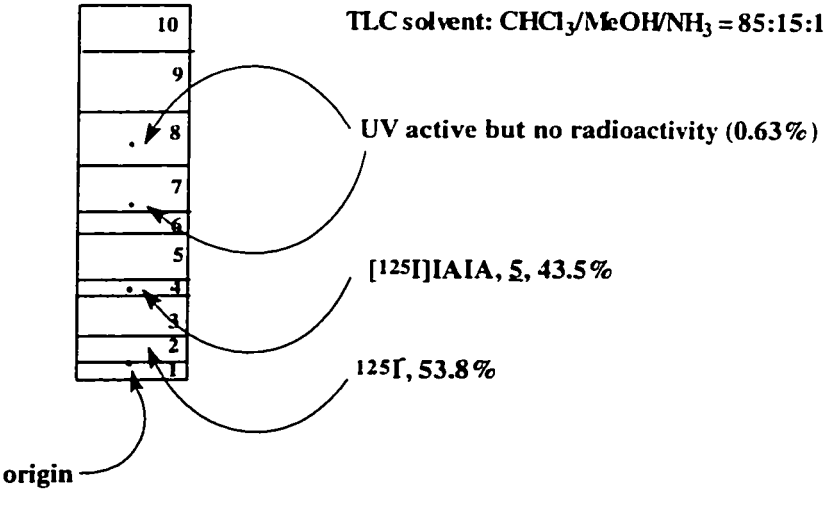

Figures 14 and 15 show that about 44% of the total radioactivity was found on Fraction 4 ([^{125}I]-5). The majority of the radioactivity remained as "free" radioiodide near the origin of the TLC plate. Some decomposition products were visible in Fractions 7 and 8 but these fractions had insignificant amounts of radioactivity.

The crude reaction mixture containing [^{125}I]-5 was purified by several chromatographic methods: column, preparative TLC, and using Sep-Pak® cartridges. Fourteen purification trials were performed (Table 19).

Table 19. Purification results for [^{125}I]IAIA (5).

Purification Trial	*Purification Method*	*Eluting Solvent System*	*Radiochemical Purity of [^{125}I]-5 after Purification (%)*
1	Silica gel column[a]	$CHCl_3$:MeOH:NH_3 85:15:10	90.7
2	Silica gel column[b]	$CHCl_3$:MeOH:NH_3 85:15:10	75.2
3	Silica gel column[c]	$CHCl_3$:MeOH:Et_3N 85:15:0.3	85.5
4	Silica gel column[c]	$CHCl_3$:MeOH:Et_3N 85:15:0.1	64.1
5	Preparative TLC[d]	$CHCl_3$:MeOH 85:15 (saturated with NH_3)	51.8
6	Preparative TLC[e]	$CHCl_3$:MeOH 85:15 (saturated with NH_3)	70.9
7	Preparative TLC[f]	$CHCl_3$:MeOH 85:15 (saturated with NH_3)	77.3

Table 19 (Cont'd). Purification results for [^{125}I]IAIA (5).

Purification Trial	*Purification Method*	*Eluting Solvent System*	*Radiochemical Purity of [^{125}I]-5 after Purification (%)*
8	Sep-Pak®cartridge[g]	1. H_2O 2. MeOH:H_2O 80:20	23.6
9	Sep-Pak®cartridge[h]	0.9% NaCl	66.8
10	Sep-Pak®cartridge[i]	0.9% NaCl	86.6
11	Sep-Pak®cartridge[i]	0.9% NaCl	96.0
12	Sep-Pak®cartridge[i]	1. 0.9% NaCl 2. H_2O	80.0
13	Sep-Pak®cartridge[i]	0.9% NaCl	94.7
14	Sep-Pak®cartridge[i]	0.9% NaCl	94.6

Notes to Table 19:

[a]Small glass column, 1x35 cm, single collection
[b]Pasteur pipette column, single collection
[c]Pasteur pipette column, 20 2-mL fractions
[d]20x20 cm glass preparative plates
[e]5x20 cm glass preparative plates
[f]5.2x15.2 cm plastic-backed preparative TLC plates
[g]10 4-mL fractions
[h]10 2-mL fractions
[i]20 2-mL fractions

Purification by silica gel columns and preparative TLC plates gave unacceptable radiochemical purity (< 95%) for animal studies. The most effective purification method appeared to be the Sep-Pak® (Waters) cartridges. The cartridge was first preconditioned with 5 mL of MeOH followed by 5 mL of 0.9% NaCl (saline). The same saline solution was used as the eluting mobile phase and it was found to be more efficient than employing water alone. Sep-Pak® thus gave the best purification

results (>95% radiochemical purity) in this study. The collection profile for Trial 13, for instance, is shown in Figure 16.

Figure 16. Collection profile for [^{125}I]IAIA (5).

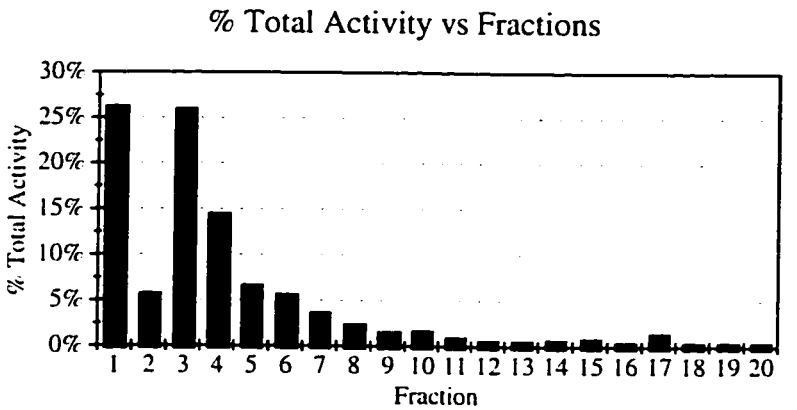

Since the labeling efficiency of 5 was relatively low, the crude reaction mixture contained substantial amounts of "free" radioiodide, complicating the purification procedures. Figure 16 shows that the first purified fraction, Fraction 1, contained significant amounts of radioactivity due to "free" radioiodide. Radioiodide was expected to first elute from the Sep-Pak® cartridge because of the reverse-phase properties of the cartridge. With its negative charge, radioiodide ion is the most polar radioactive constituent of the crude reaction mixture and thus is first eluted. Subsequent fractions (Fractions 3-8) contained the [^{125}I]-5 and a radiochemical purity of about 95% was obtained (Figure 17). The amount of radioiodide was approximately 3.3% of the total radioactivity. Fraction 3 from the analysis of the purified [^{125}I]-5 (Figure 17) contained 1.7% of radioactivity which could be residual [^{125}I]-5 due to "tailing" on TLC plates, or minor amounts of decomposed fragments. The amount of radioactivity of [^{125}I]-5 was found to be 95 μCi.

Figure 17. Radiochemical purity of [^{125}I]IAIA (5).

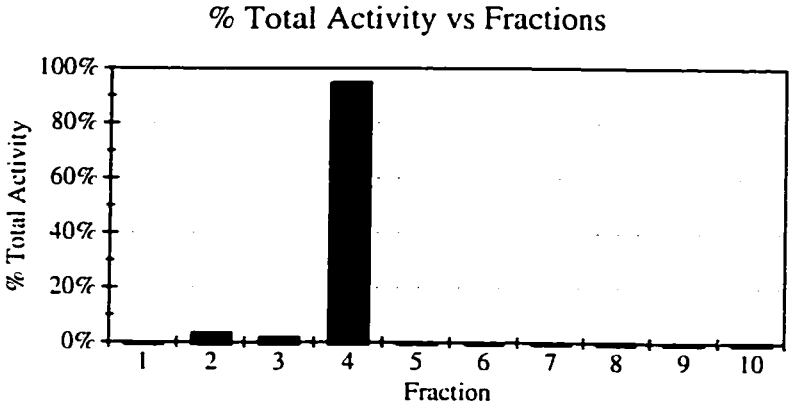

4.3.3. Biodistribution and elimination.

Tables 20 and 21 show the *in vivo* biodistribution of [^{125}I]-5 at seven time intervals in normal and tumor-bearing Balb/c mice, respectively. The specific activity of the injected compound was 1.2-1.4 GBq/mmol, with the exception in normal mice during the five time intervals (0.25 h to 4 h) where the specific activity of the injected compound was 0.4-0.6 GBq/mmol. Each animal received an intravenous bolus injection of 48-60 kBq containing 15-18 μg of [^{125}I]-5. In the latter five sets of normal mice, the activity of the injected compound was 10-11 kBq containing 8-9 μg of [^{125}I]-5. The data are presented as percent injected dose per gram of tissue and as tissue-to-blood ratios of ^{125}I activity.

Table 20. Biodistribution of [125-I]IAIA following i.v. administration in Balb/c mice at various time intervals.

	Time (Hours)						
Tissue	0.25	0.5	1	2	4	8	24
Blood	0.92 ± 0.10a	0.50 ± 0.07	0.32 ± 0.04	0.19 ± 0.04	0.15 ± 0.05	0.075 ± 0.028	0.014 ± 0.002
Kidney	2.94 ± 0.40	1.52 ± 0.23	0.79 ± 0.11	0.34 ± 0.18	0.22 ± 0.04	0.073 ± 0.032	0.018 ± 0.015
	3.19 ± 0.07b	*3.00 ± 0.10*	*2.45 ± 0.18*	*1.90 ± 1.06*	*1.51 ± 0.23*	*0.94 ± 0.11*	*1.19 ± 0.91*
GITc	7.29 ± 0.99	5.41 ± 1.76	2.38 ± 0.34	1.04 ± 0.09	0.36 ± 0.06	0.21 ± 0.07	0.061 ± 0.027
	7.99 ± 1.20	*10.67 ± 2.79*	*7.47 ± 1.42*	*5.68 ± 0.83*	*2.75 ± 1.05*	*2.91 ± 0.68*	*4.34 ± 1.79*
Liver	7.78 ± 0.28	4.84 ± 0.62	2.69 ± 0.35	1.56 ± 0.13	1.53 ± 0.32	0.56 ± 0.11	0.46 ± 0.07
	8.55 ± 0.71	*9.63 ± 0.82*	*8.34 ± 0.82*	*8.67 ± 2.05*	*10.62 ± 1.33*	*8.26 ± 2.18*	*33.92 ± 4.88*
Muscle	1.01 ± 0.12	0.57 ± 0.12	0.38 ± 0.035	0.20 ± 0.06	0.30 ± 0.06	0.10 ± 0.03	0.048 ± 0.026
	1.10 ± 0.07	*1.13 ± 0.15*	*1.20 ± 0.25*	*1.16 ± 0.49*	*2.28 ± 0.87*	*1.36 ± 0.25*	*3.40 ± 1.35*
Bone	1.15 ± 0.15	0.45 ± 0.04	0.31 ± 0.13	0.15 ± 0.07	0.41 ± 0.22	0.078 ± 0.012	0.016 ± 0.011
	1.27 ± 0.21	*0.89 ± 0.04*	*1.01 ± 0.53*	*0.91 ± 0.56*	*2.76 ± 1.63*	*1.20 ± 0.39*	*1.33 ± 0.94*
Lungs	1.86 ± 0.24	0.98 ± 0.05	0.61 ± 0.06	0.25 ± 0.03	0.26 ± 0.09	0.056 ± 0.015	0.003 ± 0.003
	2.02 ± 0.04	*1.96 ± 0.18*	*1.90 ± 0.09*	*1.40 ± 0.32*	*1.79 ± 0.57*	*0.79 ± 0.13*	*0.23 ± 0.22*
Heart	1.38 ± 0.10	0.50 ± 0.02	0.33 ± 0.02	0.08 ± 0.04	0.18 ± 0.05	0.035 ± 0.011	0.003 ± 0.003
	1.51 ± 0.11	*1.01 ± 0.11*	*1.04 ± 0.04*	*0.40 ± 0.13*	*1.34 ± 0.51*	*0.50 ± 0.10*	*0.15 ± 0.11*
Spleen	1.82 ± 0.08	0.86 ± 0.14	0.45 ± 0.09	0.15 ± 0.07	0.13 ± 0.01	0.050 ± 0.036	0.002 ± 0.002
	1.99 ± 0.14	*1.70 ± 0.09*	*1.39 ± 0.14*	*0.74 ± 0.30*	*0.92 ± 0.22*	*0.60 ± 0.28*	*0.086 ± 0.081*
Stomach	2.90 ± 0.27	2.00 ± 0.64	1.48 ± 0.11	0.86 ± 0.23	0.51 ± 0.24	0.34 ± 0.14	0.058 ± 0.007
	3.17 ± 0.23	*4.16 ± 1.85*	*4.67 ± 0.91*	*5.00 ± 2.12*	*3.25 ± 0.41*	*4.61 ± 0.84*	*4.51 ± 1.33*
Brain	0.14 ± 0.02	0.05 ± 0.04	0.03 ± 0.01	0.01 ± 0.01	0.03 ± 0.01	0.01 ± 0.01	0.002 ± 0.002
	0.16 ± 0.01	*0.10 ± 0.06*	*0.09 ± 0.05*	*0.04 ± 0.04*	*0.19 ± 0.11*	*0.10 ± 0.07*	*0.15 ± 0.15*
Carcass	1.53 ± 0.40	1.20 ± 0.05	0.81 ± 0.03	0.71 ± 0.08	0.45 ± 0.09	0.22 ± 0.08	0.093 ± 0.014
	1.64 ± 0.23	*2.40 ± 0.22*	*2.53 ± 0.38*	*3.86 ± 0.45*	*3.27 ± 1.02*	*3.03 ± 0.63*	*7.01 ± 1.71*

a - The numbers represent the mean ± standard deviation for percent of injected dose per gram of wet tissue for 3 animals.
b - Second line for each tissue represents tissue-to-blood ratio.
c - Section of intestine.

Table 21. Biodistribution of [125-I]IAIA following i.v. administration in Balb/c mice bearing EMT-6 tumors at various time intervals.

	Time (Hours)						
Tissue	0.25	0.5	1	2	4	8	24
Blood	1.32 ± 0.13a	0.82 ± 0.15	0.49 ± 0.09	0.18 ± 0.03	0.19 ± 0.03	0.051 ± 0.001	0.011 ± 0.002
Tumor	1.08 ± 0.16	0.95 ± 0.15	0.76 ± 0.18	0.28 ± 0.09	0.83 ± 0.28	0.096 ± 0.032	0.015 ± 0.006
	0.81 ± 0.05b	*1.18 ± 0.10*	*1.55 ± 0.18*	*1.56 ± 0.28*	*4.34 ± 0.80*	*2.07 ± 1.09*	*1.39 ± 0.49*
Kidney	3.92 ± 0.42	2.48 ± 0.57	1.20 ± 0.31	0.29 ± 0.08	0.20 ± 0.03	0.071 ± 0.017	0.013 ± 0.002
	2.96 ± 0.13	*3.04 ± 0.31*	*2.41 ± 0.22*	*1.65 ± 0.19*	*1.09 ± 0.01*	*1.40 ± 0.28*	*1.22 ± 0.05*
GITc	8.81 ± 0.81	6.47 ± 1.77	3.29 ± 1.05	0.81 ± 0.15	0.86 ± 0.11	0.16 ± 0.05	0.037 ± 0.006
	6.67 ± 0.49	*7.90 ± 1.25*	*6.59 ± 1.08*	*4.63 ± 0.09*	*4.65 ± 0.25*	*3.02 ± 0.42*	*3.54 ± 1.06*
Liver	13.88 ± 1.67	7.87 ± 1.04	4.25 ± 0.66	1.76 ± 0.26	1.09 ± 0.11	0.75 ± 0.05	0.32 ± 0.03
	10.48 ± 0.87	*9.77 ± 0.45*	*8.77 ± 0.36*	*10.15 ± 0.65*	*5.92 ± 0.42*	*14.96 ± 1.91*	*30.04 ± 3.36*
Muscle	1.18 ± 0.17	0.95 ± 0.21	0.79 ± 0.20	0.38 ± 0.13	0.30 ± 0.03	0.12 ± 0.03	0.048 ± 0.007
	0.90 ± 0.16	*1.17 ± 0.12*	*1.60 ± 0.15*	*2.08 ± 0.40*	*1.62 ± 0.12*	*2.22 ± 0.32*	*4.43 ± 0.47*
Bone	1.01 ± 0.13	0.91 ± 0.06	0.51 ± 0.08	0.21 ± 0.05	0.17 ± 0.03	0.06 ± 0.02	0.033 ± 0.018
	0.77 ± 0.14	*0.91 ± 0.14*	*1.06 ± 0.20*	*1.17 ± 0.09*	*0.90 ± 0.03*	*1.22 ± 0.13*	*3.56 ± 2.39*
Lungs	2.46 ± 0.22	1.53 ± 0.29	0.82 ± 0.14	0.31 ± 0.04	0.22 ± 0.03	0.055 ± 0.010	0.017 ± 0.002
	1.86 ± 0.15	*1.88 ± 0.10*	*1.69 ± 0.04*	*1.79 ± 0.10*	*1.16 ± 0.02*	*1.08 ± 0.04*	*1.56 ± 0.23*
Heart	1.44 ± 0.16	0.82 ± 0.10	0.47 ± 0.07	0.16 ± 0.02	0.12 ± 0.02	0.025 ± 0.010	0.007 ± 0.002
	1.09 ± 0.10	*1.02 ± 0.06*	*0.98 ± 0.04*	*0.94 ± 0.04*	*0.63 ± 0.02*	*0.46 ± 0.12*	*0.66 ± 0.24*
Spleen	1.83 ± 0.13	1.15 ± 0.21	0.65 ± 0.17	0.19 ± 0.04	0.14 ± 0.04	0.027 ± 0.007	0.009 ± 0.003
	1.38 ± 0.04	*1.42 ± 0.17*	*1.31 ± 0.13*	*1.09 ± 0.11*	*0.76 ± 0.11*	*0.51 ± 0.06*	*0.79 ± 0.15*
Stomach	2.70 ± 0.52	2.34 ± 0.75	1.89 ± 0.37	0.64 ± 0.14	0.90 ± 0.27	0.45 ± 0.23	0.036 ± 0.009
	2.04 ± 0.28	*2.82 ± 0.38*	*3.86 ± 0.08*	*3.68 ± 0.51*	*4.79 ± 1.12*	*8.29 ± 2.84*	*3.32 ± 0.62*
Brain	0.06 ± 0.01	0.05 ± 0.01	0.04 ± 0.01	0.01 ± 0.003	0.02 ± 0.002	0.004 ± 0.003	0.004 ± 0.003
	0.05 ± 0.01	*0.07 ± 0.02*	*0.07 ± 0.01*	*0.08 ± 0.005*	*0.10 ± 0.01*	*0.07 ± 0.05*	*0.32 ± 0.21*
Carcass	1.89 ± 0.14	1.57 ± 0.18	1.33 ± 0.15	0.80 ± 0.16	0.68 ± 0.17	0.20 ± 0.04	0.029 ± 0.006
	1.44 ± 0.22	*1.96 ± 0.24*	*2.76 ± 0.21*	*4.58 ± 0.26*	*3.62 ± 0.34*	*3.83 ± 0.37*	*2.63 ± 0.21*

a - The numbers represent the mean ± standard deviation for percent of injected dose per gram of wet tissue for 3 animals.

b - Second line for each tissue represents tissue-to-blood ratio.

c - Section of intestine.

Table 20 indicates a rapid early distribution of [^{125}I]-5 in normal mice with the brain containing the lowest radioactivity among all the organs. At longer time periods, between 4 and 24 h, brain radioactivity, in terms of percent injected dose per gram, remained very low (0.002%) when compared to other organs. These low brain-to-blood ratios (essentially <0.10 in all time periods) provided no strong evidence to suggest any metabolic trapping of [^{125}I]-5 in the normal mouse brain. Specific nucleoside and/or amine transporters or a pH-dependent trapping mechanism in neuronal tissues did not appear to be important in this preliminary study.

At 0.25 h post injection, the kidney, liver, GIT and stomach had the highest amount of radioactivity. Rapid urinary excretion of [^{125}I]-5 seemed evident and this high concentration of radioactivity persisted in the kidney through the first few hours and even at 24 h the kidney-to-blood ratio was more than 1.0. The kidney appeared to play an important role in the excretion of [^{125}I]-5 or its metabolites. The second organ of highly concentrated radioactivity, the liver, also seemed to be involved in the metabolism and excretion of [^{125}I]-5 because of its high dose per gram values at 0.25 h. Liver radioactivity continued to be high even at 24 h at which the liver-to-blood ratio rose to a remarkably high value of 34, although the corresponding dose per gram value had fallen from 7.78% at 0.25 h to 0.46% at 24 h. These high liver radioactivity values at 24 h are very unusual since this is not due to liver processing but due to liver metabolic trapping.

Table 22. Thyroid radioactivity as percent injected dose of [^{125}I]IAIA (5) per organ in normal and EMT-6 tumor-bearing Balb/c mice (n=3).

Time post injection (h)	*Percent injected dose per organ*	*Thyroid radioactivity as percentage of whole-body radioactivity*
0.25	0.39±0.01[a] ***0.66±0.46***[b]	1.15±0.21 ***0.53±0.14***
0.50	0.11±0.05 ***0.38±0.04***	0.42±0.26 ***1.00±0.01***
1	0.20±0.09 ***0.34±0.08***	0.90±0.49 ***1.20±0.24***
2	0.11±0.08 ***0.13±0.02***	0.89±0.88 ***0.91±0.25***
4	0.29±0.18 ***0.35±0.09***	3.3±2.5 ***2.6±0.3***
8	0.61±0.27 ***0.17±0.18***	12.1±0.6 ***4.4±4.9***
24	1.04±1.03 ***0.80±0.12***	27.7±24.5 ***45.0±8.7***

[a] normal Balb/c mice [b] ***EMT-6 tumor-bearing Balb/c mice***

Besides kidney and liver, the gastrointestinal tract (GIT) also had high radioactivity at 0.25 h. However, when compared to the liver, its radioactivity was much lower at 24 h with a dose per gram value of 0.061% and a GIT-to-blood ratio of 4.34. Its radioactivity could predominately be "free" radioiodide[226].

The persistently high stomach-to-blood ratios were also due to the accumulation of "free" radioiodide produced by *in vivo* deiodination[226] (Table 22). Compared to the sugar derivatives at 4 h post injection, the amount of *in vivo* de-

iodination in [^{125}I]-5 appeared to be lower ([^{125}I]-5 vs. [^{125}I]-3: t = -3.31, p = 0.0453; [^{125}I]-5 vs. [^{125}I]-4: t = -2.60, p = 0.0483). Tissue-to-blood ratios of radioactivity for these and some other representative organs are shown in Figures 18 and 19.

Figure 18. Tissue-to-blood ratios of radioactivity at various time intervals following i.v. administration of [^{125}I]IAIA (5) in normal Balb/c mice.

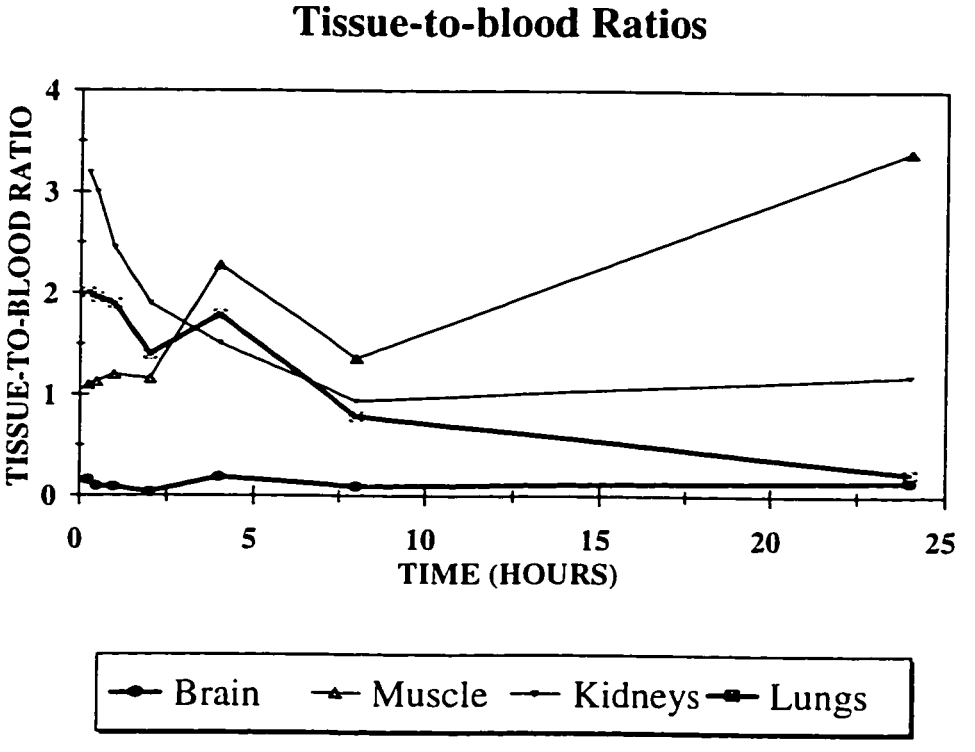

Figure 19. Tissue-to-blood ratios of radioactivity at various time intervals following i.v. administration of [^{125}I]IAIA (5) in normal Balb/c mice.

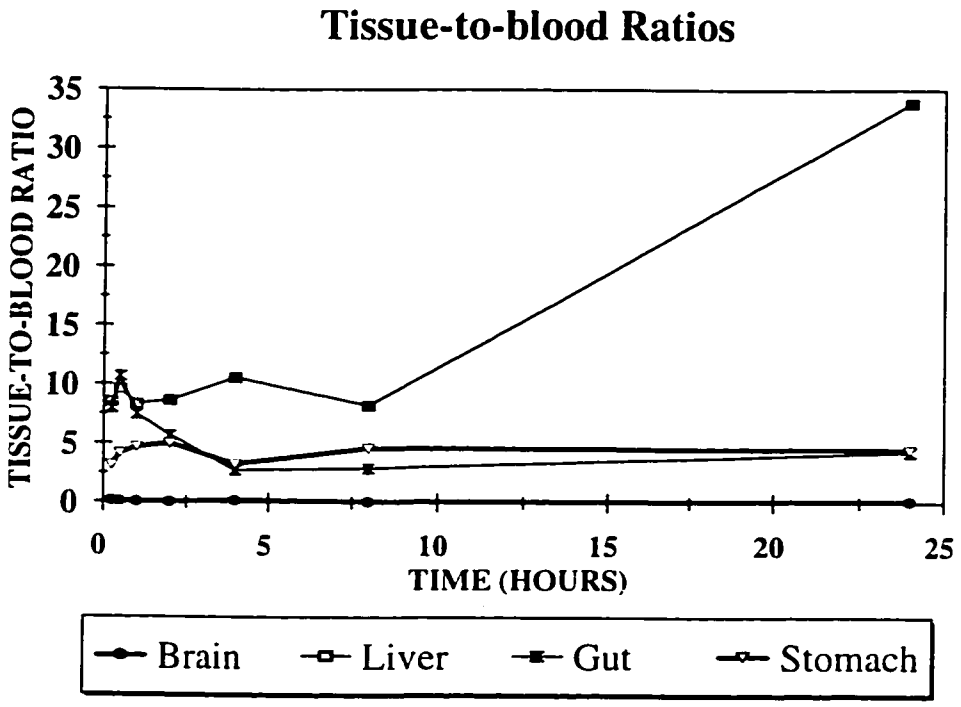

At 24 h, the muscle-to-blood ratio was unusually high. In dose per gram values, the muscle also retained high radioactivity comparable to the GIT and kidney. Some metabolic trapping of [^{125}I]-5 might also occur in muscle tissues.

The biodistribution data of [^{125}I]-5 in EMT-6 tumor-bearing Balb/c mice (Table 21) indicate once again a rapid early distribution of [^{125}I]-5 similar to the normal mice set. At 0.25 h in particular, a statistically significant difference in brain radioactivity was observed when compared to the normal mice set (dose per gram: t = 4.75, p = 0.0177; brain-to-blood ratio: t = 10.4, p = 0.00189) (Appendix 2). At longer time periods, between 4 and 24 h, brain radioactivity (dose per gram) remained very low (0.004%). With the exception of 0.25 h, there is no strong evidence to suggest any differences in brain radioactivity between the normal mice and the tumor-bearing mice

(e.g. at 24 h post injection, dose per gram: $t = -0.632$, $p = 0.562$; brain-to-blood ratio: $t = -0.812$, $p = 0.462$).

Besides the brain, the tumor contained generally lower radioactivity compared to most of the other organs at 0.25 h. This could be an indication of reduced perfusion of the tumor tissue which is known to contain a large (up to 33%) proportion of hypoxic, poorly-perfused cells[229]. Tumor radioactivity stayed fairly unchanged from 0.25 h to 1 h, followed by an apparent downward jump at 2 h. The reason for this sudden decrease in tumor radioactivity was not known, although the tumor-to-blood ratio at this time period stayed at around 1.60. At 4 h, tumor radioactivity in percent injected dose per gram rebounded to 0.83% and was higher than in other tissues with the exception of the GIT, liver, and stomach. This time interval gave the highest tumor-to-blood ratio of 4.3. This higher tumor radioactivity could be due to slower clearance of radioactivity from the tumor tissue, suggesting some mechanisms of metabolic trapping were present. However, this tumor uptake of radioactivity was relatively short-lived and fell rapidly; at 8 h, the dose per gram value had dropped from a high of 0.83% to 0.10%, an almost eight-fold decrease within four hours. Within the same four-hour period, blood radioactivity was reduced from about 0.20% to 0.05%, a fourfold decrease. Between 8 and 24 h tumor radioactivity dropped another tenfold while a fivefold decrease was observed for blood radioactivity. At 24 h blood and tumor radioactivity were comparable (0.011% and 0.015%, respectively) with a tumor-to-blood ratio of about 1.40. These results suggest that the crucial time interval for tumor uptake of radioactivity is between 2 and 4 h post injection in mice.

Thyroid radioactivity showed a very similar trend when compared to the normal mice data. Although the numbers were quite different, no strong evidence exists to show that the differences were statistically significant. For example, at 24 h (Table 22), real differences between the dose per organ (t = 0.397, p = 0.730) and percent whole-body radioactivity (t = -1.15, p = 0.333) of the thyroid could not be inferred.

At 4 h, tissue-to-blood ratios for the liver, GIT and stomach were higher than that in tumor. In terms of percent dose per gram values, the liver retained the highest amount of radioactivity (1.1%) at this time interval. The stomach and the GIT, with their values of 0.9% and 0.86%, respectively, closely followed the liver. These three organs were the only ones which contained higher radioactivity than the tumor at the time interval when the tumor-to-blood ratio was the highest. When compared to the normal mice no real differences could be inferred in these three organs (e.g. in liver, dose per gram: t = 1.84, p = 0.208; liver-to-blood: t = 4.78, p = 0.0410). Attempts to image the tumor at this time interval would be considerably hindered by the high background radioactivity in these organs. The generally high background radioactivity of the carcass would further complicate the imaging problem.

At 24 h, all tissue-to-blood ratios remained greater than 1.0 with the exception of the heart, spleen and brain. The liver-to-blood ratio was unusually high with a magnitude of 30, representing 0.32% injected dose per gram (when compared to normal mice, dose per gram: t = 2.65, p = 0.0767; liver-to-blood ratio: t = 0.939, p = 0.401). The ratios for the stomach and GIT were also high and in the range of 3.3-3.5. Muscle radioactivity for both sets of mice at this time interval appeared to be the same

(dose per gram: t = 0.0364, p = 0.974; muscle-to-blood ratio: t = -1.02, p = 0.414).

Tissue-to-blood ratios for these selected organs are shown in Figures 20 and 21.

Figure 20. Tissue-to-blood ratios of radioactivity at various time intervals following i.v. administration of [^{125}I]IAIA (5) in tumor-bearing Balb/c mice.

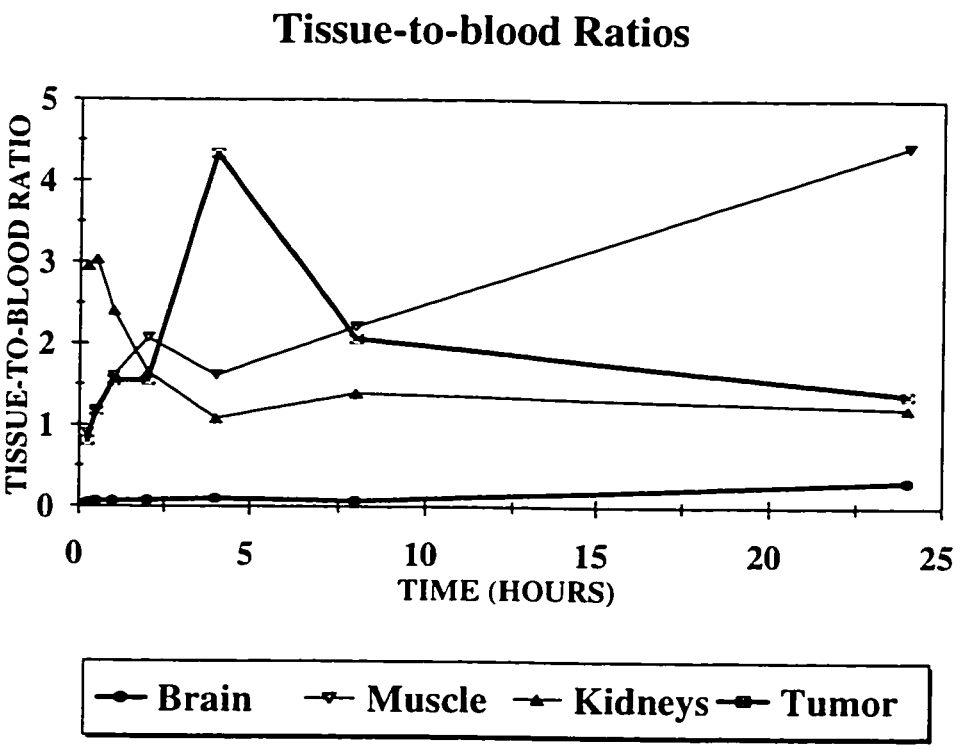

Figure 21. Tissue-to-blood ratios of radioactivity at various time intervals following i.v. administration of [^{125}I]IAIA (5) in tumor-bearing Balb/c mice.

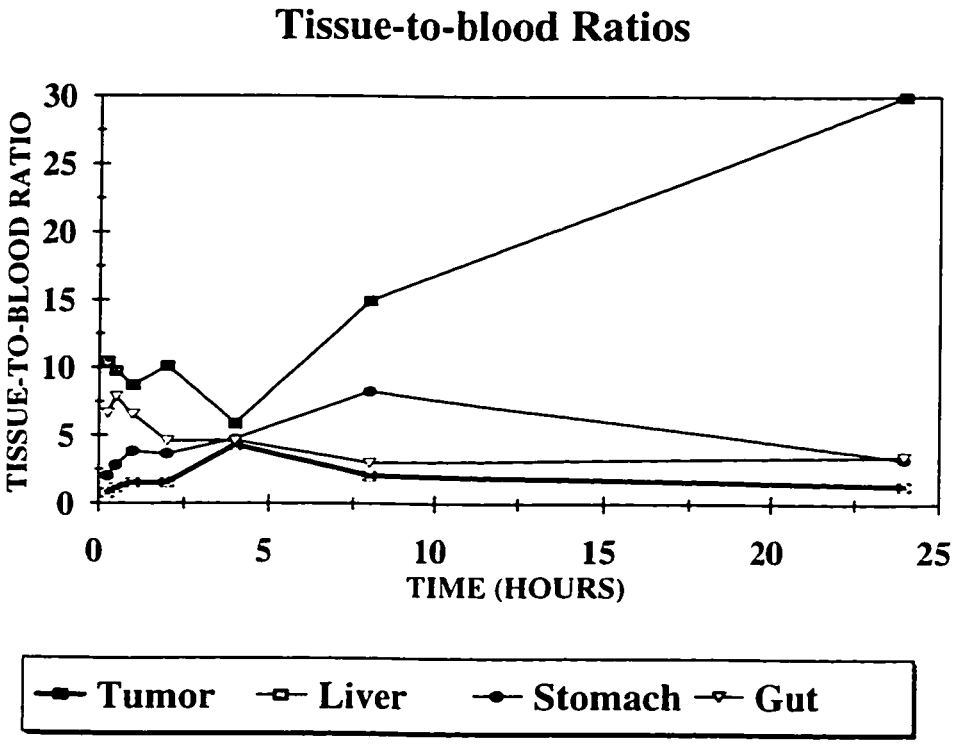

The whole-body and blood clearance data for both sets of mice are shown in Figures 22 and 23. Whole-body clearance data indicate that at 0.25 h, more than 65% and 45% of radioactivity were cleared from whole body in normal and tumor-bearing mice, respectively. There is fairly good evidence to suggest that this difference in radioactivity elimination was valid (t = -4.89, p = 0.0393), although the p-value is not small enough to suggest absolute differences at the 0.01 significance level. In all other time periods, no significant differences in whole-body clearance were observed between these two mice sets (e.g. at 4 h, t = -1.92, p = 0.194). Greater than 97% of injected radioactivity was eliminated within 24 h in both sets of mice.

Figure 22. Whole-body clearance of radioactivity following i.v. administration of [^{125}I]IAIA (5) in normal and tumor-bearing Balb/c mice.

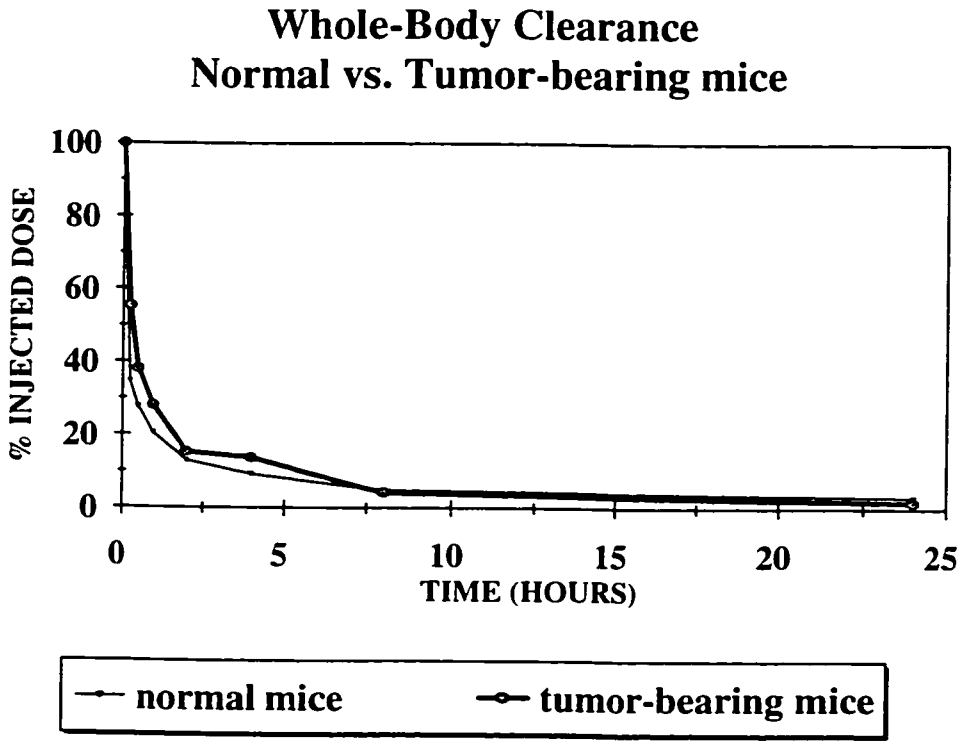

The blood clearance data for both normal and tumor-bearing mice are shown in Figure 23. Once again, there is strong evidence to suggest statistically significant differences existed between the two sets of data at 0.25 h (t = -8.42, p = 0.00352). More than 98% of blood radioactivity was eliminated within the first 15 min. In other time periods, no significant differences were observed (e.g. at 8 h, t = 1.40, p = 0.296) between the two mice sets. Greater than 99.98% of the injected radioactivity was eliminated from blood within 24 h.

Figure 23. Blood clearance of radioactivity following i.v. administration of [^{125}I]IAIA (5) in normal and tumor-bearing Balb/c mice.

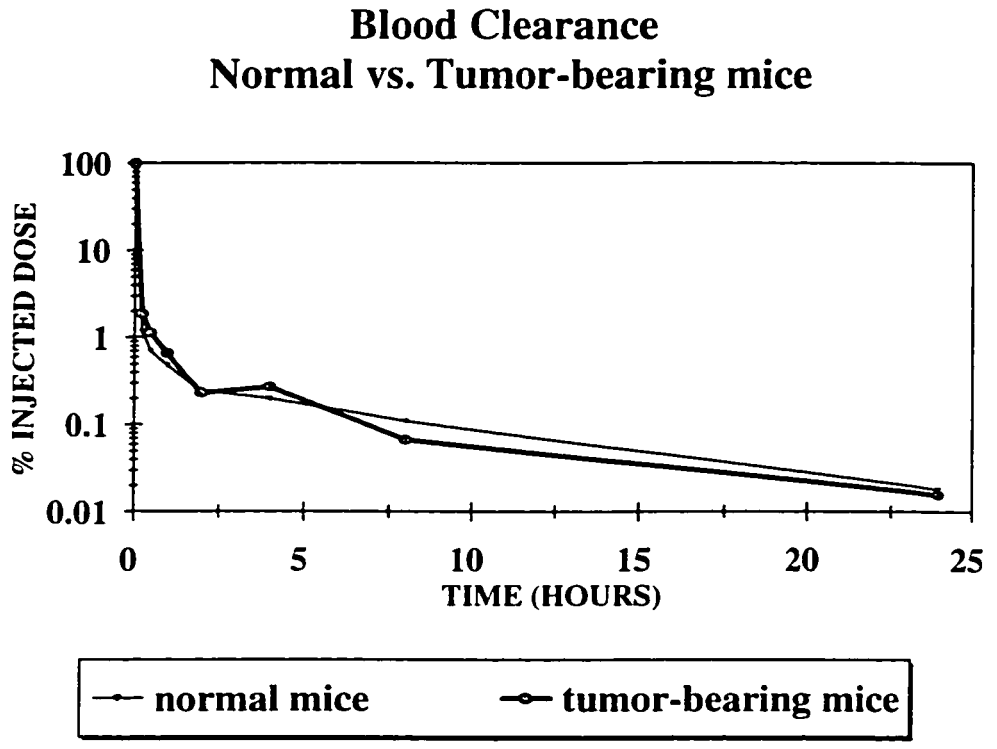

On the basis of these results, it appears that [^{125}I]IAIA (5) is trapped in EMT-6 tumors. The nature of this trapping mechanism is not known nor was it investigated, although the 2-aminoimidazole base might be back-oxidized[137,148] to reactive intermediates (hydroxylamine or nitroso) and underwent analogous macromolecular binding as in 2-nitroimidazole nucleosides, or [^{125}I]-5 could undergo a pH trapping mechanism during which the amino group is protonated at the slightly lower pH in tumors[123]. No radioactivity, however, was trapped in the brain. Despite this favorable result in tumors (tumor-to-blood ratio 4.34) 5 may not be an ideal agent for non-invasive diagnosis of hypoxic cells in tumors (especially those present in the abdomen), due to the elevated liver radioactivity up to 24 h. No time period was

found to be suitable for an imaging study, as the liver-to-blood ratio was higher than tumor-to-blood ratio, and most organs showed persistently high ratios throughout the 24 h period. The high liver radioactivity values suggested some metabolic trapping in this organ, and further studies would be required to determine the nature of this metabolic trapping.

4.3.4. Stability

The chemical and radiochemical stability of 5 were briefly assessed. It showed good chemical stability when stored in frozen water under argon at -20^{0}C. ^{1}H and ^{13}C NMR spectra showed that the compound was still intact after storage for one year.

Table 23. Chemical and radiochemical stability assessment for 5.

Compound	*Storage condition*	*Storage time*	*(Radio)chemical purity*
IAIA (5)	Frozen water, argon, -20^{0}C	1 year	5 was found to be structurally intact by ^{1}H and ^{13}C NMR
[^{125}I]IAIA ([^{125}I]-5)	Frozen saline, argon, -20^{0}C	3 days	94.5%
[^{125}I]IAIA ([^{125}I]-5)	Frozen saline, argon, -20^{0}C	2 weeks	90.6%
[^{125}I]IAIA ([^{125}I]-5)	Saline, argon, 4^{0}C	1 week	85.2%

Its radiochemical stability in saline, however, was lower. The radiochemical purity of [^{125}I]-**5** in saline at 4^{0}C was assessed one week after its preparation and it had decreased from 95% to 85%. When the storage medium was in frozen saline, its radiochemical stability was found to be improved (Table 23). Compared to [^{125}I]-**3** and [^{125}I]-**4**, [^{125}I]-**5** appeared to be less radiochemically stable.

4.4. Chemistry of glycosylation reactions between arabinofuranosyl sugars and N^2- protected 2-aminoimidazoles

4.4.1. Studies on the glycosylation reaction

Ten glycosylation trials were conducted between 2,3,5-tri-*O*-benzoyl-α-D-arabinofuranosyl bromide (64) and N^2-protected 2-aminoimidazoles (66 or 69) with various conditions (Table 24). In this study, three problems were encountered.

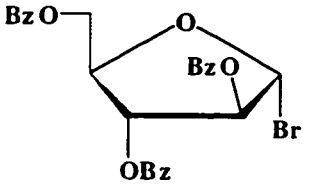

64

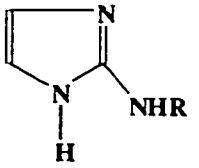

66 (R = $COCF_3$)
69 (R = $COCH_3$)

Protection of the exocyclic N^2-amino group. It was necessary to protect the reactive primary amino group on the exocyclic N^2-nitrogen. Otherwise it would compete with the N^1- and N^3-nitrogens in the imidazole ring and lead to glycosylation of the exocyclic amine. Such glycosylations have been observed in stannic chloride-catalyzed ribosylation with silylated 2-aminoimidazole which gave predominately the N^2-nucleoside (70)[191].

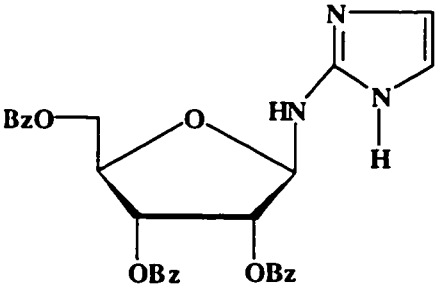

70

Table 24. Glycosylation trials between N^2-protected 2-aminoimidazoles (66 or 69) with 2,3,5-tri-*O*-benzoyl-α-D-arabinofuranosyl bromide (64).

Glyco-sylation trials	*N^2-protected 2-amino-imidazole(R= imidazole)*	*Silylation/ $Hg(CN)_2$ / K_2CO_3*	*Solvent*	*Reaction condition*	*Glyco-sylation product obtained*	*% yield*
1*	$RNHCOCH_3$	Yes/Yes/ No	CH_3CN	Reflux (82^{0}C), 12 h	Not observed	-
2*	$RNHCOCH_3$	No/Yes/ No	CH_3CN	25^{0}C, 3.5 days; 55^{0}C, 24 h; Reflux (82^{0}C), 3 h	Yes, 71	15
3A	$RNHCOCH_3$	No/Yes/ No	CH_3CN	25^{0}C, 60 h; Reflux (82^{0}C), 3 h	Yes, 71	22
3B	$RNHCOCH_3$	No/No/ Yes	CH_3CN	25^{0}C, 60 h; Reflux (82^{0}C), 3 h	Yes, 71	26
4	$RNHCOCH_3$	No/No/ Yes	CH_3CN	25^{0}C, 20 h	Yes, 71	17
5	$RNHCOCF_3$	No/No/ Yes	CH_3CN	25^{0}C, 2 h	Yes, 67	25
6	$RNHCOCF_3$	No/No/ Yes	C_6H_6/ CH_3CN	25^{0}C, 15 h	Yes, 67	44
7	$RNHCOCF_3$	No/No/ No	CH_2Cl_2	25^{0}C, 10.5 days	Yes, 67	12
8	$RNHCOCF_3$	No/No/ No	CH_2Cl_2	25^{0}C, 3.5 days	Yes, 67	23
9	$RNH_2 \bullet ½ H_2SO_4$	Yes/Yes/ No	C_6H_6	Reflux (80^{0}C), 12 h	Not observed	-

*The sugar bromide 64 was prepared by the HBr/CH_2Cl_2 method in an anomeric mixture.

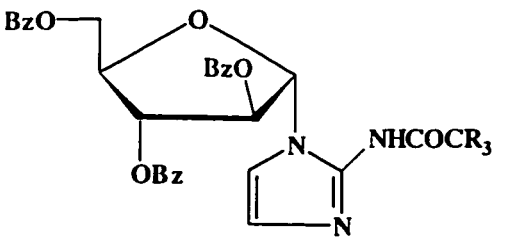

71 (R = H)
67 (R = F)

To prevent the formation of N^2-nucleosides such as 70, it is desirable to reduce the reactivity of the exocyclic primary amino group by introducing an electron-withdrawing substituent. Obviously an enormous number of nitrogen protective groups can be used. In this study, the acetyl and trifluoroacetyl groups were selected. The acetyl group is a relatively small substituent and thus could minimize steric effects during glycosylation. On the other hand, its cleavage might be more difficult because of the lack of a strong electron-withdrawing substituent. With the trifluoroacetyl group the fluorine atoms do not significantly contribute to steric effects while their electronic effects could facilitate subsequent amide cleavage. The 2-aminoimidazole derivatives containing acetyl and trifluoroacetyl groups were successfully prepared in good yields.

The sugar bromide suffered decomposition. The chemical stability of the sugar bromide 64 was initially of some concern because during the early glycosylation trials, it was observed that the modified method of sugar bromide preparation using HBr/CH_2Cl_2 (Kumar, unpublished results) gave a highly colored foam and unstable compound (TLC). Although this anomeric sugar bromide mixture could be directly used for subsequent glycosylation, it was desirable to obtain pure crystalline sugar bromide. The preparation of 64 was repeated according to published proce-

dures[157,214,215] and anomerically pure crystalline **64** was obtained in about 40% yield. Its structure was characterized ^{1}H and ^{13}C NMR and its melting point was identical to that reported in literature[214]. When stored at -20^{0}C under argon, **64** was observed to be stable for months as shown by ^{1}H NMR.

The chemical stability of **64** was also assessed in different solvents. In acetonitrile, the common solvent for glycosylation, ^{1}H NMR showed that the chemical structure of **64** had altered in three separate determination trials after 1 h, 2 h or 15 h standing time, respectively (Seki, Ohkura and Lee, unpublished results). A new compound was observed and although its identity was not investigated, acetonitrile could react with **64** at the anomeric center to give a sugar nitrile with the concomitant production of CH_3Br. In other non-participating solvents such as benzene and dichloromethane, ^{1}H NMR showed no changes in **64** after standing in these solvents for 1 h, 2 h or 15 h. Based on these observations, low glycosylation yields in this study could be due to the chemical decomposition of **64** in acetonitrile. Further evidence came from the observation in the similarity of the ^{1}H NMR spectra between the decomposed **64** and isolated side products from most glycosylation trials with acetonitrile as solvent.

Stereospecificity of the glycosylation reaction. The optimum reaction conditions for successful glycosylation were explored. Originally the goal was to synthesize the β C_1'-C_2' *trans* nucleoside because IAZA (**1A**) had been reported as the β C_1'-C_2' *trans* nucleoside (see section 4.5). Efforts to synthesize this stereo-specific nucleoside using the benzoyl protecting groups on the sugar moiety were, as expected, unsuccessful. Only the α anomer (confirmed by NOE and NOESY) was synthesized

in satisfactory yields. The effects of silylation, mercury catalysts, and solvent were examined and these were found to produce exclusively the α anomer in this study.

Silylation

The effect of silylation was examined in Trials 1 and 9 (Table 24). In this study, silylation of 2-aminoimidazole (free or protected) did not produce the glycosylation product. The use of trimethylsilyl groups to activate heterocyclic bases for condensation with glycosyl halides was reported by Nishimura *et al.*[230] to provide a new synthesis of purine and pyrimidine nucleosides. Trimethylsilyl derivatives of 2-nitroimidazole bases[231] and 2-aminoimidazole bases[191] have also been reported. Since the 2-aminoimidazole base contains an exocyclic electron-donating group, base activation by silylation may not be necessary. In both reaction trials, a complex mixture of products were observed and their ^{1}H NMR spectra did not suggest any glycosylation products. In this study, silylation was not necessary to obtain **71** or **67**, although it is not known whether silylation of Trial 6, for example, would further increase the yields.

Mercury salt catalysts

Mercury salts such as mercuric bromide ($HgBr_2$) or mercuric cyanide ($Hg(CN)_2$) are known to function as activators in both nucleoside and oligosaccharide syntheses[232]. During glycosylation, mercury is believed to form a complex with one or more nitrogen atoms on the nucleobase and glycosyl halides are attracted to the nitrogen atoms that bear the mercury groups[233]. The effect of mercury salts in the present glycosylation study appeared to be not substantial. In Trials 3A and 3B, comparable yields and same stereospecificity were obtained with or without the

presence of $Hg(CN)_2$. In subsequent glycosylation trials (4-8), **71** and **67** were obtained in useful yields without the mercury catalyst. Besides acting as base activators, mercury salts also function as acid acceptors similar to the role of molecular sieves[171,229]. The use of potassium carbonate (K_2CO_3) appeared to replace the highly toxic mercury salt as a solid acid acceptor (Trials 4-6 in this study) with reasonable yields of the glycosylation products.

Solvent

Acetonitrile is a common solvent for glycosylation but its possible role in the observed decomposition of the sugar bromide **64** suggested that it could be a participating solvent. In fact, acetonitrile is known to help direct the stereospecific synthesis of a *trans* glycosylation product[229]. If this were true, it would explain the observed formation of **71** and **67** in this study (Trials 2-6). In a polar solvent such as acetonitrile, dissociation of the bromide (or other halides) from the sugar is more favored and thus the positive charge on the orthoester intermediate **53** is more stabilized. In a less polar solvent such as dichloromethane, however, this dissociation is expected to be less favored, resulting in the formation of a tight ion pair[223] which could hinder the attack by the nucleobase on the bottom ("α") side. The *cis* nucleoside can be predominately formed in this special violation of the *trans* rule. However, this solvent effect appears to be in a delicate balance with the directing effect of the 2' participating group on the sugar. For example, in Trials 7 and 8, dichloromethane did not appear to change the stereospecificity of the glycosylation reactions (^{1}H NMR), even though it is not a participating solvent.

An interesting side product was observed in glycosylation trials 3-6. This compound was identified to be the benzoylated N^1,N^3-bis(arabinofuranosyl)2-acetamidoimidazole (72) or its trifluoroacetamido counterpart (73) depending on the starting 2-aminoimidazole derivative.

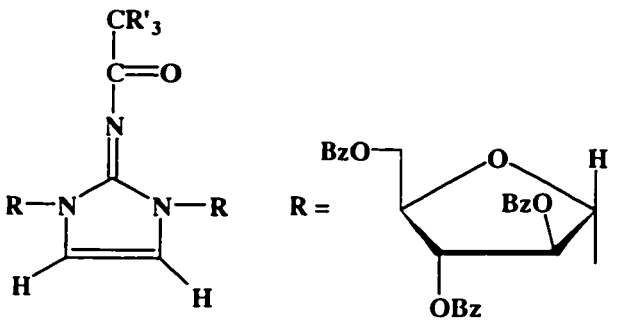

72 (R' = H)
73 (R' = F)

There was a literature precedent for the formation of a "bis" glycosylation product. Pedersen *et al.*[234] isolated analogous "bis" compounds (α configuration) in the glycosylation reactions between silylated 6-substituted uracils with methyl 2,3,5-tri-*O*-benzoyl-α-D-arabinofuranoside (63) in the presence of TMS triflate in acetonitrile at room temperature for 5 days. In their study, the yields of the "bis" compounds exceeded those of the desired α nucleoside to such an extent that in one case the yield of the "bis" compound was 81% and that of the α nucleoside was only 1.5%. In the present study, the yield of 72 was about 16-19% and that of 73 was 7% while the desired glycosylation products were obtained in 22-26% and 44%, respectively (Table 24). In contrast to literature precedents, 72 and 73 were not the major products.

The structures assigned to 72 and 73 were supported by their ^{1}H NMR data. The imidazole signals converged to a singlet due to the symmetrical nature of each molecule. The integration patterns on the ^{1}H NMR spectra also revealed a 1:1 ratio between the two imidazole protons and C_1' protons on the sugar, implying that there were two C_1' protons present. These 2 C_1' protons showed downfield shifts[234] up to 0.24 ppm for 72 and 0.28 ppm for 73 relative to their monoglycosylated counterparts. The slight downfield shifts were probably due to the electron-withdrawing effects of the conjugated exocyclic amides, especially in 73 which contains the trifluoro-acetamide. Unambiguous identification of these "bis" compounds came from low resolution Fast atom bombardment (FAB) mass spectra where the $M+H^+$ peaks were 1014 and 1068 for 72 and 73, respectively. The mechanism of their formation was not determined, although potassium carbonate and acetonitrile could play a role. Acetonitrile was also the glycosylation solvent used by Pedersen *et al*[234].

In summary, these glycosylation trials suggested that the optimum glycosylation reaction was Trial 6 where the desired α nucleoside was isolated in 44% yield.

4.4.2. Studies on the deprotection reactions.

Seven deprotection reaction trials were performed on selected glycosylation products (Table 25). The deprotection reactions included debenzoylation with NH_3/MeOH on the sugar moiety and subsequent amide cleavage on the nucleobase under basic conditions. In the first three reactions the intermediates 74 or 68 were isolated prior to further amide cleavage reaction. In the remaining reactions, these intermediates were not isolated.

Table 25. Deprotection reactions of selected glycosylation products.

De-protection reaction	*Selected glycosylated product (Trial) and base derivative*	*De-benzoylation Conditions*	*% yield of amide*	*Amide cleavage condition*	*AIA (6) & % yield*
1	2[a], $RNHCOCH_3$	NH_3/MeOH 4^0C, 15 h	**74**, 74%	Et_2NH/CH_3CN, reflux, 5 h	Not observed
2	3A, $RNHCOCH_3$	NH_3/MeOH 4^0C, 22 h	**74**, 73%	EtOH/KOH/ H_2O, reflux, 3 h	Yes, 50%
3	5, $RNHCOCF_3$	NH_3/MeOH 25^0C, 15 h	**68**, 42%	Not performed	-
4A	6, $RNHCOCF_3$	NH_3/MeOH 25^0C, 20 h	ND	1. NH_3/MeOH, 25^0C, 4 days 2. NH_3/MeOH, reflux, 1 h 3. NH_3/H_2O, reflux, 30 min	Not observed (side product formed)
4B	6, $RNHCOCF_3$	NH_3/MeOH 25^0C, 20 h	ND	1. NH_3/MeOH, reflux, 1 h 2. NH_3/H_2O, reflux, 30 min	Not observed
5	6, $RNHCOCF_3$	NH_3/MeOH 25^0C, 18 h	ND	NH_3/H_2O, reflux, 30 min	Yes, 44% (side product formed)
6	4, $RNHCOCH_3$	NH_3/MeOH 25^0C, 21 h	ND	EtOH/KOH, reflux, 3 h	Not observed

ND = Not Determined (and not isolated).
[a]Trials for glycosylation from Table 24.

The debenzoylation reactions with NH_3/MeOH (at 4 or 25^{0}C) were carried out according to published procedures[1,157,191] and were generally successful (Trials 1-3).

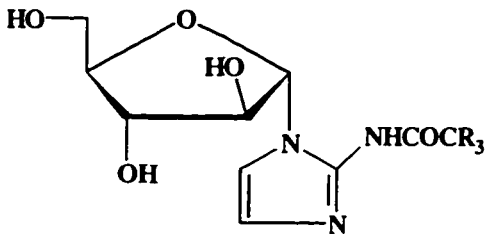

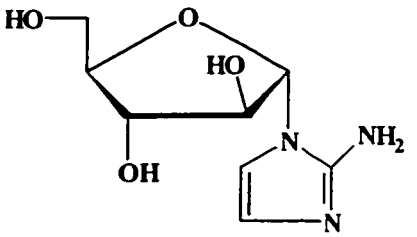

74 (R = H)
68 (R = F)

6

The cleavage of the amides proved to be more difficult than the debenzoylation reactions. The acetamide 74 was cleaved in refluxing ethanol and aqueous base to give 50% of AIA (6). Although methanolic ammonia (25^{0}C, 4 days) was not able to cleave the trifluoroacetamide 68, reflux in 29% ammonia water for 30 min afforded 6 in 44% yields. Cleavage of the trifluoroacetamide required less vigorous reaction conditions to be cleaved as expected. In Trial 5, in particular, a side product was observed after work-up and purification by reverse-phase HPLC. This side product had similar ^{1}H NMR data and mass fragmentation patterns to 6 but eluted faster in reverse-phase HPLC. Table 26 provides a comparison of ^{1}H NMR and mass data between these two compounds.

The identical molecular weights obtained for both compounds suggested that they are isomers. In ^{1}H-^{1}H COSY, a cross peak between H_2' and H_5' was observed in the side product but not in 6. In NOE results, a generally lower enhancement was observed in the side product, suggesting slightly shorter spatial distances among the protons. This difference in NOE enhancement was particularly noticeable at H_2' when the imidazole proton C_5-H was irradiated (1.0% in the side product and 12.3% in 6).

when the imidazole proton C_5-H was irradiated (1.0% in the side product and 12.3% in 6).

Table 26. Comparison of ^{1}H NMR and mass data of the unknown side product and AIA (6).

	Unknown side product	*AIA (6)*
^{1}H NMR (D_2O):		
-Imidazole protons	δ6.90 & 6.69	δ6.83 & 6.56
-H_1'	δ5.52	δ5.45
-$J_{1'-2'}$	5.5 Hz	6.2 Hz
-^{1}H-^{1}H COSY	H_2' has cross peaks with H_5'	H_2' has no cross peaks with H_5'
-^{1}H-^{1}H NOESY	NOESY cross peaks at: • C_5-H (imidazole) - H_2' • H_1' - H_2' • H_1' - H_3' & H_4'	NOESY cross peaks at: • C_5-H (imidazole) - H_2'
-NOE correlation results		H_1'*: C_5-H (1.9%) H_2 (3.3%) H_3 (5.0%) H_5 (1.0%) C_5-H*: C_4-H (5.6%) H_1' (2.6%) H_2' (12.3%) H_4 (2.5%)
^{1}H NMR (CD_3CN):		
-Imidazole protons	δ6.89 & 6.74	δ6.76 & 6.48
-H_1'	δ5.61	δ5.40
-$J_{1'-2'}$	3.42 Hz	5.38 Hz
-NOE	H_1'*: C_5-H (2.5%)** H_2 (1.6%) H_3 (1.2%) C_5-H*: C_4-H (4.2%) H_1' (1.3%) H_2' (1.0%) H_4 (0.7%)	

*Irradiated proton in NOE experiments.
**NOE intensity enhancement.

Table 26 (Cont'd). Comparison of ^{1}H NMR and mass data of the unknown side product and AIA (6).

	Unknown side product	*AIA (6)*
LR FAB MS:	(M+H$^+$) 216 (100) 207 (17.46) 185 (47.53) 115 (41.72) 93 (67.87) 84 (37.59) 75 (18.95) 57 (15.68)	(M+H$^+$) 216 (69.24) 207 (9.96) 185 (79.85) 115 (18.76) 93 (100) 84 (21.84) 75 (25.51) 57 (19.62)
HR FAB MS:	Found: 216.0995 Calcd: 216.0984 ($C_8H_{14}O_4N_3$)	Found: 216.0991 Calcd: 216.0984 ($C_8H_{14}O_4N_3$)
Reverse-phase HPLC retention time (H_2O, 0.6 mL/min):	8.48 - 9.56 min	11.02 - 12.09 min

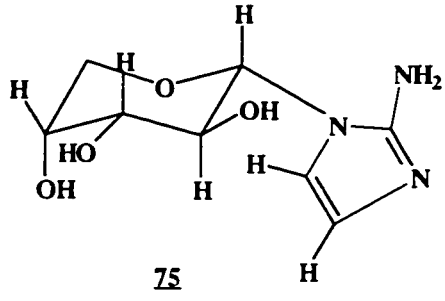

75

Based on these observations, the proposed structure for this side product is 75, the arabinopyranose counterpart of 6 (Seki, Ohkura, and Lee, unpublished results). The pyranose structure of the sugar could explain the difference in NOE results since the pyranose ring is more flexible and may increase the spatial separation among the protons. Differences in chemical shifts of H_1' and $J_{1'-2'}$ coupling constants also provided some support for the proposed structure. Furthermore, neither of the ^{1}H

NMR spectrum of **6** nor **75** changed at elevated temperature (80^0C), suggesting the observed ^{1}H NMR differences at 25^0C were not due to intramolecular dymanics such as hindrance to internal rotation[186] (Seki and Ohkura, unpublished results). Thus **6** and **75** do not have identical chemical structures. Although there is good support for the proposed structure of **75**, this proof is not absolute and the possibility of a β counterpart is still not precluded. Further studies are currently in progress (Seki and Ohkura, unpublished results).

In summary, the glycosylation products **71** and **67** were successfully deprotected in two steps to afford **6** in about 50% yields.

4.5. Investigations that led to the conclusion of the chemical structure of α-IAZA (1A)

4.5.1. Initial observation: Studies with AIA (6)

As described in section 4.3.1., AIA (6) was prepared by chemical reduction from AZA (7) and chemical synthesis from D-(-)-arabinose (61). The ^{1}H NMR spectra of both compounds were found to be virtually identical (Table 27). This initial observation raised the question of the anomeric configuration of 6 reduced from 7. Because of the *trans* rule of nucleoside synthesis[160], a C_1'- C_2' *trans* (α) nucleoside is expected from glycosylated 6. To determine the anomeric configuration of glycosylated 6, ^{1}H-^{1}H COSY (Figure 24), ^{1}H-^{1}H NOESY (Figure 25) and NOE correlation experiments were performed (Table 27).

Table 27. ^{1}H NMR data comparison between the two AIA (6) nucleosides synthesized by two different methods.

	Glycosylated AIA (6)	*Reduced AIA (6)*
^{1}H NMR (D_2O)	Imidazole protons (C_4-H & C_5-H): δ6.53 (1.8 Hz) & δ6.81 (1.8 Hz) H_1': δ5.43 ($J_{1',2'}$ = 6.3 Hz) H_2': δ4.36 H_3': δ4.08 H_4': δ4.01 H_5': δ3.68 & 3.59	Imidazole protons (C_4-H & C_5-H): δ6.48 (2 Hz) & 6.77 (2 Hz) H_1': δ5.40 ($J_{1',2'}$ = 6 Hz) H_2': δ4.33 H_3': δ4.06 H_4': δ3.99 H_5': δ3.66 & 3.56
^{1}H-^{1}H COSY (D_2O)	H_1' X H_2' H_2' X H_1' & H_3' H_3' X H_2' & H_4' H_4' X H_3' & H_5' H_5' X H_4' & H_5' C_4-H X C_5-H C_5-H X C_4-H	Not performed.

Table 27 (Cont'd). ^{1}H NMR data comparison between the two AIA (6) nucleosides synthesized by two different methods.

	Glycosylated AIA (6)	*Reduced AIA (6)*
^{1}H-^{1}H NOESY (D_2O)	H_2' X C_5-H (imidazole proton)	Not performed.
NOE correlation results (D_2O)	H_1'*: C_5-H (1.9%) H_2' (3.3%) H_3' (5.0%) H_5' (1.0%) C_5-H*: C_4-H (5.6%) H_1' (2.6%) H_2' (12.3%) H_4' (2.5%)	Not performed on 6 but on **IAIA 5(CD_3OD)**: H_1'*: C_5-H (1.6%) H_2' (3.6%) H_3' (2.0%) C_5-H*: H_1' (2.4%) H_2' (5.5%) H_4' (1.0%)
	Structure shown in 6 (NOE).	Structure shown in 5 (NOE).

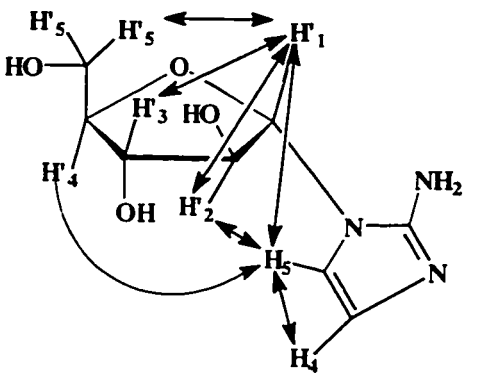

6 (NOE)

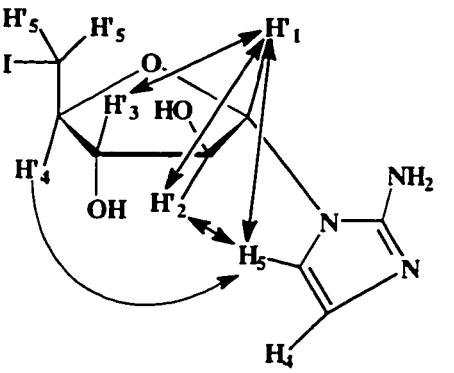

5 (NOE)

^{1}H-^{1}H NOESY (Figure 25) and NOE correlation results both indicated the spatial interactions between the H_2' proton on the sugar and the C_5-H proton on the imidazole ring (6(NOE)). These observations strongly suggest an α nucleoside. If it were β, strong NOE enhancement signals (12.3%) would be very unlikely.

Figure 24. ^{1}H-^{1}H COSY spectrum of AIA (6).

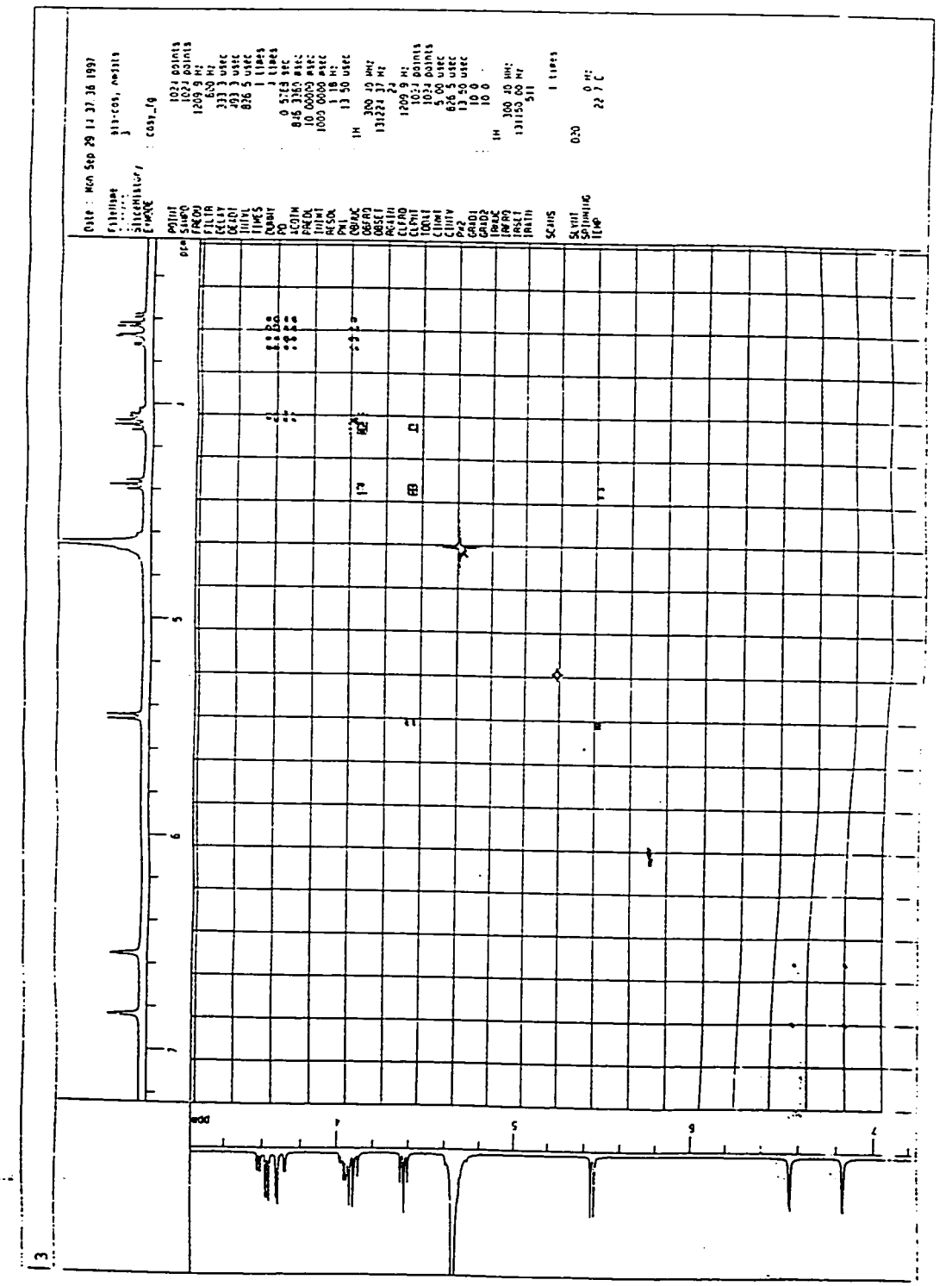

Figure 25. ^{1}H-^{1}H NOESY spectrum of AIA (6).

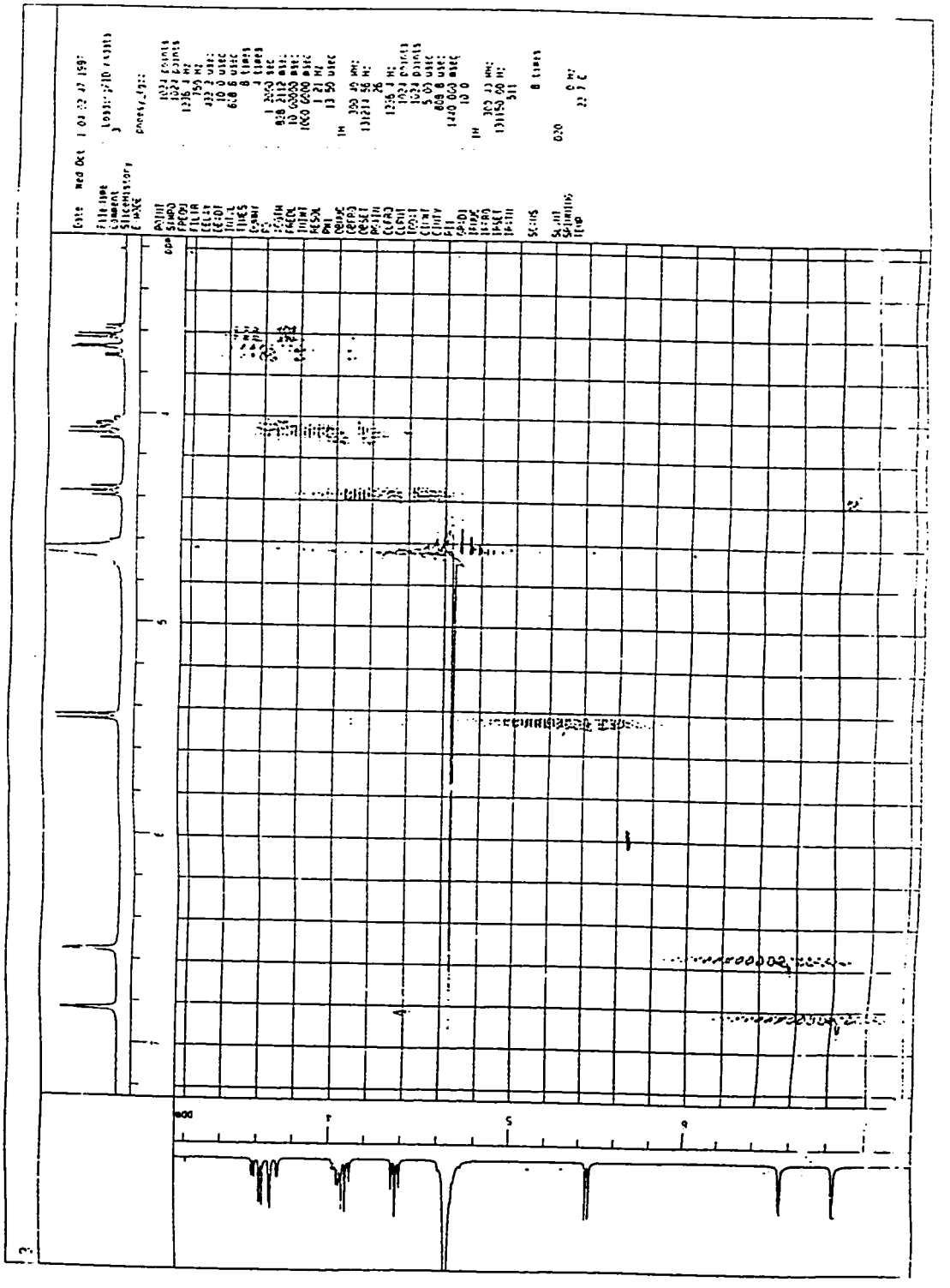

Other NOE correlations (H_4' and C_5-H; H_1' and H_3') gave additional support for the α configuration of **6** and was consistent with literature observations[188,235]. Molecular orbital (MO) calculations (PM3 method[236], MOPAC version 94) on **6** predicted that the spatial distances between **C_5-H-H_2'**, C_5-H-H_4' and H_1'-H_3' are **2.073**, 3.563, and 3.916 Å, respectively (Figure 26) (Seki and Ohkura, unpublished results). Because an NOE signal falls off with the inverse sixth power of distance, protons must be within approximately 5 Å of each other for an NOE between them to be observed[189]. These predicted spatial distances are well within 5 Å and thus are very likely to be observed. The corresponding distances for β-AIA (**76**) were predicted to be **4.716**, 4.468, and 4.126 Å, respectively (Figure 27) (Seki and Ohkura, unpublished results). These larger spatial distances in the β anomer (especially in C_5-H-H_2' where the distance is more than doubled) are not likely to generate a strong NOE signal[188,235]. The dihedral angle ϕ between the C_1'-H and C_2'-H bonds in **6** was predicted to be about -110.62^0 (Figure 28) which corresponds to a theoretical C_1'-C_2' coupling constant of about 1 Hz by the Karplus equation. This theoretical coupling constant is consistent with the small coupling constant reported for C_1'-C_2' *trans* arabinofuranosyl nucleosides[157,231]. The higher (6 Hz) coupling constant observed for **6** was also within the limits of empirical results[186]. It should be emphasized that these MO calculations are performed on molecules in isolation and do not take into account any solvent effects. Nevertheless, these calculations provide a theoretical framework for intramolecular distances and dihedral angles.

Figure 26. MO calculations on AIA (6) of intramolecular distances relevant in NOE correlation studies (Seki and Ohkura, unpublished results).

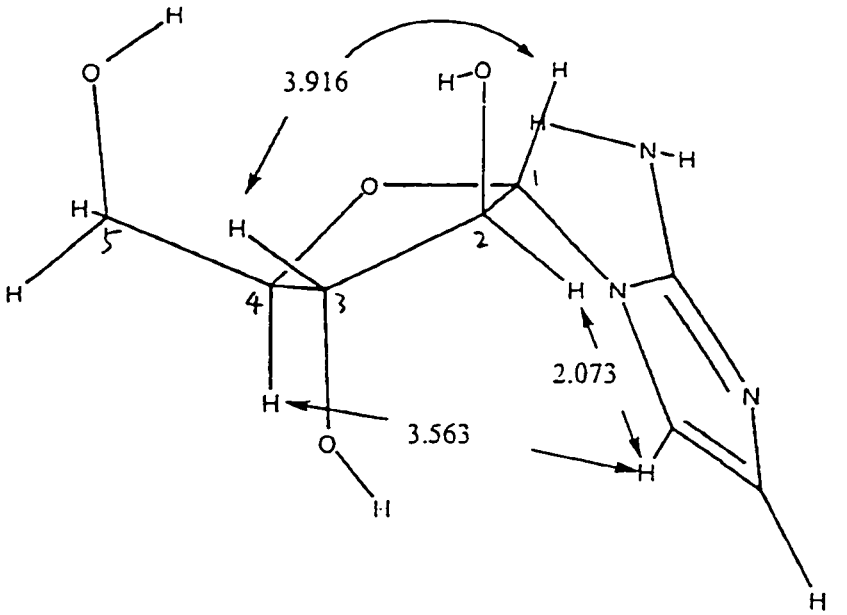

Figure 27. MO calculations on β-AIA (76) of intramolecular distances relevant in NOE correlation studies (Seki and Ohkura, unpublished results).

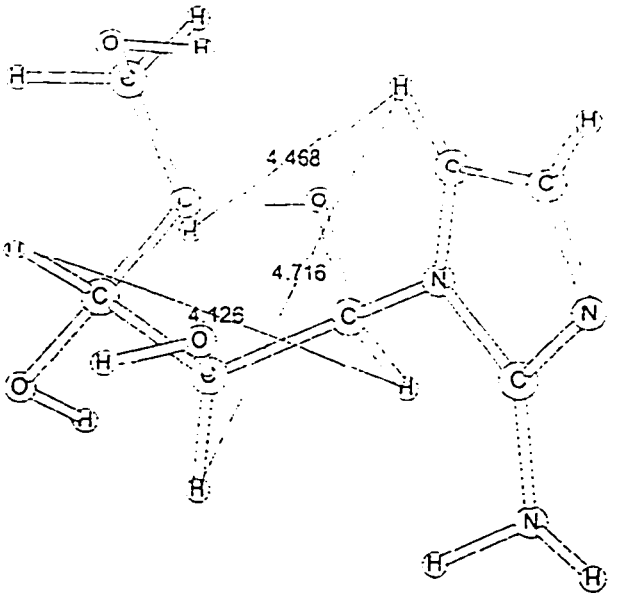

Figure 28. MO calculations on AIA (6): dihedral angles and other selected intramolecular distances (Seki and Ohkura, unpublished results).

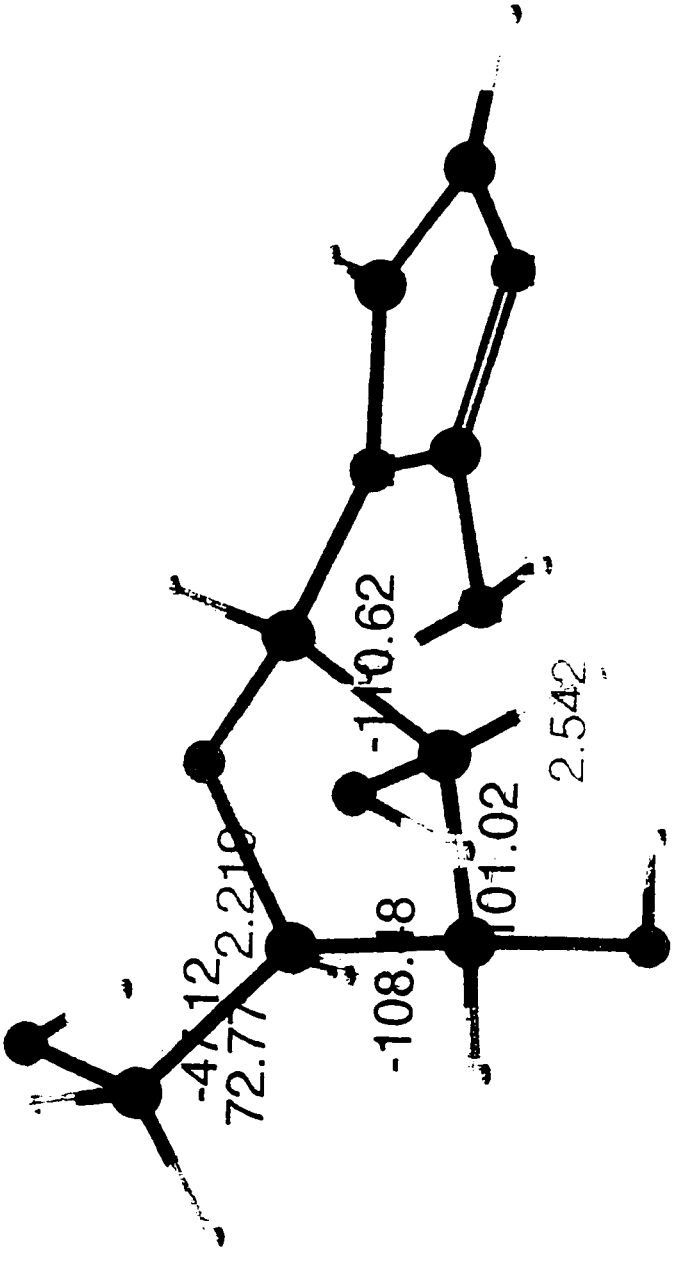

If 6 has the α configuration, the logical extension will be the same α configuration of AZA (7) which was used to prepare 6. Chemical reduction and subsequent iodination are not expected to change the anomeric configuration of the nucleoside. NOE correlation results of IAIA (5) confirmed this speculation. NOE enhancements were observed at H_2' and H_4' when C_5-H on the imidazole was irradiated (5 (NOE)).

Based on these NOE observations, if AZA (7) is the α nucleoside, then IAZA (1A) will also be α. The next piece of evidence to support this claim involved the previously reported glycosylation methods and ^{1}H NMR data of 7 and 1A.

4.5.2. Literature evidence

^{1}H NMR data

The first indications that the reported β-IAZA (77) could actually be the α nucleoside came from a publication by Chapman *et al*[157]. In that paper, the synthesis of α-IAZA (1A) itself was reported and it has a small (~ 1.5 Hz) H_1'-H_2' coupling constant. The reported ^{1}H NMR data of 1A and other related compounds are shown in Table 28.

In a paper by Sakaguchi *et al.*[231], the ^{1}H NMR data (in DMSO-d_6) for both α- and β-AZA (7 and 78) were reported. In particular, the coupling constant between H_1' and H_2' was also found to be very small (1.5 Hz or less). Furthermore, the H_1'-H_2' coupling constants of their benzoylated counterparts were 0.4 Hz and 4.6 Hz for α and β anomers, respectively. These two papers show that α-AZA (7) has a smaller H_1'-H_2' coupling constant than its β counterpart.

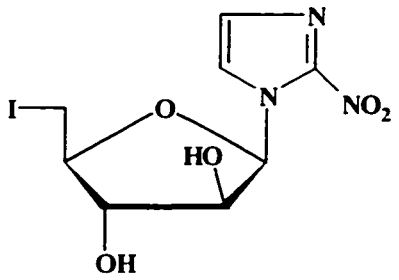

77

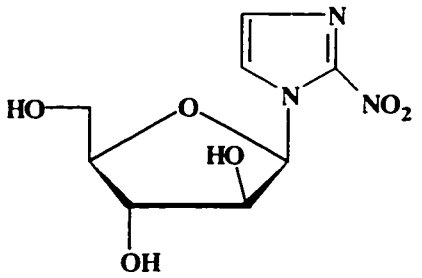

78

Table 28. ^{1}H NMR and melting point data reported in literature.

Literature	*Chemical shift(δ)*	*H_1'-H_2' coupling constant ($J_{1'2'}$)(Hz)*	*Melting point (^0C)*
Schneider *et al.*[154]	DMSO-d_6:		
α-AZA (7):	**6.30**	**1.47**	153-155
α-IAZA (1A):	**6.39**	**1.48**	not reported
Sakaguchi *et al.*[220]	DMSO-d_6:		
α-AZA (7):	**6.29**	**broad singlet**	160
β-AZA (78):	**6.60**	not reported	172
Mannan *et al.*[1]	CD_3OD:		
β-AZA (78):	**6.29**	**1.3**	192-193
β-IAZA (77):	**6.52**	**singlet**	122

In Mannan *et al.*[1], the synthesis of β-IAZA (77) was reported and the observed H_1'-H_2' coupling constants of β-AZA (78) and β-IAZA (77) therein raised further questions of anomeric configuration. This β-AZA (78) had remarkably similar ^{1}H NMR characteristics as the α-AZA (7) reported in the previous two papers (Table 28).

Although the H_1'-H_2' coupling constant cannot always be used for anomeric assignment of nucleosides, an H_1'-H_2' coupling constant of about 1 Hz is often indicative of a C_1'-C_2' *trans* (α) nucleoside (see section 2.3.2.1.). Therefore, the small H_1'-H_2' coupling constant reported for **77** could actually belong to that of the α counterpart in accordance with previous published results[157,231].

The ribose examples also gave some support for the above ^{1}H NMR data. It is true that α- and β-AZA (**7** and **78**) are not equivalent to their ribose counterparts (**79** and **80**, respectively), but *arabino* α and *ribo* β nucleosides are both considered to be C_1'-C_2' *trans* because the configuration around C_1' and C_2' would be identical[181]. Their anomeric protons should have virtually identical chemical shifts. The ^{1}H NMR data (in DMSO-d_6) of **79** and **80** were reported by Prisbe *et al*[191].

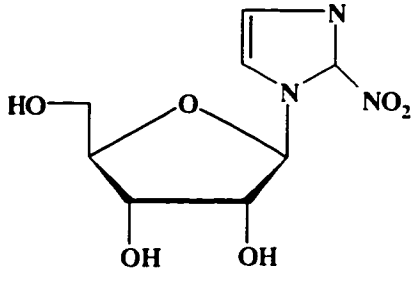

79

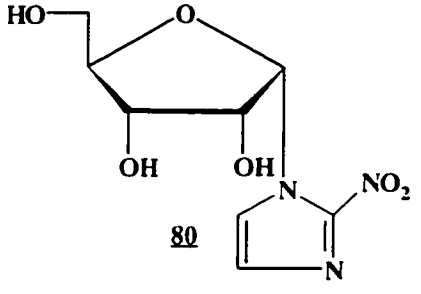

80

δ6.21 (H_1', $J_{1'-2'}$ = 1 Hz) **δ6.52 (H_1', $J_{1'-2'}$ = 4.5 Hz)**

Comparison of these ^{1}H NMR data revealed that **79** (C_1'-C_2' *trans* nucleoside) had very similar chemical shifts and H_1'-H_2' coupling constants as **7** (also a C_1'-C_2' *trans* nucleoside). The same inference was reached with the C_1'-C_2' *cis* nucleosides **80** and β-AZA **78**). Although speculations on the H_1'-H_2' coupling constant in ribosyl nucleosides cannot always be extended to their arabinofuranosyl counterparts, a small

value was indeed reported in **79**. Therefore, the ribose examples gave further support that a C_1'-C_2' *trans* nucleoside has a smaller (~ 1 Hz) H_1'-H_2' coupling constant than a C_1'-C_2' *cis* nucleoside.

Glycosylation methods

The glycosylation methods reported in literature also shed some light on the possibility of obtaining β-IAZA. The preparation of a C_1'-C_2' *cis* nucleoside has traditionally been difficult due to the *trans* rule of nucleoside synthesis[160] (see section 2.3.1.). Although there was an exception reported for this *trans* rule[191], C_1'-C_2' *trans* nucleosides almost always predominate. Table 29 shows that variations in reaction conditions could have a significant effect on the yields of the α and β nucleosides. In the Mannan[1] and Kumar (unpublished results) methods, one major anomer (β) predominated. In the Sakaguchi[231] method, the yields of the α nucleoside exceeded the β by about fivefold. The Chapman group[157] reported approximately equal yields of both the α and β nucleosides. Seki and Ohkura (unpublished results) repeated the Chapman method and observed that there was no β nucleosides. They observed a compound with an R_f value higher than that of the α nucleoside, *but it was not the β nucleoside as reported in the Chapman group.* These observations suggest that the β nucleoside is very difficult to prepare and the glycosylation reaction could be very sensitive to different reaction conditions. The reported 69% yield of the β protected nucleoside previously reported[1] thus is not consistent with these observations.

Table 29. Glycosylation methods reported in literature.

Literature	*Sugar bromide* ***64***	*Silylation of 2-nitro-imidazole*	*$Hg(CN)_2$*	*Reaction conditions*	*Glycosylation results*
Sakaguchi *et al.*[231]	-HBr-HOAc method -anomeric mixture (1 eq)	Yes (1.5 eq)	Yes (1 eq)	CH_3CN, RT, 2 days	**α (32.9%)** β (7.2%)
Mannan *et al.*[1]	-HBr/HOAc method -pure α (1 eq)	No	Yes (2.1 eq)	CH_3CN RT, 6 h	"β" (69%) no "α" was reported
Kumar *et al.* (unpublished results)	-HBr/CH_2Cl_2 -anomeric mixture (1 eq)	Yes (1.17 eq)	Yes (2.26 eq)	CH_3CN 50^0C, 15 h	1 major product ("β")
Schneider *et al.*[157]	-HBr/HOAc method -pure α (1 eq)	No	Yes (2.5 eq)	CH_3CN 40^0C, 4 h; RT, 16 h	**α (22.7%)** β (21.5%)
Seki and Ohkura (unpublished results)	-HBr/HOAc method -pure α (1 eq)	No	Yes (2.5 eq)	CH_3CN 40^0C, 4 h; RT, 16 h	**α (major)** no β observed

In summary, two types of literature evidence (^{1}H NMR and glycosylation methods) gave strong support for the α configuration of the reported β-IAZA (**77**). To confirm that the Mannan and Kumar methods actually produced the α nucleosides, previous ^{1}H NMR spectra were reexamined. The next section is devoted to this reinvestigation.

4.5.3. Previous ^{1}H and ^{13}C NMR data of AZA and IAZA

Four independent syntheses of AZA and IAZA have been performed and the ^{1}H and ^{13}C NMR data recorded therein were reexamined. Table 30 provides a brief summary of the NMR data, and Figures 29 and 30 show the ^{1}H-^{1}H COSY and ^{1}H-^{1}H ROESY spectra of IAZA, respectively.

Table 30. ^{1}H and ^{13}C NMR data for previous AZA and IAZA syntheses.

Batch # of AZA & IAZA	*AZA*	*IAZA*
1 (Data was published in Mannan *et al*[1])	^{1}H NMR (CD_3OD): **H_1': δ6.44 ($J_{1',2'}$ = 1.3 Hz)** ^{13}C NMR (CD_3OD): **C_1': δ97.1334**	^{1}H NMR ($CD_3OD/CDCl_3$): **H_1': δ6.5156 ($J_{1',2'}$ = singlet)** ^{13}C NMR ($CD_3OD/CDCl_3$): **C_1': δ95.9895**
2 (unpublished results)	NMR data was not available.	NMR data was not available.
3 (unpublished results)	^{1}H NMR (CD_3OD): **H_1': δ6.44 ($J_{1',2'}$ = singlet)** ^{13}C NMR data was not available.	^{1}H NMR (CD_3OD): **H_1': δ6.48 ($J_{1',2'}$ = singlet)** ^{13}C NMR data was not available.
4 (unpublished results)	^{13}C NMR data was not available.	^{1}H NMR (CD_3OD): **H_1': δ6.49 ($J_{1',2'}$ = singlet)** ^{1}H-^{1}H COSY (CD_3OD): **H_1' X C_5-H** **H_1' X C_4-H** ^{1}H-^{1}H ROESY (CD_3OD): **C_5-H X H_4'** **C_5-H X H_2'** **H_1' X H_3'** ^{13}C NMR (CD_3OD): **C_1': δ97.542**

Figure 29. ^{1}H-^{1}H COSY spectrum of IAZA (1A) (Kumar, unpublished results).

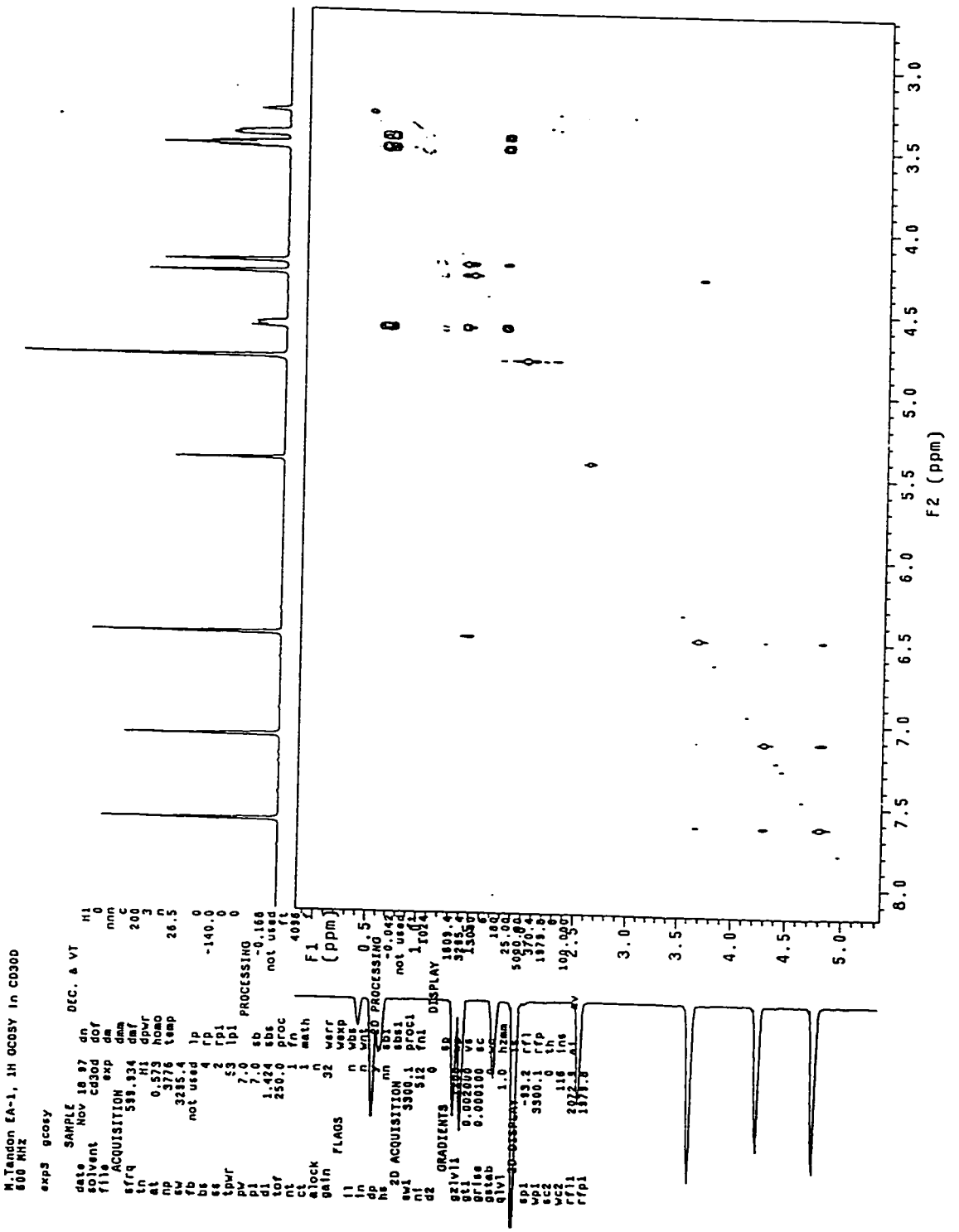

Figure 30. ^{1}H-^{1}H ROESY spectrum of IAZA (1A) (Kumar, unpublished results).

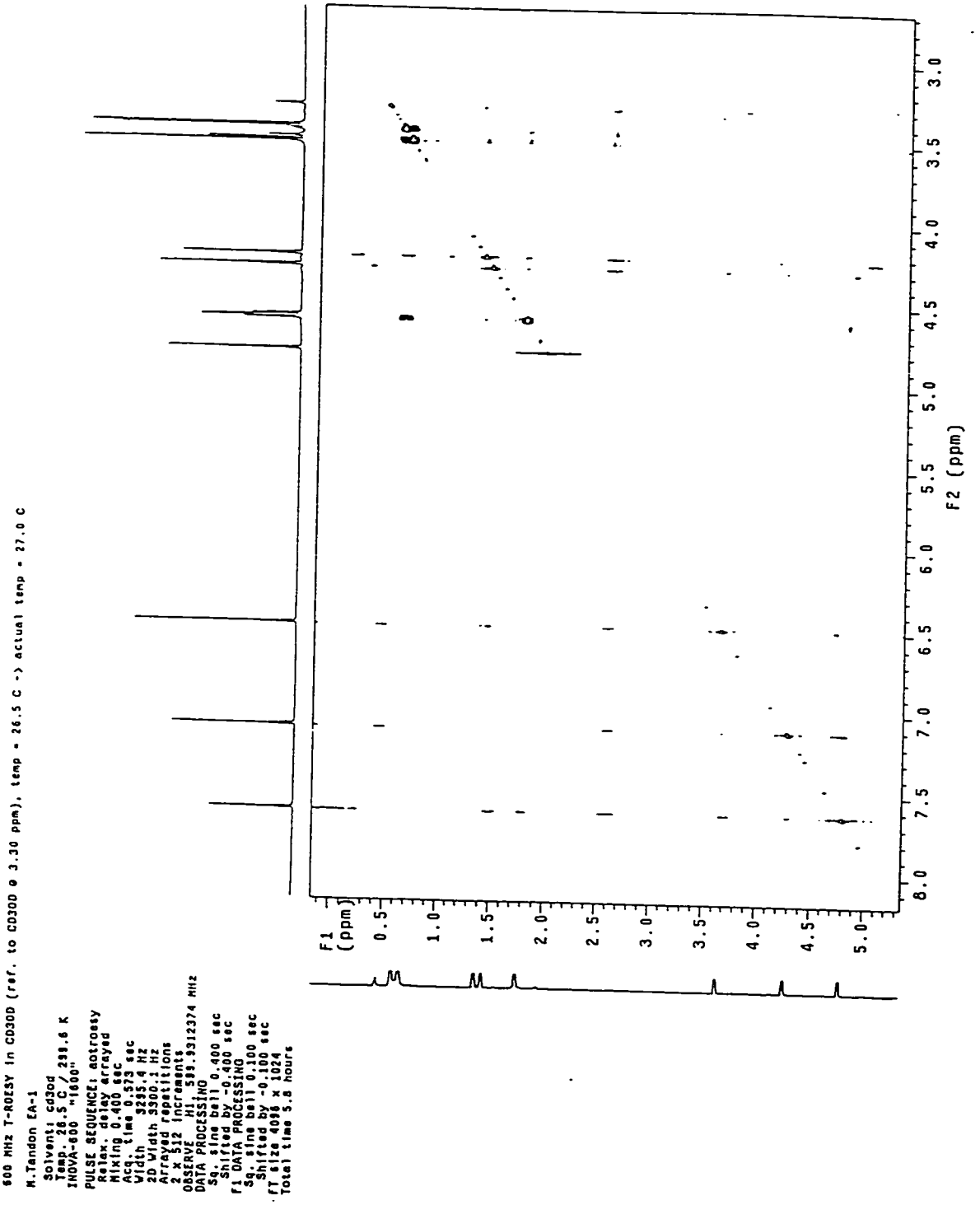

There are two noteworthy points in Table 30. First, these NMR data provide strong evidences that the anomeric configuration of all four batches of compounds are identical. Second, both AZA and IAZA had small H_1'-H_2' coupling constants (~ 1 Hz and even singlets). ^1H-^1H COSY (Figure 29) and ROESY (rotating frame NOESY, Figure 30) data further suggest the spatial proximity of the imidazole protons to H_2' and H_4' protons. These observations strongly indicate that these nucleosides have the α configuration (see section 4.5.2.).

Reexaminations of previous NMR data of AZA and IAZA led to the same conclusions. The final and absolute piece of proof came after X-ray crystallography structure analyses of AZA and IAZA.

4.5.4. X-ray crystallography structure analyses

X-ray crystallography provides an attractive method for the determination of the absolute configuration of an anomeric compound (see section 2.3.2.3.). Two samples were submitted for X-ray structure analyses: IAZA (Batch #4) (Kumar, unpublished results) and AZA (Seki and Ohkura, unpublished results). The structures are shown in Figures 31 and 32, respectively. In both cases, the anomeric configurations of the nucleosides are unambiguously α.

These investigations all led to the conclusion of the α configuration of the IAZA reported in Mannan *et al*[1]. In summary, these two initial indications are crucial in this determination:

1. A small (~ 1 Hz) H_1'-H_2' coupling constant will indicate α-IAZA (**1A**).
2. The *trans* rule of nucleoside synthesis will almost always produce a C_1'-C_2' *trans* nucleoside.

Figure 31. X-ray crystallography structure analysis of IAZA (1A) (Kumar, unpublished results).

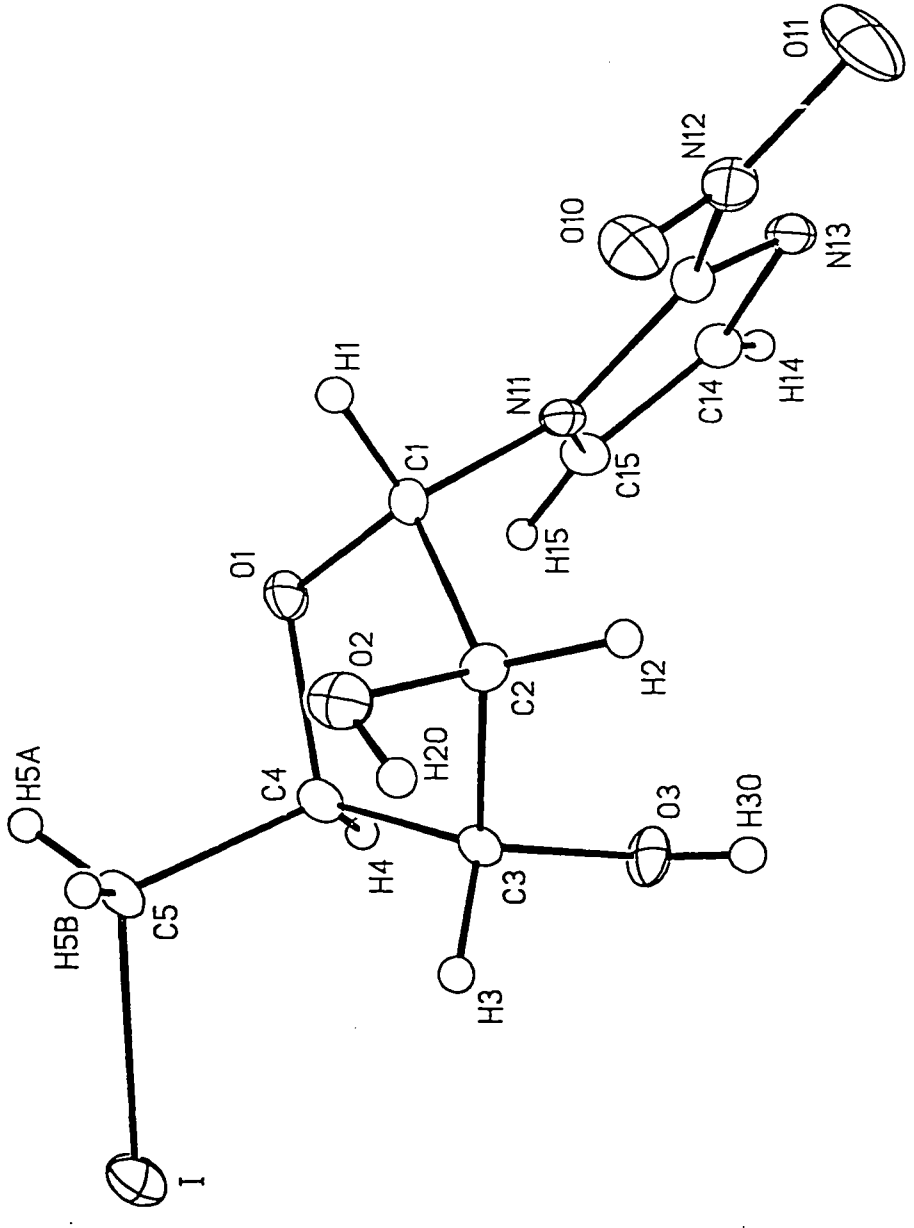

Figure 32. X-ray crystallography structure analysis of AZA (7) (Seki and Ohkura, unpublished results).

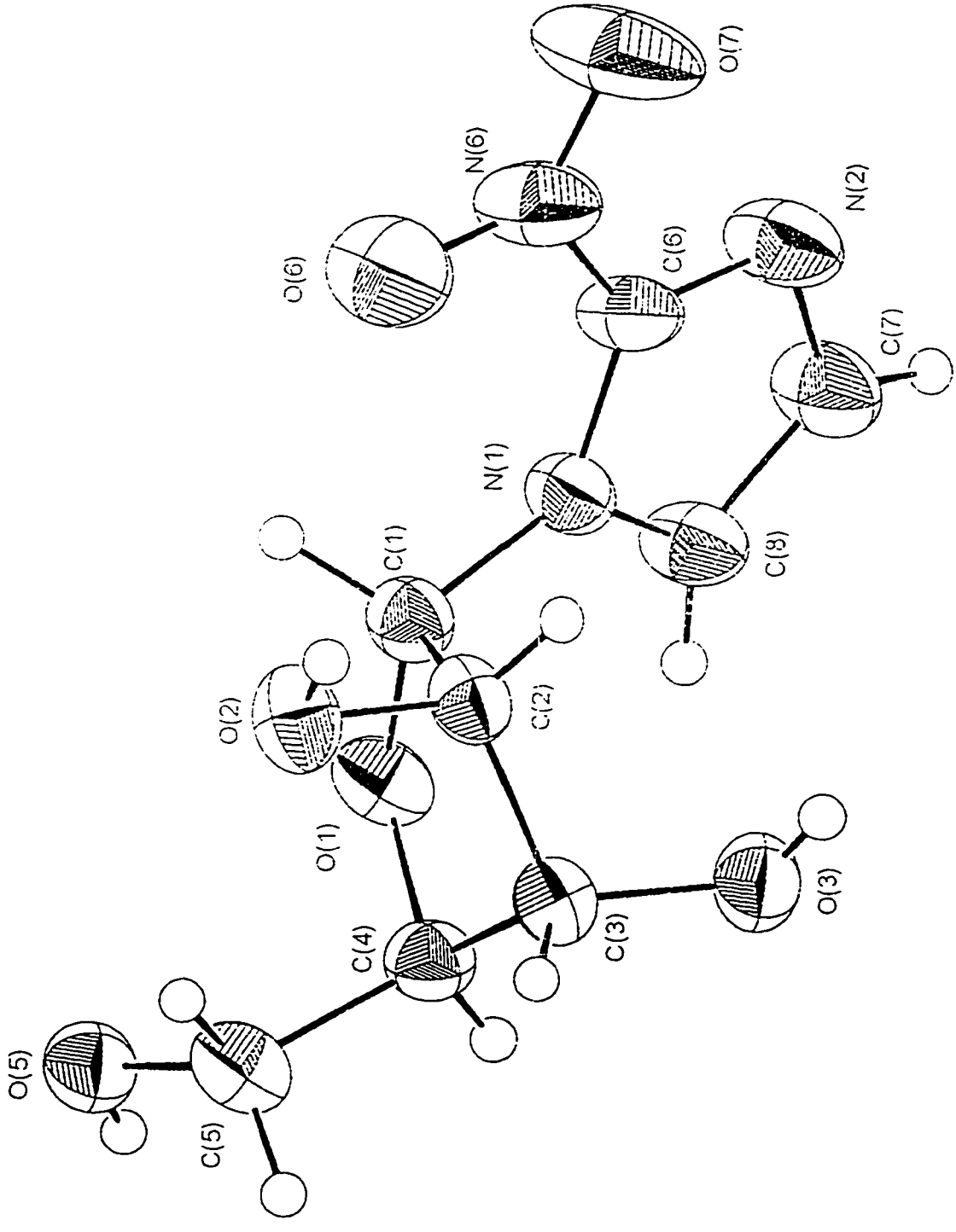

5. Conclusions

The primary objective of the research described in this thesis was to evaluate the potential of two kinds of radioiodinated metabolites from [^{123}I]IAZA (**1A**) as SPECT brain and tumor imaging agents. The chemistry, radioiodination and biological studies of these proposed metabolites, together with investigations on the sugar-2-aminoimidazole glycosylation reaction and the anomeric configuration of **1A**, reported in the previous chapters have now led to the following conclusions.

1. The abnormal brain uptake of radioactivity observed in [^{123}I]IAZA patients could not be explained by this study on radioiodinated [^{123}I]IAZA metabolites. The sugar analogs **3** and **4** showed no active accumulation of brain radioactivity in the mouse brain. The amino analog of IAZA (**5**) also showed no brain uptake of radioactivity in both normal and tumor-bearing mice. The nature of this observed brain uptake in 3 out of 10 advanced cancer patients is still unknown.
2. In *in vivo* biodistribution studies with tumor-bearing mice, [^{125}I]-**5** exhibited a moderately high tumor-to-blood ratio of 4.34 at 4 h post injection. But at the same time other tissues, especially the liver, had persistently higher ratios than the tumor, even at 24 h post injection. The high liver radioactivity at 24 h suggests metabolic trapping in this organ, and further study would be needed to determine the nature of this metabolic trapping. *In vivo* deiodination followed by subsequent accumulation of radioactivity in thyroid was common to all the radioiodinated metabolites. However, [^{125}I]-**5** appeared to be more radiochemically stable *in vivo* (at 4 h post injection) than its sugar counterparts. The renal route is an important route for excretion for all the metabolites, although in [^{125}I]-**5** liver and GIT

radioactivity noted in the high tissue-to-blood ratios suggests that the hepatobiliary elimination route is equally, if not more, important. More than 95% of the injected dose was eliminated within 4 h after injection for the sugar metabolites **3** and **4**, and greater than 97% was excreted within 24 h for **5**.

3. The sugar analogs were synthesized by chemical cleavage of the N^1-glycosidic bond of **58B** and **1B**. Alternatively they were prepared from commercially available D-(-)-arabinose (**61**) because the former method involves the degradation of a costly synthetic end product IAZA (**1A**). Radioiodination of these sugars was achieved by exchange labeling in the pivalic acid "melt" method. Over 90% radiochemical yields were obtained with both sugars. Purification was achieved by column chromatography (silica gel) and the radiochemical purity of both sugars determined thereafter was >98%. Since the radiochemical stability of [^{125}I]-**4** in saline was low, 20% ethanol in saline was selected and found to be a suitable solution medium for animal injection.

4. The sugar derivative (amino nucleoside) **5** was also prepared by two different methods. The first method involved the chemical reduction of AZA (**7**) with hydrogen in the presence of palladium-carbon and subsequent iodination. A less costly method is the direct glycosylation of a 2-aminoimidazole derivative (**66** or **69**) with the protected sugar bromide **64**. The desired α-nucleoside **67** was achieved in 44% yield. Two methods of the radioiodination of **5** were studied. The solvent exchange method in 2-propanol was preferred due to its shorter reaction time when compared to the pivalic acid "melt" method. In both methods, radiochemical yields of 40-45% were obtained. Purification of [^{125}I]-**5** was

achieved by reverse-phase Sep-Pak® cartridges and the radiochemical purity determined thereafter was >95%.

5. Ten glycosylation trials between a 2-aminoimidazole derivative (**66** or **69**) and the protected sugar bromide **64** were performed. The desired glycosylation product was obtained in 8 of the 10 trials with an average yield of about 23%. The problem of the reactive exocyclic, primary amino group on the imidazole base was solved by introducing the acetamide and the trifluoroacetamide as the protective groups. The HBr/HOAC method was preferred for the preparation of the sugar bromide **64** because crystalline and anomerically pure α-bromide could be obtained and characterized by melting point and ^{1}H NMR. This crystalline bromide was observed to be stable when stored under argon at -20^{0}C for up to 6 months. However, its chemical stability in acetonitrile was low. This problem was circumvented by dissolving the sugar bromide in benzene and subsequent dropwise addition to acetonitrile. Silylation and mercury catalysts were found to be unnecessary in this study. The glycosylation reaction with the trifluoroacetamide **66** gave the best yields (44%) and **67** was characterized by ^{1}H and ^{13}C NMR, ^{1}H-^{1}H COSY, ^{1}H-^{13}C correlation studies, ^{1}H-^{1}H NOESY, NOE correlation studies and FAB mass spectrometry. These results strongly suggest that **67** has an α configuration.

6. Although no β nucleoside was observed in the glycosylation reactions, a "bis" glycosylation product (**71** or **72**) was isolated. Its chemical structure was proven by ^{1}H NMR and FAB mass spectrometry. The latter method gave the strongest

support because of the high molecular weights (>1,000) obtained in both compounds.

7. Seven deprotection reactions were performed on selected glycosylation products. These deprotection reactions involved debenzoylation with NH_3/MeOH and subsequent cleavage of the amides. The second deprotection step was more difficult and produced **6** in about 50% yield. An isomer of **6** was isolated and its proposed structure is the arabinopyranose counterpart of **6** (**75**). Further confirmation is necessary for this proposed structure.

8. The possibility of α-IAZA (**1A**) and not the previously assigned β was explored. Studies with AIA (**6**), literature evidence (^{1}H NMR data and glycosylation methods), previous ^{1}H and ^{13}C NMR data of AZA and IAZA, and X-ray crystallography structure analyses on AZA and IAZA all led to the conclusion that IAZA is actually the α anomer.

References

1. Mannan RH, Somayaji VV, Lee J, Mercer JR, Chapman JD and Wiebe LI, "Radioiodinated 1-(5-Iodo-5-deoxy-β-D-arabinofuranosyl)-2-nitroimidazole (Iodoazomycin Arabinoside:IAZA): A Novel Marker of Tissue Hypoxia", *J Nucl Med*, **32(9)**:1764-1770 (1991).
2. Parliament MB, Chapman JD, Urtasun, RC McEwan AJ, Golberg L, Mercer JR, Mannan RH and Wiebe LI, "Non-invasive assessment of human tumor hypoxia with ^{123}I-Iodoazomycin arabinoside: preliminary report of a clinical study", *Brit J Cancer*, **65(1)**:90-95 (1992).
3. Wiebe LI and Stypinski D, "Pharmacokinetics of SPECT radiopharmaceuticals for imaging hypoxic tissues", *Q J Nucl Med*, **40(3)**:270-284 (1996).
4. Groshar D, McEwan AJB, Parliament MB, Urtasun RC, Golberg LE, Hoskinson M, Mercer JR, Mannan RH, Wiebe LI and Chapman JD, "Imaging Tumor Hypoxia and Tumor Perfusion", *J Nucl Med*, **34(6)**:885-888 (1993).
5. Al-Arafaj A, Ryan EA, Hutchison K, Mannan RH, Mercer J, Wiebe LI and McEwan AJB, "An evaluation of iodine-123 iodoazomycinarabinoside as a marker of localized tissue hypoxia in patients with diabetes mellitus", *Eur J Nucl Med*, **21(12)**:1338-1342 (1994).
6. Zimmerman M and Siedenberg J, "Deoxyribosyl transfer.I. Thymidine phosphorylase and nucleoside 2-deoxyribosyl transferase in normal and malignant tissues", *J Biol Chem*, **239(8)**:2618-2621 (1964).
7. Desgranges C, Razaka G, Rabaud M and Bricaud H, "Catabolism of thymidine in human blood platelets. Purification and properties of thymidine phosphorylase", *Biochim Biophys Acta*, **654(2)**:211-218 (1981).
8. Tovell DR, Samuel J, Mercer JR, Misra HK, Xu L, Wiebe LI, Tyrrel DL and Knaus EE, "The *in vitro* evaluation of nucleoside analogues as probes for use in the non-invasive diagnosis of herpes simplex encephalitis", *Drug Design Del*, **3(3)**:213-221 (1988).
9. Watanabe KA, Su TL, Klein RS, Chu CK, Matsuda A, Chun MW, Lopez C and Fox JJ, "Nucleosides 123. Synthesis of antiviral nucleosides: 5-substituted 1-(2-deoxy-2-halogeno-β-D-arabinofuranosyl)cytosines and -uracils. Some structure-activity relationships", *J Med Chem*, **26(2)**:152-156 (1983).
10. Saha GB, MacIntyre WJ and Go RT, "Radiopharmaceuticals for brain imaging", *Semin Nucl Med*, **24(4)**:324-349 (1994).
11. Som P, Atkins HL, Bandoypadhyay D, Fowler JS, MacGregor RR, Matsui K, Oster ZH, Sacker DF, Shiue CY, Turner H, Wan CN, Wolf AP and Zabinski SV, "A Fluorinated Glucose Analog, 2-Fluoro-2-deoxy-D-glucose(F-18): Nontoxic Tracer for Tumor Detection", *J Nucl Med*, **21(7)**:670-675 (1980).
12. Minn H, Joensuu H, Ahonen A and Klemi P, "Fluorodeoxyglucose Imaging: A Method to Assess the Proliferative Activity of Human Cancer *In Vivo*", *Cancer*, **61(9)**:1776-1781 (1988).
13. Kalaria RN and Harik SI, "Nucleoside Transporter of Cerebral Microvessels and Choroid Plexus", *J Neurochem*, **47(6)**:1849-1856 (1986).

14. Kung HF and Blau M, "Regional intracellular pH shift: a proposed mechanism for radiopharmaceutical uptake in brain and other tissues", *J Nucl Med*, **21(2)**:147-152 (1980).
15. Hawkins RA, Hoh C, Glaspy J, Choi Y, Dahlbom M, Rege S, Messa C, Nietszche E, Hoffman E, Seeger L, Maddahi J and Phelps ME, "The Role of Positron Emission Tomography in Oncology and Other Whole-Body Applications", *Semin Nucl Med*, **22(4)**:268-284 (1992).
16. Gallagher BM, Ansari A, Atkins H, Casella V, Christman DR, Fowler JS, Ido T, MacGregor RR, Som P, Wan CN, Wolf AP, Kuhl DE and Reivich M, "Radiopharmaceuticals XXVII. ^{18}F-Labeled 2-Deoxy-2-Fluoro-D-Glucose as a Radiopharmaceutical for Measuring Regional Myocardial Glucose Metabolism In Vivo: Tissue Distribution and Imaging Studies in Animals", *J Nucl Med*, **18(10)**:990-996 (1977).
17. Gallagher BM, Fowler JS, Gutterson NI, MacGregor RR, Wan CN and Wolf AP, "Metabolic Trapping as a Principle of Radiopharmaceutical Design: Some Factors Responsible for the Biodistribution of [^{18}F]2-Deoxy-2-Fluoro-D-Glucose", *J Nucl Med*, **19(10)**:1154-1161 (1978).
18. Phelps ME, "Positron computed tomography studies of cerebral glucose metabolism in man: theory and application in nuclear medicine", *Sem Nucl Med*, **11(1)**:32-49 (1981).
19. Alavi A, Reivich M, Greenberg J, Hand P, Rosenquist A, Rintelmann W, Christman D, Fowler J, Goldman A, MacGregor R and Wolf A, "Mapping of functional activity in brain with ^{18}F-fluoro-deoxyglucose", *Sem Nucl Med*, **11(1)**:24-31 (1981).
20. Henry TR, Englel J Jr and Mazziotta JC, "Clinical Evaluation of interictal fluorine-18-fluorodeoxyglucose PET in partial epilepsy", *J Nucl Med*, **34(11)**:1892-1898 (1993).
21. Salmon E, Sadzot B, Maquet P, Degueldre C, Lemaire C, Rigo P, Comar D and Franck G, "Differential diagnosis of Alzheimer's disease with PET", *J Nucl Med*, **35(3)**:391-398 (1994).
22. Herholz K, Perani D, Salmon E, Franck G, Fazio F, Heiss WD and Comar D, "Comparability of FDG-PET studies in probable Alzheimer's Disease", *J Nucl Med*, **34(9)**:1460-1466(1993).
23. Tommasino C, Grana C, Lucignani G, Torri G and Fazio F, "Regional cerebral metabolism of glucose in comatose and vegetative state patients", *J Neurosurg Anesthes*, **7(2)**:109-116 (1995).
24. Meyer M, Gast T, Raja S and Hubner K, "Increased F-18 FDG accumulation in an acute fracture", *Clin Nucl Med*, **19(1)**:13-14 (1994).
25. Perani D, Vallar G, Paulesu E, Alberoni M and Fazio F, "Left and right hemisphere contribution to recovery from neglect after right hemisphere damage - an [^{18}F]FDG PET study of two cases", *Neuropsychologica*, **31(2)**:115-125 (1993).
26. Huber M, Kittner B, Hojer C, Fink GR, Neveling M and Heiss WD, "Effect of propentofylline on regional cerebral glucose metabolism in acute ischemic stroke", *J Cereb Blood Flow Metab*, **13(3)**:526-530 (1993).

27. Eberling JL, Richardson BC, Reed BR, Wolfe N and Jagust WJ, "Cortical glucose metabolism in Parkinson's disease without dementia", *Neurobiol Aging*, **15(3)**:329-335 (1994).
28. Herholz K, "FDG PET and differential diagnosis of dementia", *Alzheimer's Disease & Assoc Disorders*, **9(1)**:6-16 (1995).
29. Pappata S, Chabriat H, Levasseur M, Legault-Demare F and Baron JC, "Marchiafava-Bignami disease with dementia: severe cerebral metabolic depression revealed by PET", *J Neural Trans Parkinson's Disease & Dementia Sec*, **8(1-2)**:131-137 (1994).
30. Heiss WD, Pawlik G, Herholz K, Wagner R and Wienhard K, "Regional cerebral glucose metabolism in man during wakefulness, sleep, and dreaming", *Brain Res*, **327(1-2)**:362-366 (1985).
31. Wu J, Buchsbaum MS and Gillin JC, American Psychiatry Association, Chicago, May 9-14, 1987.
32. Yamada S, Kubota K, Kubota R, Ido T and Tamahashi N, "High accumulation of fluorine-18-fluorodeoxyglucose in turpentine-induced inflammatory tissue", *J Nucl Med*, **36(7)**:1301-1306 (1995).
33. Okazumi S, Enomoto K, Fukunaga T, Kikuchi T, Asano T, Isono K, Arimizu N, Imazeki K, Ito Y and Yamamoto H, "Evaluation of the cases of benign disease with high accumulation on the examination of 18F-fluorodeoxyglucose PET[Japanese]", *Kaku Igaku - Jap J Nucl Med*, **30(12)**:1439-1443 (1993).
34. Kim CK, Alavi JB, Alavi A, Reivich M, "New grading system of cerebral gliomas using positron emission tomography with F-18 fluorodeoxyglucose", *J Neuro-Oncol*, **10(1)**:85-91(1991).
35. Delbeke D, Meyerowitz C, Lapidus RL, Maciunas RJ, Jennings MT, Moots PL, Kessler RM, "Optimal cutoff levels of F-18 fluorodeoxyglucose uptake in the differentiation of low-grade from high-grade brain tumors with PET", *Radiology*, **195(1)**:47-52 (1995).
36. Ishizu K, Sadato N, Yonekura Y, Nishizawa S, Magata Y, Tamaki N, Tsuchida T, Okazawa H, Tanaka F, Miyatake S *et al*, "Enhanced detection of brain tumors by [18F]fluorodeoxyglucose PET with glucose loading", *J Comput Assist Tomogr*, **18(1)**:12-15 (1994).
37. Ishizu K, Nishizawa S, Yonekura Y, Sadato N, Magata Y, Tamaki N, Tsuchida T, Okazawa H, Miyatake S, Ishikawa M, *et al*, "Effects of hyperglycemia on FDG uptake in human brain and glioma", *J Nucl Med*, **35(7)**:1104-1109 (1994).
38. Holthoff VA, Herholz K, Berthold F, Widemann B, Schroder R, Neubauer I and Heiss WD, "In vivo metabolism of childhood posterior fossa tumors and primitive neuro-ectodermal tumors before and after treatment", *Cancer*, **72(4)**:1394-1403 (1993).
39. Schifter T, Hoffman JM, Hanson MW, Boyko OB, Beam C, Paine S, Schold SC, Burger PC and Coleman RE, "Serial FDG-PET studies in the prediction of survival in patients with primary brain tumors", *J Comput Assist Tomogr*, **17(4)**:509-561 (1993).

40. Hoffman JM, Waskin HA, Schifter T, Hanson MW, Gray L, Rosenfeld S and Coleman RE, "FDG-PET in differentiating lymphoma from nonmalignant central nervous system lesions in patients with AIDS", *J Nucl Med*, **34(4)**:567-575 (1993).
41. Buchpiguel CA, Alavi JB, Alavi A and Kenyon LC, "PET versus SPECT in distinguishing radiation necrosis from tumor recurrence in the brain", *J Nucl Med*, **36(1)**:159-164 (1995).
42. Sols A and Crane RK, "Substrate specificity of brain hexokinase", *J Biol Chem*, **210**:581-595 (1954).
43. Sokoloff L, Reivich M, Kennedy C, Des Rosiers MH, Patlak CS, Pettigrew KD, Sakurada O and Shinohara M, "The [^{14}C]deoxyglucose method for the measurement of local cerebral glucose utilization: Theory, procedure, and normal values in the conscious and anesthetized albino rat", *J Neurochem*, **28(5)**:897-916 (1977).
44. Coe EL, "Inhibition of glycolysis in ascites tumor cells preincubated with 2-deoxy-2-fluoro-D-glucose", *Biochim Biophys Acta*, **264(2)**:319-327 (1972).
45. Bessell EM, Foster AB and Westwood JH, "The Use of Deoxyfluoro-D-glucopyranoses and Related Compounds in a Study of Yeast Hexokinase Specificity", *Biochem J*, **128(2)**:199-204 (1972).
46. Kuhl D, Reivich M, Wolf A, Greenberg J, Phelps M, Ido T, Casella V, Fowler J, Gallagher B, Hoffman E, Alavi A and Sokoloff L, "Determination of local cerebral glucose utilization by means of radionuclide computed tomography and (F-18)-2-fluoro-2-deoxy-D-glucose", *J Nucl Med*, **18(6)**:614 (1977)(Abstr).
47. Bessell EM and Thomas P, "The Effect of Substitution at C-2 of D-Glucose 6-Phosphate on the Rate of Dehydrogenation by Glucose 6-Phosphate Dehydrogenase (from Yeast and from Rat Liver)", *Biochem J*, **131(1)**:83-89 (1973).
48. Kobayashi Y and Taguchi T, "Fluorinated Vitamin D_3 Analogs Syntheses and Biological Activities". In: Filler R and Kobayashi Y (eds) *Biomedicinal Aspects of Fluorine Chemistry*, Tokyo:*Kodansha Ltd*, 33-53 (1982).
49. Hamacher K, Coenen HH and Stocklin G, "Efficient stereospecific synthesis of no-carrier-added 2-[^{18}F]-fluoro-2-deoxy-D-glucose using aminopolyether supported nucleophilic substitution", *J Nucl Med*, **27(2)**:235-238 (1986).
50. Warburg O, *The Metabolism of Tumors*, New York: Richard R. Smith Inc., 129-169 (1931).
51. Sweeney MJ, Ashmore J, Morris HP and Weber G, "Comparative biochemistry of heopatomas IV. Isotope studies of glucose and fructose metabolism in liver tumors of different tumor growth rates", *Cancer Res*, **23(6)**:995-1002 (1963).
52. Kubota K, Kubota R and Yamada S, "FDG Accumulation in Tumor Tissue", *J Nucl Med*, **34(3)**:419-421 (1993).
53. Shiue CY and Wolf AP, "The Syntheses of 1-[^{11}C]-D-Glucose and Related Compounds for the Measurement of Brain Glucose Metabolism", *J Labelled Compd Radiopharm*, **22(2)**:171-182 (1985).
54. Raichle ME, Larson KB, Phelps ME, Grubb RL Jr., Welch MJ and Ter-Pogossian MM, "In vivo measurement of brain glucose transport and metabolism employing glucose-11C", *Am J Physiol*, **228(6)**:1936-1948 (1975).

55. Weiss ES, Hoffman EJ, Phelps ME, Welch MJ, Henry PD, Ter-Pogossian MM and Sobel BE, "External detection and visualization of myocardial ischemia with 11C-substrates in vitro and in vivo", *Circ Res*, **39(1)**:24-32 (1976).
56. Raichle ME, Welch MJ, Grubb RL Jr, Higgins CS, Ter-Pogossian MM and Larson KB, "Measurement of regional substrate utilization rates by emission tomography", *Science*, **199(4332)**:986-987 (1978).
57. Kones RJ, "Insulin, adenyl cyclate, ions and the heart", *Trans NY Acad Sci*, **36(8)**:738-774 (1974).
58. Hara T, Nozaki T, Karasawa T, Iio M and Izuchi R, "(^{11}C)-1-Glucose and mannose as specific tumor markers", *J Labelled Compd Radiopharm*, **21(11-12)**:1213-1214 (1984).
59. Powers WJ, Dagogo-Jack S, Markham J, Larson KB and Dence CS, "Cerebral transport and metabolism of 1-^{11}C-D-glucose during stepped hypoglycemia", *Ann Neurol*, **38(4)**: 599-609 (1995).
60. Spence AM, Graham MM, Muzi M, Freeman SD, Link JM, Grierson JR, O'Sullivan F, Stein D, Abbott GL and Krohn KA, "Feasibility of imaging pentose cycle glucose metabolism in gliomas with PET: studies in rat brain tumor models", *J Nucl Med*, **38(4)**:617-624 (1997).
61. Fowler JS, Lade RE, MacGregor RR, Shiue C, Wan CN and Wolf AP, "Agents for the armamentarium of regional metabolic measurement in vivo via metabolic trapping: ^{11}C-2-deoxy-D-Glucose and halogenated deoxyglucose derivatives", *J Labelled Compd Radiopharm*, **16(1)**:7-9 (1979).
62. MacGregor RR, Fowler JS, Wolf AP, Shiue CY, Lade RE and Wan CN, "A Synthesis of 2-deoxy-D-[1-^{11}C]glucose for regional metabolic studies: Concise communication", *J Nucl Med*, **22(9)**:800-803 (1981).
63. Alavi A, Reivich M, Greenberg J, Fowler J, Christman D, MacGregor R, Shiue C, Jones S, London J and Wolf A, "Determination of local cerebral glucose metabolism in man using deoxy glucose and positron emission tomography", *J Nucl Med*, **23(5)**:P13(1982)(Abstr).
64. Russel JAG and Wolf AP, "The test-retest paradigm: The subject as his own reference", *J Nucl Med*, **25(5)**:P33 (1984)(Abstr).
65. Kloster G, Muller-Platz CM and Laufer P, "3-[^{11}C]-Methyl D-glucose, a potential agent for regional cerebral glucose utilization studies: synthesis, chromatography and tissue distribution in mice", *J Labelled Compd Radiopharm*, **18(6)**:855-863 (1981).
66. Turton DR, Sohanpal SK and Pike VW, "A modified procedure for the preparation of the radiopharmaceutical, 3-O-(^{11}C)Methyl-D-Glucose", *J Labelled Compd Radiopharm*, **21(11-12)**:1211-1212 (1979).
67. Laufer P and Kloster G, "Remote control synthesis of 3-[^{11}C]-methyl-D-glucose", *Int J Appl Radiat Isot*, **33(9)**:775-776 (1982).

68. Kloster G, Stocklin G, Vyska K, Freundlieb C, Hock A, Feinendegen LE, Traupe H and Heiss WD, "3-[^{11}C]-Methyl-D-glucose, an agent for the assessment of regional glucose transport across the blood-brain barrier". In: Cox PH (ed), *Progress in Radiopharmacology Vol 3*, Den Haag, Nijhoff, 199-211 (1982).
69. Tenth International Symposium on Cerebral Blood Flow and Metabolism, St Louis, Missouri, USA June 19-23, 1981, *J Cereb Blood Flow Metab*, **1**:Suppl 1, S505 (1981).
70. Thorell JO, Stone-Elander S, von Holst H and Ingvar M, "Synthesis of [1-^{11}C]D-glucosamine and evaluation of its in vivo distribution in rat with PET", *Appl Radiat Isot*, **44(5)**:799-805 (1993).
71. Tewson TJ, Welch MJ and Raichle ME, "[^{18}F]-labeled 3-deoxy-3-fluoro-D-glucose: synthesis and preliminary biodistribution data", *J Nucl Med*, **19(12)**:1339-1445 (1978).
72. Goodman MM, Elmaleh DR, Kearfott KJ, Ackerman RH, Hoop B Jr, Brownell GL, Alpert NM and Strauss HW, "F-18-labeled 3-deoxy-3-fluoro-D-glucose for the study of regional metabolism in the brain and heart", *J Nucl Med*, **22(2)**:138-144 (1981).
73. Knust EJ, Machulla HJ, Baldwin RM, Chen T and Feinendegen LE, "Synthesis of, and animal experiments with, *N*-isopropyl-*p*-^{123}I-iodo-amphetamine (IMP) and ^{18}F-3-deoxy-3-fluoro-D-glucose (3-FDG) as tracers in brain and heart diagnostic studies", *Nuklearmedizin* **23(1)**:31-34 (1984).
74. Nakada T, Kwee IL, Card PJ, Matwiyoff NA, Griffey BV and Griffey RH, "Fluorine-19 NMR imaging of glucose metabolism", *Mag Res Med*, **6(3)**:307-313 (1988).
75. Barnett JE, Holman GD and Munday KA, "Structural requirements for binding to the sugar-transport system of the human erythrocyte", *Biochem J*, **131(2)**:211-221 (1973).
76. Goodman MM, Kabalka GW and Longford CPD, "Synthesis of Fluorine-18 labeled 4-fluoro-4-deoxy-D-glucose as a potential brain, heart and tumor imaging agent", *J Labelled Compd Radiopharm*, **32**:568-569 (1993).
77. Fujiwara T, Kubota K, Sato T, Matsuzawa T, Tada M, Iwata R, Itoh M, Hatazawa J, Sato K, Fukuda H and Ido T, "*N*-[^{18}F]Fluoroacetyl-D-glucosamine: A Potential Agent for Cancer Diagnosis", *J Nucl Med*, **31(10)**:1654-1658 (1990).
78. Toole BP, Biswas C and Cross J, "Hyaluronate and invasiveness of the rabbit V2 carcinoma", *Proc Natl Acad Sci USA*, **76(12)**:6229-6303 (1979).
79. Lehninger AL, *Biochemistry*, 2nd ed, New York:Worth (1975).
80. Tada M, Oikawa A, Iwata R, Fujiwara T, Kubota K, Matsuzawa T, Sugiyama H, Ido T, Ishiwata K and Sato T, "An efficient, one-pot synthesis of 2-deoxy-2-[^{18}F]fluoroacetamido-D-glucopyranose (*N*-[^{18}F]fluoroacetyl-D-glucosamine): a potential diagnostic imaging agent", *J Labelled Compd Radiopharm*, **27(11)**:1317-1324 (1989).
81. Winterbourne DJ, Barnaby RJ, Kent PW and Mian N, "Incorporation of N-fluoro-acetyl-D-glucosamine into hyaluronate by rabbit tracheal explants in organ culture", *Biochem J*, **182(3)**:707-716 (1979).

82. Tada M, Matsuzawa T, Ohrui H, Fukuda H, Ido T, Takahashi T, Shinohara M and Komatsu K, "Synthesis of some 2-deoxy-2-fluoro-[^{18}F]-hexopyranoses: potential diagnostic imaging agents", *Heterocycles*, **22(3)**:565-568 (1984).
83. Tada M, Matsuzama T, Yamaguchi K, Abe Y, Fukuda H and Itoh M, "Synthesis of ^{18}F-labeled 2-deoxy-2-fluoro-D-galactopyranoses using acetyl hypofluorite procedure", *Carbohydr Res*, **161**:314-317 (1987).
84. Fukuda H, Yamaguchi K, Matsuzama T *et al*, "2-deoxy-2-[^{18}F]fluoro-D-galactose: a new tracer for the evaluation of liver function by PET. I. Evaluation of toxicity and radiation dose", *Kaku Igaku - Jpn J Nucl Med*, **24**:165-169 (1987).
85. Fukuda H, Yamaguchi K, Matsuzama T *et al*, "2-deoxy-2-[^{18}F]fluoro-D-galactose: a new probe for the evaluation of liver function by PET. II. A first clinical PET study of the liver in normal volunteers", *Kaku Igaku - Jpn J Nucl Med*, **24**:871-874 (1987).
86. Ishiwata K, Ido T, Imahori Y, Yamaguchi K, Fukuda H and Matsuzawa T, "Accumulation of 2-deoxy-2-[^{18}F]fluoro-D-galactose in the liver by phosphate and uridylate trapping", *Int J Radiat Appl Instrum Part B. Nucl Med Biol*, **15(3)**:271-276 (1988).
87. Fukuda H, Takahashi J, Fujiwara T, Yamaguchi K, Abe Y, Kubota K, Sato T, Miyazawa H, Hatazawa J, Tada M, Ishiwata K and Ido Tatsuo, "High Accumulation of 2-Deoxy-2-Fluorine-18-Fluoro-D-Galactose by Well-Differentiated Hepatomas of Mice and Rats", *J Nucl Med*, **34(5)**:780-786 (1993).
88. Schwarz RT and Datema R, "Inhibitors of protein glycosylation", *Trends Biochem Sci*, **5(3)**:65-67 (1980).
89. Haradahira T, Maeda M, Omae H and Kojima M, "Synthetic routes for labeling of 2-deoxy-2-fluoro-D-hexoses with fluorine-18", *J Labelled Compd Radiopharm*, **21(11-12)**:1218-1219 (1984).
90. Fukuda H, Matsuzawa T, Abe Y, Endo S, Yamada K, Kubota K, Hatazawa J, Sato T, Ito M, Takahashi T, Iwata R and Ido T, "Experimental study for cancer diagnosis with positron-labeled fluorinated glucose analogs: [^{18}F]-2-fluoro-2-deoxy-D-mannose: a new tracer for cancer detection", *Eur J Nucl Med*, **7(7)**:294-297 (1982).
91. Adam MJ, McCarter JD and Withers SG, "Synthesis and Evaluation of 2-Deoxy-2-[^{18}F]-Fluoro-β-Mannosyl Fluoride as a Mechanism-based Imaging Probe for Glycosi-dase Enzymes", *J Labelled Compd Radiopharm*, **32**:116-117 (1993).
92. McCarter JD, Adam MJ and Withers SG, "Synthesis of 2-Deoxy-2-[^{18}F]-Fluoro-β-Mannosyl [^{18}F]-Fluoride as a Potential Imaging Probe for Glycosidases", *J Labelled Compd Radiopharm*, **31(12)**:1005-1009 (1992).
93. Takahashi T, Ido T, Shinohara M, Iwata R, Fukuda H, Matsuzawa T, Tada M and Orui H, "Syntheses of ^{18}F-deoxy-aldohexoses and their comparative study", *J Labelled Compd Radiopharm*, **21(11-12)**:1215-1217 (1984).
94. Haradahira T, Kato A, Maeda M, Kanazawa Y, Yamada M, Torii Y, Ichiya Y and Masuda K, "Synthesis and *in vivo* behavior of F-18 labeled analog of D-Talose: 2-deoxy-2-[^{18}F]fluoro-D-talose", *J Labelled Compd Radiopharm*, **32**, 552-554(1993).

95. Haradahira T, Maeda M, Kato A, Kanazawa Y, Yamada M, Torii Y, Ichiya Y and Masuda K, "Metabolic pathway of 2-deoxy-2-[^{18}F]fluoro-D-talose in mice: trapping in tissue after phosphorylation by galactokinase", *Nucl Med Biol*, **21(2)**:269-276 (1994).
96. Chen M and Whistler RL, "Metabolism of D-Fructose", *Adv Carbohydr Chem Biochem*, **34**:286-343 (1977).
97. Gumaa KA and McLean P, "The Kinetic Quantitation of ATP:D-Glucos-6-Phosphotransferases", *FEBS Lett*, **27(2)**:293-297 (1972).
98. Haradahira T, Tanaka A, Maeda M, Ichiya Y and Masuda K, "Synthesis and Biodistribution of F-18 Labeled Analog of D-Fructose: 1-Deoxy-1-[^{18}F]fluoro-D-fructose", *J Labelled Compd Radiopharm*, **35**:339-340 (1994).
99. Kloster G, Laufer P, Wutz W and Stocklin G, "^{75}Br- and ^{123}I-Analogues of D-glucose as potential radiopharmaceuticals", *J Labelled Compd Radiopharm*, **19(11-12)**:1626-1628 (1982).
100. Kloster G, Laufer P, Wutz W and Stocklin G, "D-Glucose derivatives labelled with ^{75,77}Br and ^{123}I", *J Labelled Compd Radiopharm*, **20(3)**:391-415 (1983).
101. Kloster G, Laufer P, Wutz W and Stocklin G, "^{75,77}Br- and ^{123}I-Analogues of D-Glucose as Potential Tracers for Glucose Utilization in Heart and Brain", *Eur J Nucl Med*, **8(6)**:237-241 (1983).
102. Zhou YG, Shiue CY and Wolf AP, "Syntheses of radiobrominated 2-deoxy-2-bromo-D-mannose for the measurement of cerebral glucose metabolism in vivo", *J Labelled Compd Radiopharm*, **19(11-12)**:1623-1625 (1982).
103. Zhou YG, Shiue CY, Wolf AP and Arnett CD, "Synthesis and biodistributions of [Br-82]2-deoxy-2-bromo-D-glucose (^{82}Br-2-Br-DG) and [Br-82]-2-deoxy-2-bromo-D-mannose (^{82}Br-2-Br-DM)", *J Nucl Med*, **23(5)**:P105 (1982)(Abstr).
104. Tsuya A and Shigematsu A, Diagnostische Mittel Patent Application 28 17 336, 10 pages, Federal Republic of Germany (1979).
105. Abbadi M, Mathieu J-P and Morin C, "A Synthesis of 4-Deoxy-4-iodo-D-glucose Suitable for Radiolabeling", *J Labelled Compd Radiopharm*, **39(6)**:487-492 (1997).
106. Honda S and Takiura K, "Iodinolysis of C-2 mercurated hexose derivatives", *Carbohydr Res*, **34**:45 (1974).
107. Magata Y, Saji H, Arano Y, Horiuchi K, Torizuka K and Yokayama A, "Procurement of radioiodinated glucose derivative and its biological character", *J Nucl Med Biol* **14(1)**:7-13 (1987).
108. Lutz T, Dougan H, Rihela T, Hudon M, Cohen P, Jamieson WRE and Lyster DM, "The effect of iodine position on uptake in the mouse using an isomeric series of 2-deoxy-2-*O*-([^{123}I]-Iodobenzyl)glucoses", *J Labelled Compd Radiopharm*, **29**:535-545 (1991).
109. Maley F and Lardy HA, "Synthesis of *N*-substituted glucosamines and their effect on hexokinase", *J Biol Chem*, **214**:765-773 (1955).
110. Magata Y, Saji H, Ohmomo Y, Tanaka C, Konishi J and Yokoyama A, "Development of a Novel Radioiodinated Glucose Derivative with interaction to hexokinase", *J Labelled Compd Radiopharm*, **31(4)**:317-328 (1992).

111. Lutz T, Dougan H, Rihela T, Vo CV and Lyster DM, "^{123}I-Iodobenzoylglucosamines: Glucose analogues for heart", *J Labelled Compd Radiopharm*, **33(4)**:327-344 (1993).
112. Magata Y, Inagaki M, Ohmomo Y, Yamada Y, Saji H and Yokoyama A, "Synthesis and biological evaluation of esterified radioiodinated glucose derivative", *J Labelled Compd Radiopharm*, **30**:300-301 (1991).
113. Adam MJ and Withers SG, "2-Fluoro-2-Iodo-Mannose and -Glucose as Potential SPECT Imaging Agents.", *J Labelled Compd Radiopharm*, **35**:250 (1994).
114. McCarter JD, Adam MJ and Withers SG, "Syntheses, radiolabelling, and kinetic evaluation of 2-deoxy-2-fluoro-2-iodo-D-hexoses for medical imaging", *Carbohydr Res*, **266**:273-277 (1995).
115. Goodman MM and Knapp FF Jr, "Synthesis and distribution of (E)-3-C-[^{125}I]iodovinyl-D-allose: A new strategy for the preparation of in vivo stable radioiodinated carbohydrates", *J Nucl Med*, **26(5)**:P121 (1985)(Abstr).
116. Flanagan R, Lentle BR and Wiebe LI, "Synthesis of 6-radioiodo-6-deoxy-D-galactose, and its tissue distribution and excretion in rats". In: Sorenson JA (ed), *Radiopharmaceuticals II: Proceedings 2nd International Symposium on Radiopharmaceuticals*, March 19-22, Seattle, Washington, 119-128 (1979).
117. Brunet M-D, Morin C and Vidal M, "Ester Derivatives in Transport of ^{123}I-labelled D-glucose analogues", *J Labelled Compd Radiopharm*, **37**:164-166 (1995).
118. Comet M, Desruet M-D, Guezzi C, Morin C and Vidal M, "Preliminary evaluation of [^{123}I]6'-deoxy-6'-iodo-D-maltose as a glucose transporter binding ligand", *J Labelled Compd Radiopharm*, **40**:684-686 (1997).
119. Mercer JR, *Pharmacy 443. Radiopharmaceutical Sciences 1*, Faculty of Pharmacy and Pharmaceutical Sciences, University of Alberta, Edmonton, Alberta, Canada (1997).
120. Berne RM and Levy MN, "Skeletal physiology". In: Berne RM and Levy MN (eds), *Physiology 3rd ed*, St Louis: Mosby Yearbook, 292-308 (1993).
121. Berne RM and Levy MN, "The peripheral circulation and its control". In: Berne RM and Levy MN (eds), *Principles of Physiology 2nd ed*, St Louis: Mosby Yearbook, 313-322 (1996).
122. Tannock IF, "Cell Proliferation". In Tannock IF and Hills RP (eds), *The Basic Science of Oncology, 2nd ed*, 154-177 (1992).
123. Chapman JD, "Tumor Oxygenation". In: Bertino JR (ed), *Encyclopedia of Cancer Vol III*, San Diego: Academic Press, 1914-1925 (1997).
124. Dewey DL, "Effect of oxygen and nitric oxide on the radiosensitivity of human cells in tissue culture", *Nature*, **186(4727)**:780-782 (1960).
125. Gentner NE and Paterson MC, "Damage and Repair from Ionizing Radiation". In: Hurst A and Nasim A (eds), *Repairable Lesions in Microorganisms*, London: Academic Press, 57-84 (1984).
126. Gray LH, Conger AD, Ebert M, Hornsey S and Scott OCA, "The concentration of oxygen dissolved in tissues at the time of irradiation as a factor in radiotherapy", *Br J Radiol*, **26(312)**:638-648 (1953).

127. Stone HB, Brown JM, Phillips TL and Sutherland RM, "Oxygen in Human Tumors: Correlations between Methods of Measurement and Response to Therapy", *Radiat Res*, **136(3)**:422-434 (1993).
128. Asquith JC, Watts ME, Patel K, Smithen CE and Adams GE, "Electron Affinic Sensitization V. Radiosensitization of Hypoxic Bacteria and Mammalian Cells in Vitro by some Nitroimidazoles and Nitropyrazoles", *Radiat Res*, **60(1)**:108-118 (1974).
129. Stratford IJ, O'Neill P, Sheldon PW, Silver AR, Walling JM, Adams GE, "RSU1069, a nitroimidazole containing an aziridine group. Bioreduction greatly increases cytotoxicity under hypoxic conditions", *Biochem Pharmacol*, **35(1)**:105-109 (1986).
130. Brown JM, "The mechanisms of cytotoxicity and chemosensitization by misonidazole and other nitroimidazoles", *Int J Radiat Oncol Biol Phys*, **8(3-4)**:675-682 (1982).
131. Garrecht BM and Chapman JD, "The labelling of EMT-6 tumours in BALB/C mice with ^{14}C-misonidazole", *Br J Radiol*, **56(670)**:745-753 (1983).
132. Chapman JD, Franko AJ and Sharplin J, "A marker for hypoxic cells in tumours with potential clinical applicability", *Br J Cancer*, **43(4)**:546-550 (1981).
133. Edwards DI, "Nitroimidazole drugs - action and resistance mechanisms. I. Mechanisms of action", *J Antimicrob Chemother*, **31(1)**, 9-20 (1993).
134. Brown JM and Workman B, "Partition coefficients as a guide to the development of radiosensitizers which are less toxic than misonidazole", *Radiat Res*, **82(1)**:171-190 (1980).
135. Perez-Rayes E, Kalyanaraman B and Mason RP, "The reduction metabolism of metronidazole and ronidazole by aerobic liver metabolism", *Mol Pharmacol*, **17(2)**:239-244 (1980).
136. Rauth AM, McClelland RA, Michaels HB and Batistella R, "The oxygen dependence of the reduction of nitroimidazoles in a radiolytic model system", *Int J Radiat Oncol Biol Phys*, **10(8)**:1323-1326 (1984).
137. Whitmore GF and Varghese AJ, "The biological properties of reduced nitroheterocyclics and possible underlying biochemical mechanisms", *Biochem Pharmacol*, **35(1)**:97-103 (1986).
138. Varghese AJ and Whitmore, "Binding to cellular macromolecules as a possible mechanism for the cytotoxicity of misonidazole", *Cancer Res*, **40(7)**:2165-2169 (1980).
139. Chapman JD, Baer K and Lee J, "Characteristics of the metabolism-induced binding of misonidazole to hypoxic mammalian cells", *Cancer Res*, **43(4)**:1523-1528 (1981).
140. Varghese AJ and Whitmore GF, "Cellular and chemical reduction products of misonidazole", *Chem-Biol Interact*, **36(2)**:141-151 (1981).
141. McClelland RA, Panicucci R and Rauth AM, "Electrophilic Intermediate in the Reactions of a 2-(hydroxylamino)imidazole. A Model for Biological Effects of Reduced Nitroimidazoles", *J Am Chem Soc*, **107(6)**:1762-1763 (1985).

142. Biaglow JE, Varnes ME, Astor M and Hall EJ, "Non-protein thiols and cellular response to drugs and radiation", *Int J Radiat Oncol Biol Phys*, **8(3-4)**:719-723 (1982).
143. Bump EA, Taylor YC and Brown JM, "Role of gluatathione in the hypoxic cell cytotoxicity of misonidazole", *Cancer Res*, **43(3)**:997-1002 (1983).
144. Varghese AJ, Gulyas S and Mohindra JK, "Hypoxia-dependent of 1-(2-nitro-1-imidazolyl)-3-methoxy-2-propanol by Chinese hamster ovary cells and KHT tumor cells in vitro and in vivo", *Cancer Res*, **36(10)**:3761-3765 (1976).
145. Flockhart IR, Malcolm SL, Martin TR, Parkins CS, Ruane RJ and Troup D, "Some aspects of the metabolism of misonidazole", *Br J Cancer* **37**:Suppl III, 264-267 (1978).
146. Varghese AJ and Whitmore GF, "Detection of a reactive metabolite of misonidazole in human urine", *Int J Radiat Oncol Biol Phys*, **10(8)**:1361-1363 (1984).
147. Mulcahy RT, Gipp JJ, Ublacker GA and McClelland RA, "Enhancement of melphalan (L-PAM) toxicity by reductive metabolites of 1-methyl-2-nitro-imidazole, a model nitroimidazole chemosensitizing agent", *Biochem Pharmacol*, **40(12)**:2671-2676 (1990).
148. Brezden CB, McClelland RA and Rauth M, "Mechanism of the selective hypoxic cytotoxicity of 1-methyl-2-nitroimidazole", *Biochem Pharmacol*, **48(2)**:361-370 (1994).
149. Mannan RH, "Radioiodinated sugar-coupled 2-nitroimidazoles: novel non-invasive markers of hypoxic tumor tissue", *Ph.D. Thesis*, University of Alberta, Edmonton, Alberta, Canada (1991).
150. Nunn A, Linder K and Strauss HW, "Nitroimidazoles and imaging hypoxia", *Eur J Nucl Med*, **22(3)**:265-280 (1995).
151. Jette DC, Wiebe LI, Flanagan RJ, Lee J and Chapman JD, "Iodoazomycin Riboside (1-(5'-Iodo-5'-deoxyribofuranosyl)-2-nitroimidazole), a Hypoxic Cell Marker, *Radiat Res*, **105(2)**:169-179 (1986).
152. Wiebe LI, Jette DC, Chapman JD, Flanagan RL and Meeker BE, "Iodoazomycin Riboside [1-(5'-Iodo-5'-deoxyribofuranosyl)-2-nitroimidazole], a Hypoxic Cell Marker. In Vivo Evaluation in Experimental Tumors". In: Winkler C (ed), *Nuclear Medicine in Clinical Oncology*, Heidelberg:Springer-Verlag, 402-207 (1986).
153. Moore RB, Chapman JD, Mercer JR, Mannan RH, Wiebe LI, McEwan AJ and McPhee MS, "Measurement of PDT-Induced Hypoxia in Dunning Prostate Tumors by Iodine-123-Iodoazomycin Arabinoside", *J Nucl Med*, **34(3)**:405-413 (1993).
154. Stypinski D, "Pharmacokinetics and Dosimetry of Radiolabelled Iodoazomycin Arabinoside (IAZA)", *Ph.D. Thesis*, University of Alberta, Edmonton, Alberta, Canada (1998).
155. Liu, H, "Evaluation of brain hypoxia with radiolabelled IAZA in the Gerbil Stroke Model", *M.Sc. Thesis*, University of Alberta, Edmonton, Alberta, Canada (1997).

156. Mercer JR, Mannan RH, Somayaji VV, Lee J, Chapman JD and Wiebe LI, "Sugar-coupled 2-nitroimidazoles: novel *in vivo* markers for hypoxic tumor tissue". In: Maddelena, Snowdon and Boniface (eds), *Advances in Radiopharmacology, proceedings of the Sixth International Symposium on Radiopharmacology*, Wollongong, Austria:Wollongong University Press, 104-113 (1990).
157. Schneider RF, Engelhardt EL, Stobbe CC, Fenning MC and Chapman JD, "The synthesis and radiolabeling of novel markers of tissue hypoxia of the iodinated azomycin nucleoside class", *J Labelled Compd Radiopharm*, **39(7)**:541-557 (1997).
158. Mannan RH, Mercer JR, Wiebe LI, Kumar P, Somayaji VV and Chapman JD, "Radioiodinated Azomycin Pyranoside (IAZP): A Novel Non-Invasive Marker for the Assessment of Tumor Hypoxia", *J Nucl Med Biol*, **36(1)**:60-67 (1992).
159. Mannan RH, Mercer JR, Wiebe LI, Somayaji VV and Chapman JD, "Radioiodinated 1-(2-Fluoro-4-iodo-2,4-dideoxy-β-L-xylopyranosyl)-2-nitroimidazole: A Novel Probe for the Noninvasive Assessment of Tumor Hypoxia", *Radiat Res*, **132(3)**:368-374 (1992).
160. Baker BR, Joseph JP and Schaub RE, "Puromycin. Synthetic Studies XIV", *J Am Chem Soc*, **77(22)**:5905-5910 (1955).
161. Reist EJ, Benitez A, Goodman L, Baker BR and Lee WW, "Potential Anticancer Agents. LXXVI. Synthesis of Purine Nucleosides of β-D-Arabinofuranose", *J Org Chem*, **27(9)**:3274-3279 (1962).
162. Ikehara M and Ogiso Y, "Studies of nucleosides and nucleotides-LIV. Purine cyclonucleosides-19. Further investigations on the cleavage of the 8,2'-O-anhydro linkage. A new synthesis of 9-β-D-arabinofuranosyladenine", *Tetrahedron*, **28**:3695-3704 (1972).
163. Sowa T and Tsunoda K, "Novel Synthesis of Anhydronucleosides *via* the 2',3'-*O*- Sulfinate of Purine Nucleosides as Intermediates", *Bull Chem Soc Japan*, **48(11)**:3243-3245 (1975).
164. Chattopadhyaya JB and Reese CB, "Reaction of 8,2'-*O*-Cycloadenosine with Hydrazine and Amines. Convenient Preparations of 9-β-D-Arabinofuranosyladenine and its Derivatives", *JCS Chem Commun*, 414-415 (1977).
165. Brodbeck U and Moffatt JG, "Carbodiimide-Sulfoxide Reactions. IX. Synthesis of 2'- and 3'-Keto Derivatives of Cytidine", *J Org Chem*, **35(10)**:3552-3558 (1970).
166. Sakairi N, Hirao I, Zama Y and Ishido Y, "Chemical conversion of some ribonucleosides into the corresponding β-D-arabinofuranosyl derivatives", *Nucleosides & Nucleotides*, **2(3)**:221-229 (1983).
167. Niaz GR, Khan F and Ifzal SM, "Synthesis of Spongouridine", *Karachi Uni J Sci* **8(1-2)**:67-70 (1980).
168. Ranganathan R and Larwood D, "Facile conversion of adenosine into new 2'-substituted-2'-deoxy-arabinofuranosyladenine derivatives: stereospecific synthesis of 2'-azido-2'-deoxy-, 2'-amino-2'-deoxy-, and 2'-mercapto-2'-deoxy-β-D-arabinofuranosyladenines", *Tet Lett*, **45**:4341-4344 (1978).

169. Sugawara T, Ishikura T, Itoh T and Mizuno Y, "Studies on the chemical synthesis of potential antimetabolites. 32. Synthesis of β-D-pentofuranosyl-deazaadenines as candidate inhibitors for S-adenosylhomocysteinases and methyltransferases", *Nucleosides & Nucleotides*, **1(3)**:239-251 (1982).
170. Gosselin G, Bergogne M-C and Imbach J-L, "Obtention d'arabinofuranno-nucleosides par transformation chimique de certains xylofurannonucleosides [French]", *Nucleosides & Nucleotides*, **3(3)**:265-275 (1984).
171. Glaudemans CPJ and Fletcher HG Jr, "Syntheses with Partially Benzylated Sugars. III. A Simple Pathway to a "*cis*-Nucleoside," 9-β-D-Arabino-furanosyladenine (Spongoadenosine), *J Org Chem*, **28(11)**:3004-3006 (1963).
172. Shen TY, Lewis HM and Ruyle WV, "Nucleosides I. A New Synthesis of 1-β-D-Arabinofuranosyl Pyrimidine Nucleosides", *J Org Chem*, **33(3)**:835-838 (1965).
173. Keller F, Botvinick IJ and Bunker JE, "An Improved Synthesis of 9-β(-D-Arabinofurnaosyl)-2-chloroadenine", *J Org Chem*, **32(5)**:1644-1646 (1967).
174. Cheriyan UO and Ogilvie KK, "Preparation of 9-β-D-arabinofuranosylguanine (araG)", *Nucleosides & Nucleotides*, **1(3)**:233-237 (1982).
175. Ibrahim-Lodgemann F, Mackenzie G and Shaw G, "Glycosylation of 5-hydroxy-4-cyanoimidazole", *Nucleosides & Nucleotides*, **4(1&2)**:199-200 (1985).
176. Seela F, Bourgeois W and Winter H, "Synthesis of pyrrole[3,2-c]pyridine and pyrazolo[3,4-d]pyrimidine β-D-arabinonucleosides via nucleobase anion glycosylation", *Nucleosides & Nucleotides*, **10(1-3)**:713-714 (1991).
177. Barker R and Fletcher HG Jr, "2,3,5-Tri-O-benzyl-D-ribosyl and L-arabinosyl Bromides", J *Org Chem*, **26(11)**: 4605-4609 (1961).
178. IUPAC-IUBMB Joint Commission on Biochemical Nomenclature (JCBN), "Nomenclature of Carbohydrates (Recommendations 1996)", *J Carbohydr Chem*, **16(8)**:1191-1280 (1997).
179. Smith CW, Sidwell RW, Robins RK and Tolman RL, "Azapurine Nucleosides. Synthesis and Antiviral Activity of 7-Amino-3-α-D-arabinofuranosyl-*v*-triazolo [4,5-*d*]pyrimidine and Related Nucleosides", *J Med Chem*, **15(9)**:883-887 (1972).
180. Tolman RL, Robins RK and Townsend LB, "Pyrrolopyrimidine Nucleosides II. The Total Synthesis of 7-β-D-Ribofuranosyl pyrrolo [2,3-d] pyrimidines Related to Toyocamycin", *J Heterocycl Chem*, **4(3)**:230-238 (1967).
181. Darnall KR and Townsend LB, "3-β-D-Arabinofuranosyladenine", *J Heterocycl Chem*, **3(3)**:371-373 (1966).
182. Karplus M, "Contact Electron-spin coupling of Nuclear Magnetic Moments", *J Chem Phys*, **30(11)**:11-15 (1959).
183. Rousseau RJ, Robins RK and Townsend LB, "The Synthesis of 2-Nitro-1-β-D-ribofuranosylimidazole (Azomycin Riboside)", *J Heterocycl Chem*, **4(3)**:311-312 (1967).
184. Beier RC and Mundy BP, "Assignment of anomeric configuration and identification of carbohydrate residues by ^{13}C NMR: arabino- and ribopyranosides and furanosides", *J Carbohydr Chem*, **3(2)**:253-266 (1984).

185. Silverstein RM , Bessler GC and TC Morrill, *Spectrometric Identification of Organic Compounds 5th ed*, New York: John Wiley & Sons, 267-284 (1991).
186. Gunther H, *NMR Spectroscopy: Basic principles, concepts, and applications in chemistry 2nd ed*, Chichester: John Wiley & Sons, 392-462 (1995).
187. Toth G, Rosemeyer H and Seela F, "Unambiguous assignment of anomeric configuration of nucleosides by NOE-difference spectroscopy", *Nucleosides & Nucleotides*, **8(5&6)**:1091-1092 (1989).
188. Rosemeyer H, Toth G and Seela F, "Assignment of anomeric configuration of D-ribo-, arabino-, 2'-deoxyribo-, and 2',3'-dideoxyribonucleosides by NOE difference spectroscopy", *Nucleosides & Nucleotides*, **8(4)**:587-597 (1989).
189. Eliel EL, Wilen SH and Mander L, *Stereochemistry of Organic Compounds*, NewYork: John Wiley & Sons, 991-1118 (1994).
190. Nishimura T, Shimizu B and Iwai I, "Optical rotatory dispersion of the anomeric nucleosides and nucleotides", *Biochim Biophys Acta*, **157(2)**:221-232 (1968).
191. Prisbe EJ, Verheyden JPH and Moffatt JG, "5-Aza-7-deazapurine Nucleosides.2. Synthesis of Some 8-(D-Ribofuranosyl)imidazo[1,2-*a*]-1,3,5-triazine Derivatives", *J Org Chem*, **43(25)**:4784-4794 (1978).
192. Seevers RH and Councell RE, "Radioiodination Techniques for Small Organic Molecules", *Chem Rev*, **82(6)**:575-590 (1982).
193. Weichert JP, Van Dort ME, Groziak MP and Councell RE, "Radioiodination via Isotope Exchange in Pivalic Acid", *J Radiat Appl Instrum Part A. Appl Radia Isot Int*, **37(8)**:907-911 (1986).
194. Eisenhut M, "Simple labelling of omega-phenyl fatty acids by iodine isotope exchange", *Int J Appl Radiat Isot*, **33(7)**:499-504 (1982).
195. Elias H and Lotterhos HF, "Notiz über eine neue Methode zur Raiojod-Markierung durch Halogenaustausch in Acetamid-Schmelzen [German]", *Chem Ber*, **109(4)**:1580-1583 (1976).
196. Mangner TJ, Wu J and Wieland DM, "Solid-Phase Exchange Radioiodination of Aryl Iodides. Facilitation by Ammonium Sulfate", *J Org Chem*, **47(8)**:1484-1488 (1982).
197. Iwashina T, Kumar R, Knaus EE and Wiebe LI, "An efficient, high specific activity radioiodination of 5-(1-hydroxy/methoxy-2-iodoethyl)-2'-deoxyuridine by isotope exchange labelling in pivalic acid melt", *J Labelled Compd Radiopharm*, **28(3)**:247-255 (1990).
198. Zea-Ponce Y, Baldwin RM, Zoghbi SS and Innis RB, "Formation of 1-[^{123}I]-Iodobutane in Labeling [^{123}I]Iomazenil by Iododestannylation: Implications for the Reaction Mechanism", *Appl Radiat Isot*, **45(1)**:63-68 (1994).
199. Srivastava SC, "Is There Life After Technetium: What is the Potential for Developing New Broad-Based Radionuclides?", *Sem Nucl Med*, **26(2)**:119-131 (1996).
200. Ter-Pogossian MM, "The Origins of Positron Emission Tomography", *Sem Nucl Med*, **22(3)**:140-149 (1992).

201. Koeppe RA and Hutchins GD, "Instrumentation for Positron Emission Tomography: Tomographs and Data Processing and Display Systems", *Sem Nucl Med*, **22(3)**:162-181 (1992).
202. Hoh CK, Schiepers C, Seltzer MA, Gambhir SS, Silverman DHS, Czernin J, Maddahi J and Phelps ME, "PET in Oncology: Will it Replace the Other Modalities?", *Sem Nucl Med*, **27(2)**:94-106 (1997).
203. Devous MD Sr, "SPECT Functional Brain Imaging". In: Kramer EL and Sanger JJ (eds), *Clinical SPECT Imaging*, New York: Raven Press, 97-128 (1995).
204. Kanno I, Uemura K, Miura S and Miura Y, "HEADTOME: A Hybrid Emission Tomograph for Single Photon and Positron Emission Imaging of the Brain", *J Comput Assist Tomogr*, **5(2)**:216-226 (1981).
205. Hirose Y, Ikeda Y, Higashi K *et al*, "A Hybrid Emission Computed Tomograph HEADTOME II", *IEEE Trans Nucl Sci*, **NS-29**:520-523 (1982).
206. Kanno I, Miura S, Yamamoto S, Iida H, Murakami M, Takahashi K and Uemura K, "Design and Evaluation of a Positron Emission Tomograph: HEADTOME III", *J Comput Assist Tomogr*, **9(5)**:931-939 (1985).
207. Kanno I, Iida H, Miura S, Yamamoto S, Amano M, Hirose Y, Murakami M, Takahashi K, Sasaki H, Shishido F *et al*, "Design concepts and preliminary performances of stationary-sampling whole-body high resolution positron emission tomography: HEADTOME IV[Japanese]", *Kaku Igaku - Jpn J Nucl Med*, **26(4)**: 477-85 (1989).
208. Drane WE, Abbott FD, Nicole MW, Mastin ST and Kuperus JH, "Technology for FDG SPECT with a Relatively Inexpensive Gamma Camera", *Radiology*, **191(2)**:461-465 (1994).
209. Chen EQ, MacIntyre WJ, Go RT, Brunken RC, Saha GB, Wong C-Y O, Neumann DR, Cook SA and Khandekar SP, "Myocardial Viability Studies Using Fluorine-18-FDG SPECT: A Comparison with Fluorine-18-FDG PET", *J Nucl Med*, **38(4)**:582-586 (1997).
210. Barinaga M, "New Imaging Methods Provide A Better View Into the Brain", *Science*, **276(5321)**:1974-1976 (1997).
211. Taubes G, "Play of Light Opens a New Window into the Body", *Science*, **276(5321)**:1991-1993 (1997).
212. Hebden JC, Arridge SR and Delpy DT, "Optical imaging in Medicine: I. Experimental techniques", *Phys Med Biol*, **42(5)**:825-840 (1997).
213. Arridge SR and Hebden JC, "Optical imaging in Medicine: II. Modelling and reconstruction", *Phys Med Biol*, **42(5)**:841-853 (1997).
214. Ness RK and Fletcher HG Jr, "The Anomeric 2,3,5-Tri-*O*-benzoyl-D-arabinosyl Bromides and Other D-Arabinofuranose Derivatives", *J Am Chem Soc*, **80(8)**, 2007-2010 (1958); Fletcher HG Jr, "The Anomeric Tri-*O*-benzoyl-D-arabinofuranosyl Bromides", *Methods Carbohydr Chem* **2**:228-230 (1963).
215. Wright RS and Khorana HG, "Phosphorylated Sugars. V. Syntheses of Arabinofuranose and Arabinopyranose 1-Phosphates", *J Am Chem Soc*, **80(8)**, 1994-1998 (1958).
216. Montgomery EM and Hudson CS, "Crystalline Alpha-Methyl-*d*-arabinofuranoside", *J Am Chem Soc*, **59(6)**:992-993 (1937).

217. Serianni AS and Barker R, "[^{13}C]-Enriched Tetroses and Tetrafuranosides: An Evaluation of the Relationship between NMR Parameters and Furanosyl Ring Conformation", **49(18)**:3292-3300 (1984).
218. Gorin PAJ and Mazurek M, "Carbon-13 and proton nuclear magnetic resonance studies on methyl aldofuranosides and their *O*-alkyl derivatives", *Carbohydr Res*, **48**:171-186 (1976).
219. Mizuno Y, Kaneko C and Oikawa Y, "Syntheses of Potential Antimetabolites. XV. Syntheses of a Sulfonate Analog of Adenosine 5'-Phosphate and an Alternative Synthesis of 5'-8-*S*-Anhydroadenine Nucleosides and 5'-Deoxy-spongoadenosine and Its Isomers", *J Org Chem*, **39(10)**:1440-1444 (1974).
220. Fargher RG and Pyman FL, "XXVI. - Nitro-, Arylazo-, and Amino-glyoxalines", *J Chem Soc Trans*, **115(1)**:217-260 (1919).
221. Heinisch G and Reusser W, "2-Dialkylaminoacylamino-imidazole als potentielle Lokalanästhetica [German]", *Sci Pharm*, **42(1)**:19-33 (1974).
222. Hanessian S and Banoub J, "Preparation of 1,2-*trans*-Glycosides in the Presence of Stannic Chloride", *Methods Carbohydr Chem*, **8**:243-245 (1980).
223. Watanabe KA, Hollenberg DH and Fox JJ, "Nucleosides LXXXV. On mechanisms of nucleoside synthesis by condensation reactions", *J Carbohydr Nucleosides Nucleotides*, **1(1)**:1-37 (1974).
224. Green JW, "The Glycofuranosides", *Adv Carbohydr Chem*, **21**:95-142 (1966).
225. Garegg PJ, Regberg T, Stawinski J and Stromberg R, "A Phosphorous Nuclear Magnetic Resonance Spectroscopic Study of the Conversion of Hydroxyl Groups into Iodo Groups in Carbohydrates using the Iodine-Triphenyl-phosphine-Imidazole Reagent", *JCS Perkin Trans II*, 271-274 (1987).
226. Gross J, "Iodine and bromine Part 1. Iodine Metabolism". In: Comar CL and Bronner F (eds), *Mineral Metabolism an Advanced Treatise Vol II (Part B)*, New York: Academic Press, 221-262 (1962).
227. Murray RK, "Metabolism of Xenobiotics". In: Murray RK, Granner DK, Mayes PA and Rodwell VW (eds), *Harper's Biochemistry 24th ed*, Stamford, Connecticut: Appleton & Lange, 750-756 (1996).
228. Hanessian S and Lavallee P, "Direct Replacement of Primary Hydroxyl Groups by Halogen", *Methods Carbohydr Chem*, **7**:49-55 (1976).
229. Moulder JE and Rockwell S, "Hypoxic fraction of solid tumors: Experimental techniques, methods of analysis and a survey of existing data", *Int J Radiat Oncol Biol Phys*, **10(5)**:695-712 (1984).
230. Nishimura T, Shimizu B and Iwai S, "A New Synthetic Method of Nucleosides", *Chem Pharm Bull*, **11(11)**:1470-1472 (1963).
231. Sakaguchi M, Larroquette CA and Agrawal KC, "Potential Radiosensitizing Agents. 6. 2-Nitroimidazole Nucleosides: Arabinofuranosyl and Hexopyranosyl Analogues", *J Med Chem*, **26(1)**:20-24 (1983).
232. Khan SH and Hindsgaul O, "Chemical Synthesis of oligosaccharides". In: Fukuda M and Hindsgaul O (eds), *Frontiers in Molecular Biology - Molecular Glycobiology*, IRL Press, 206-229 (1994).

233. Montgomery JA and Thomas HJ, "The Relationship of the Structure of Mercury Derivatives of Purines to Their Reaction with Acylglycosyl Halides", *J Org Chem*, **31(5)**:1411-1413 (1966).
234. Jorgenson PT, El-Barbary AA and Pedersen EB, "Synthesis of α-Arabinose Nucleosides from 6-Substituted Uracils", *Liebigs Ann Chem*, 1-5 (1993).
235. Bourgeois W and Seela F, "Synthesis of *ara*-3,7-Dideazaadenosine and Related Pyrrolo[3,2-*c*]pyridine D-Arabinofuranosides", *J Chem Soc Perkin Trans I*, 279-283 (1991).
236. Stewart JJP, "Optimization of Parameters for Semiempirical Methods I. Method", *J Comput Chem*, **10(2)**:209-220 (1989).

Appendices

Appendix 1. Brief assessment on the SPECT images obtained from 10 selected [^{123}I]IAZA advanced cancer patients[2,4] during 1991-1994.

Codes used in assessing radioactivity uptakes: 0 - no uptake; 1 - low uptake; 2 - moderate uptake; 3 - high uptake

Patient #1: Male, 57.

Date of Imaging: June 29, 1994.
Immediate images: Brain: 0 Liver: 3
24 h images: **Brain: 1** Liver: 3

Patient #2: Female, 67.

Date of Imaging: June 21, 1994.
Immediate images: Brain: 1 Liver: 3
24 h images: **Brain: 3** Liver: 3

Patient #3: Male, 56.

Date of Imaging: June 28, 1994.
Immediate images: Brain: 0 Liver: 3
24 h images: **Brain: 1** Intestines: 3

Patient #4: Female, 33.

Date of Imaging: not available.
Immediate images: Brain: 0 Liver: 3
24 h images: **Brain: 1** Intestines: 3

Patient #5: Male, 44.

Date of Imaging: April 21, 1993.
Immediate images: Brain: 0 Liver: 3
18 h images: **Brain: 3** Liver/Intestines: 3 (Figure 1)

Patient #6: Female, 66.

Date of Imaging: February 23, 1993.
Immediate images: Brain: 0 Liver: 3
20 h images: **Brain: 1** Liver/Intestines: 3

Patient #7: Male, no age was given.

Date of Imaging: April 30, 1992.
Immediate images: Brain: 0 Liver: 3
21 h images: **Brain: 1** Liver: 3

Patient #8: Male, no age was given.

Date of Imaging: June 25, 1992.
Immediate images: Brain: 1 Liver: 3
24 h images: **Brain: 2** Liver: 3

Patient #9: Male, no age was given.

Date of imaging: November 26, 1991.
Immediate images: Brain: 0 Liver: 3
18-25 h images: **Brain: 1** Liver: 3

Patient #10: Female, no age was given.

Date of imaging: June 12, 1991.
Immediate images: Brain: 0 Liver: 3
17 h images: **Brain: 1** Liver: 3

Appendix 2. Sample calculations of the two-sample *t*-test.

Data: Brain-to-blood ratios, [^{125}I]IAIA (5)

Sample 1: *Normal* = normal Balb/c mice
Sample 2: *Tumor* = EMT-6 tumor bearing Balb/c mice

t-Test: Two-Sample Assuming Unequal Variances

0.25h	*Normal*	*Tumor*
Mean	0.155567	0.0461
Variance	0.000278	5.41E-05
Observations	3	3
Hypothesized Mean Difference	0	
df	3	
t Stat	10.4115	
*p**(T<=*t*) one-tail	0.000946	
t Critical one-tail**	4.540707	
*p**(T<=*t*) two-tail	0.001891	
t Critical two-tail**	5.840848	

t-Test: Two-Sample Assuming Unequal Variances

0.50h	*Normal*	*Tumor*
Mean	0.0997	0.066467
Variance	0.005632	0.000362
Observations	3	3
Hypothesized Mean Difference	0	
df	2	
t Stat	0.743482	
p(T<=*t*) one-tail	0.267333	
t Critical one-tail	6.964547	
p(T<=*t*) two-tail	0.534666	
t Critical two-tail	9.924988	

t-Test: Two-Sample Assuming Unequal Variances

1h	*Normal*	*Tumor*
Mean	0.029	0.0347
Variance	0.000292	0.000203
Observations	3	3
Hypothesized Mean Difference	0	
df	4	
t Stat	-0.44349	
p(T<=*t*) one-tail	0.34017	
t Critical one-tail	3.746936	
p(T<=*t*) two-tail	0.680341	
t Critical two-tail	4.60408	

t-Test: Two-Sample Assuming Unequal Variances

2h	*Normal*	*Tumor*
Mean	0.039933	0.0791
Variance	0.003106	3.11E-05
Observations	3	3
Hypothesized Mean Difference	0	
df	2	
t Stat	-1.21126	
p(T<=*t*) one-tail	0.174748	
t Critical one-tail	6.964547	
p(T<=*t*) two-tail	0.349496	
t Critical two-tail	9.924988	

t-Test: Two-Sample Assuming Unequal Variances

4h	*Normal*	*Tumor*
Mean	0.192433	0.099667
Variance	0.016981	0.000148
Observations	3	3
Hypothesized Mean Difference	0	
df	2	
t Stat	1.22771	
p(T<=*t*) one-tail	0.172221	
t Critical one-tail	6.964547	
p(T<=*t*) two-tail	0.344442	
t Critical two-tail	9.924988	

t-Test: Two-Sample Assuming Unequal Variances

8h	*Normal*	*Tumor*
Mean	0.0533	0.0743
Variance	0.005682	0.004022
Observations	2	3
Hypothesized Mean Difference	0	
df	2	
t Stat	-0.32475	
p(T<=*t*) one-tail	0.388095	
t Critical one-tail	6.964547	
p(T<=*t*) two-tail	0.77619	
t Critical two-tail	9.924988	

t-Test: Two-Sample Assuming Unequal Variances

24h	*Normal*	*Tumor*
Mean	0.145667	0.316367
Variance	0.063656	0.068914
Observations	3	3
Hypothesized Mean Difference	0	
df	4	
t Stat	-0.81203	
p(T<=*t*) one-tail	0.231167	
t Critical one-tail	3.746936	
p(T<=*t*) two-tail	0.462334	
t Critical two-tail	4.60408	

*The *p*-value, *p*, is the probability of obtaining a mean as extreme or more extreme than the observed sample mean. The smaller *p* is, the stronger the belief that a difference is not a random occurrence.

**Statistical analyses were performed at the significance level of 0.01.

IMAGE EVALUATION TEST TARGET (QA-3)

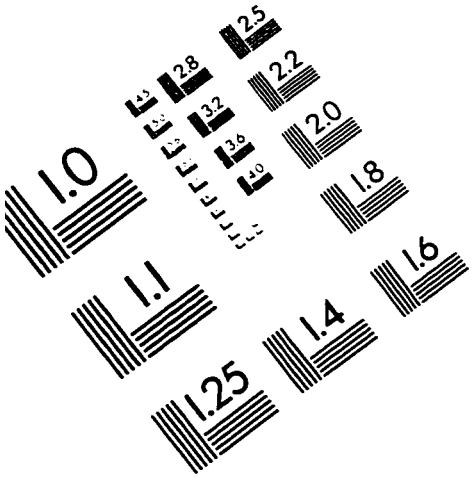

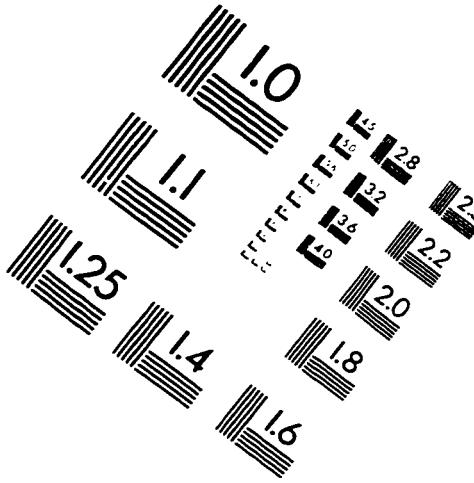

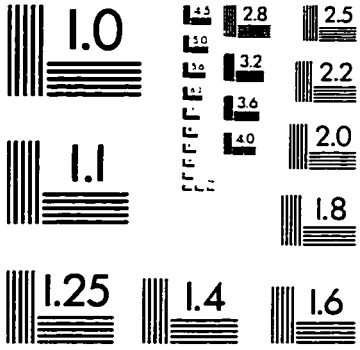

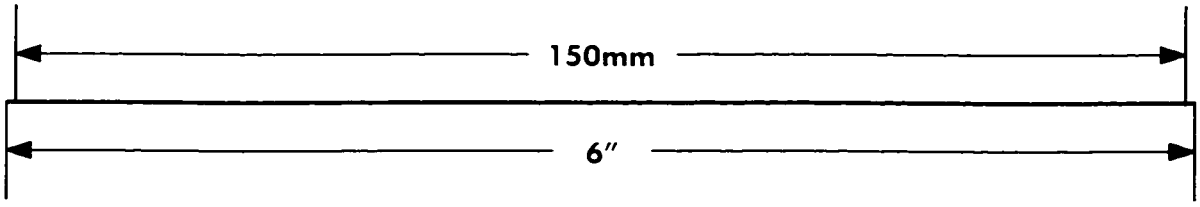

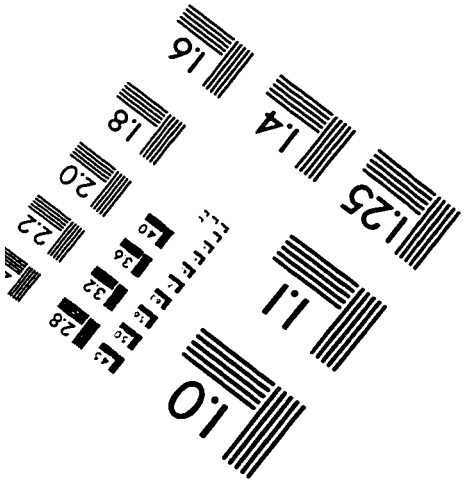

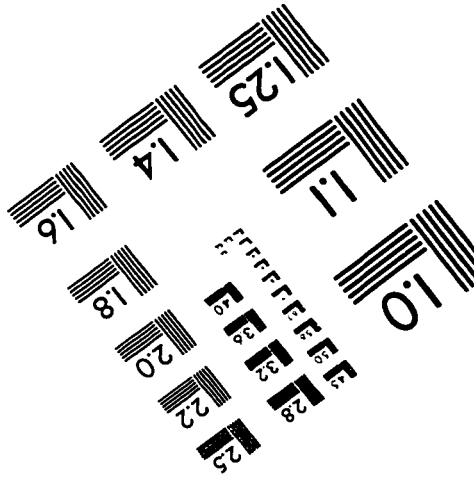

APPLIED IMAGE, Inc
1653 East Main Street
Rochester, NY 14609 USA
Phone: 716/482-0300
Fax: 716/288-5989

© 1993, Applied Image, Inc., All Rights Reserved